United States
Environmental Protection
Agency

Industrial Environmental Research
Laboratory
Research Triangle Park NC 27711

EPA-600/7-80-017c
January 1980

EPA

Advanced Combustion Systems for Stationary Gas Turbine Engines: Volume III. Combustor Verification Testing

Interagency Energy/Environment R&D Program Report

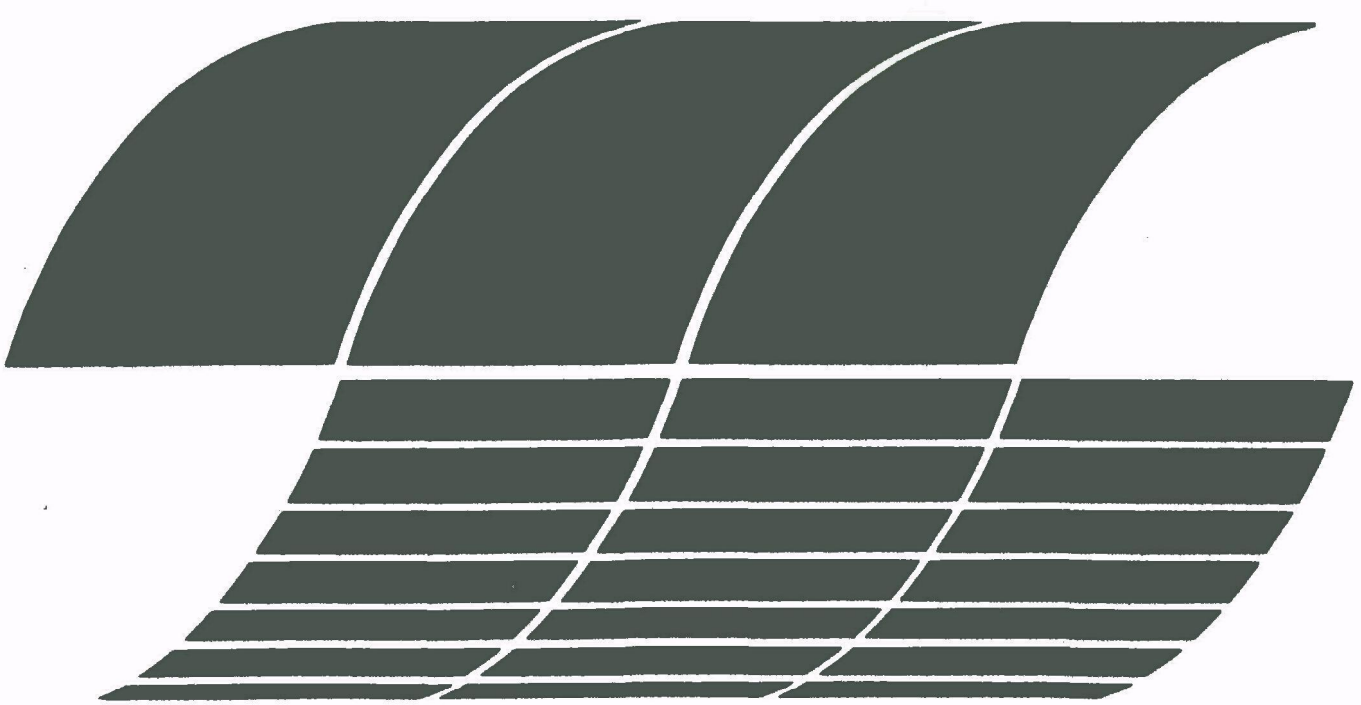

RESEARCH REPORTING SERIES

Research reports of the Office of Research and Development, U.S. Environmental Protection Agency, have been grouped into nine series. These nine broad categories were established to facilitate further development and application of environmental technology. Elimination of traditional grouping was consciously planned to foster technology transfer and a maximum interface in related fields. The nine series are:

1. Environmental Health Effects Research
2. Environmental Protection Technology
3. Ecological Research
4. Environmental Monitoring
5. Socioeconomic Environmental Studies
6. Scientific and Technical Assessment Reports (STAR)
7. Interagency Energy-Environment Research and Development
8. "Special" Reports
9. Miscellaneous Reports

This report has been assigned to the INTERAGENCY ENERGY-ENVIRONMENT RESEARCH AND DEVELOPMENT series. Reports in this series result from the effort funded under the 17-agency Federal Energy/Environment Research and Development Program. These studies relate to EPA's mission to protect the public health and welfare from adverse effects of pollutants associated with energy systems. The goal of the Program is to assure the rapid development of domestic energy supplies in an environmentally-compatible manner by providing the necessary environmental data and control technology. Investigations include analyses of the transport of energy-related pollutants and their health and ecological effects; assessments of, and development of, control technologies for energy systems; and integrated assessments of a wide range of energy-related environmental issues.

EPA REVIEW NOTICE

This report has been reviewed by the participating Federal Agencies, and approved for publication. Approval does not signify that the contents necessarily reflect the views and policies of the Government, nor does mention of trade names or commercial products constitute endorsement or recommendation for use.

This document is available to the public through the National Technical Information Service, Springfield, Virginia 22161.

EPA-600/7-80-017c

January 1980

Advanced Combustion Systems for Stationary Gas Turbine Engines: Volume III. Combustor Verification Testing

by

R.M. Pierce, C.E. Smith,
and B.S. Hinton

Pratt and Whitney Aircraft Group
United Technologies Corporation
P.O. Box 2691
West Palm Beach, Florida 33402

Contract No. 68-02-2136
Program Element No. INE829

EPA Project Officer: W.S. Lanier

Industrial Environmental Research Laboratory
Office of Environmental Engineering and Technology
Research Triangle Park, NC 27711

Prepared for

U.S. ENVIRONMENTAL PROTECTION AGENCY
Office of Research and Development
Washington, DC 20460

FOREWORD

This report was prepared by the Government Products Division of the Pratt & Whitney Aircraft Group (P&WA) of United Technologies Corporation under EPA Contract No. 68-02-2136, "Advanced Combustion Systems for Stationary Gas Turbine Engines." It is Volume III of the final report which encompasses work associated with the accomplishment of Phases III and IV of the subject contract from 1 January 1978 through 12 April 1979. The originator's report number is FR-11405.

Contract 68-02-2136 was sponsored by the Industrial Environmental Research Laboratory of the Environmental Protection Agency (EPA), Research Triangle Park, North Carolina under the technical supervision of Mr. W. S. Lanier.

The authors wish to acknowledge the valuable contributions made to this program by Mr. W. S. Lanier, whose skillful management and insight have been a key factor in the success of the Rich Burn/Quick Quench combustor design concept.

The Pratt & Whitney Aircraft Program Manager is Mr. Robert M. Pierce; the Deputy Program Manager is Mr. Clifford E. Smith. Mr. Stanley A. Mosier is Technology Manager for Fuels and Emissions Programs at the Government Products Division of Pratt & Whitney Aircraft Group. Mr. Bruce S. Hinton has been a principal contributor to the technical effort in Phases III and IV.

Special recognition is due Mr. E. R. Robertson of the Component Design and Integration Group, who was responsible for all drafting, hardware fabrication, and data processing activities. The skillful assistance of Mr. R. Taber of the Instrumentation Laboratory in setting up and operating the gas analysis equipment is also acknowledged.

CONTENTS

ILLUSTRATIONS (Continued)

ILLUSTRATIONS (Continued)

ILLUSTRATIONS (Continued)

ILLUSTRATIONS (Continued)

ILLUSTRATIONS (Continued)

LIST OF TABLES

SUMMARY

This report describes an exploratory development program to identify, evaluate, and demonstrate dry techniques for significantly reducing production of NO_x from thermal and fuel-bound sources in burners of stationary gas turbine engines.

Duty cycle analyses were conducted to identify current and projected dominant operating modes and requirements of stationary gas turbine engines. These analyses indicate that the propensity for NO_x to be generated in combustors of stationary gas turbine engines will increase significantly in the future as compression ratios and turbine inlet temperatures are increased to improve thermal efficiency and net plant heat rate. In ten years, uncontrolled thermal NO_x generation is predicted to double over today's levels; in 20 years, the factor is predicted to triple.

An extensive survey was made of candidate combustor design concepts and an analytical study was accomplished from which those concepts considered to have significant potential for reducing production of NO_x were identified. The initial compilation of 26 design concepts included many variations of basic strategies such as fuel-rich combustion, ultra lean combustion, heat removal, fuel prevaporization, and fuel-air premixing. An assessment of the NO_x-control effectiveness of each concept was made using a combustor streamtube computer code. The code employs a modular approach in the prediction of combustor emissions (NO_x, CO, and unburned hydrocarbons), with submodels for the internal flow field, physical combustion (including droplet vaporization and droplet burning), hydrocarbon thermochemistry, and NO_x kinetics.

The results of the computer studies were drawn upon to select a group of concepts for experimental screening in a bench scale combustor test rig. An erector-set approach was followed in the experimental program, making possible the rapid evaluation of many different concepts and combinations of concepts. About half the NO_x reduction techniques evaluated were based on fuel-lean burning, and half were based on fuel-rich burning. Two successful approaches were ultimately identified, and their performance relative to the program goals was assessed. It was concluded that one of the two concepts, referred to by the descriptive name "Rich Burn/Quick Quench," showed significant potential for application in stationary gas turbine engines, and was capable of meeting or exceeding all program exhaust emission goals.

Based on this assessment, the Rich Burn/Quick Quench concept was selected for implementation into the design of a full-scale (25 megawatt engine size) gas turbine combustor. In carrying out the full-scale design, reference was made to parametric data generated in the bench-scale experimental program which showed an inverse relationship between NO_x concentration levels and combustor primary zone residence time. Because direct scaling of combustor features cannot be employed, it was necessary to execute a separate but parallel design in larger scale, reproducing the essential processes of the basic Rich Burn/Quick Quench concept.

Two configurations of the full-scale prototype combustor were designed and constructed. The first provided a primary zone residence time about half as great as that utilized in the bench-scale combustor, but greater than that available in a representative 25 megawatt engine having on-board (in-line) burner cans. The second configuration was shorter in length, meeting the basic envelope requirements of the representative engine. Tests of the two configurations were conducted to verify proper implementation of the design concept, and to demonstrate the exhaust emission characteristics attainable in the full-scale design.

The test results were very positive, showing that the Rich Burn/Quick Quench concept can produce substantial reductions in NO_x for both nitrogenous and non-nitrogenous petroleum distillate fuels. All program exhaust emission goals were met. Comparison of the general emission characteristics to those documented earlier for the bench-scale combustor showed good agreement and indicated the same general dependence of NO_x concentrations on primary zone residence time. Extrapolation of the results to greater values of residence time indicates that further substantial reductions in NO_x can be achieved given increased combustor length. A second major implication of the test results is that the Rich Burn/Quick Quench concept may be directly applicable to heavy fuels. Having demonstrated substantial reductions in the quantities of NO_x formed due to fuel-bound nitrogen (which may be present in coal-derived and shale-derived feedstocks), the Rich Burn/Quick Quench concept may hold the answer to a second major difficulty, lack of fuel volatility. Under fuel-rich burning conditions NO_x formed initially due to heterogeneous burning of nonvolatile droplets can be reduced to N_2. Operation of the existing prototype combustor on heavy fuels (coal-derived, shale-derived or petroleum residual fuel) may show substantial reductions in NO_x when these fuels are fired.

SECTION 1

INTRODUCTION

Gas turbine engines currently in use by the electric utilities and by industry account for a relatively small portion of the total quantity of oxides of nitrogen (NO_x) emitted from stationary sources in this country. On a local scale, however, the gas turbine can be a significant contributor to air quality degradation, especially in the vicinity of engine installations where the NO_x background level is already objectionably high. The impact of stationary gas turbines may become even more significant in the future. Along with the present modes of utilization, combined cycle and industrial cogeneration applications are being projected. In these applications the advanced engine technology needed to provide higher cycle efficiencies, and to accommodate the anticipated firing of coal-derived, shale-derived, and petroleum residual fuels, will make it more difficult to meet proposed emission regulations.

Until recently, gas turbine combustors have been designed without regard for exhaust emissions. Initial attempts to control NO_x by modifying existing designs were generally unsuccessful. Although water injection was identified as a potential solution, this approach is expensive and ineffective when nitrogen-laden fuels must be burned. In light of these findings, it was clear that new design concepts specifically addressing exhaust emissions should be considered.

Under EPA Contract 68-02-2136, an exploratory development program was undertaken to identify, evaluate, and demonstrate alternative combustor design concepts for significantly reducing the production of NO_x in stationary gas turbine engines. The investigations were directed toward dry combustion control techniques suitable for use in a 25 megawatt (nominal) engine. Operation on both petroleum distillate fuels (non-nitrogenous and nitrogen bound) and low Btu* gaseous fuels was specified. Program goals were 50 ppmv NO_x (at 15% O_2) for non-nitrogenous fuels (oil and gas), and 100 ppmv NO_x (at 15% O_2) for oil or gas containing 0.5% nitrogen by weight. The goal for CO was 100 ppmv (at 15% O_2).

Accomplishment of the overall objective was effected via complementary analytical and experimental programs. Intrinsic in the support activities were combustor analytical model and engine duty cycle analyses, bench-scale screening tests of promising NO_x reduction concepts and, finally, full-scale evaluation tests of combustors incorporating the most promising NO_x reduction techniques.

The program was accomplished in four phases. The first phase consisted of an analytical investigation of combustion concepts considered to have potential for reducing the production of NO_x. In the second phase of work, a number of promising low NO_x production concepts were bench-tested to select the best candidate for implementation into the design of a full-scale, 25-megawatt-size, utility gas turbine engine combustor. In Phase III, a full-scale low NO_x combustor was designed and fabricated. Verification testing of the prototype combustor was conducted in Phase IV, and guidelines regarding the applicability of the demonstrated low NO_x design technology to stationary gas turbine engines were generated.

*Refer to Appendix B for SI unit conversion

SECTION 2

PHASE III — COMBUSTOR DESIGN AND RIG PREPARATION

In Phase III, the design of a full-scale combustor incorporating the successful NO_x reduction concept demonstrated in the bench-scale screening experiments of Phase II was carried out. This section describes the analytical and experimental procedures used in preparing the design, and describes the fabrication of the prototype combustor.

2.1 REVIEW OF PHASE I AND PHASE II RESULTS

In the first two phases of work, a review and analytical study had been conducted to identify concepts that might have potential for reducing the production of NO_x from thermal and fuel-bound sources of nitrogen in stationary gas turbine engine combustors. The most promising of these had been evaluated experimentally in bench-scale hardware. Of two successful design concepts that emerged from this study, the Rich Burn/Quick Quench concept was selected as the basis for the full-scale combustor design executed in Phase III.

The key elements of the Rich Burn/Quick Quench concept are identified in Figure 1. A premixing chamber is provided in which the fuel is prevaporized and premixed with air to form a homogeneous rich mixture. The prepared mixture is introduced into a primary zone section of the combustor and burned without the further addition of airflow. The rich burning process is terminated in a final step involving very rapid dilution, which provides the airflow needed to achieve an overall lean exit plane equivalence ratio. The success of this concept, which does not differ in its essential features from many previous proposals for a rich-burn, quick-quench approach to NO_x reduction, was largely a matter of execution, and of the selection and refinement of techniques for achieving the idealized conditions called for in the basic concept.

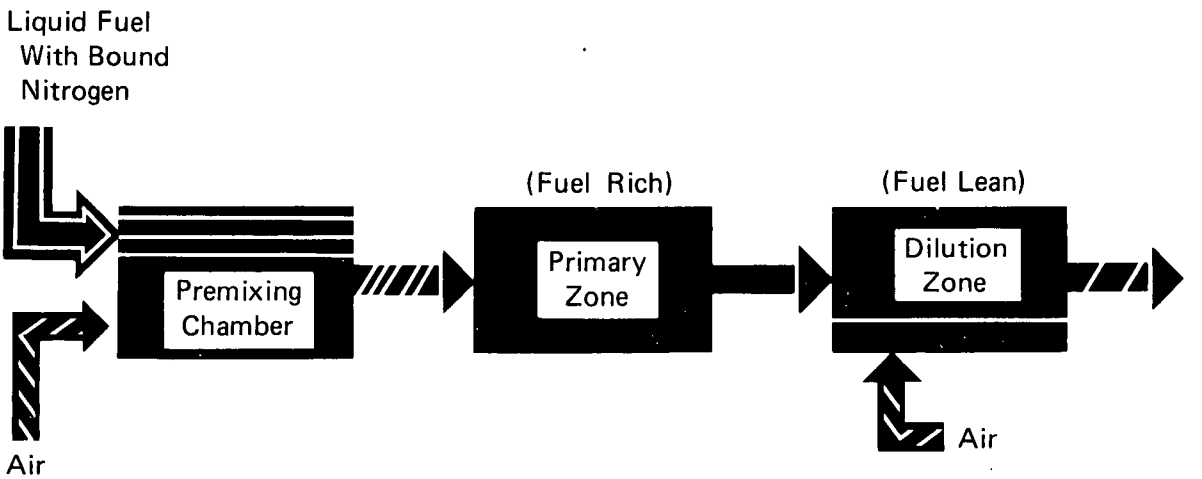

Figure 1. Rich Burning Concept Burner Components

The arrangement of representative rich burner bench-scale hardware tested in Phase II is shown in Figure 2. A single, high-velocity premixing passage was provided, terminating in a swirler that served to stabilize the flame in the primary zone of the combustor. All the air entering the primary zone came through the premixing passage. At design point, the primary zone operated fuel rich. It was followed by a dilution section designed for very rapid quenching of the fuel-rich gases leaving the primary zone.

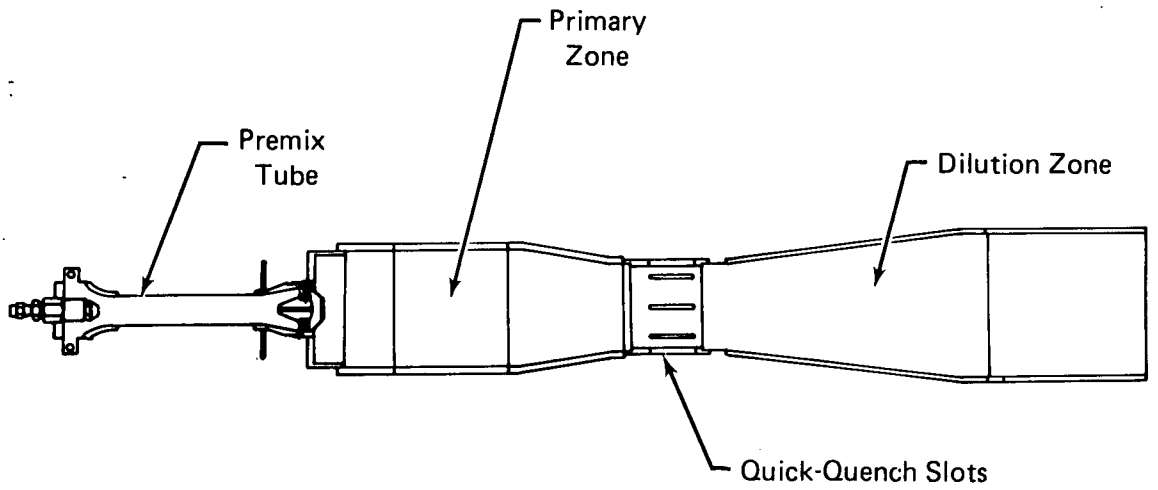

Figure 2. Rich Burner Arrangements

Tests of the rich burner were conducted at elevated pressures and temperatures simulating actual engine operating conditions. In Figure 3, data are shown from tests conducted at 150 psia, at inlet air temperatures of 650°F and 750°F. By staging the amount of air that entered the premixing tube, it was found that low NO_x concentration levels could be achieved over a range of overall (exit-plane) equivalence ratios. At the primary air settings shown (7 and 14%), NO_x concentrations of 60 ppmv and lower were demonstrated using No. 2 fuel with 0.5% nitrogen (as pyridine). Even lower concentrations were demonstrated using non-nitrogenous fuel. In Figure 4, representative bench-scale data points are presented for the Rich Burn/Quick Quench concept, demonstrating low NO_x concentration levels over a wide range of operating conditions using No. 2 fuel.

2.2 DESIGN APPROACH

The objectives adopted for the design of the full-scale prototype combustor reflect the requirements of conventional gas turbine combustion systems (temperature rise, pressure drop, and others), as well as the stated emission goals of the current experimental development program. It was intended that the NO_x reduction technology generated in this program be compatible with current state-of-the-art design practice for stationary gas turbine engines in the 25-megawatt-size range. The design requirements for the full-scale combustor are presented in Table I.

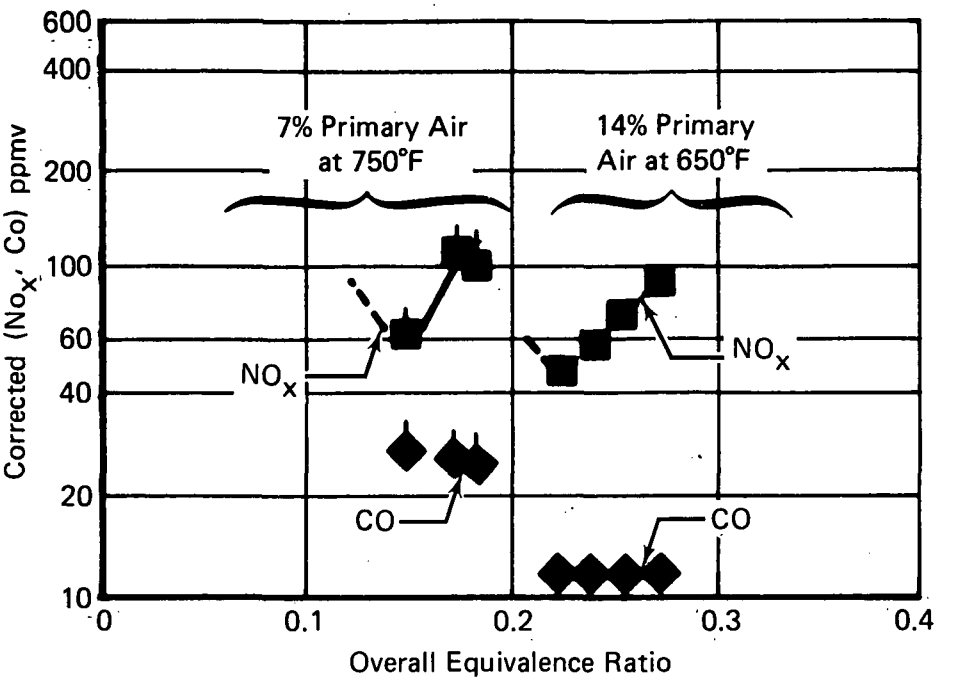

Figure 3. Rich Burner Simulated Engine Cycle Characteristics (150 psia, 0.5% Nitrogen)

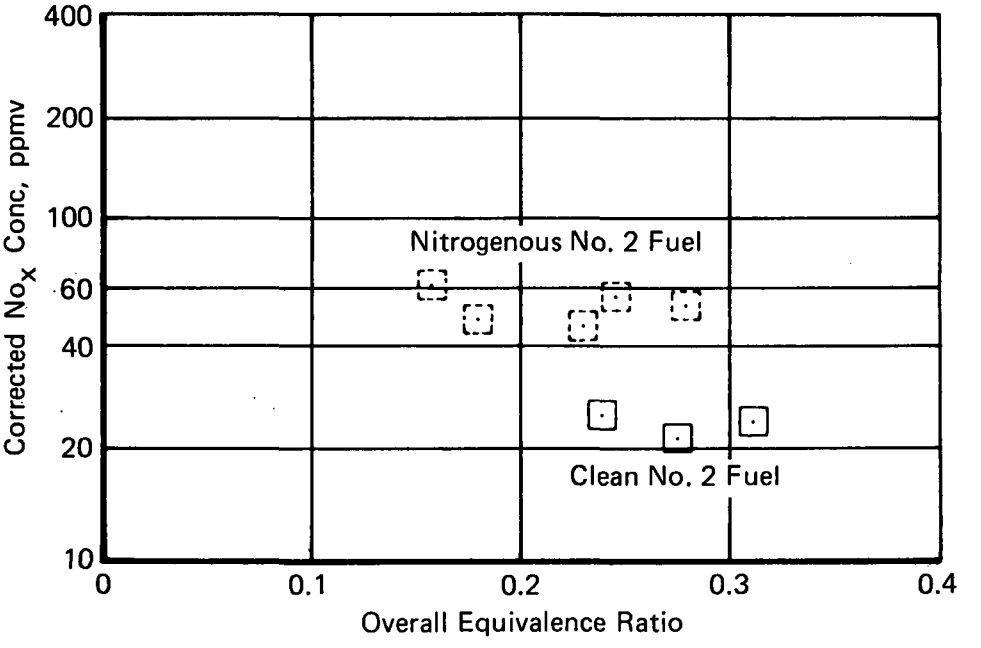

Figure 4. Rich Burn/Quick Quench Combustor Emission Trends

TABLE I
DESIGN REQUIREMENTS FOR THE
FULL-SCALE PROTOTYPE COMBUSTOR*

Type Combustor:	can (1 of 8, internally mounted)
Basic Dimensions:	10-in. dia, 20-in. length

Design Point Requirements:

	(Baseload)	*(Idle)*
Airflow -	31 lb_m/sec	7.8 lb_m/sec
Pressure -	188 psia	40 psia
Inlet Temperature -	722°F	285°F
Temperature Rise -	1160°F	625°F

Pressure Drop:	3% combustor, 2.5% diffuser
Lean Blowout:	0.006 fuel-air ratio (burner exit)

Exhaust Emissions (max. at any setting):

	(0% Fuel N)	*(0.5% Fuel N)*
NO_x	50 ppmv at 15% O_2	100 ppmv at 15% O_2
CO	100 ppmv at 15% O_2	100 ppmv at 15% O_2

Execution of the design of the full-scale combustor was based in large part upon the data generated in the bench-scale combustor program. It is important to point out that while these results may have provided a full characterization of the bench-scale combustor itself, they could not be used directly to specify the complete design of the full-scale combustor. Scaling criteria dictate that there can be no exact and complete correspondence between a prototype combustor and its subscale model, with regard to physical dimensions, operating conditions, and combustion performance. In lieu of direct scaling, a partial modeling approach was taken, as described in this section. In the basic features of the full-scale combustor, and in the areas of primary air staging (to control stoichiometry), combustor aerodynamics, liner cooling, and residence times, an attempt was made to reproduce the essential processes of the rich-burning concept, as identified and defined parametrically in the bench-scale test results. The design of the full-scale combustor was executed separately, drawing upon analytical modeling techniques and upon the bench testing of key components (particularly the full-scale premix tube) to verify that the essential processes of the concept were successfully reproduced.

2.3 BASIC DESIGN CONCEPT

The basic features and demonstrated results (from Phase II bench-scale testing) of the Rich Burn/Quick Quench concept, in summary form, are as follows:

Arrangement — Two combustion zones are arranged in series: a fuel-rich primary zone and a fuel-lean secondary zone, separated by a reduced diameter "quick-quench" section. A diagram of the bench-scale configuration as tested, is shown in Figure 2, with the major zones identified.

*Refer to Appendix B for SI unit conversion

Critical Features — Four key requirements for low exhaust emissions have been identified, using distillate and low Btu gaseous fuels:

- All the air entering the primary zone must be premixed with fuel to prevent the formation of an interface between the desired homogenous, fuel-rich mixture and air; in particular, liner cooling airflow cannot be discharged into the primary combustion region. This interface is considered to be a region where diffusion burning (combustion occurring at near stoichiometric conditions) predominates and has been shown to result in a substantial increase in NO_x in the combustor exhaust (refer to the results of bench scale Scheme 29-22A, Volume II of this report).

- For fuels with bound nitrogen, minimum NO_x concentration levels are obtained at primary zone equivalence ratios near 1.3. Non-nitrogenous fuels exhibit similar NO_x characteristics (at lower levels) up to the minimum point of the NO_x "bucket." Beyond this point, the NO_x concentration, corrected to 15% O_2, remains essentially constant with increasing equivalence ratio. However, it should be noted that equivalence ratios approaching and exceeding 1.5 could produce unacceptable quantities of smoke. This has the implication that primary zone airflow staging would not be necessary for non-nitrogenous fuels over the range of primary zone equivalence ratios from a value giving acceptable NO_x (perhaps 1.1 to 1.2) to a value where smoke formation is still acceptable (perhaps 1.4 to 1.5). In a typical 25 megawatt gas turbine this would represent an operating range (for acceptable emissions) from about 60% of baseload to peak load conditions. However, the optimum value of primary zone equivalence ratio is near 1.3 for both non-nitrogenous and nitrogen bearing fuels.

- Quick-quench air is added at a single site; it must be introduced in a manner that produces vigorous admixing, approximating a step change in composition and temperature.

- To attain acceptable CO concentrations at the burner exit plane, temperature (and therefore, fuel-air ratio) must be maintained high enough within the secondary zone to consume the large quantities of CO discharged from the fuel-rich primary zone. The temperature also must not be allowed to become excessive as appreciable NO_x formation in the fuel-lean secondary zone would result. The temperature range generally accepted for the oxidation of CO without appreciable NO_x formation with the residence time constraints of onboard gas turbine combustors is from about 2100 to about 2800°F. This implies the need to rapidly dilute the fuel-rich products from the primary combustion volume to a lean stoichiometry with a temperature in that range. Consequently, it is desirable to

introduce only part of the remaining airflow (not entering the primary zone) into the quick-quench region, leaving a final quantity to be introduced later in the secondary zone to achieve the desired combustor exit temperature. It is also acknowledged that, for ideal operation of the Rich Burn/Quick Quench concept at low power settings (low overall equivalence ratios), the quick-quench airflow should also be varied in proportion to the amount of flow restricted from the primary zone in an effort to maintain efficient combustion in the secondary zone to consume CO.

Emission Characteristics — The emission characteristics, or "signature," of the basic concept are shown in Figure 5, as generated at a constant airflow setting by varying the burner fuel flowrate. This "signature" has two notable features:

- A peak in the CO curve, to the right of which (at 0.2 exit plane equivalence ratio and higher) measured concentration levels are low;

- A minimum point or "bucket" in the NO_x curve, which corresponds approximately to a primary zone equivalence ratio of 1.3. The NO_x curve "bucket" represents the unique low emission design point of the basic emission signature.

  It should be noted that the data shown in Figure 5 are representative of fuels containing significant bound nitrogen. Non-nitrogenous fuels exhibit the same CO characteristics and the same NO_x characteristics (but at a lower level) up to the "bucket." Beyond that point, the NO_x emission remains nearly constant with increasing equivalence ratio.

Variable Primary Zone Airflow — Variable geometry can be employed to shift the low emission design point over a broad range of exit plane equivalence ratios, as shown in Figure 3. As described in Reference 1, the NO_x "bucket" can be shifted in this manner while maintaining an essentially fixed CO characteristic. Again, variable geometry may not be necessary for clean fuels over a limited operating range.

Residence Time Requirements — The minimum NO_x concentration levels attained (at the bottom of the NO_x curve "bucket") have been shown to decline with increasing primary zone residence time. This characteristic results in basic design tradeoffs among primary zone length (residence time), combustor pressure drop, and resultant NO_x concentration levels.

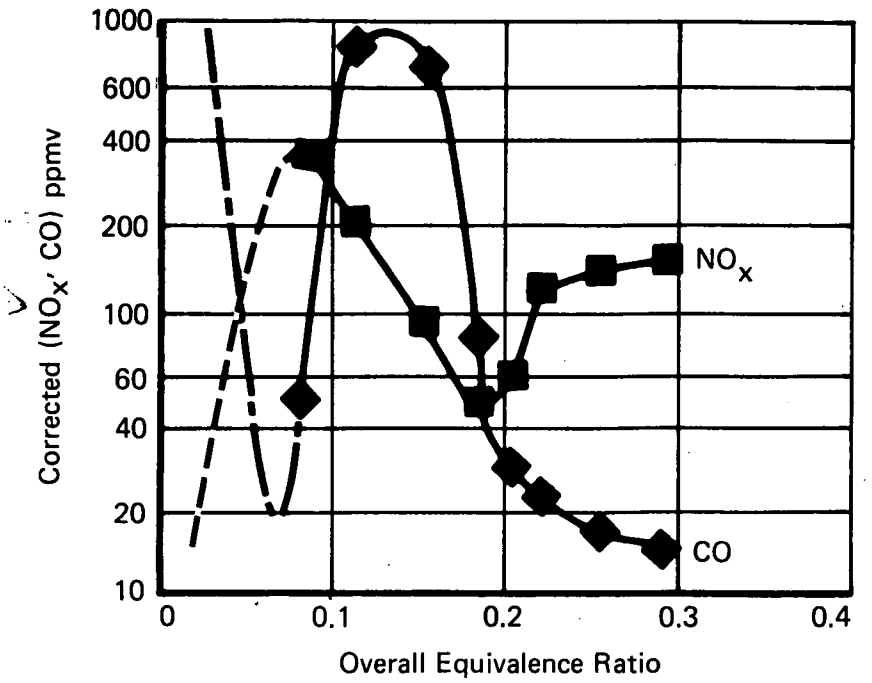

Figure 5. Rich Burner Characteristics (50 psia, 600°F, 0.5% Nitrogen

2.4 INITIAL COMBUSTOR SIZING AND SELECTION OF BASIC FEATURES

To initiate the design of the full-scale combustor, studies were conducted to identify the critical features of the bench-scale combustor and to determine what methods might be employed to reproduce the essential processes of the Rich Burn/Quick Quench concept. As stated, the bench-scale combustor hardware cannot be "scaled-up" directly to produce a full-scale design. However, the parametric data from the bench-scale combustor can be used to characterize the essential processes of the basic concept. To achieve emission characteristics in full scale comparable to those demonstrated in bench scale, it is necessary to execute a second design (in larger scale), reproducing the critical features of the smaller combustor and setting up the same basic physical processes.

Preliminary design activity was directed toward defining the size and basic features of the full-scale Rich Burn/Quick Quench combustor. Initial sizing calculations indicated that a primary zone length roughly twice that of a representative engine combustor might be necessary to achieve NO_x concentration levels in the 50 ppmv range, when No. 2 fuel with 0.5% nitrogen is burned. This conclusion was based on bench-scale data in which the tradeoff between primary residence time and the minimum achievable NO_x concentration level had been documented by varying the diameter and the length of the primary zone of the combustor. The bench-scale combustor configurations tested are shown in Figure 6. Primary zone diameters of three, five, and six inches were included. Two lengths were tested, 9 and 18 in. (measured from the premix tube swirler to the centerline of the quick-quench slots), and in one configuration an enlarged premixing tube (designed to pass 70% more airflow) was evaluated. The results obtained are presented in Figure 7 in terms of the tradeoff between the minimum attainable NO_x concentration* levels and the primary zone residence time.**

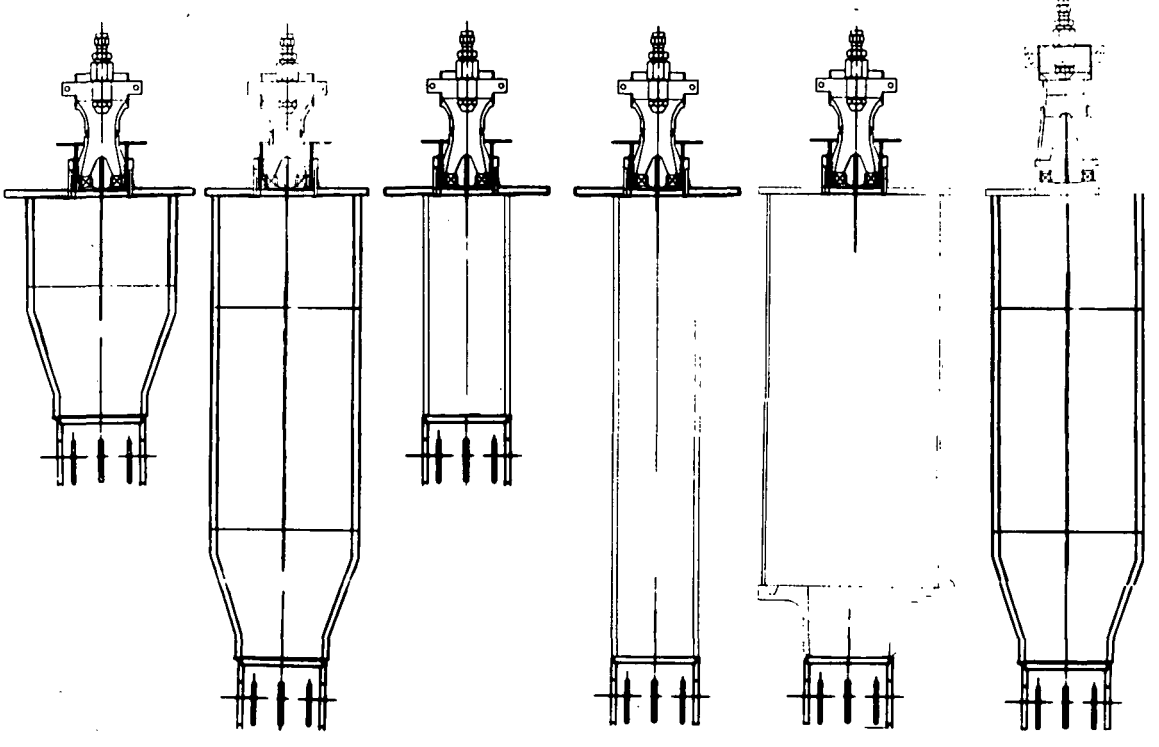

Figure 6. Bench-Scale Test Configurations Used to Determine Primer Zone Residence Requirements

* The "minimum attainable NO_x concentration" is measured at the bottom of the "bucket" in the characteristic NO_x curve of the Rich Burn/Quick Quench concept, illustrated in Figure 5.

** cold flow residence time $= \frac{\text{primary zone length}}{\text{cold flow reference velocity}}$

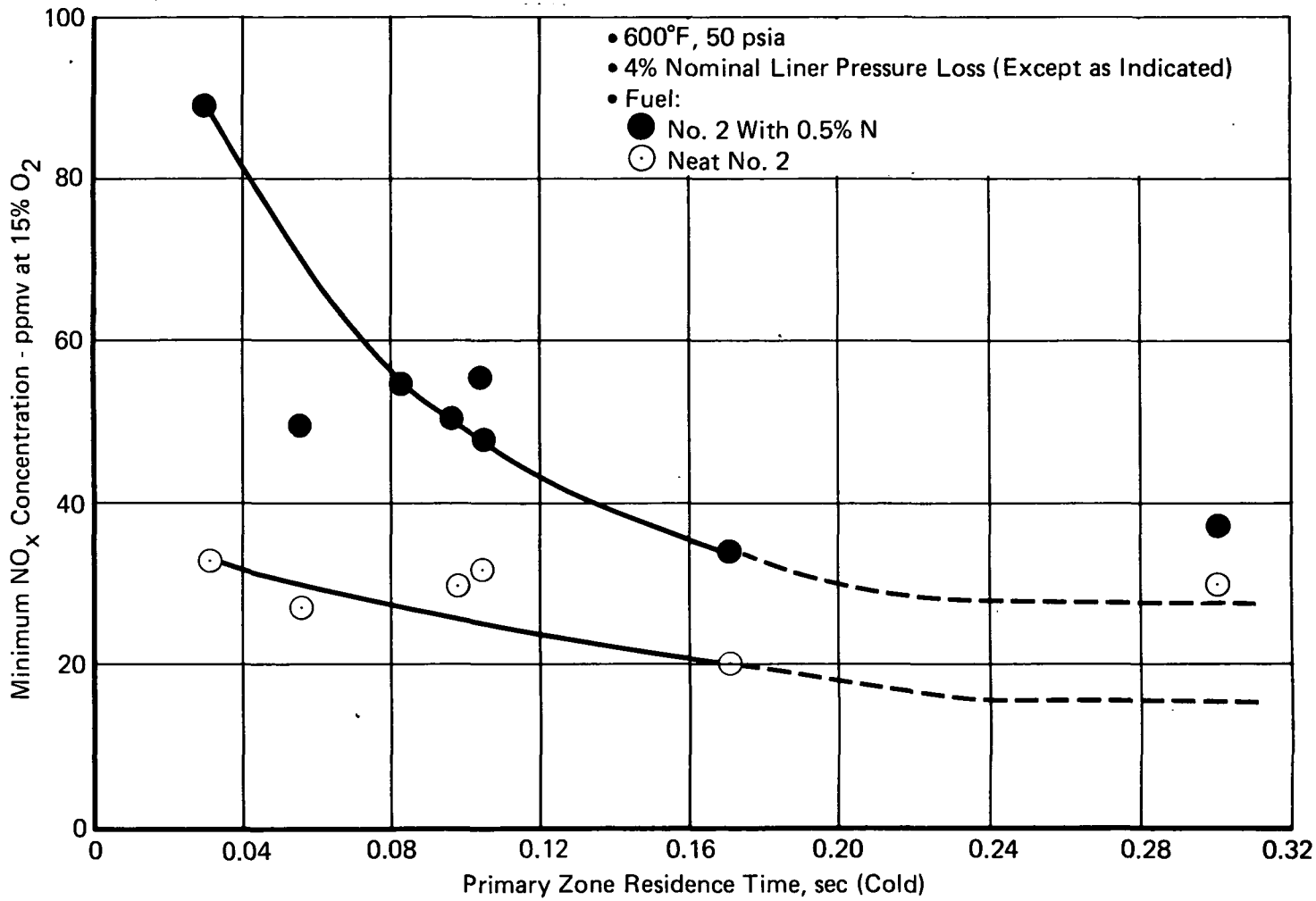

Figure 7. Variation in Minimum NO_x Concentration With Primary Zone Residence Time for Bench-Scale Tests of the Rich Burn/Quick Quench Concept

In the design of the full-scale combustor, the general relationship between residence time and NO_x concentration levels depicted in Figure 7 was adopted. It was assumed that the absolute levels demonstrated in the bench-scale combustor (50 to 60 ppmv over a broad range of operating conditions, as illustrated in Figure 4) were ultimately achievable in the full-scale combustor. To select a design-point value of the primary zone residence time, several factors were considered:

1. If an absolute value of residence time equal to that which had been utilized in the bench-scale combustor were adopted, a primary zone length about 2.5 times greater than the nominal length available in a representative 25-megawatt engine combustor would be required.

2. Primarily because of an inherently lower surface-to-volume ratio, it was reasoned that the full-scale combustor might not require the full value of residence time established for the bench-scale combustor.

3. For an initial configuration, a value equal to half the residence time utilized in the bench-scale combustor was selected.

4. Because more than one value of primary zone residence time would be required to establish the exact residence time dependence (and to establish whether the data being obtained fall on the negative slope portion or the flat portion of the curve in Figure 7) it was decided that a second configuration of the full-scale combustor, differing in primary zone length, should also be tested.

Consideration was also given to the front-end configuration of the full-scale combustor. By varying the number of premix tubes, it was possible to trade system complexity against overall combustor length. A single premixing tube was less complex because of more straightforward variable-geometry actuating requirements (the valving of airflow would be required in conjunction with only one premixing passage). On the other hand, multiple premixing tubes (six, for example) would require a more complex mechanical system, but could offer reduced length and might be expected to produce a more uniform fuel-air distribution within the primary zone.

The preliminary design activity led to a "first cut" configuration of the combustor, shown in Figure 8, which had the following basic features:

1. A single centrally mounted premix tube having a velocity versus length schedule similar to that of the smaller tubes employed in the bench-scale test program. Variable inlet vanes (not shown) were provided at the premixing tube entrance to regulate the primary zone airflow. The premix tube was offset slightly with respect to the centerline of the combustor in order to be in-line with an engine diffuser passage.

2. An extended length primary zone (65% of the overall combustor length) was provided for increased residence time.

3. A primary liner cooling scheme was provided that did not call for the discharge of spent cooling air into the combustion region of the primary zone. Airflow from the primary-liner convective cooling passage was discharged into the aft dilution section through openings in the wall at the dump plane of the combustor.

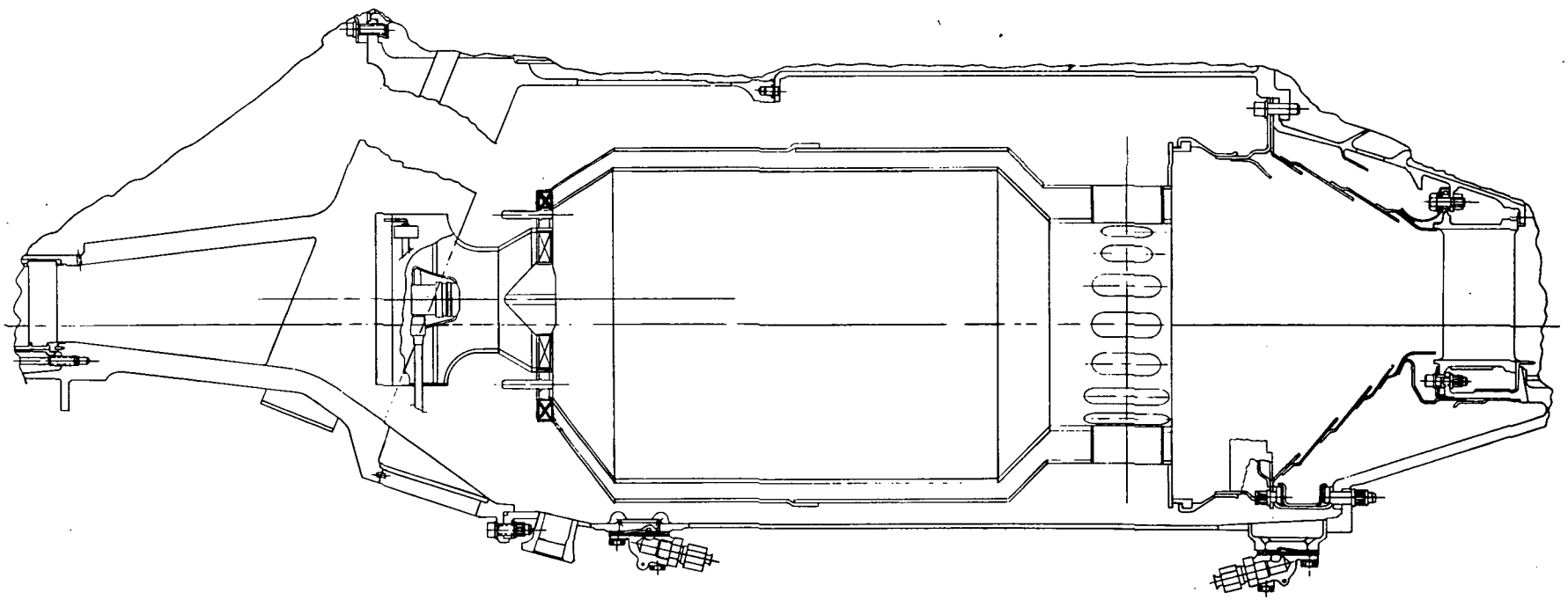

Figure 8. "First-Cut" Configuration of Full-Scale Combustor

4. The quick-quench section was designed to provide strong mixing, so that an abrupt termination of the primary zone rich-burning process could be achieved. An area ratio of 2.8 to 1 was adopted in the "necked-down" section of the combustor, matching the optimum value determined in the bench-scale tests.

5. The aft dilution section of the combustor was extended into the engine transition duct to maximize the available length for oxidation of CO, while still maintaining an extended-length primary zone in the interest of achieving low NO_x.

After consideration had been given to the sizing and basic features of the combustor, subsequent design work was concentrated in two areas: the final refinement and verification of the primary liner cooling scheme; and the evaluation of possible design tradeoffs that might be made in the interest of reducing combustor overall length to conform to the available space within a representative engine envelope. In the following paragraphs, a brief review of the work performed in the primary liner cooling study is presented, and bench-scale rig data indicating the tradeoff between secondary zone length and CO concentration levels are discussed.

2.5 PRIMARY ZONE LINER COOLING

An analytical effort was undertaken to design a convectively cooled combustor liner compatible with the Rich Burn/Quick Quench concept. A scheme was required that did not call for the discharge of spent cooling air into the combustion region of the primary zone. To meet this requirement, the feasibility of utilizing impingement cooling was investigated initially. Preliminary calculations were performed for the bench-scale burner rather than the full-scale burner so that model predictions could be verified by bench-scale experimental data. The heat load to the primary liner, under its most severe operating condition (unity equivalence ratio), was predicted using a liner design computer program, which took into account both convective and radiative heat transfer. At operating conditions of 50 psia and 600°F, the predicted heat load was 5×10^4 Btu/ft^2 hr. In subsequent analyses, a second computer code was used to predict the convective heat transfer coefficient resulting from a given impingement hole size, spacing and gap, assuming an allowable 1500°F metal temperature on the outer surface of the liner. Intial results indicated that a hole diameter of 0.060 in., and a transverse hole and row spacing of 0.5 in. would be sufficient to cool a 10-in. length of the primary liner without dumping any cooling air into the combustion region. This hole pattern required approximately 25% of the burner airflow. The spent cooling flow would be subsequently discharged into the burner as dilution air at the throat of the quick-quench section.

A feasibility test of the impingement cooling concept was carried out in the bench-scale rig. The burner configuration, shown in Figure 9, consisted of a double-wall primary liner made up of concentric cylindrical/conical pieces. The outer piece contained a plurality of small holes through which the liner cooling airflow entered, impinging on the surface of the inner piece. The annular passage between the pieces led to the necked-down section of the burner, where spent cooling air was discharged through the quick-quench slots. In the initial test of this configuration, failure of the inner liner wall occurred. Examination of the hardware indicated that the longitudinal ribs separating the inner and outer pieces had constrained the inner wall, preventing thermal expansion. As a result, buckling of the inner wall occurred, and the effectiveness of the impingement cooling technique was compromised leading to failure. A second configuration was built up without longitudinal ribs. Upon retesting, the new liner also exhibited signs of buckling, this time in the axial direction, which compromised the effectiveness of the film-cooling process, and once again led to failure of the inner liner.

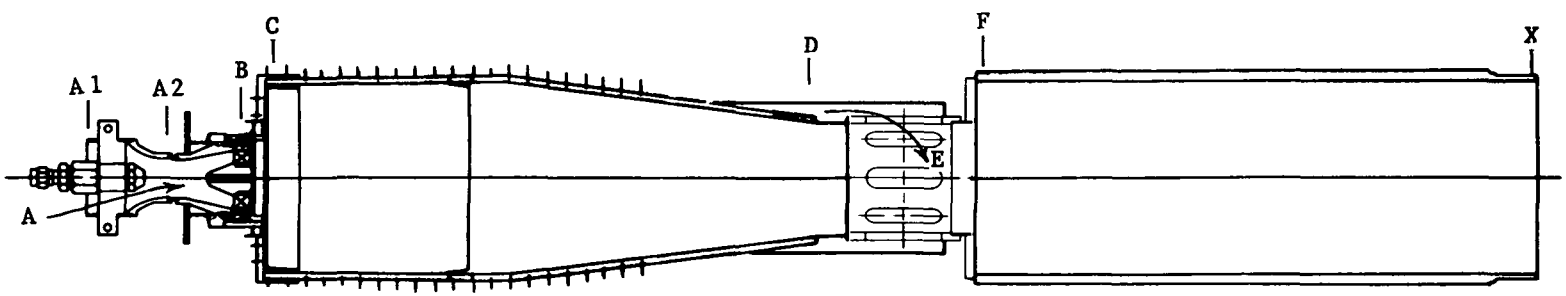

Figure 9. Impingement Cooling Scheme Implemented in the Rich Burn/Quick Quench Bench-Scale Combustor

Despite these outcomes, analytical predictions continued to indicate that the impingement cooling technique could meet the cooling requirements of the Rich Burn//Quick Quench combustor. However, a review of the bench-scale test results indicated that other questions remained to be answered, and that additional analyses and experimental verification tests should be undertaken to verify that an adequate flowrate of cooling air had been provided. In particular, it appeared that an expanded analysis of the aerodynamic characteristics of the convective cooling channel was needed. A revised analytical procedure was formulated after the analysis of Reference 2. The aerodynamic effects treated by the model included the pressure losses arising from friction, heat and mass addition, and sudden expansion. Both convective and radiative heat transfer processes were included. Predictions made using the expanded model indicated that the proper flowrate within the convective cooling passage (roughly 30% of the total burner airflow) could be readily achieved under the impingement cooling scheme only if the cooling airflow were discharged at low velocity (to avoid an excessive loss due to sudden expansion).

It was also indicated that the required cooling might be accomplished without the use of impingement jets if other means of achieving adequate turbulence within the cooling passage could be provided. One alternative suggested by the analysis was the use of swirling flow within the passage. According to this concept, swirl vanes would be provided at the entrance to the convective cooling passage. A "first-cut" configuration of this arrangement, shown in Figure 10, illustrates the swirl cooling concept. To verify the results of the analytical studies, and to assess the effectiveness of the swirl cooling technique, a short series of bench-scale experiments was carried out. The data generated in these experiments were used as a standard of comparison for the analytical model predictions with regard to the influence of burner airflow rate, inlet pressure, and inlet air temperature on the primary liner wall temperature level. Two liner convective cooling schemes were evaluated: a swirling scheme and a nonswirling scheme, shown in Figures 10 and 11. Both schemes were the same except at the entrance to the cooling passage. A photograph of the experimental hardware is shown in Figure 12. The tests conducted indicated that there was no appreciable difference in the cooling effectiveness of the two schemes. Based on these results, the swirl cooling scheme was dropped from further consideration.

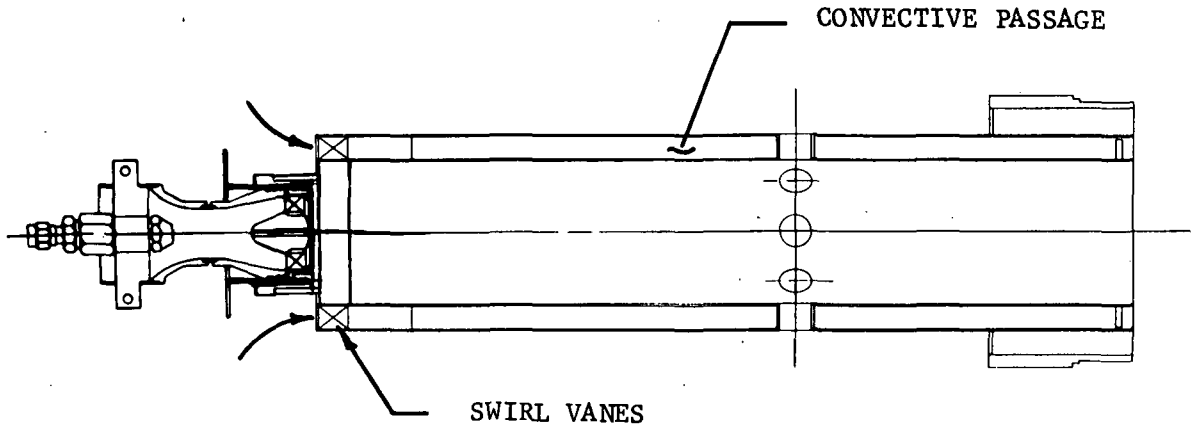

Figure 10. Liner Convective Cooling Scheme With Inlet Swirl for Increased Turbulence (Scheme 29-73A)

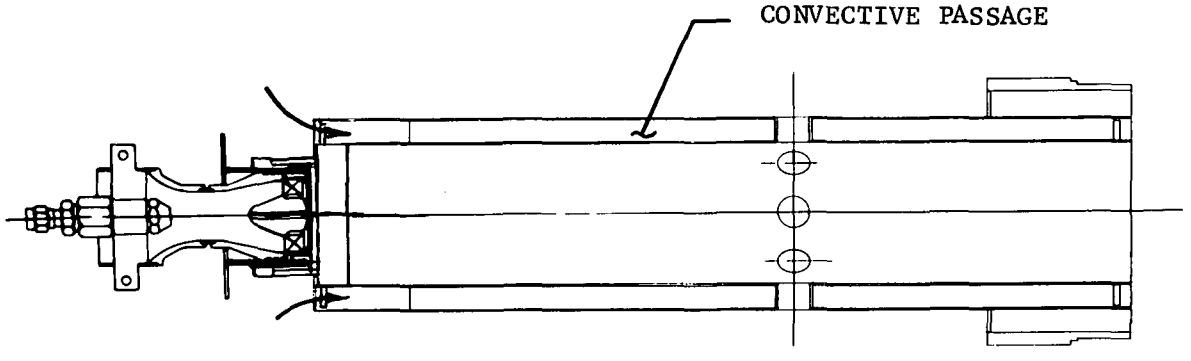

Figure 11. Liner Convective Cooling Scheme Nonswirling Case (Scheme 29-76A)

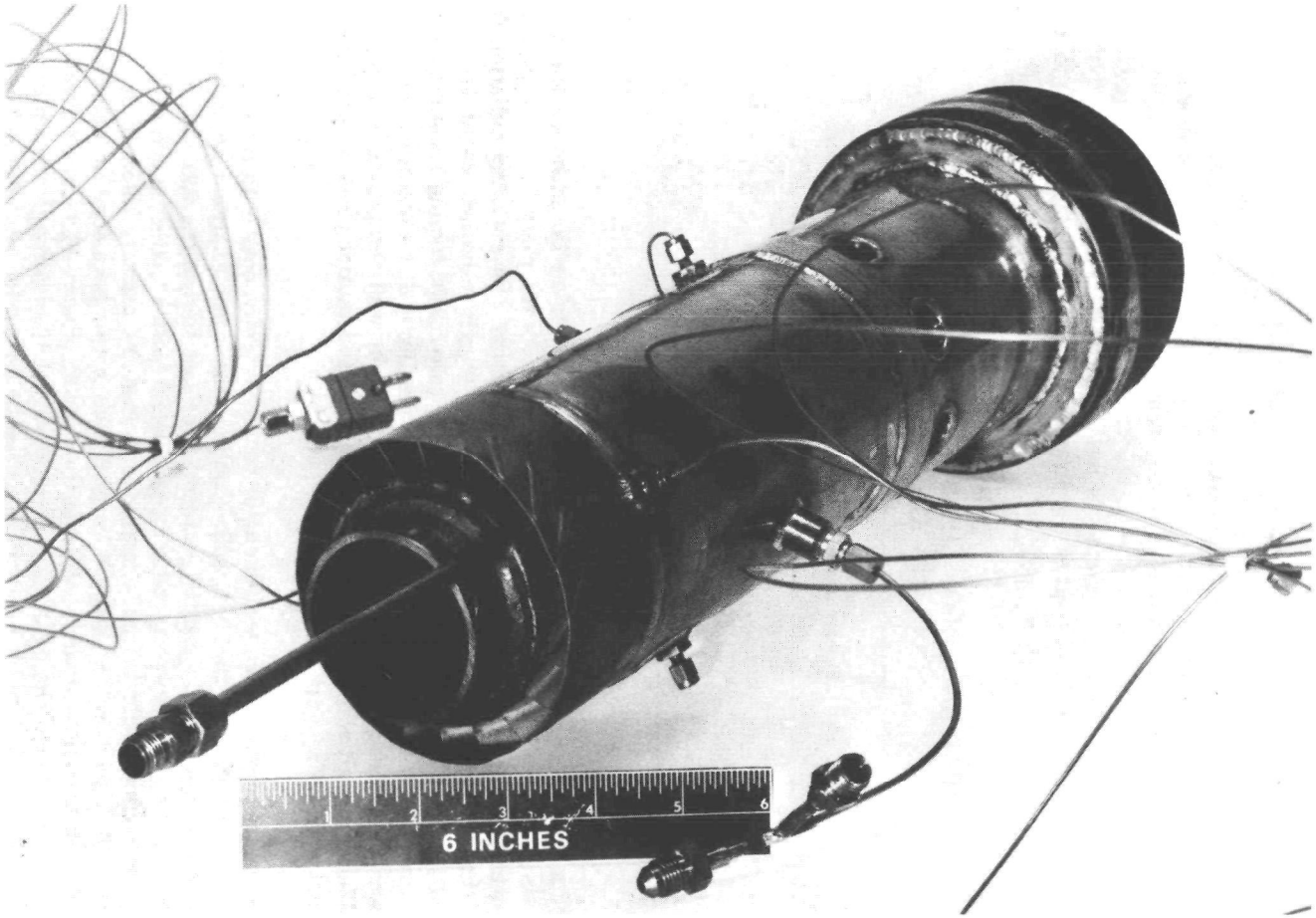

Figure 12. Bench-Scale Combustor Configuration Used in Heat-Transfer Model Verification

During testing with the nonswirl cooling scheme, five different cases were investigated to assess the effect of pressure, mass flow and inlet temperature, and to compare experimental data with data from the analytical model. Table II presents the five cases investigated and compares the experimental cooling flow with the calculated cooling flow predicted by the model. The cooling flow was determined experimentally with total and static pressure probes mounted in the cooling passage. Agreement between experimental and analytical values was within 10%. The inlet temperature effect on wall temperature is presented in Figure 13. The experimental wall temperatures were determined by averaging two wall thermocouples located 5 and 7 in. downstream from the dome. The two temperatures measured are believed to be indicative of the overall average liner temperature. Agreement between the model and the experimental data is very close. An increase in inlet temperature from 400° to 600°F roughly increased the maximum wall temperature (at an overall FA of 0.070) from 1300 to 1600°F.

TABLE II
COMPARISON OF MEASURED AND PREDICTED
COOLING AIR FLOWRATES*

				Cooling Air Flowrate	
Case	P_B *(psia)*	*Temperature (°F)*	*Liner Pressure Drop (pct)*	*Measured (pps)*	*Calculated (pps)*
1	50	600	2.2	0.80	0.78
2	100	600	1.4	1.36	1.26
3	50	600	4.8	1.19	1.17
4	50	600	6.0	1.29	1.31
5	500	400	4.6	1.31	1.27

The mass flow effect on wall temperature is shown in Figure 14. Although the agreement here is less satisfactory, the trends are believed accurate. As the mass flow was increased, the convection heat transfer was increased roughly in proportion. However, the radiation from the hot gas to the hot wall remained nearly the same. Since radiation accounts for a large percentage of the heat transferred into the wall, and convective cooling accounts for most of the heat removed from the hot wall, a trend of decreasing wall temperature with increasing mass flow was considered logical. The pressure effect on wall temperature is presented in Figure 15. The increased wall temperature due to increased burner pressure predicted by the model was not verified by experimental data.

A common technique for enhancement of cooling effectiveness is to increase the surface area on the cooling side of the hot wall. Cooling fins were analyzed to determine their effectiveness. Heat transfer calculations performed for cast fins on the cooled side of the inner liner indicated that a primary zone wall temperature of 1536°F could be achieved if 43.2% of the total burner airflow could be made available to cool the primary liner. In order to ensure that this relatively high percentage could be provided, it was necessary to make a revision to the "first-cut" configuration of the Full-Scale Combustor (Figure 8) to allow discharge of the primary cooling air through the quick-quench slots rather than through the sudden expansion dump farther downstream. This arrangement, shown in Figure 16, was adopted in combination with the cast-fin inner liner as the best available alternative for primary liner cooling.

*Refer to Appendix B for SI unit conversion

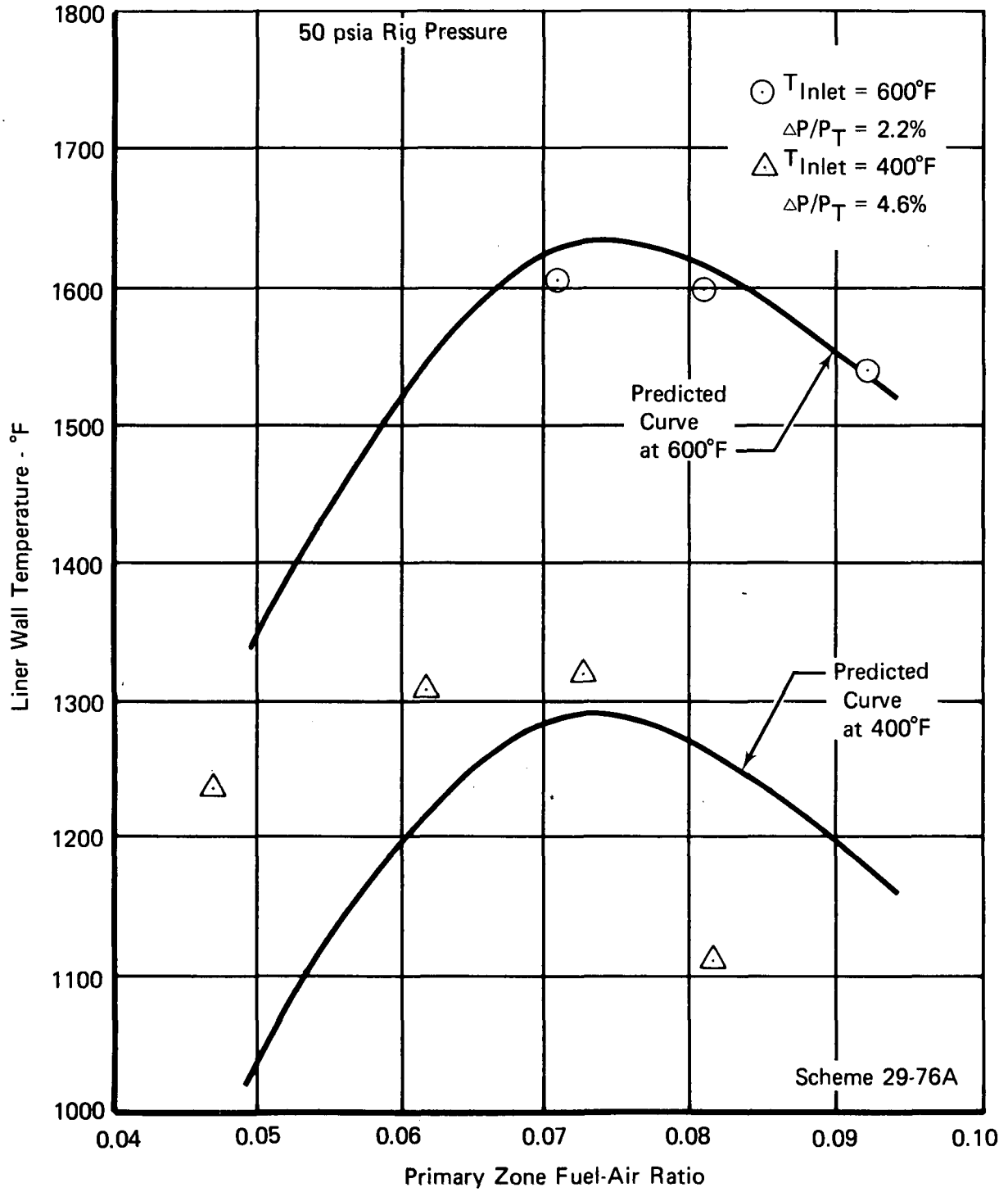

Figure 13. Variation in Measured and Predicted Liner Temperatures With Inlet Air Temperature and Fuel-Air Ratio (Bench-Scale Rig Data)

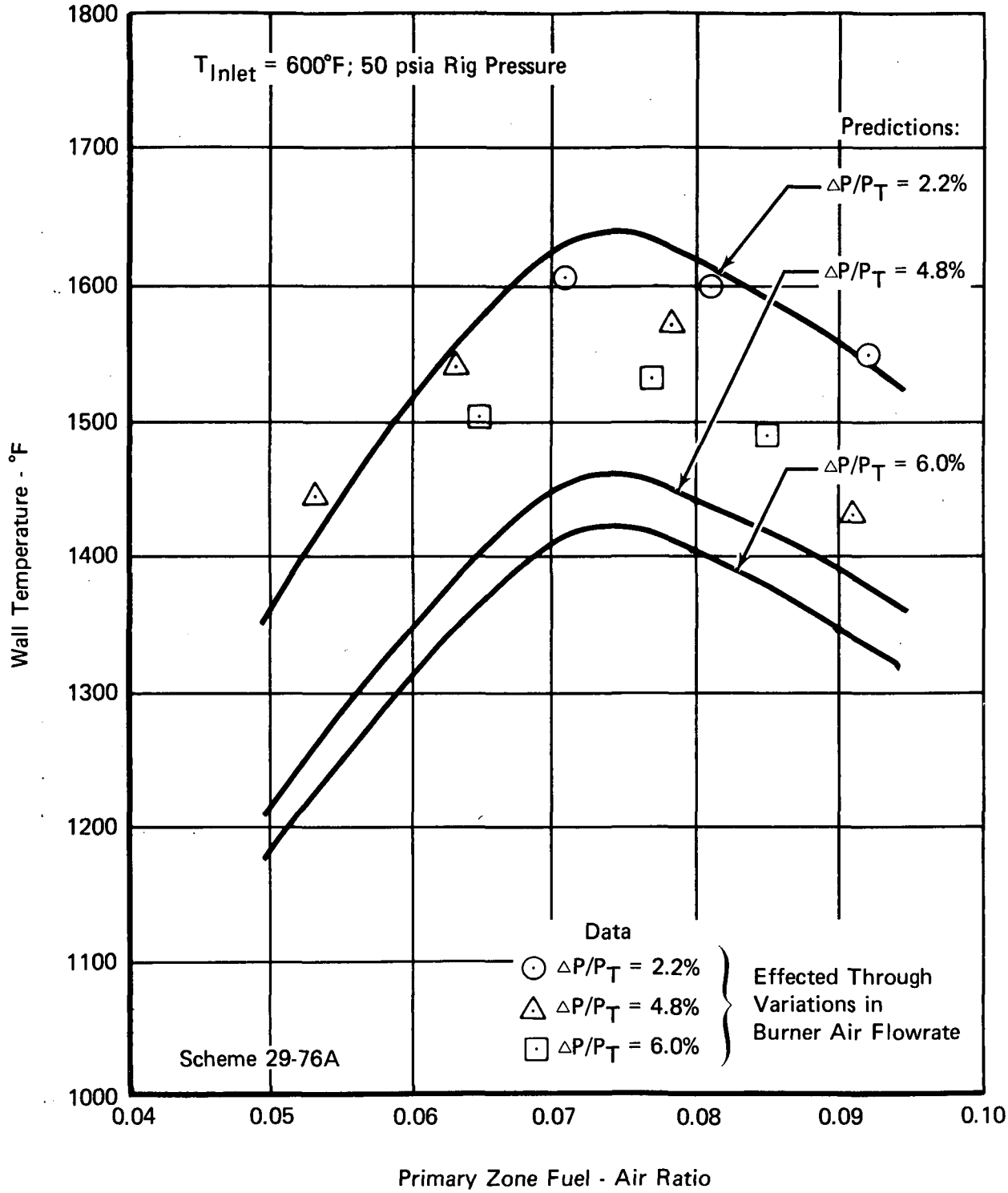

Figure 14. Variation in Measured and Predicted Liner Temperatures With Burner Air Flowrate and Fuel-Air Ratio (Bench-Scale Rig Data)

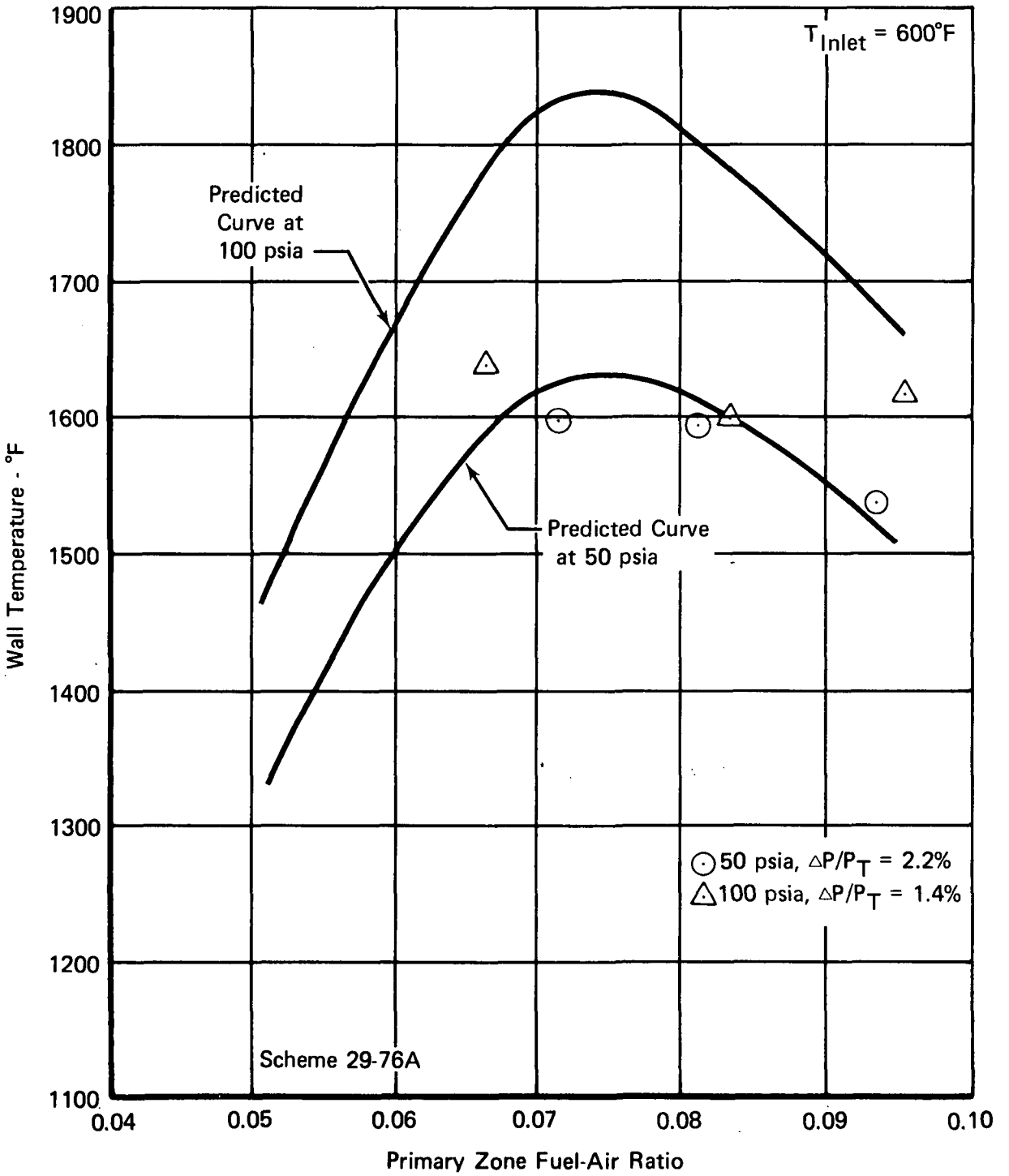

Figure 15. Variation in Measured and Predicted Liner Temperatures With Rig Pressure and Fuel-Air Ratio (Bench-Scale Rig Data)

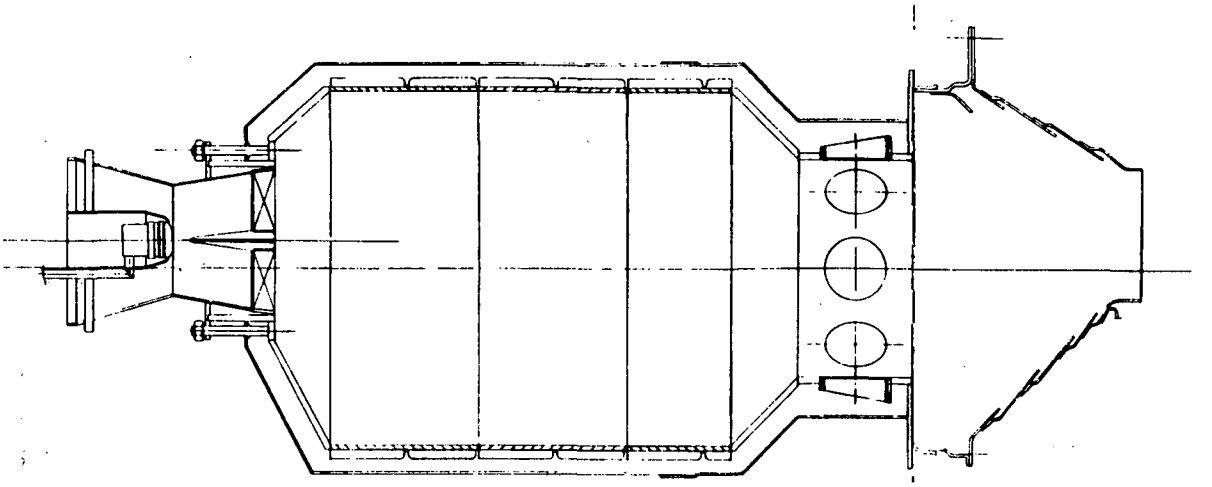

Figure 16. Final Configurations of the Full-Scale Prototype Combustor

2.6 RESIDENCE TIME CONSIDERATIONS

The "first-cut" configuration of the full-scale combustor represented a compromise solution to the problem of achieving low concentration levels of NO_x and CO within the limited length of a representative engine combustor compartment. The configuration allocated most of the available combustor length to the primary zone in the interest of achieving lower NO_x. It was understood that this arrangement might result in higher CO concentration levels because the rear section of the combustor had been radically truncated and the secondary zone had been combined with the engine transition piece.

A brief series of bench-scale rig tests was conducted to generate data showing the tradeoff between secondary zone length and CO concentration levels. The combustor configuration tested (Figure 17) provided full power-range primary airflow (20% of total), and had no dilution section except for the dump piece at the end of the slotted quick-quench section. Gas sample measurements were taken at the dump plane (2½ in. downstream of the slot centerline), and at a location in the exit duct (9½ in. downstream of the slot centerline). Data were already on hand for gas sample measurements taken at a far-downstream position (approximately 8 ft downstream of the combustor, where a "fully-mixed-out" sample was routinely measured).

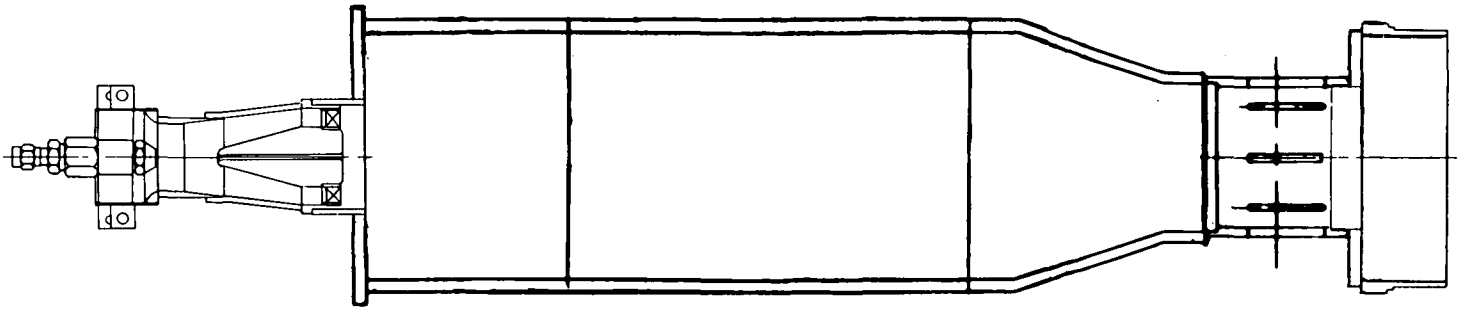

Figure 17. Bench-Scale Burner Configuration Used in Secondary Zone Length Studies (Scheme 29-77A)

The measurements taken at the dump plane showed very high CO concentration levels (above the 3000 ppmv maximum analyzer range), indicating that the oxidation of CO had only begun at this plane, as might be expected. The data recorded at the other locations are shown in Figure 18. There is clear evidence that the CO oxidation process is a gradual one, which has not been fully completed at the "upstream" sample location. By increasing the residence time (through a lowering of the reference velocity), a lower concentration level was achieved. However, this level still did not match the "fully-reacted" concentration level (approximately 8 ppmv) measured at the far-downstream probe.

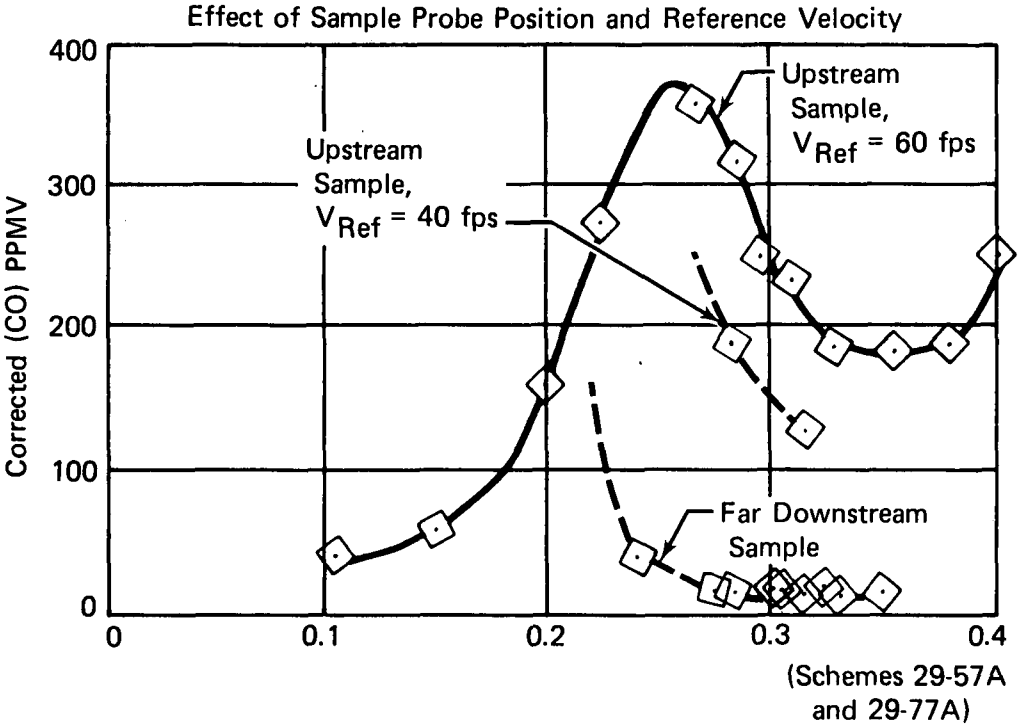

Figure 18. Carbon Monoxide Characteristics of Rich Burn/Quick Quench Combustor

These results indicated that the truncated dilution section of the "first-cut" engine-retrofit combustor configuration was too short for the completion of the CO oxidation process. This conclusion was in agreement with streamtube analytical model predictions, which indicated that a 10- to 15-in. length would be required to produce CO concentrations in the 10 ppmv range. The exact tradeoff between secondary zone length and CO concentration levels would, of course, have to be determined in rig tests of the full-scale combustor.

With regard to the design compromises involved in reducing the combustor overall length to conform to the available space within a representative engine combustion section envelope, it was decided to adopt the tradeoff incorporated in the "final" configuration shown in Figure 16. The very short length of this engine-compatible version (ECV) of the full-scale combustor was, however, viewed as an item of concern. In order to meet the reduced-length requirement, residence times in the primary zone and, in particular, in the dilution section had been decreased below the design-point values derived from bench-scale rig data. While these lower residence times might eventually prove to be adequate for achieving the program exhaust emission goals, a better demonstration of the basic Rich Burn/Quick Quench design concept could almost certainly be gained by conducting tests of a "stretched" configuration of the full-scale combustor. It was decided that a second configuration of the full-scale combustor hardware, of different overall length, should be assembled and tested. In addition to the engine-compatible version described (Figure 16), the full residence-time (FRT) configuration was designed as shown in Figure 19.

The FRT and ECV combustor configurations differed in two main areas: (1) primary zone length in the ECV was 12.5 in. compared to 18 in. in the FRT combustor; (2) a louver-cooled dilution piece was added just downstream of the quick-quench section in the FRT combustor, yielding an increase of 8 in. in the length of the secondary zone. It should be noted that, even though the FRT combustor provided an 18-in. long primary zone and an extended length secondary zone in comparison to the ECV combustor, neither configuration was an optimum design in terms of attainable NO_x emission levels. An increase in primary zone length beyond that provided in the FRT configuration may exhibit further reductions in NO_x emissions.

2.7 PRIMARY AIR STAGING

The bench-scale test results from Phase II had consistently shown that minimum NO_x concentration levels were achieved when the primary zone equivalence ratio was maintained near a value of 1.3. In order to achieve this value over a broad range of combustor exit plane equivalence ratios (engine power settings), a method of varying the amount of airflow admitted to the primary zone was required. At the baseload setting, slightly more than 20% of the total combustor airflow is called for in the primary zone; at idle, approximately 10% is required.

The method of primary air staging selected for the full-scale combustor is depicted in Figure 20. A variable damper, consisting of two sets of vanes (one movable, one fixed) was mounted at the inlet plane of the premix tube. The variable damper can be adjusted to achieve a 2:1 variation in premix tube airflow. At the full-open setting, only a nominal pressure drop (less than 0.1%) was incurred by airflow passing through the vanes. A large number of narrow vanes was employed to minimize wake formation in the incoming airflow. In going from the full-open to the full-restricted setting, the total damper travel required was only about 10 deg (or 0.25 in. at the maximum diameter).

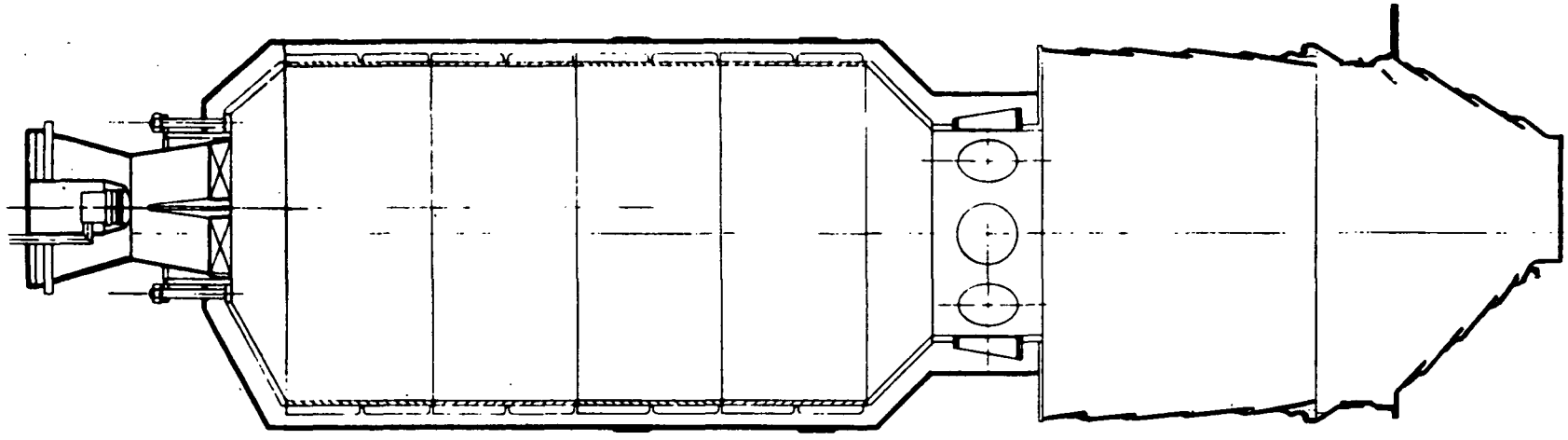

Figure 19. Final Residence Time Configuration of the Full-Scale Prototype Combustor

Figure 20. Premix Tube Variable Damper Mechanism

2.8 COMBUSTOR INTERNAL AERODYNAMICS

The combustor internal airflow distribution is determined by several factors, which include the relative areas of openings in the combustor liner, the pressure/velocity distribution of the approach airflow, and the combustor internal geometry (cross-sectional area as a function of length). The full-scale prototype combustor must meet a prescribed schedule of internal equivalence ratios, and, therefore, must be designed for a specific internal airflow distribution.

The Rich Burn/Quick Quench concept calls for a "necked-down" shape that produces locally high velocities in a quick-quench section for the purpose of vigorous mixing. An analysis of the effect of these high velocities on the combustor pressure drop and airflow distribution showed that significant "mixing losses" are incurred in the quick-quench section. These losses must be considered in tailoring the liner hole pattern to achieve the required airflow splits (these mixing losses are believed to be desirable and, in general, to be indicative of the high rate of mixing achieved in that section of the combustor).

To ensure an accurate determination of the liner hole areas required in the full-scale prototype combustor, a computer model was formulated to simulate the aerodynamic processes described above. The model accepts as input, a prescribed fractional airflow distribution, the inlet air temperature and pressure, the fuel flowrate, and the required liner pressure drop. The cross-sectional area profile of the combustor is also input, and an external pressure distribution may be specified. The calculation is performed in a downstream-marching fashion, beginning with an initial guess for the premix tube airflow in lb/sec. At each of several stations along the length of the burner, the pressure drops associated with various components and processes are computed. These pressure drops include the following: (1) premix tube entrance and blockage losses (both at the variable damper and at the fuel injector); (2) swirler pressure loss; (3) momentum pressure loss; (4) mixing loss in the quick-quench section; (5) mixing loss in the dilution zone. At the exit plane, a check is made on the overall pressure drop. If it agrees with the specified input value, the solution is complete. Otherwise, a new value for the premix tube airflow rate is assumed, and the computation is repeated. The final solution includes the total airflow that can be passed through the combustor for a given overall pressure drop and specified distribution, and the schedule of hole areas required to achieve that distribution.

Several cases were run with the aerodynamic model for the purpose of sizing the holes in the quick-quench section of the combustor and in the dilution zone. The results verified that a major source of combustor pressure drop is the "mixing loss" in the quick-quench section. The model computes as "mixing loss" the total pressure drop due to mass addition (from the one-dimensional momentum equation). In the quick-quench section, the mass added through the penetration holes is assumed to have zero axial velocity. This flow must be accelerated, along with the approach flow from the primary zone, to a uniform axial velocity consistent with the cross-sectional area of the "necked-down" (quick-quench) section of the burner. The smaller the diameter of the "necked-down" section, the greater the required acceleration, and the greater the resultant total pressure drop.

The full-scale prototype combustor design called for a 6-in. dia quick-quench section (in conjunction with a 10-in. dia primary zone section). The pressure drop incurred in this section was substantial, according to the aerodynamic model. In order to pass the quantity of airflow required in a representative engine, the model predicted that an overall combustor pressure drop of 5.5% would be required. At the combustor design-point pressure drop of 3%, calculations indicated that only 66% of the design-point airflow would pass through the combustor. The controlling factor in these results was the "mixing loss" incurred in the quick-quench section of the combustor. This section has a throttling effect on the combustor flowrate. The higher the axial velocity in the "necked-down" passage (i.e., the smaller the diameter), the lower the quantity of airflow (from both primary and quick-quench sources) that can pass through that section without an increase in burner pressure drop.

To illustrate the results described, four of the cases run with the aerodynamic model have been summarized and are presented in Table III through Table VI. In Table III, predictions for the prototype combustor operating at 3% pressure drop and at a baseload power setting are shown. The data include computed flow properties at selected stations along the length of the combustor. The stations are identified in Figure 21. It may be seen from the tables that there is a progressive decline in total pressure caused by the losses incurred at the various stations. Table III and Table IV show cases for 3% pressure drop, (at idle it was assumed that the premix tube damper is adjusted to provide higher blockage). Table V and Table VI show cases for 5.5% pressure drop. Note that the total airflow passed by the combustor at 3% pressure drop, as shown in Table III (22 pps), is only about two-thirds the amount required (31 pps) in a representative engine test. On the other hand, the amount passed at 5.5% pressure drop (29.7 pps) closely approaches the requirement.

The predicted results were verified experimentally in tests of the bench-scale combustor, as shown in Figure 22. Good agreement with the experimental data was demonstrated. The predictions indicated that the selected diameter of the quick-quench section (6-in.) was too small to pass the airflow required in an engine-compatible design. If ultimately substantiated by test results, these results would dictate an increase in the diameter of the quick-quench section. Calculations performed using the model also indicated that an increase in diameter to 8 in. would be required to provide full design-point airflow at 3% pressure drop. There was another alternative as well. Full design-point airflow could be achieved using the selected geometry if a pressure drop of 5.5% was available. This value coincides with the total combustion system pressure drop (diffuser plus combustor) of the representative engine. By placing ram scoops at the entrance to the primary liner cooling passage (which carries airflow to the quick-quench slots), and by positioning the premix tube to capture high-velocity air at the diffuser dump plane, it was reasoned that recovery of most of the compressor-exit total pressure might be achieved, thereby making available to the primary and secondary zones of the combustor a pressure drop nearly equal to the 5.5% value required.

TABLE III.
AERODYNAMIC MODEL CALCULATIONS FOR FULL-SCALE PROTOTYPE COMBUSTOR*

- Configuration for 3% Pressure Drop
- Baseload Power Setting (Damper Open)

Station	*1*	*2*	*3*	*4*	*5*	*6*	*7*	*8*
Wa(cum) — pps	4.50	4.50	4.50	4.50	4.50	13.60	13.60	22.064
Equivalent ratio (local)	0.0	1.300	1.300	1.300	1.300	0.430	0.430	0.265
T_t — °F	722	722	722	3686	3686	2494	2494	1878
P_S — psia	187.61	186.63	186.85	186.77	186.32	180.99	182.39	179.14
P_T — psia	188.00	187.41	186.95	186.85	186.85	184.14	182.74	182.36
Velocity — fps	91.7	121.7	46.7	78.5	202.2	420.1	139.2	377.5
Mach No.	0.055	0.073	0.028	0.026	0.067	0.163	0.054	0.164

TABLE IV.
AERODYNAMIC MODEL CALCULATIONS FOR FULL-SCALE PROTOTYPE COMBUSTOR*

- Configuration for 3% Pressure Drop
- Idle Power Setting (Damper at Minimum Setting)

Station	*1*	*2*	*3*	*4*	*5*	*6*	*7*	*8*
Wa(cum) — pps	0.5558	0.5558	0.5558	0.5558	0.5558	3.286	3.286	5.536
Equivalent ratio (local)	0.0	1.300	1.300	1.300	1.300	0.220	0.220	0.131
T_t — °F	285	285	285	3406	3406	1318	1318	921
P_S — psia	39.98	39.58	39.59	39.58	39.55	38.58	38.81	38.24
P_T — psia	40.00	39.61	39.59	39.58	39.58	39.10	38.87	38.80
Velocity — fps	33.5	44.2	17.4	38.2	102.8	285.6	97.1	262.1
Mach No.	0.025	0.033	0.013	0.013	0.034	0.141	0.048	0.146

*Refer to Appendix B for SI unit conversion

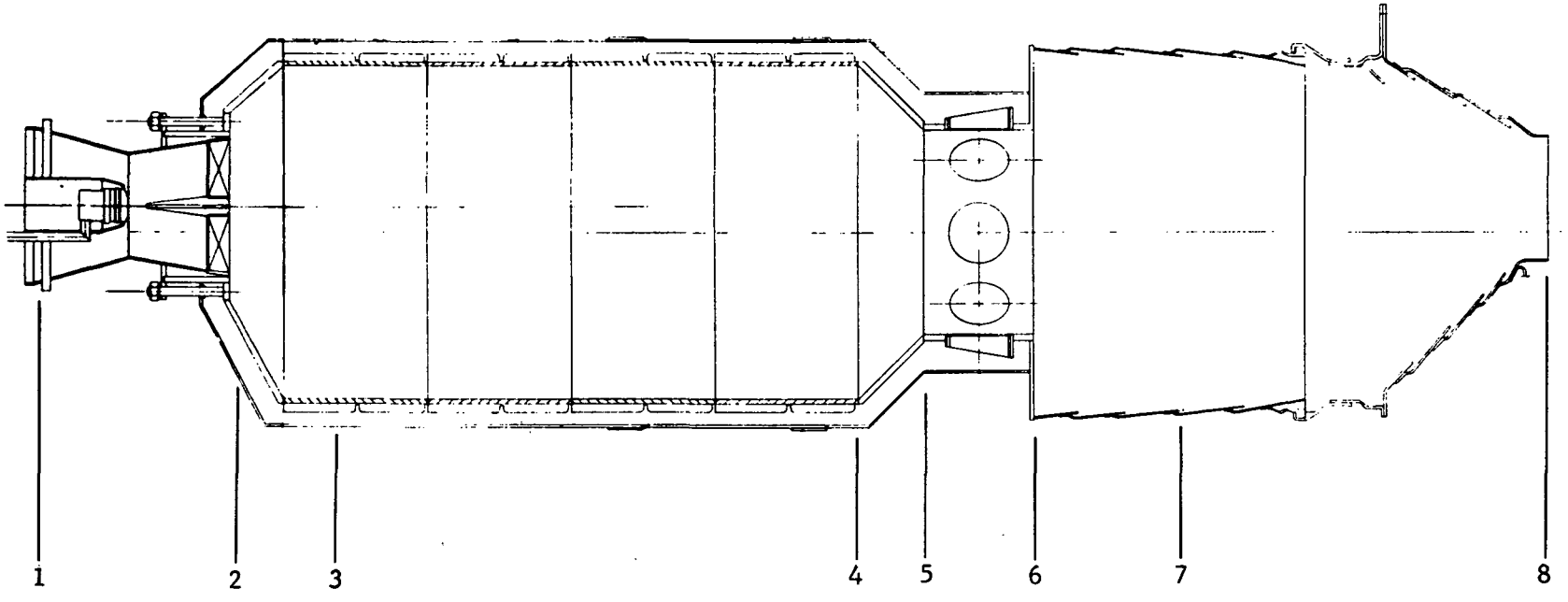

Figure 21. Identification of Stations Referred to in the Aerodynamic Model Calculations

TABLE VI.
AERODYNAMIC MODEL CALCULATIONS FOR FULL-SCALE PROTOTYPE COMBUSTOR*

- Configuration for 5.5% Pressure Drop
- Idle Power Setting (Damper at Minimum Setting)

Station	*1*	*2*	*3*	*4*	*5*	*6*	*7*	*8*
Wa(cum) — pps	0.7394	0.7394	0.7394	0.7394	0.7394	4.3794	4.3794	7.4494
Equivalent ratio (local)	0.0	1.300	1.300	1.300	1.300	0.219	0.219	0.129
T_t — °F	285	285	285	3406	3406	1317	1317	914
P_S — psia	39.97	39.23	39.24	39.23	39.18	37.40	37.83	36.76
P_T — psia	40.00	39.29	39.25	39.24	39.24	38.36	37.93	37.80
Velocity — fps	44.2	58.9	22.7	52.9	141.0	392.2	129.4	363.6
Mach No.	0.033	0.044	0.017	0.018	0.048	0.194	0.064	0.203

TABLE V.
AERODYNAMIC MODEL CALCULATIONS FOR FULL-SCALE PROTOTYPE COMBUSTOR*

- Configuration for 5.5% Pressure Drop
- Baseload Power Setting (Damper Open)

Station	*1*	*2*	*3*	*4*	*5*	*6*	*7*	*8*
Wa(cum) — pps	6.035	6.035	6.035	6.035	6.035	18.105	18.105	29.658
Equivalent ratio (local)	0.0	1.300	1.300	1.300	1.300	0.433	0.433	0.265
T_t — °F	722	722	722	3686	3686	2505	2505	1875
P_S — psia	187.30	185.72	185.94	185.78	184.97	175.15	177.74	171.71
P_T — psia	188.00	186.94	186.12	185.93	185.93	180.98	178.38	177.66
Velocity — fps	123.4	163.4	61.7	108.7	271.6	578.4	191.1	524.4
Mach No.	0.074	0.098	0.037	0.036	0.090	0.224	0.074	0.228

*Refer to Appendix B for SI unit conversion

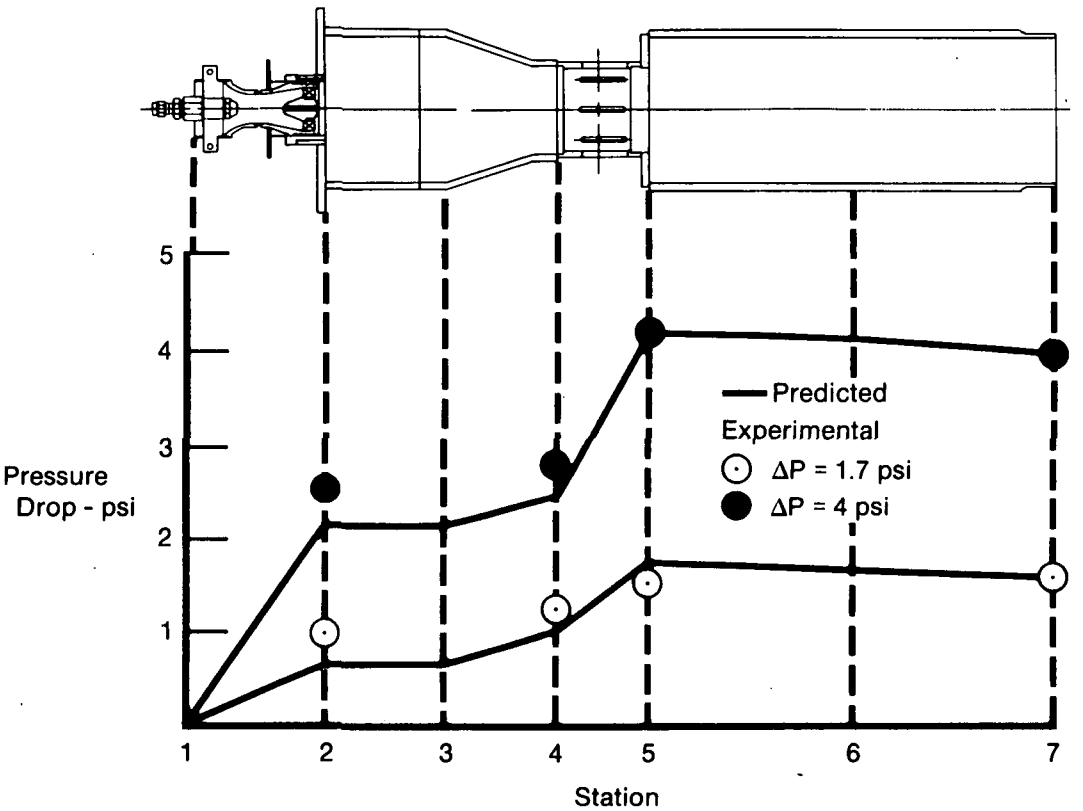

Figure 22. Comparison of Predicted and Experimental Pressure Drop Characteristics of the Bench-Scale Combustor

2.9 PREMIX TUBE

Good fuel preparation (effective prevaporization and premixing) is important in the design of the full-scale combustor. If the airflow entering the primary zone has not been sufficiently admixed with fuel to form a reasonably homogeneous mixture, it is possible that diffusion burning could take place between the incoming air and the droplets or localized pockets of fuel-rich gases already present. Because diffusion burning proceeds at near-peak flame temperatures, it is the authors' opinion that significant concentration levels of NO_x could be formed in the primary zone under these circumstances. Such levels may not be reduced to molecular nitrogen later in the combustion process.

In order to provide uniform premixing (and prevaporization) of the fuel and air that are introduced into the primary zone, a number of candidate designs for the full-scale premix tube were proposed and evaluated (both analytically and experimentally) during the Phase III design effort. In the course of these evaluations, a considerable body of design data was gathered. These data were assembled to form a premix tube design system. In this section, a brief description of the design system is presented. Several of the premix tube designs described in the discussions of the design system were evaluated in tests of the full-scale combustor, and will be described further in Section 3.

2.9.1 Atomization

Atomization of the liquid fuel and optimization of droplet sizes is important for two reasons. First, fuel vaporization is dependent on fuel drop size; the smaller the fuel droplet, the faster it vaporizes. Because vaporization is usually one of the attainable goals of a premix system, atomization determines the premixing length required for vaporization. Second, even if complete vaporization is not attained, it can be expected that very small droplets ($< 20\mu m$) will behave like vapor in the combustion process as vaporization of a small droplet occurs nearly instantaneously as it approaches the flame-front. Thus, small premixed fuel droplets in air can approach the performance of a perfectly premixed, prevaporized system.

Of the various atomization techniques available, air atomization has perhaps the greatest potential for producing fine droplets in premix tubes. In order to optimize air atomization, three general directions of fuel injection or combinations thereof can be used:

1. Downstream axial injection (low fuel velocities)
2. Upstream axial injection
3. Cross-stream (radial or tangential) fuel injection.

All these types of injection provide a high relative velocity between the fuel and air, thus promoting good atomization.

The empirical correlation for droplet size that follows was derived from References 3-12, which include theoretical analyses and experimental data for liquid jets, sheets and droplets. The correlation has the form:

$$SMD = K(d_f)^a(\nu_f)^b(\sigma_f)^c(\rho_f)^d(\rho_a)^e(V_a)^f$$

where K, a, b, c, d, e, and f are constants.

The correlation is a function of the following variables:

- ν_f — viscosity of fuel
- σ_f — surface tension of fuel
- ρ_f — density of fuel
- ρ_a — density of air
- V_a — velocity of air (relative to fuel)
- d_f — characteristic initial dimension of fuel (diameter, thickness, etc.); in this case, d_f was taken as the diameter of the fuel orifice corrected for the discharge coefficient (about 0.6).
- $\frac{W_a}{W_f}$ — atomizing airflow to fuel flow ratio.

In the references cited, other parameters have been shown to have a negligible influence on the Sauter Mean Diameter (SMD).

The last parameter, W_a/W_f, is a droplet interference and interaction term that can, under certain circumstances, be eliminated from the list. If all of the airflow passing through the premix tube is used in the atomization process, the air-to-fuel ratio can be expected to range from about 10 in fuel-rich premix tubes ($\phi = 1.3$) to about 20 in fuel-lean premix tubes. It has been shown (Reference 3) that for values greater than five, the air-to-fuel ratio does not play a significant role in the atomization process. In the design of full-scale combustor hardware, the term W_a/W_f was eliminated from the equation.

Table VII gives a list of the exponents a through f from the various references. In reviewing the references, it was apparent that some of the constants were remarkably consistent (particularly b, c, and f) while others varied. By the use of dimensional analysis, three exponents can be calculated from three selected exponents. The following equation was derived:

$$SMD = K(d_f)^{0.375}(\nu_f)^{0.25}(\sigma_f)^{0.375}(\rho_f)^{-0.125}(\rho_a)^{-0.5}(V_a)^{-1.0} \quad (1)$$

TABLE VII.
THE EFFECT OF IMPORTANT PARAMETERS
ON DROPLET SIZE *

Drop	*a*	*b*	*c*	*d*	*e*	*f*	*Reference*
$2\bar{r}$	0.5	0.33	0.16	−0.16	−0.33	−0.66	3
$2\bar{r}$	—	0.66	0.33	−0.33	−0.66	−1.33	3
$2\bar{r}$	0.5	0.25	0.25	−0.25	−0.25	−0.75	4
MMD	0.16	0.34	0.41	−0.84	—	−1.33	5
$2\bar{r}$	—	—	0.50	−0.5	—	−1.0	6
$2\bar{r}$	0.375	0.25	0.375	−0.375	−0.25	−0.75	7
SMD	—	—	0.33	−0.37	−0.3	−1.0	8
SMD	0.375	0.25	0.375	0.25	−0.875	−1.0	2
SMD	—	—	—	—	—	−0.75	9
$2\bar{r}$	—	—	0.33	−0.16	−0.16	−0.66	10
$2\bar{r}$	0.166	0.333	0.50	−0.125	−0.66	−1.33	11
SMD	0.375	0.25	0.375	−0.125	−0.5	−1.0	

$$SMD = K(d_f)^a(\nu_f)^b(\sigma_f)^c(\rho_f)^d(\rho_a)^e(V_a)^f$$

The proportionality constant K was determined to be 48 in Reference 8. Equation (1) allows the designer to predict actual SMD values, provided that the value of d_f is known. Also, equation (1) allows the designer to evaluate the effects of changing pertinent parameters. It should be noted that air velocity is the single most important parameter in the atomization of a liquid fuel. As a typical example, an air velocity of 400 fps at ambient pressure is predicted to shatter a thin kerosene jet (0.062 in.) into droplets with a SMD of 16 μm.

*Refer to Appendix B for SI unit conversion

2.9.2 Distribution

In addition to atomization, the proper distribution of fuel in a premix tube must be achieved. Poor fuel distribution results in incomplete atomization due to droplet interaction effects, slower vaporization, and mixture nonuniformity. If a premix system is properly optimized, the fuel must be uniformly distributed throughout the airstream by the time the mixture enters the main combustor.

In tests of smaller bench-scale premix tubes (1-in. dia), experience has shown that centrally mounted pressure-atomizing fuel nozzles are capable of properly distributing the fuel. In tests of larger, full-scale premix tubes (3-in. dia), two techniques appear to offer potential for a uniform fuel distribution. First, a centrally mounted injector can be used in combination with an inlet-plane mixing device such as a swirler. An example of this type of fuel distribution system is shown in Figure 23. The swirling airstream produced by preswirl vanes centrifuges larger droplets outboard and transports smaller droplets by turbulence. Care must be exercised in the design of this type distribution system both, in the avoidance of reverse flow zones and the avoidance of excessive wall wetting by the fuel. Second, multiple injection sources can be used with or without mixing devices. Figure 24 shows two premix tubes using multiple injectors, one with and one without a mixing device.

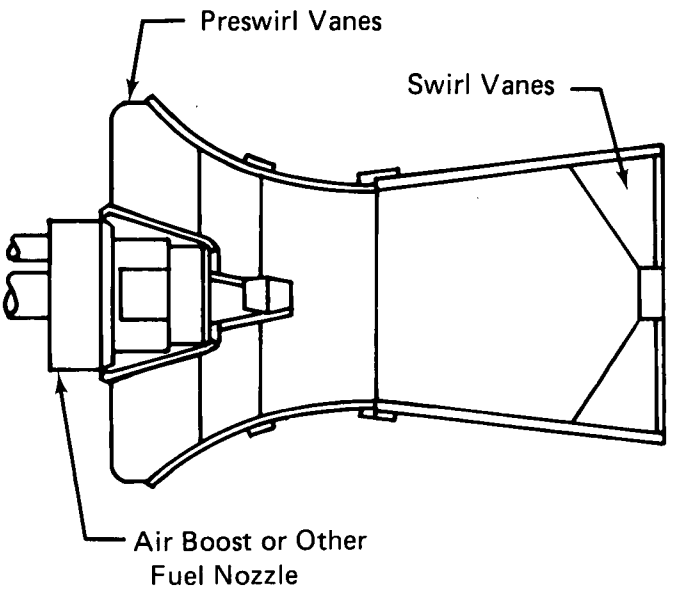

Figure 23. A Typical Centrally-Mounted Fuel Injector With a Mixing Device

Simple radial fuel injectors mounted on the wall of a cylindrical premix tube can also be employed. This approach offers the advantage of providing a uniform fuel distribution without the complexity of a mixing device. Radial injection also eliminates all internal blockage and provides a "clean" premix tube design. However, the provisions for fuel penetration must be carefully determined to properly distribute the fuel without excessive wall wetting. Designs of this type can be undertaken using the three penetration design curves for radial fuel injection from References 13, 14 and 15. These are shown to be in fairly good agreement in Figure 25. Data from Reference 5 are also plotted in Figure 25.

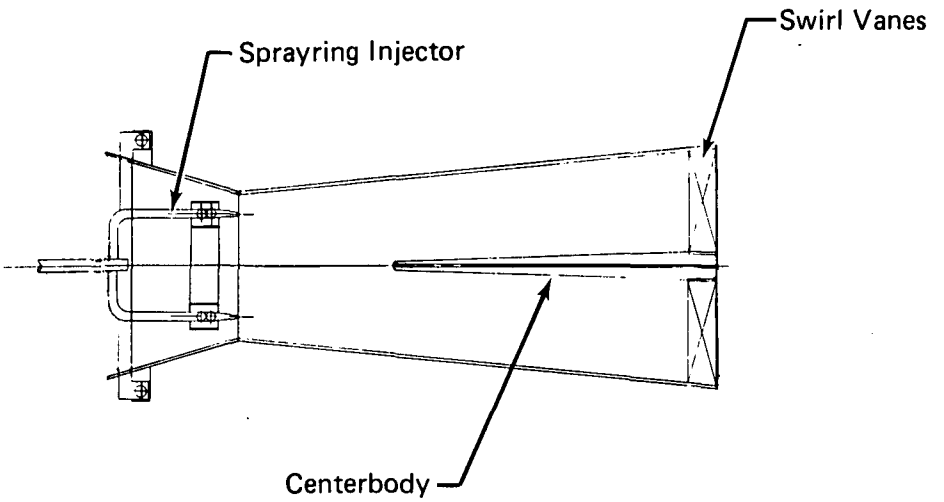

(a) Without Mixing Device

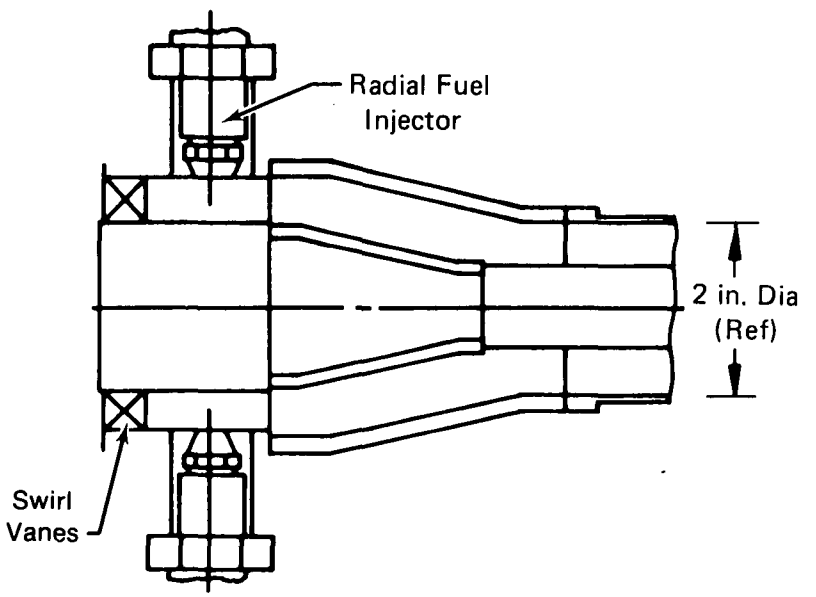

(b) With Mixing Device (Preswirl Vanes)

Figure 24. Representative Multiple Fuel Injector Premix Tubes

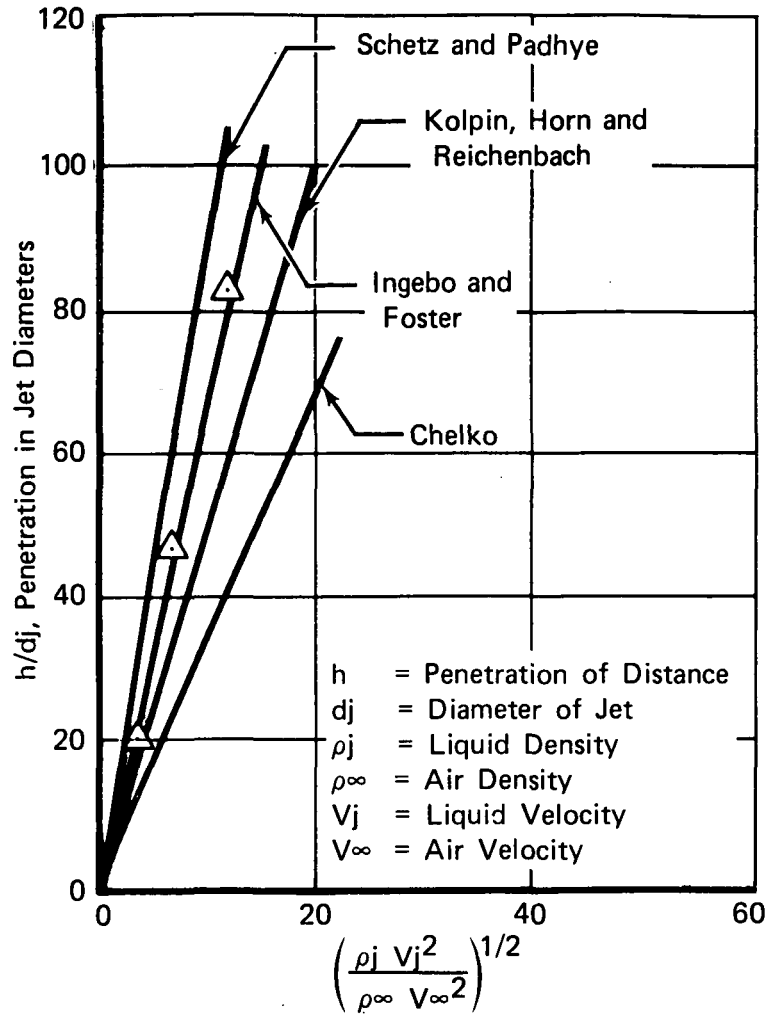

Figure 25. Liquid Jet Penetration in Airstream

A promising candidate design for optimum fuel distribution was the radial "spoke" design shown in Figure 26. Each spoke has multiple orifice injectors which tangentially feed the fuel into the airstream. The injection system shown has 12 spokes and 36 individual orifices spaced on an equal area basis. Reference 16 employed a similar fuel injection system and obtained excellent premixing results. This design was evaluated extensively in tests of the full-scale combustor described in Section 4.

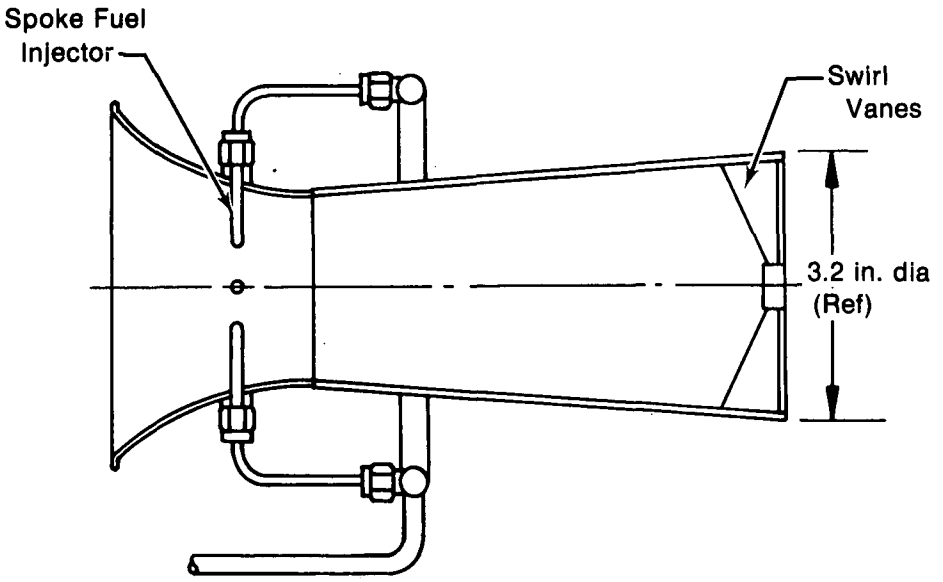

Figure 26. Radial "Spoke" Premix Tube Design

2.9.3 Pressure Loss

In order to design a premix tube that passes the desired airflow and meets the requirement for overall combustor pressure drop, an assessment was made of the pressure losses of the various parts of the premix tube. Three major sources of pressure loss were identified in premix tubes of the design shown in Figure 26: internal blockage loss, diffuser boundary layer loss, and swirler dump loss.

In sizing the premix tubes used in this program, internal blockage loss was calculated from the one-dimensional momentum equation. Diffuser boundary layer loss was calculated from diffuser pressure recovery maps available in the literature. Swirler dump loss was calculated from the one-dimensional equation of motion assuming a one-dynamic head loss based on the discharge area of the swirler. By summing the losses of the various components and iterating to a specific overall loss, the required "size" of the premix tube was determined.

2.9.4 Candidate Premix Tube Designs

The premix tube design system described was compared to the results of previous development activity, both in-house and that reported in the literature, involving many alternative premix tube configurations. Designs incorporating various fuel injectors (centrally-mounted, wall-mounted, spray bars, air-boost, air-blast, and pressure-atomizing), various flameholding devices (inlet and exit swirlers, bluff bodies), and various provisions for fuel-spreading (inlet swirl, vortex generators, and multiple-point sources) were represented in the background data. It was found that while the design system outlines the principles and techniques that should be employed in the execution of various designs, it does not provide a means of selecting a specific combination of design features from the many alternatives available.

To ensure that a combination of features best suited for the particular application intended are selected, it is essential that candidate premix tube designs be evaluated experimentally. Ideally, a number of alternative configurations are selected for evaluation in component tests prior to the actual mating of the premix tube to the combustor. In these tests, the predicted performance of the designs can be verified, and a basis of demonstrated performance can be established for selecting design features.

A number of alternative configurations for the premix tube of the full-scale combustor were selected and evaluated experimentally as part of the design effort. In Section 4, the chronological development of this component verification activity is documented. Among the designs subsequently built and tested, are those depicted in Figures 23, 24 and 26. The premix tubes, shown in Figures 16 and 19 in conjunction with the ECV and FRT combustor designs, were the initial configurations proposed. The approach taken (experimental verification of a number of proposed designs) ultimately produced a superior premix tube design, and provided a means for identifying and correcting deficiencies in the configurations initially proposed.

2.10 CONSTRUCTION OF THE FULL-SCALE COMBUSTOR AND RIG HARDWARE

The purpose of the Verification Testing planned in Phase IV was to ensure proper implementation of the Rich Burn/Quick Quench concept in full-scale burner hardware, and to demonstrate (at intermediate pressure and under ideal air-feed conditions) a level of performance consistent with program goals for exhaust emissions and conventional performance requirements. The full-scale combustor hardware was constructed to facilitate the modifications that were anticipated during the test program. Bench-scale parametric data had indicated that combustor residence times in excess of those available in current in-line engine combustors might be required if very low concentration levels of CO and NO_x were to be achieved. Therefore, the combustor hardware was constructed in such a manner that two configurations of different overall length could be assembled and tested. The primary liner was made up of 4-in. long cast liner sections that could be welded together to form any desired total length. Tests of both an engine-length combustor (the ECV configuration) and an extended-length combustor (the FRT configuration) were planned. Modifications to the configuration of the premix tube in the course of the test program were also anticipated, because of the difficult design requirements for this component. A modular approach was adopted allowing the premix tube and fuel injectors to be bolted to the combustor as a unit.

The final layout drawing of the FRT combustor prior to the start of the verification test program is shown in Figure 27. The ram scoop shown at the entrance to the primary liner cooling passage (which carries airflow to the quick-quench slots) was added as a means of recovering a greater fraction of compressor-exit total pressure. This technique, in conjunction with good premixing tube pressure-recovery characteristics, would provide an effective combustor pressure drop of nearly 5.5%. As discussed in Section 2.8, analytical model predictions had indicated that a pressure drop on that order would be required to overcome mixing losses in the quick-quench section of the prototype combustor.

The design features of the full-scale (FRT) combustor are summarized in Table VIII. A photograph of the FRT combustor during construction is shown in Figure 28. The premixing tube and primary liner shroud were not attached in this figure. The fully-assembled configuration is shown in Figure 29, except for the premixing tube damper mechanism. A view of the damper is shown in Figure 20. The ECV configuration of the full-scale combustor, which was constructed by modifying the FRT combustor hardware, is described in Section 3.10.

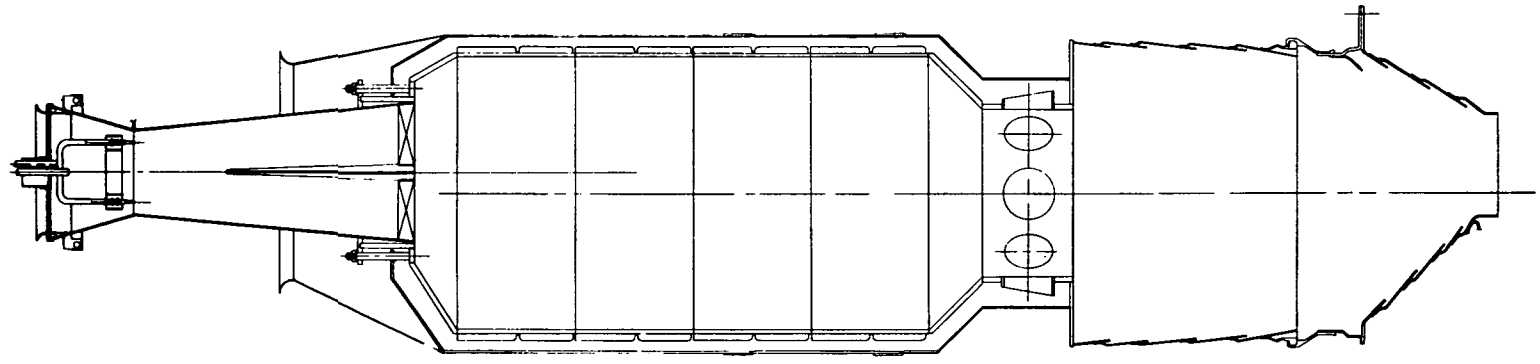

Figure 27. Final Layout of the Full Residence Time (FRT) Configuration of the Full-Scale Combustor Prior to the Verification Test Program

TABLE VIII
SUMMARY OF FULL RESIDENCE TIME (FRT) COMBUSTOR DESIGN FEATURES*

Type Combustor	Combustor Can, Convective Primary Zone Cooling, Film Dilution Zone Cooling
Length (Primary)	19.0 in.
Length (Dilution)	8.0 in.
Length (Overall)	45.0 in.
Outer Diameter	11.25 in.
Inner Diameter	9.8 in.
Combustor Reference Area (Primary)	75.4 in. sq
Type Nozzle	Dual sprayring with 16 holes (0.030 dia)
Swirler	4.874 in. OD, 0.56 in. ID, 20 vanes with centerbody
Combustor Material	
Outer Liner	Type 347 SST
Inner Liner	Stellite 31 (X40)
Combustor Wall Thickness	
Outer Liner	0.0625 in.
Inner Liner	0.125 in. on dia with 0.125 high fins
Design Point Conditions	
Fuel-Air Ratio	0.0189
Volumetric Heat Release Rate Based on:	2.05×10^6 Btu/(ft^3-hr-atm)
Inlet Pressure	188 psia
Combustor Airflow	31.5 lb/s
Combustor Reference Velocity (PrimaJry)	29.0 f/s
Combustor Total Pressure Loss	5.5%

*Refer to Appendix B for SI unit conversion

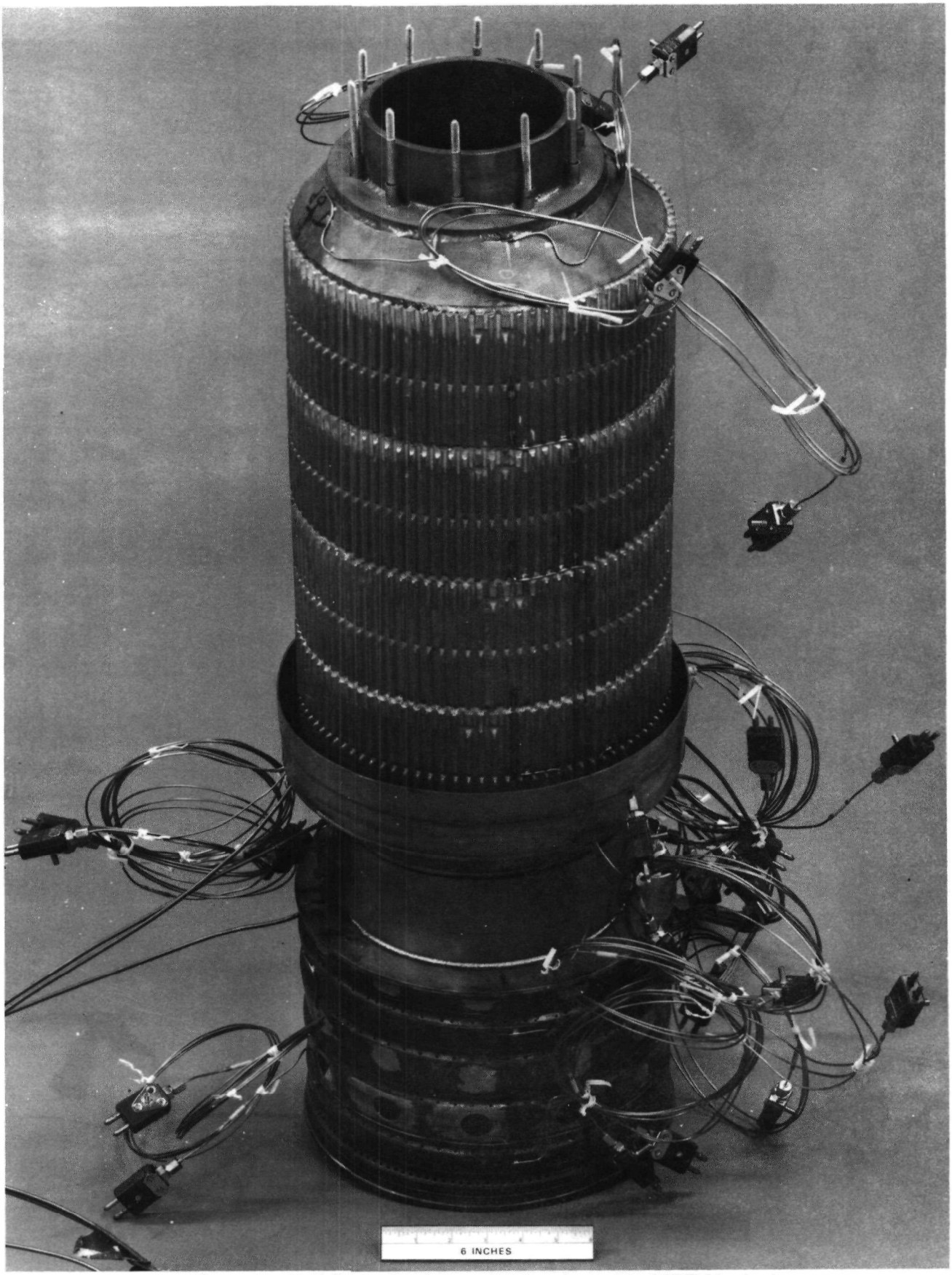

Figure 28. Full-Scale Combustor During Assembly (FRT Version)

*Figure 29. Full-Scale Combustor Fully Assembled (**FRT Version**)*

2.10.1 Experimental Rig Hardware and Test Stand Preparation

A layout diagram of the combustor test rig is presented in Figure 30. The combustor was mounted in a large-diameter cylindrical duct or plenum case and fitted to a sector-annular exit transition liner. Exhaust flow from the combustor was discharged through the transition liner into a traverse case, which contains a moveable probe with gas sample, temperature and pressure instrumentation. Downstream of the traverse case, an exit transition duct was provided, with a viewing port for monitoring the burner during intermediate-pressure testing. A remotely operated backpressure valve was located in the exhaust duct to permit various operating pressure levels to be set.

A continuous mixed-out gas sample was abstracted from the rig exhaust stream at a location approximately six feet from the exit plane of the combustor. The abstraction of gas samples was also provided for through the exit traverse probe.

Rig instrumentation was provided to measure pertinent airflow rates, the pressure and temperature of the inlet air, the combustor pressure drop, the exit temperature pattern, wall temperatures, wall static pressures, the fuel flowrate, as well as combustor exhaust emissions. A schematic diagram of rig instrumentation is shown in Figure 31. A venturi meter was provided for the total rig inlet airflow, covering a range from 5 to 25 pps with measurement uncertainties of $\pm 0.5\%$. Combustor inlet total temperatures and pressures are measured in the inlet plenum at near-stagnation conditions. Three shielded chromel/alumel thermocouples and three static pressure ports are provided. The thermocouple readings have associated uncertainties of $\pm 0.7\%$ including test stand circuitry. Fuel flowrates were measured by turbine-type flow transducers and were displayed on digital voltmeter readouts. Total uncertainty for these instruments is $\pm 0.5\%$. Rotameters were provided in the lines for approximate readings used in setting test-point conditions.

Combustor exit total temperature and total pressure measurements, along with continuous gas sampling for emission analysis, were taken with the traverse probe shown in Figure 30. Nine platinum/platinum-rhodium thermocouples were equally spaced between ten sample ports on the traverse probe. For exit total pressure measurement, the gas sample line was closed and a pressure transducer was used to measure the pressure. The gas sample traverse probe was air-cooled to maintain a proper sample temperature.

The analysis of gaseous emissions from the combustor was accomplished using the system shown in Figure 32. The gas sample was cooled in the probe to approximately 300°F, thereby quenching high-temperature oxidation reactions, but maintaining an amount of heat adequate to prevent the loss of unburned hydrocarbons by condensation. The gas sample was conducted through an electrically heated transfer line to the gas-sample analysis system. The sample transfer time was less than 2 sec. Instruments were provided for analyzing the different constituent gases. Concentrations of unburned hydrocarbons were measured using a Beckman 402 flame-ionization detector. Concentrations of carbon monoxide and carbon dioxide were measured by nondispersive infrared analyzers. Determinations of nitric oxide and total NO_x concentrations were made using a Thermoelectron chemiluminescent-type analyzer. Concentrations of oxygen were determined using a Beckman Model Series 742 polargraphic analyzer. All temperatures and pressures necessary for monitoring the operation of the gas-sampling system were measured using instrumentation maintained in the gas analysis cart. Filters and gas driers were located within this system to ensure the proper conditioning of the exhaust gas sample. The calibration gases were traceable to National Bureau of Standards reference material. Check calibrations of the testing standards against the primary standards were made periodically to ensure their continued accuracy.

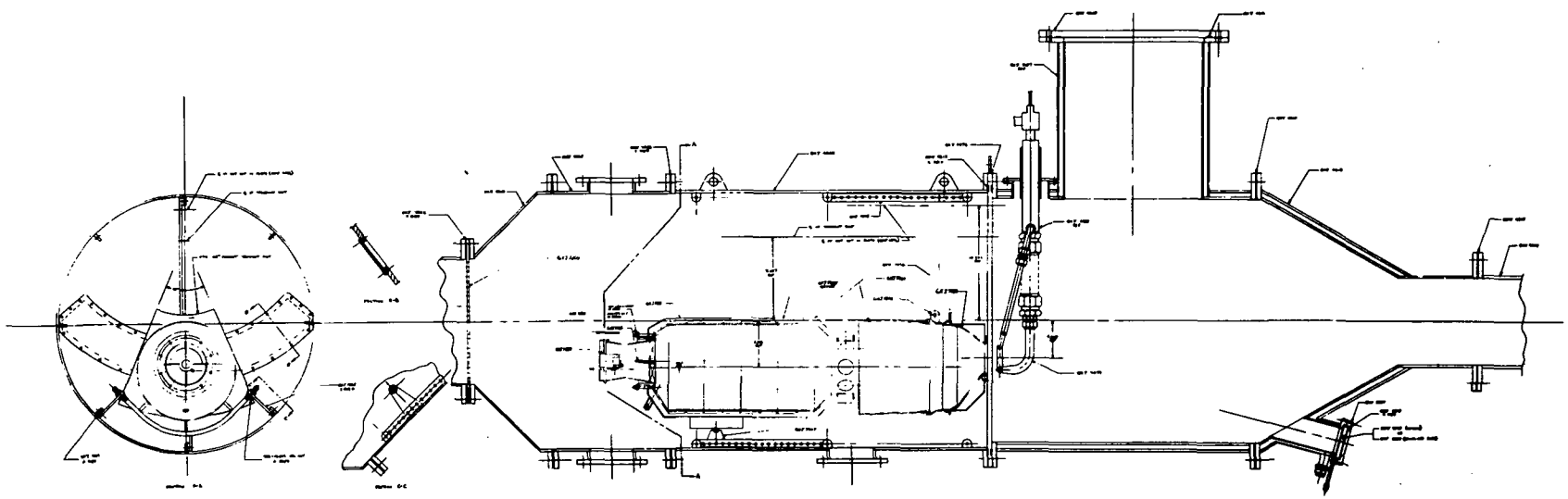

Figure 30. Layout of the B-2 Rig Showing the FRT Combustor

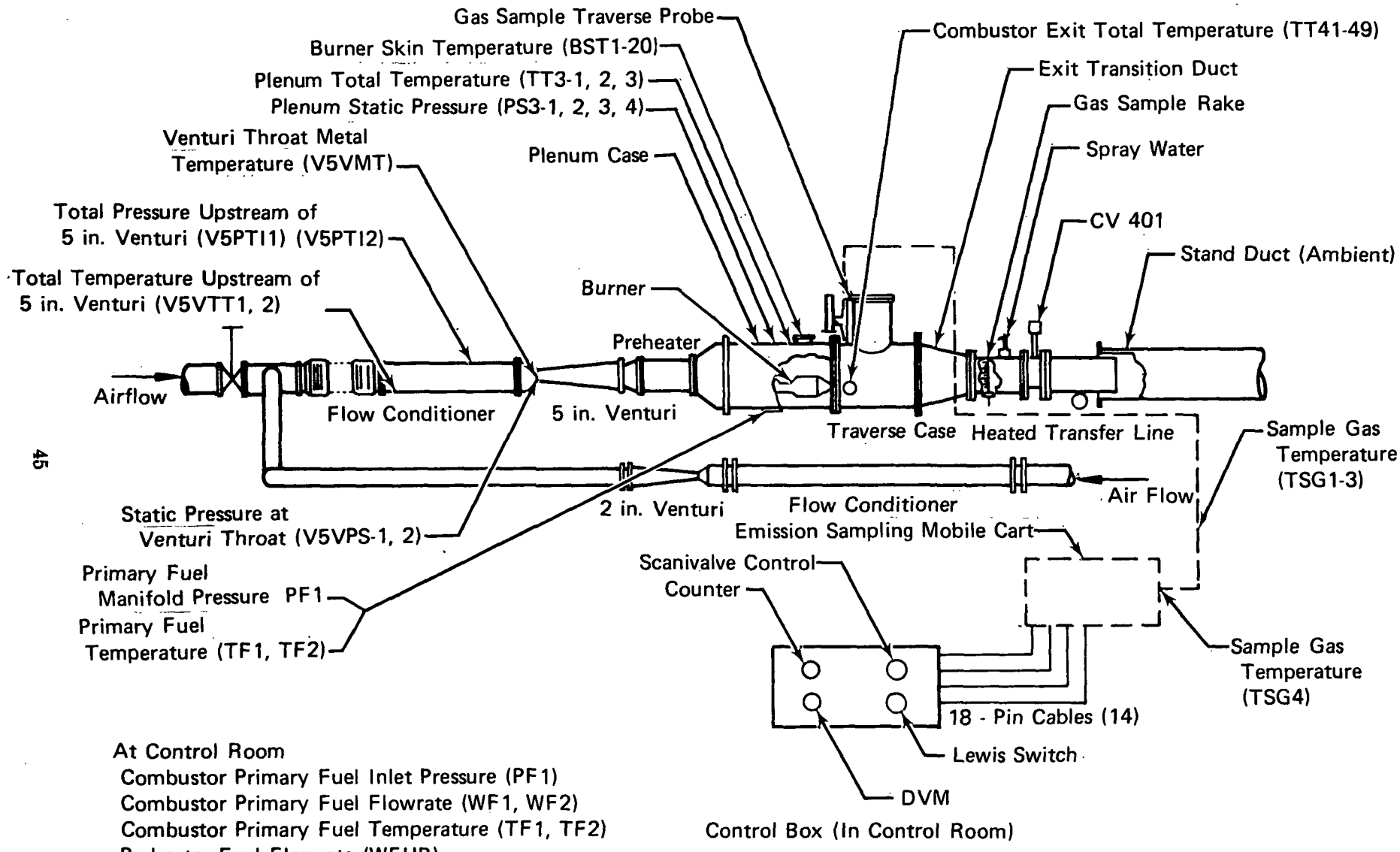

Figure 31. Schematic Diagram of Rig Instrumentation System

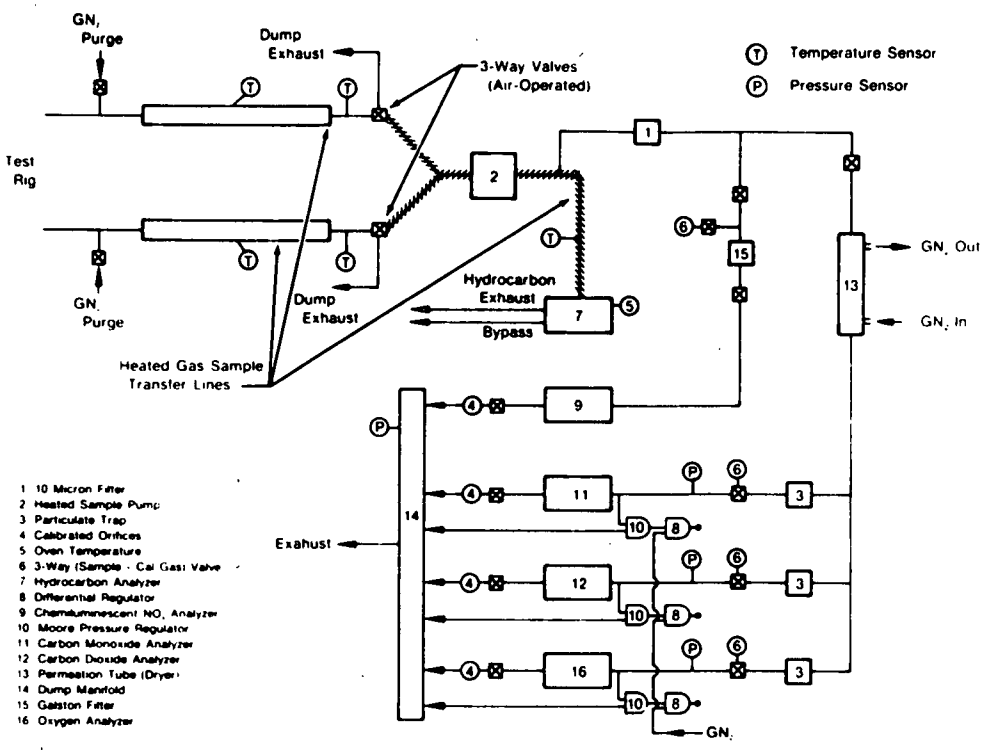

Figure 32. B-2 Sample-Gas Analysis System

Combustor instrumentation was provided to measure primary zone airflow, primary zone cooling airflow, primary zone skin temperatures, and dilution zone skin temperatures. Primary zone airflow was calculated using the static pressure measured at the throat of the premix tube, the upstream total pressure measurement, and the calibrated cross-sectional area of the premix tube. Cooling shroud airflow was determined from total and static pressures measured in the cooling passage. Approximately twelve chromel/alumel thermocouples were mounted on the primary zone liner wall to monitor liner wall temperatures. The dilution zone was instrumented with approximately eight chromel/alumel thermocouples.

SECTION 3

PHASE IV — VERIFICATION TESTING

In Phase IV, the experimental evaluation of the full-scale combustor was accomplished. As in the bench scale test program, tests were conducted at a nearly constant airflow setting (constant pressure drop) while fuel flow was varied to map an emission "signature," in an attempt to study the basic characteristics of the combustor. In an engine, pressure, temperature, and airflow vary with power setting. Both the Full-Residence-Time Version (FRT) and the Engine Compatible Version (ECV) of the combustor were tested to obtain an emission "signature" at several points over a range of conditions spanning the operating requirements of a commercially available 25 megawatt stationary gas turbine engine. Three fuels were used in the test program: No. 2 distillate; No. 2 with 0.5% N (as pyridine), and a distillate cut shale oil.

The experimental program consisted of two parallel parts: component tests of various configurations of the full-scale premix tube (involving cold flow calibration and preliminary combustion tests), and verification testing of the complete full-scale combustor.

Component tests of the various candidate premix tube designs were conducted initially in support of the full-scale combustor design effort. As described in Section 2.9.4; preliminary component tests of this type serve to verify the predicted performance of a candidate premix tube design. In the course of the full-scale combustor verification test program, additional component testing of modified or alternative premix tube configurations was also carried out to verify proper functioning of revised designs.

In Section 3.1 the experimental procedures used in the evaluation of the premix tube designs are described in their entirety. The verification tests of the complete full-scale combustor and the related data analysis are then described in their entirety in Section 3.2. The discussion of each of the two parallel verification efforts is arranged in chronological order within its own subsection.

3.1 PREMIX TUBE COMPONENT TESTS

Tests were conducted to verify the performance of candidate premix tube designs prior to their use in the full-scale combustor. This extensive experimental effort was conducted initially in support of the combustor design effort, and later in support of the full-scale combustor verification test program. In this subsection the premix tube tests are described in chronological order and grouped according to the immediate objectives of the experiments.

3.1.1 *Initial Design Verification*

Several configurations of the preliminary premix tube designs proposed for use in the ECV and FRT combustors (depicted in Figures 16 and 19) were evaluated experimentally in a series of cold flow and combustion tests following initial fabrication. These preliminary tests were conducted to verify the general performance of the initially proposed configurations.

First, an investigation was conducted to determine the patterns of dispersion of liquid produced in the premixing passage by three candidate fuel injectors. Two centrally mounted fuel nozzles were evaluated: (a) an air-blast design; and (b) a simplex pressure atomizing nozzle (85 GPH, 80 deg cone angle). An initial concern in the design of the premixing tube had

been the possibility that a centrally-mounted fuel injector might not disperse fuel over the entire cross section of the premixing tube. To help ensure that a design providing complete dispersion would be available, an alternative configuration, consisting of a spray ring injector, was also fabricated and tested.

The three injectors were evaluated in cold flow tests of a wooden premix tube model at ambient air temperature and pressure, using water as the test fluid. Air velocities were set to match the engine design requirements. The distribution of liquid in the flow field (measured at the premix tube exit plane, with the swirler removed) was determined by collecting water samples at various radial locations using a point source probe. The results of these measurements were as follows:

1. The centrally mounted pressure atomizing nozzle did not fully disperse the liquid over the entire cross section of the flow field. As shown in Figure 33, a sharply center-peaked profile was obtained.

2. The centrally mounted air-blast nozzle produced a similar pattern, with a somewhat higher concentration of liquid toward the center. Photographic documentation of this result is shown in Figure 34.

3. The sprayring injector produced a nearly uniform distribution over the entire cross-section, as shown in Figure 35.

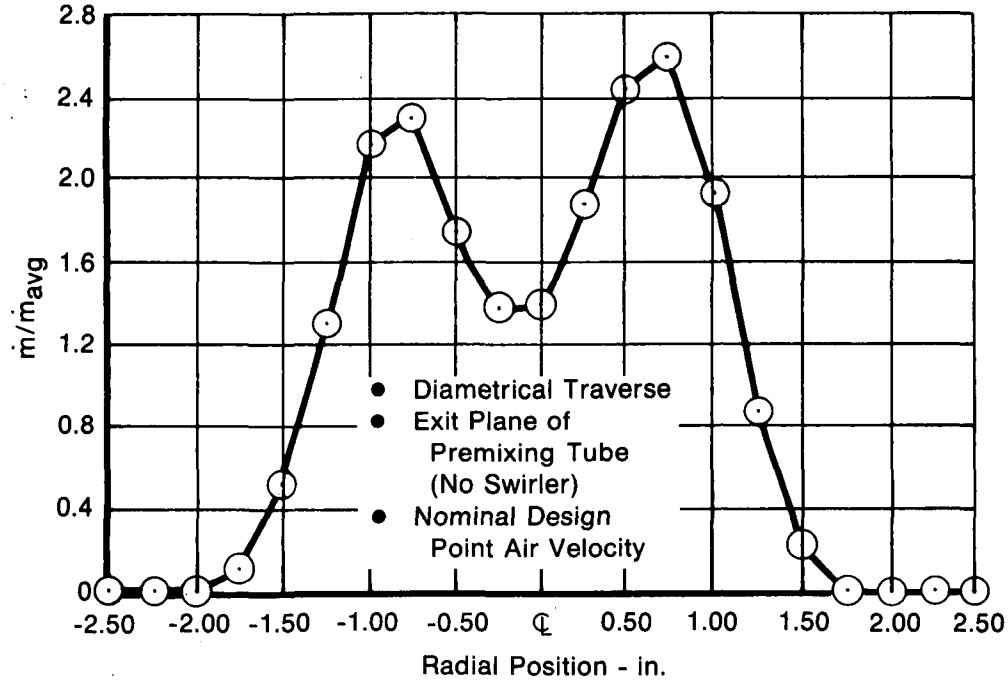

Figure 33. Measured Distribution (Normalized) of Liquid Obtained Using Simplex Pressure Atomizing Fuel Injector

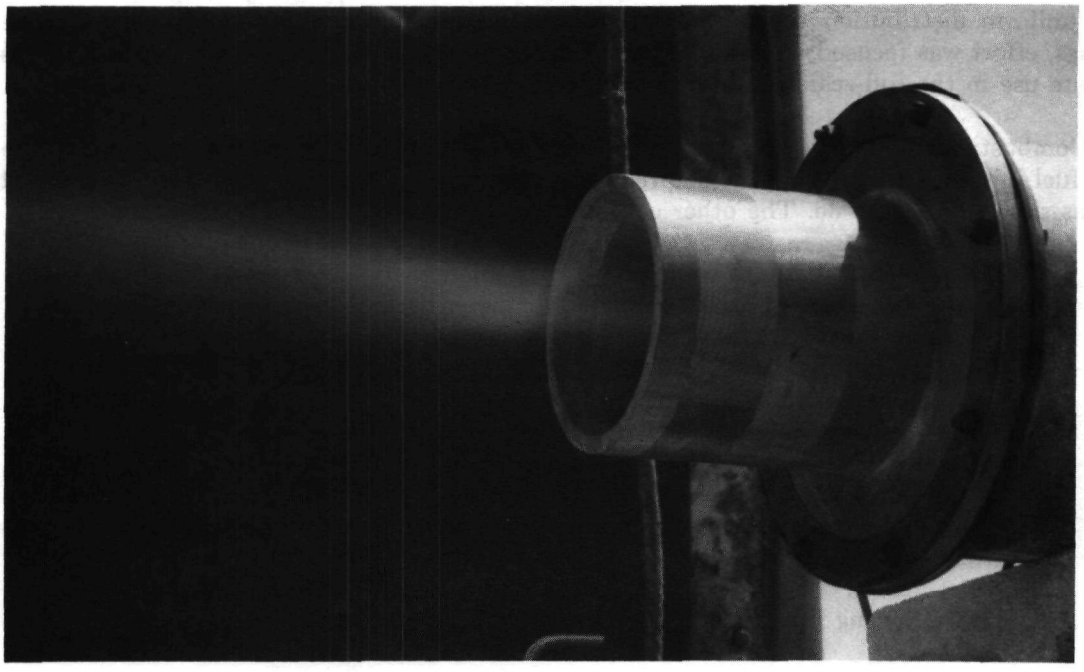

Figure 34. Liquid Distribution Pattern Produced by Centrally-Mounted Air-Blast Nozzle (Nominal Design Point Air Velocity, Equivalent Ratio = 1.0)

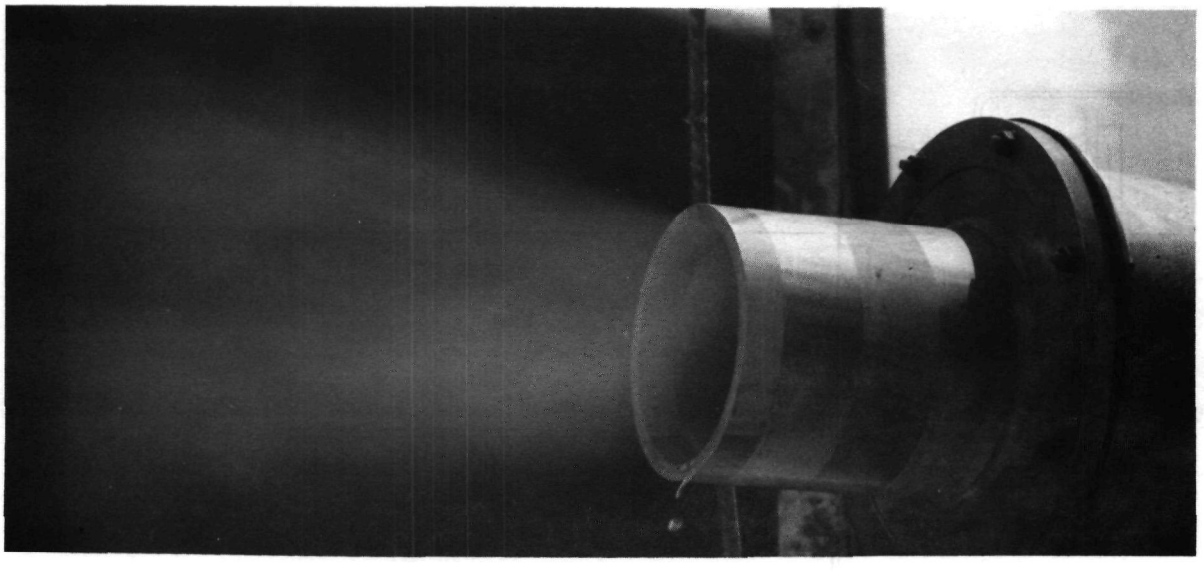

Figure 35. Liquid Distribution Pattern Produced by Spray-Ring Injector (Nominal Design Point Air Velocity, Equivalent Ratio = 1.0)

Dispersion pattern test results clearly indicated that the sprayring design produced a more uniform distribution than either of the centrally mounted injectors. Based on these findings, effort was focused on the refinement of the sprayring design, with a view toward its ultimate use in the full-scale combustor.

Combustion tests of the premixing tube and swirler were also conducted with each of the three fuel injectors. In these tests, the premixing tube was secured to an 8-in. dia sheet-metal liner as shown in Figure 36. The other configurations evaluated were as follows.

1. The air-blast nozzle in conjunction with a larger diameter premixing tube and swirler (Figure 37). An increased diameter became necessary in light of the analytical predictions described in Section 2.8, which indicated that the entire burner pressure drop of three percent would be unavailable to the premixing tube (because of the "mixing loss" incurred in the quick-quench section), and that a larger effective swirler flow area would be required.

2. The simplex pressure atomizing nozzle (Figure 38) in the large diameter premixing tube.

3. The sprayring injector (Figure 39) in the large diameter premixing tube.

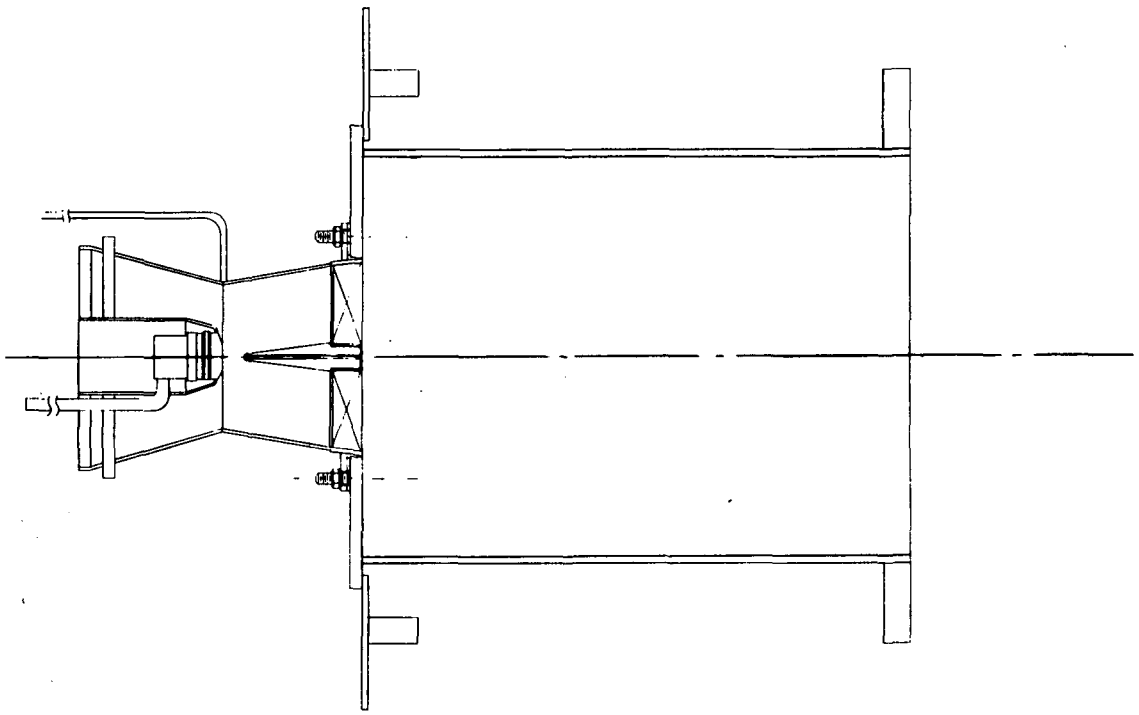

Figure 36. Combustor Test Configuration — Centrally-Mounted Air-Blast Nozzle

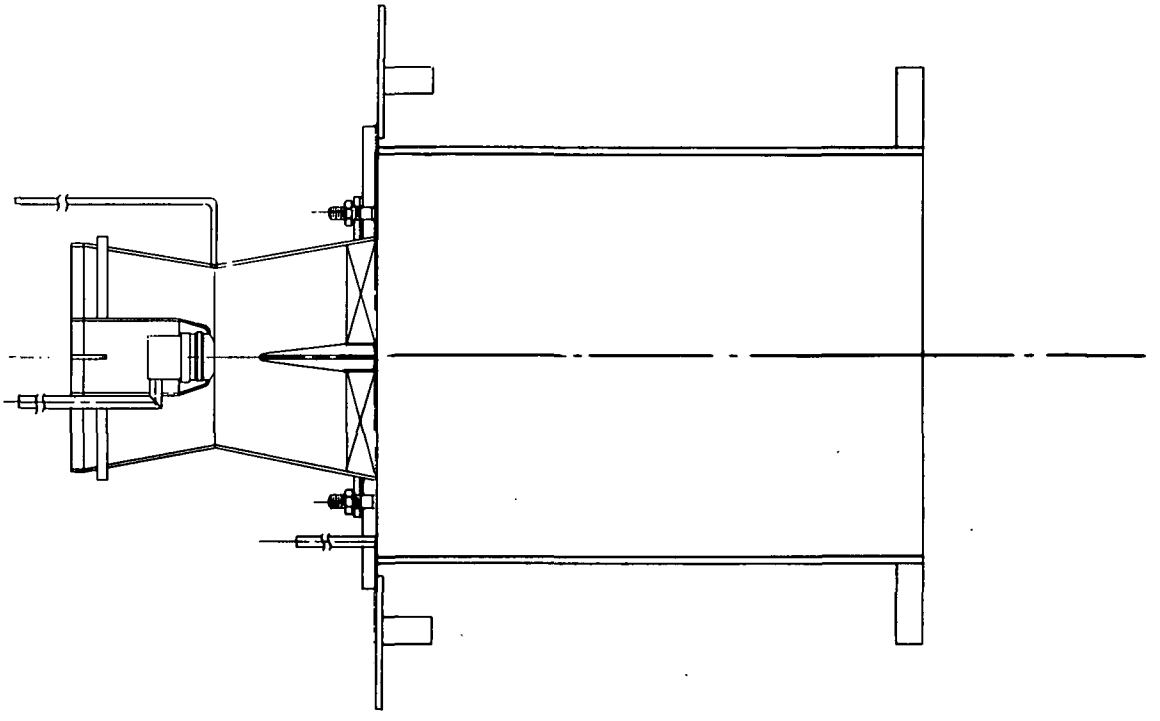

Figure 37. Combustor Test Configuration — Centrally-Mounted Air-Blast Nozzle in Large Diameter Premix Tube

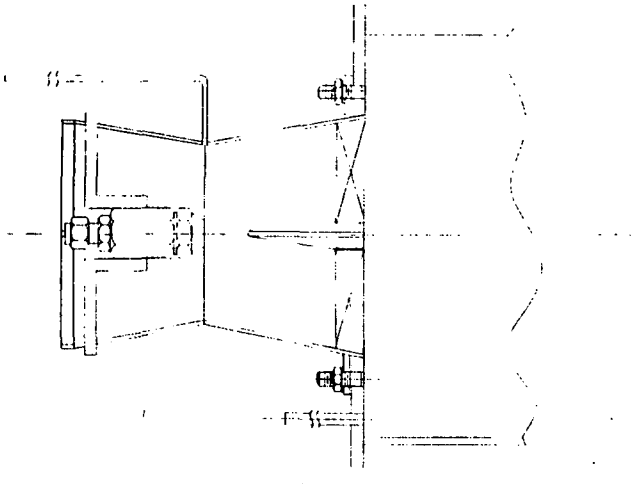

Figure 38. Combustor Test Configuration — Simplex Pressure Atomizing Nozzle

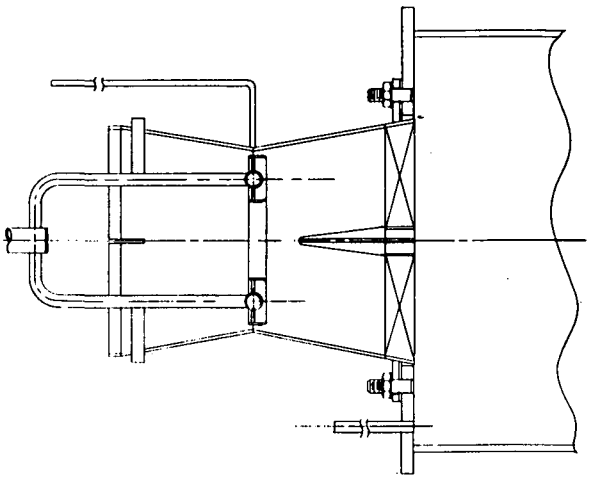

Figure 39. Combustor Test Configuration — Spray-Ring Injector

The premixing tube assembly was mounted in the bench-scale rig, and tests were conducted at 50 psia and 600°F inlet air pressure and temperature. In these tests the entire complement of rig airflow was passed through the premixing tube; there was no dilution of the primary zone exhaust products. Exhaust emission data were recorded over a range of equivalence ratios from about 0.4 to 1.4.

Representative NO_x data are shown in Figure 40 for the air-blast nozzle, and in Figure 41 for the simplex nozzle. The curves each exhibit peak concentrations near an equivalence ratio of 1.0, as expected. At fuel-rich equivalence ratios moreover, the two curves are nearly identical. However, the air-blast injector exhibited a much sharper rate of increase in NO_x at fuel-lean equivalence ratios, and a higher peak concentration. These results were interpreted as an indication that the air-blast injector had provided slightly better premixing (therefore exhibiting a steeper NO_x curve indicative of premixed burning as opposed to diffusion burning).

NO_x emission data were not obtained for the sprayring injector because of flashback conditions encountered during the test of that piece. Flame was held upstream of the swirler, leading to its complete destruction. The cause of the failure was determined to be an incorrect angle of divergence of the aft section of the premixing tube. Although called out as 6 deg, the angle was measured and found to be 11 deg. This excessively large angle of divergence was believed to have caused flow separation and flashback. To correct this problem, the aft section of the premixing tube was rebuilt to the correct specifications.

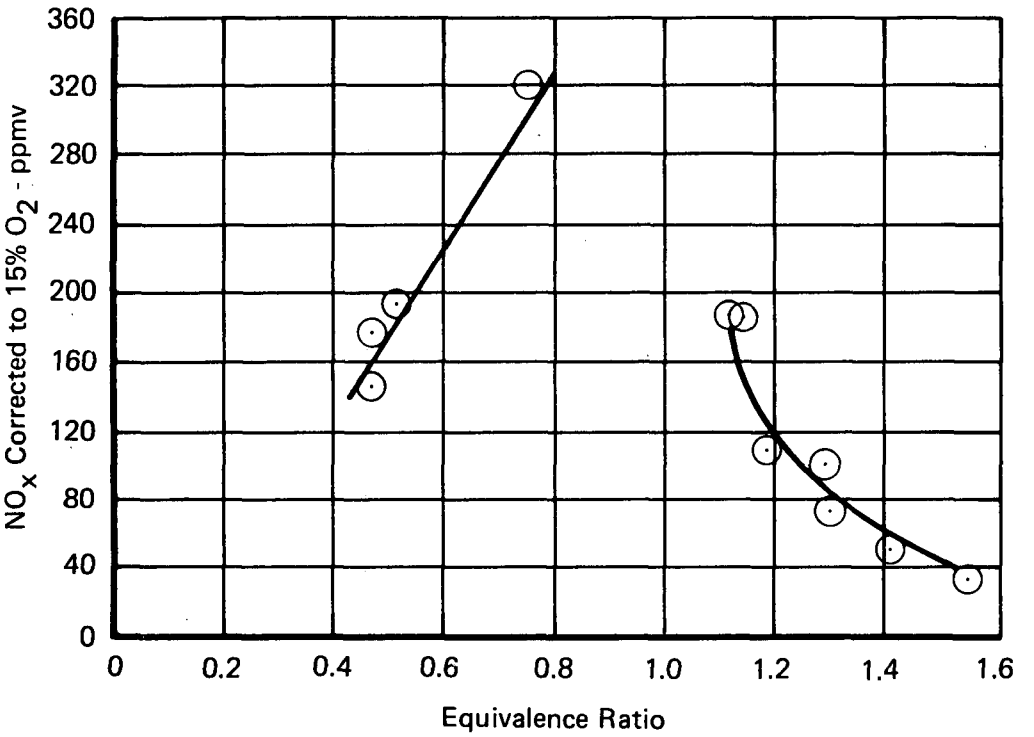

Figure 40. Variation in NO_x Concentration With Equivalence Ratio for Prototype Premixing Tube With Centrally-Mounted Air-Blast Nozzle (Scheme 26-05A)

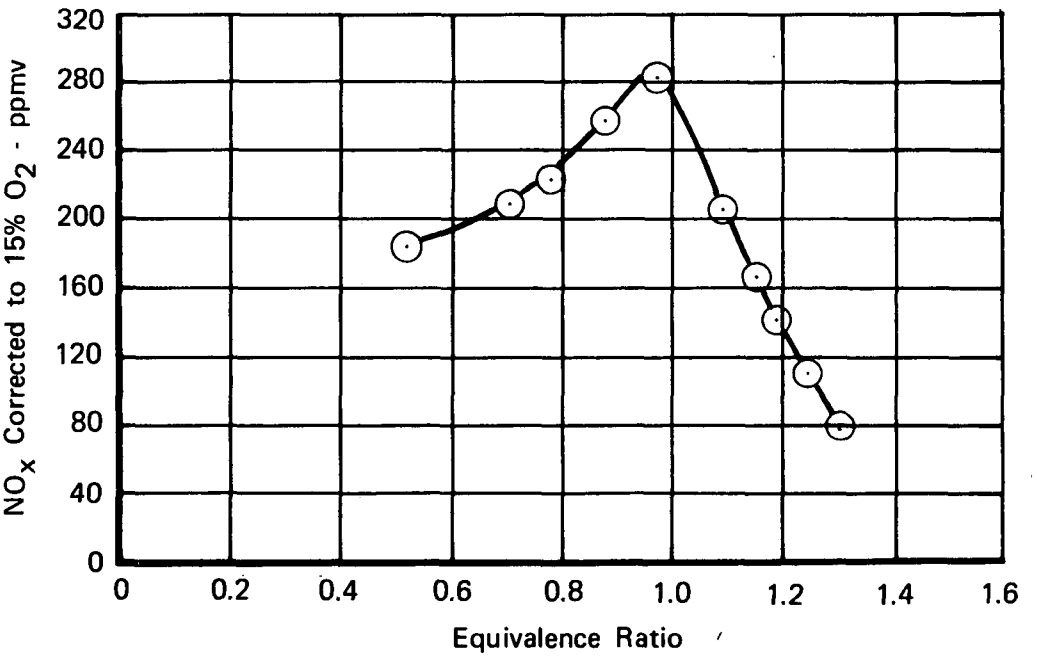

Figure 41. Variation in NO_x Concentration With Equivalence Ratio for Prototype Premixing Tube With Simplex Pressure Atomizing Nozzle (Scheme 26-06A)

Further tests were conducted to verify proper functioning of the rebuilt hardware, and to evaluate other features of the premixing tube design, particularly those associated with the sprayring injector. Initially, six series of cold flow tests were performed, in which the profiles of total and static pressure were measured at various locations in the flow field of the premixing tube. It was verified that the rebuilt aft section of the premixing tube did not generate separated flow. However, several features of the sprayring injector produced wake regions of appreciable size in the flowstream. These included the fuel injector ring, which was made of 0.32 in. OD tubing, and to a degree, the inner and outer splash plates (see Figure 42). Modifications were made to both these features as follows (see Figure 43):

1. The fuel injector ring (0.32-in. diameter) was replaced by two stacked fuel injector rings of 3/16-in. diameter. A wedge-shaped trailing-edge piece was also added to help prevent separation.

2. The outer splash plate was replaced by an outer conical partition extending upstream nearly to the inlet plane, and downstream to the throat. It was reasoned that fully developed flow would be established on both sides of the partition, preventing the formation of a wake at the trailing edge. At the same time the partition would still function as a splash plate, and would prevent fuel wetting of the premix tube wall.

3. The inner splash plate was removed altogether. It was reasoned that jet-on-jet impingement occurring in the high-velocity airstream at the center of the premixing passage might provide adequate atomization.

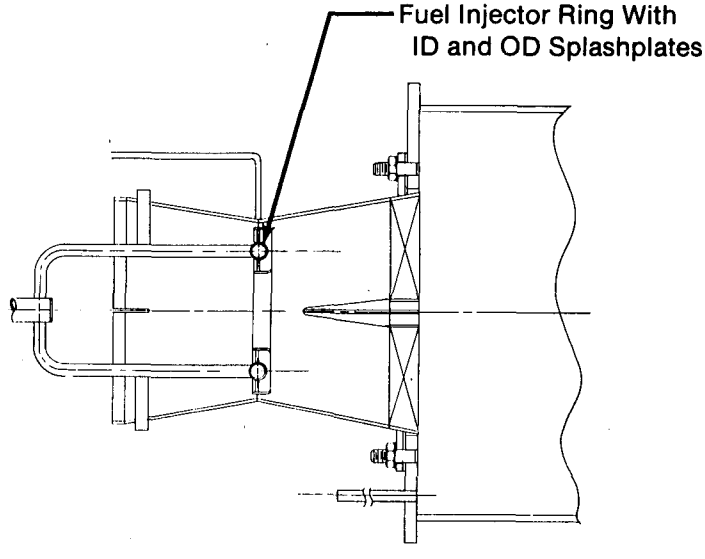

Figure 42. Premixing Tube Scheme 26-07A Showing Initial Design of the Spray-Ring Fuel Injector

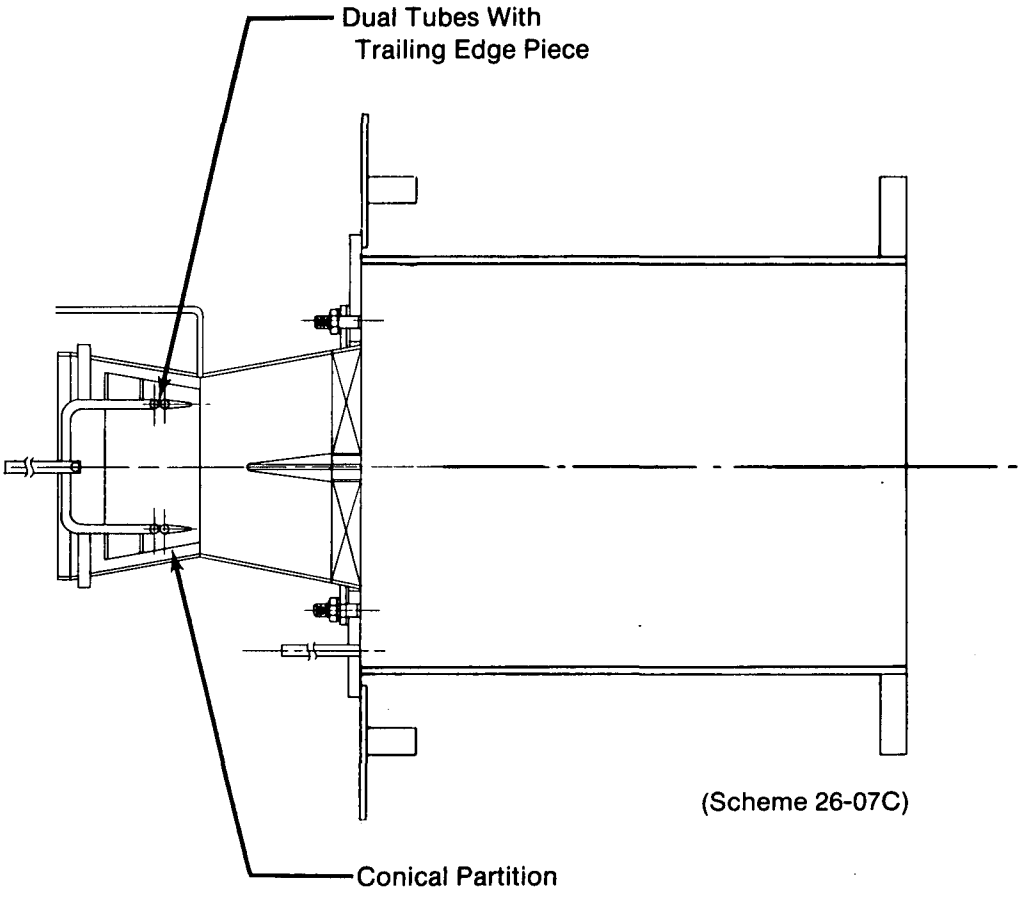

Figure 43. Intermediate Configuration of the Fuel Injector Spray Ring

The modifications described were among those evaluated in subsequent cold flow tests. Pressure traverse data indicated that the wakes associated with the fuel injector ring had effectively been eliminated. However, there were still local regions of low velocity associated with the trailing edge of the conical partition. It appeared that a mismatch of the velocities on either side of partition tended to develop as a result of small nonuniformities in the approach airflow.

Subsequent modifications to the conical partition produced no apparent improvement, and the piece was finally eliminated in favor of an outer splash plate similar to the original design. Pressure traverse data indicated that no significant wake regions were generated by the new splash plate/injector arrangement.

The revised configuration, shown in Figure 44, was evaluated in combustion tests. The premixing tube was mounted in the bench-scale rig, and tests were conducted at 50 psia and 600°F inlet air pressure and temperature. The entire complement of rig airflow was passed through the premixing tube; again there was no dilution of the primary zone exhaust products. Exhaust emission data were recorded over a range of equivalence ratios from about 0.4 to 1.4.

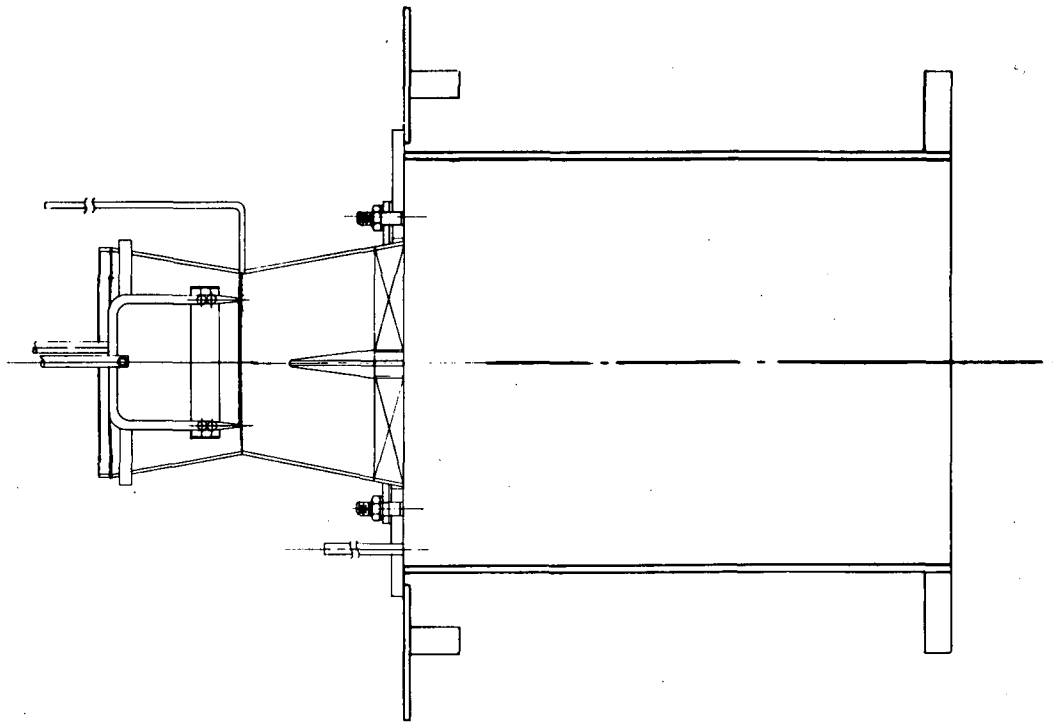

Figure 44. Revised Design of the Splashplate/Injector Ring Arrangement

Representative NO_x data are shown in Figure 45. Included for reference are the data previously shown for the original centrally mounted airblast fuel nozzle. The two sets of data are nearly identical at fuel-rich equivalence ratios. However, the sprayring design produced a significantly lower NO_x concentration at the single fuel-lean condition tested. These results were taken to indicate that the sprayring injector provided better premixing than the airblast nozzle during fuel-lean operation. More significant, however, was the fact that refinements made to the premixing tube itself (correcting the angle of divergence), and to the sprayring successfully eliminated the flashback problem previously encountered.

In the initial experiments described, proper functioning of the premix tube with regard to flashback-free operation, an even fuel distribution, and good exhaust emission characteristics had been verified. The tests had been performed using the basic premixing tube without the variable damper piece. Furthermore, the combustion tests had been made at elevated pressure in a rig chamber having no provision for visual observation of the general flame appearance.

Further tests were conducted in which cold flow pressure measurements were made with the variable damper installed, and combustion tests were conducted at atmospheric pressure in an ambient discharge rig allowing visual observation of the premixed flame. In addition to the basic premix tube previously tested, an extended-length version, providing higher throat velocities for improved atomization and longer length for increased residence time to allow more fuel vaporization to occur, was also designed and evaluated.

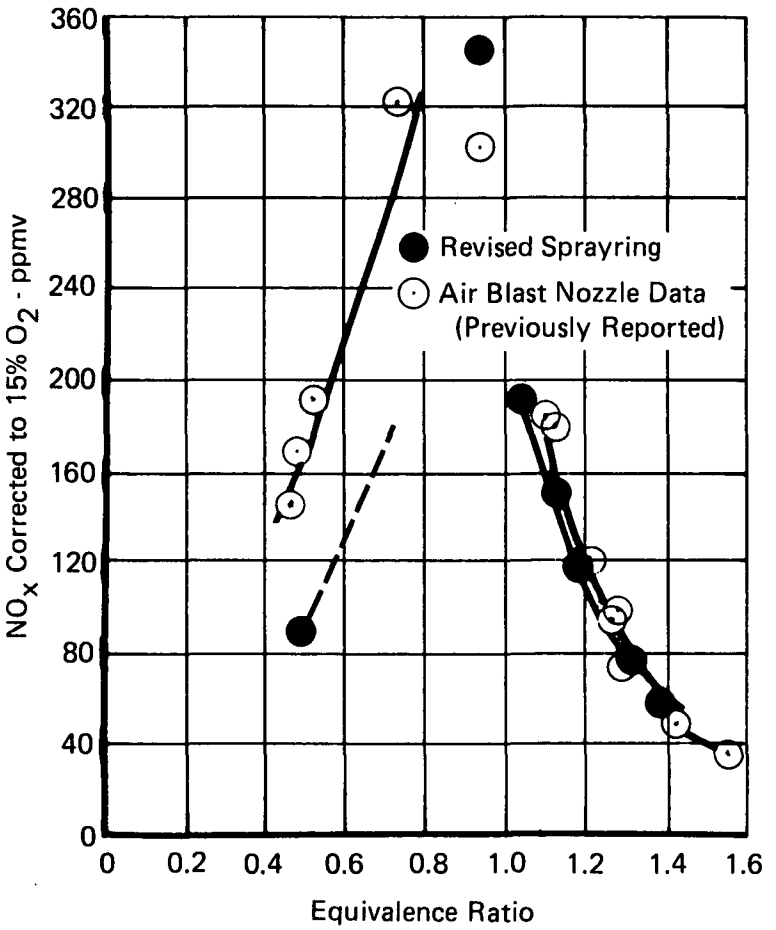

Figure 45. Comparison of Variation in NO_x Concentration With Equivalence Ratio for Revised Spraying Design and Centrally-Mounted Air-Blast Nozzle

The experiments carried out and pertinent results were as follows:

1. The variable damper device was evaluated in conjunction with the basic premix tube in the configuration shown in Figure 46. First, cold flow measurements were made of the profiles of total and static pressure in the premixing passage (at the throat of the venturi). In these tests the fuel injector was removed so that flow field characteristics due to the variable damper could be determined. With the damper in the full-open position it was found that there was no serious disruption of the flow field. However, with the damper fully restricted, there was evidence of reverse flow, as may be seen from the data presented in Figure 47. The test piece was examined and a slight misalignment was found between the fixed and movable damper plates. This misalignment was believed to have produced a non-uniform circumferential distribution in the flow field, and may have been responsible for the reverse flow observed. Another possible contributing factor was a step discontinuity that was present in the wall of the premixing tube, at the inlet plane (see Figure 46). Both these conditions were corrected prior to subsequent combustor tests with the damper in the fully restricted position.

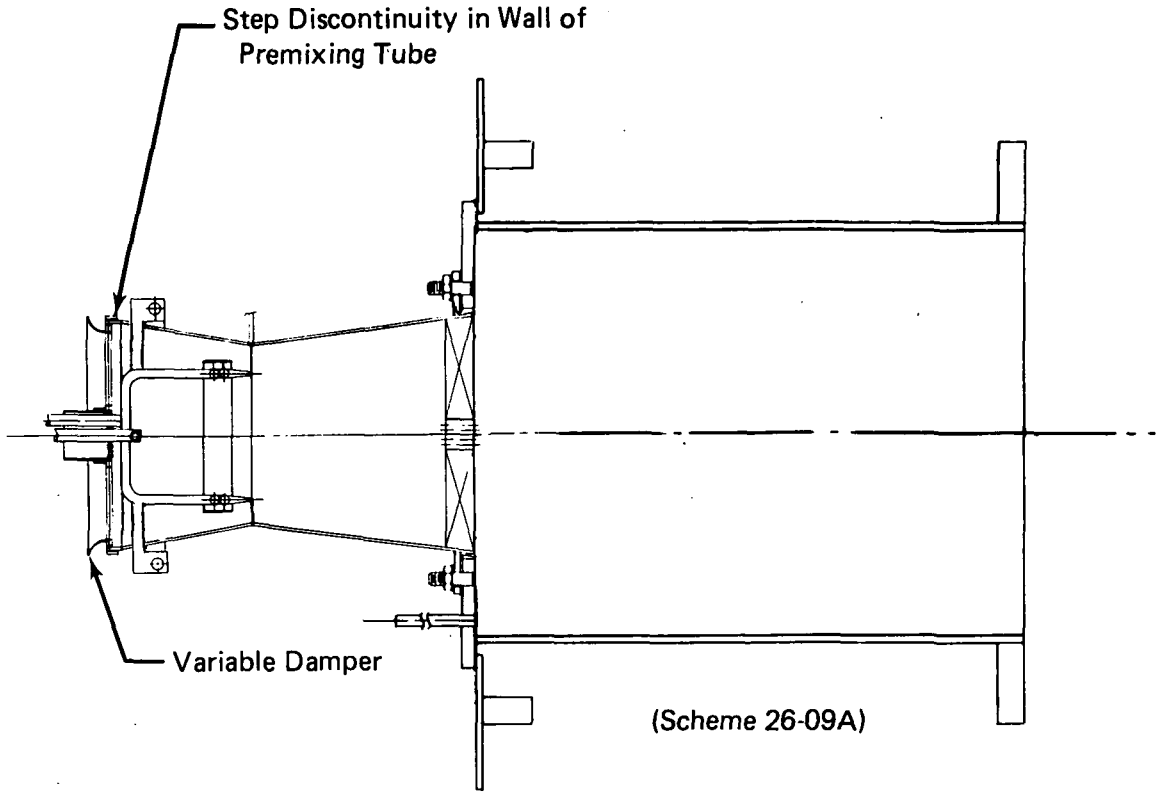

Figure 46. Basic Initial Premix Tube Configuration With Variable Damper Mechanism Installed

2. Combustion tests were performed initially using the configuration tested in the cold flow experiments, with the damper in the fully open position. Visual observations of the flame indicated that there was a slight concentration of fuel toward the center of the premixing passage. There were also indications of isolated regions of liquid burning (regions of luminous flame). Otherwise, the appearance of the flame was generally acceptable.

3. The premixing tube was modified as shown in Figure 48. An inner splashplate was added to the fuel injector sprayring in an attempt to eliminate the central region of high fuel concentration observed in the previous scheme. The wall of the premixing passage was also reworked to eliminate the step discontinuity at the inlet plane. Combustion tests were performed with the damper in the open position. It was found that the central region of high fuel concentration had been dispersed slightly, taking on an annular rather than a cylindrical form (as evidenced by the appearance of the region of luminous flame). The fraction of the flame observed to be luminous was somewhat diminished with respect to the previous scheme.

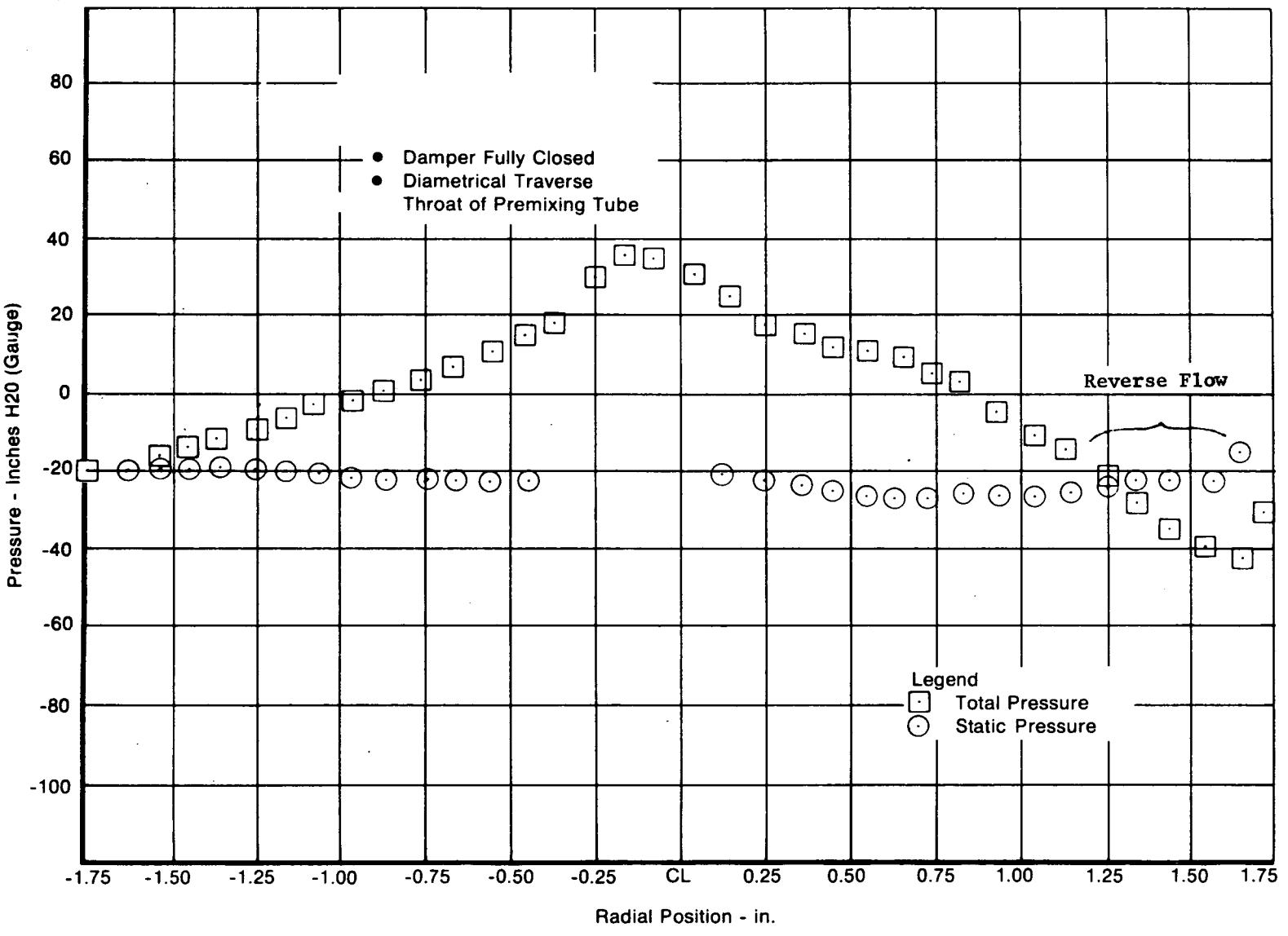

Figure 47. Pressure Transverse Data for Basic Premixing Tube With Variable Damper

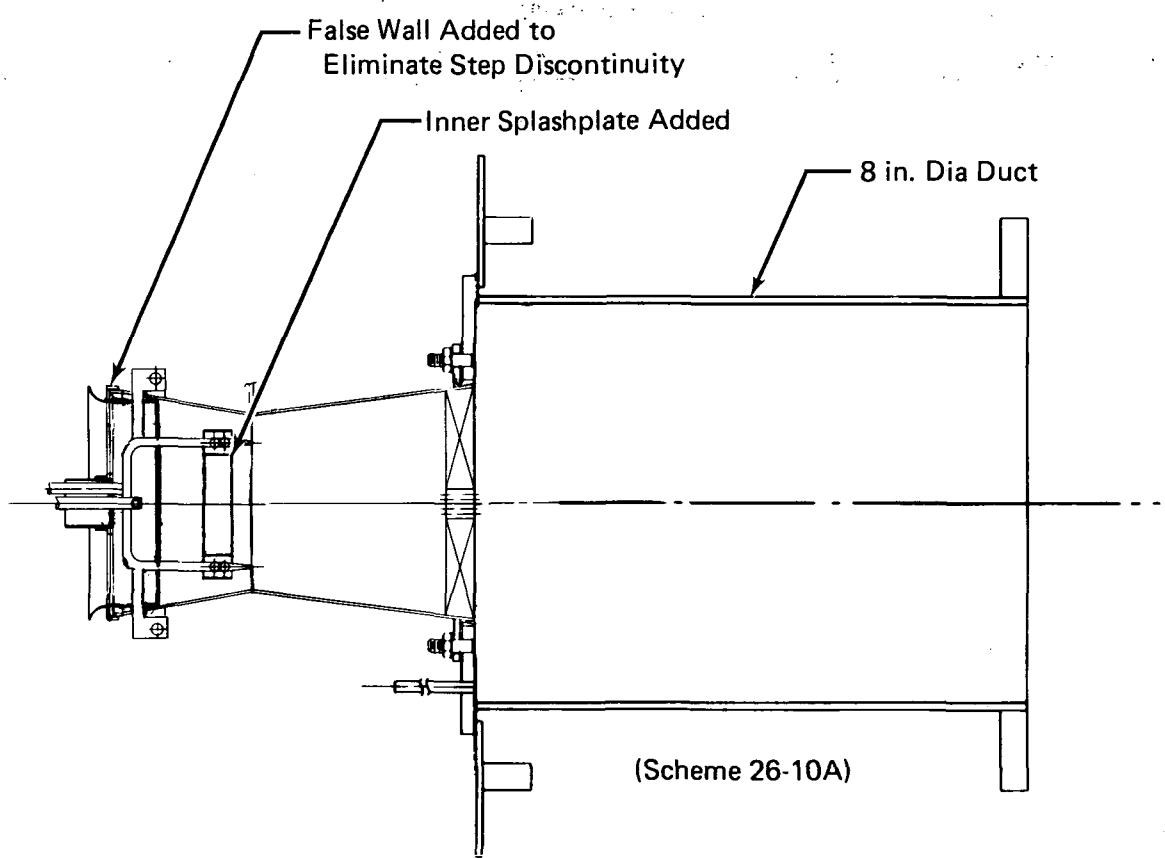

Figure 48. Modified Configuration of the Basic Initial Premix Tube Configuration

4. Combustion tests were performed again using the same premixing tube configuration, after modifications had been made to the test rig to eliminate a condition of acoustic resonance. (In atmospheric combustion tests resonant conditions often occur and can affect the combustion process; changes in the dimensions of the burning duct usually eliminate the problem.) The modified configuration is shown in Figure 49. Tests conducted with this arrangement were free of acoustic resonance. There was no apparent change in the combustion process with respect to the previous test series.

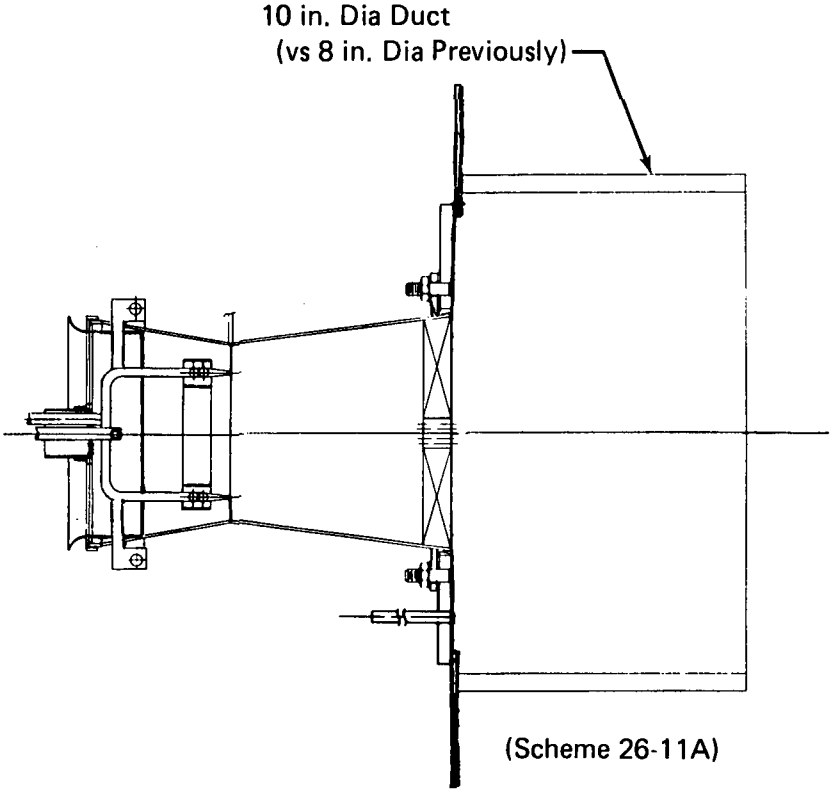

Figure 49. Burner Duct Modified to Eliminate Acoustic Resonance

5. An extended-length premixing tube was also evaluated in combustion tests at atmospheric pressure. The configuration, shown in Figure 50, differed from the short-length design previously evaluated in that a longer divergent section was provided. Given the same swirler diameter and the same angle of divergence (these two specifications are nominally the same for the short and long premixing tubes), the longer divergent section made it possible to specify a smaller diameter for the premixing tube venturi throat. The smaller diameter was expected to produce a higher mixture velocity and to result in better fuel atomization and a wider margin against flashback. The increased length also provided a longer residence time for more complete fuel vaporization. The extended-length configuration was constructed as an alternative (and more conservative) approach to providing high-quality fuel-air mixture preparation. Visual observations of the

flame made during initial combustion tests indicated that very high quality premixing had been achieved. There was a total absence of luminous flame at fuel lean equivalence ratios. At fuel-rich settings (slightly beyond the design point equivalence ratio of 1.3) the flame became orange while retaining the same texture and semitransparent quality associated with a blue flame under fuel-lean conditions. These observations indicated near-perfect premixing and a high degree of fuel vaporization.

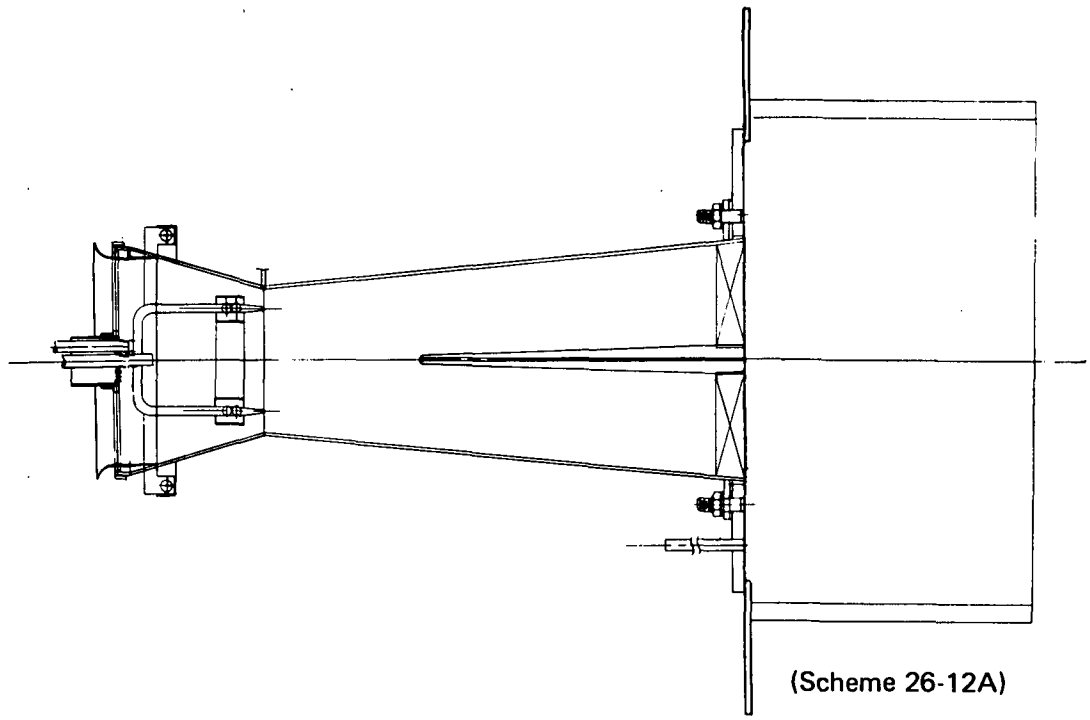

Figure 50. Extended-Length Premix Tube

A photograph of the flame under fuel-rich conditions is presented in Figure 51. (Although reproduced in this report in black and white, the uniform consistency and absence of luminous flame are apparent.)

The extended-length premixing tube was also tested with the variable damper fully restricted (simulating idle conditions). Visual observations indicated the same excellent premixed flame reported in the previous test series.

Based on the very good overall performance of the extended-length premix tube, the configuration shown in Figure 50 was selected for use in the full-scale combustor verification test program.

Further component tests were conducted to calibrate the airflow capacity of the premix tube as a function of the pressure differential between inlet stagnation pressure and the static pressure at the throat of the premixing passage. The measurements taken provided an indication of the total pressure loss taken across the variable damper, and were necessary for use in the computation of the premix tube airflow at various damper settings during the full-scale combustor verifications tests. A calibration graph was generated (Figure 52) and incorporated into the data reduction program.

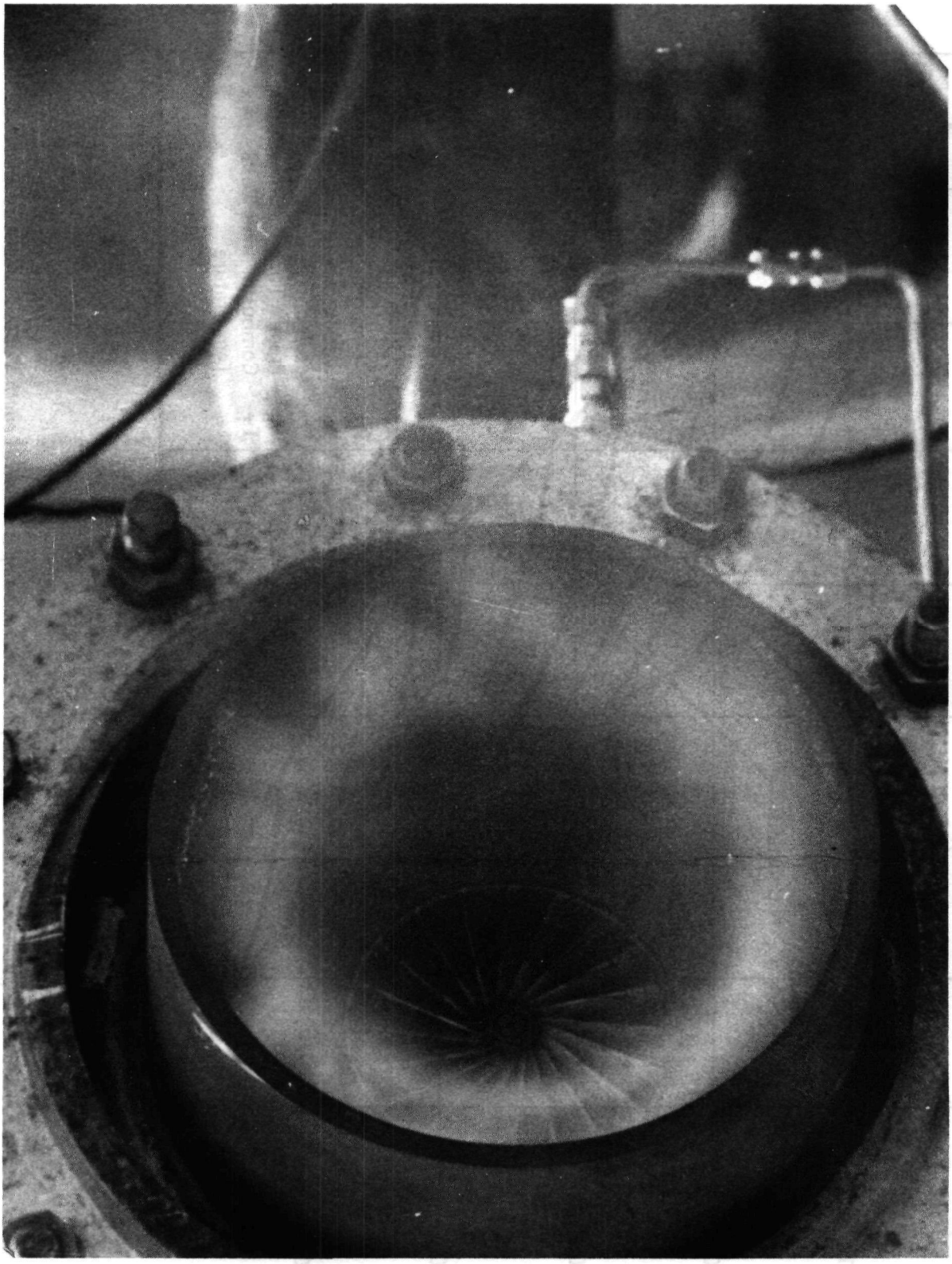

Figure 51. Premixed Flame Produced by Extended-Length Premixing Tube During Ambient Operation (Nominal Design Point Air Velocity Equivalence Ratio = 1.4 Nominal)

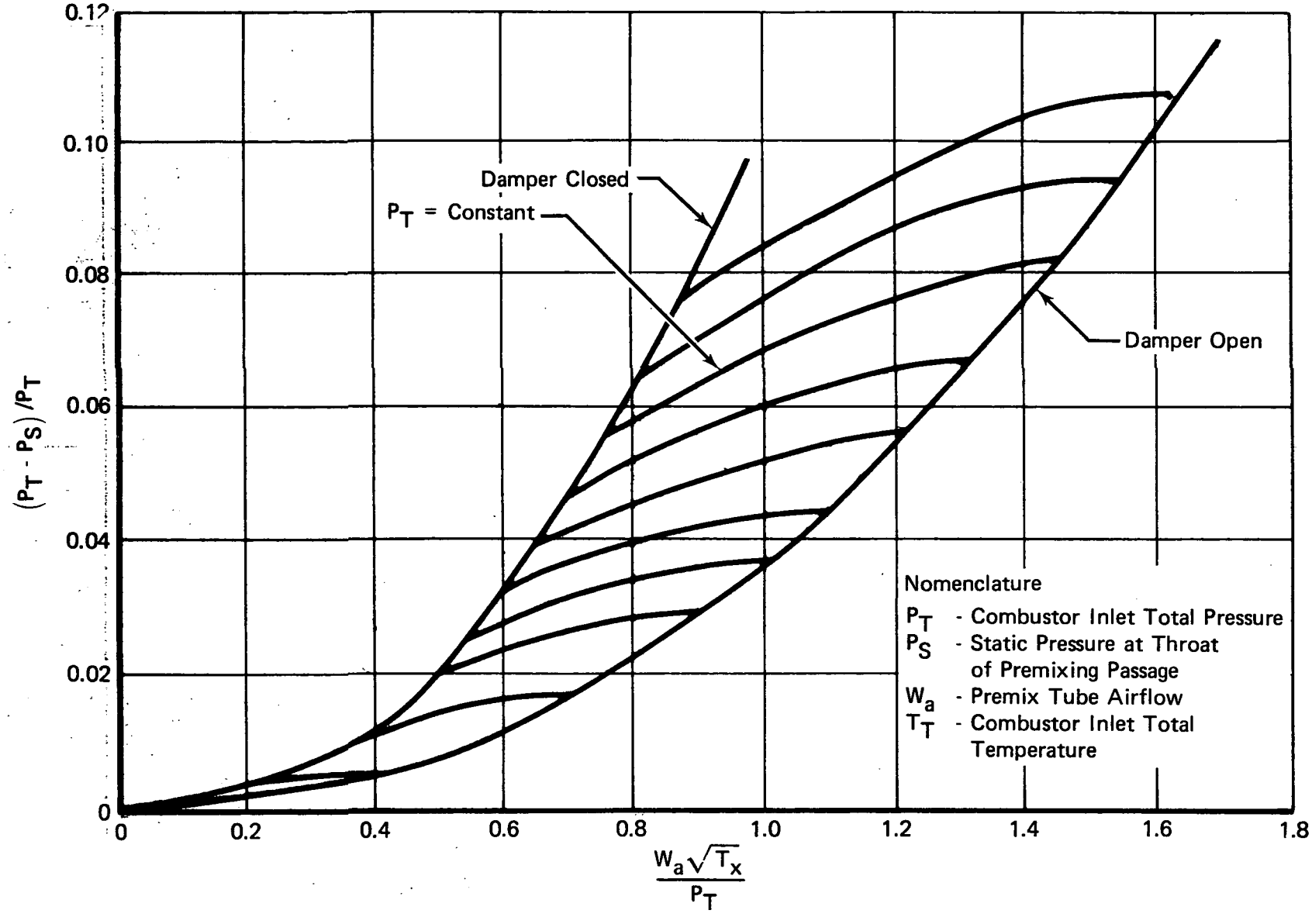

Figure 52. Premix Tube Airflow Calibration of Extended-Length Tube

3.1.2 Bench Tests in Support of the Full-Scale Combustor Test Program

During initial verification tests of the full-scale combustor (described in Section 3.2.1) inadequate performance of the extended-length premix tube was observed in terms of poor-quality fuel preparation and the occurrence of flashback. To determine whether the difficulties encountered were due to deficiencies in the design of the premix tube (and not due to rig-related causes) further component tests of the extended-length configuration were conducted.

Both flow visualization and combustion tests were performed, as summarized in Table IX. Initially, combustion tests were conducted using Scheme 26-13A, the actual configuration tested in the full-scale combustor. These tests were intended to resolve the apparent discrepancy between the poor premixing quality observed in the full-scale combustor test and the excellent quality observed in the original bench tests of the same premix tube (Figure 51). Visual observations made during the repeat premix tube test indicated that the flame quality was poor, having a luminous appearance indicative of diffusion burning. This result matched that of the full-scale combustor test, and was much worse than the original bench test results. Because contaminated fuel had at one point inadvertently been introduced into the full-scale combustor rig, resulting in partial plugging of the fuel injector sprayring, it was postulated that some foreign material might still be present (even though the sprayring had been thoroughly back-flushed following the incident with contaminated fuel and visual spray tests performed which indicated that all jets were flowing), causing a maldistribution of fuel in the premixing passage. Rather than cut apart the sprayring to perform a thorough examination, it was decided to fabricate a new fuel injector assembly identical to the original.

TABLE IX
BENCH PREMIX TUBE TESTS PERFORMED IN SUPPORT OF THE FULL-SCALE COMBUSTOR VERIFICATION TEST PROGRAM*

Scheme	*Type Test*	*Purpose*	*Results*
26-13A	Combustion	Retest of full-scale combustor rig premix tube	Poor flame quality (luminous, opaque) matching B-2 rig results
26-14A	Combustion	New sprayring. No possibility of contamination.	Poor flame quality (luminous, opaque) matching B-2 rig results
26-13B	Flow Visualization	Check fuel atomization and distribution	No discernable deterioration in spray characteristics
26-14B	Flow Visualization	Check fuel atomization and distribution	No discernable deterioration in spray characteristics
26-15A	Combustion	Centrally mounted simplex nozzle 85 GPH, 80 deg.	Poor flame quality (luminous, opaque, and concentrated in center
26-16A	Combustion	Centrally mounted simplex nozzle 35 GPH, 90 deg	Flame quality better than 26-15A, but still unacceptable
26-17A	Combustion	Centrally mounted simplex nozzle 12 GPH, 90 deg.	Acceptable flame quality (traces of luminous flame)

*Refer to Appendix B for SI unit conversion

The second fuel injector assembly, designated Scheme 26-14A, was also subjected to combustion tests. Once again, the flame quality was poor, matching the results obtained in the full-scale combustor rig test. This outcome did not shed any light on the reasons for poor functioning of the premix tube, and served to perpetuate rather than resolve the original discrepancy between the good initial component test results and the later very poor full-scale combustor results. In fact, it had been found impossible to duplicate the initial bench-rig test results which had shown excellent flame quality.

In an attempt to find a cause for the apparently consistent and repeatable deterioration in premixing quality associated with the sprayring design of the full-scale premixing tube, a series of flow visualization tests were subsequently conducted. Both the original sprayring injector and the second duplicate sprayring were evaluated. In these tests there was found to be no difference (within the limits of visual observation) between the two sprayrings (Schemes 26-13B and 26-14B). The general results (atomization and distribution of the liquid in the premix tube airstream) were judged comparable to those obtained during flow visualization tests performed initially for the original sprayring injector. These observations shed no new light on the question of deteriorated premixing performance.

Having found no explanation for the observed poor flame quality in the above-described combustion and flow visualization tests (no anomaly in the functioning of the sprayring for example, and no evidence that the original tests may have been erroneous or nonrepresentative), it was decided that the most productive approach leading to the restoration of excellent quality premixing and flame appearance consisted in the evaluation of alternative fuel injector designs. It was reasoned that the performance of the sprayring injector might have been marginal all along, providing high quality premixing on some occasions, and poor quality on others, in response to changes in secondary factors.

3.1.3 Verification Tests of Alternative Fuel Injectors

The testing of alternative fuel injectors was begun with three candidate configurations having centrally mounted fuel injectors of the same basic type (pressure atomizing with 12, 35, and 85 GPH nozzle designations). Combustion tests were conducted to determine the effect of rated flow capacity (and the resultant variation in fuel droplet diameter distribution that occurs when the three nozzles are compared at the same flowrate) on flame appearance. It was found that flame appearance improved (a lower incidence of opaque luminous flame) as lower capacity nozzles (better atomization) were inserted and tested. The smallest nozzle (12 GPH) exhibited generally acceptable flame appearance, while the two larger nozzles were judged unacceptable because of excessive luminous flame. The largest nozzle (85 GPH) was also judged unacceptable because of a poor fuel distribution pattern (fuel concentrated in the center of the passage).

The choice of a centrally mounted fuel injector for testing as an alternative to the original sprayring design was predicated upon the need for improved fuel atomization. The substantial presence of opaque luminous flame observed in the component and full-scale combustion tests had indicated that the burning of sheets of fuel or very large droplets had taken place. By the substitution of a centrally mounted simplex (pressure atomizing) or airblast fuel injector of known performance, good initial atomization of the fuel (upon injection into the premix passage) could be assured.

Not only the atomization of the fuel, but also the distribution (in an even pattern across the premix passage) must be provided in an acceptable fuel injector design. The original sprayring design had provided good fuel distribution by virtue of its ring arrangement (which allows the fuel to be introduced through 16 jets into equal-area sectors). Centrally mounted fuel injectors on the other hand introduce the fuel at a single point source, and rely upon the

penetration of the spraycone (radially outward across the premix passage) to provide an even-pattern distribution. Because small droplets do not penetrate well in a high velocity airstream, there is a trade-off between penetration (distribution) and the degree of atomization associated with a centrally mounted fuel nozzle. It was believed possible that an aerodynamic method of spreading the fuel across the premix passage might be required in conjunction with centrally mounted injectors.

Preliminary designs were prepared of several candidate fuel injectors, including: (a) centrally mounted air-blast and pressure-atomizing nozzles in conjunction with inlet swirl vanes (which provide aerodynamic spreading of the fuel); (b) centrally mounted air-boost nozzles (requiring an external compressor) in conjunction with swirl-vane and vortex aerodynamic spreading devices; and (c) modified sprayring injectors.

The specific configurations proposed and evaluated were as follows:

(a) Air-Blast and Pressure-Atomizing Nozzles

As stated, the choice of centrally-mounted fuel injectors predicated upon the apparent need for improved atomization. By the substitution of a centrally mounted pressure-atomizing or air-blast fuel injector of known performance, good initial atomization of the fuel (upon introduction into the premix passage) could be assured. To enhance the prospects for achieving an even distribution, two aerodynamic methods of spreading small fuel droplets across the premix passage were proposed: (1) moderate inlet swirl (5 to 10 deg vanes); and (2) vortex spreaders (multiple small swirlers — 4 or 8 in number — mounted in a ring around the central fuel injector). The two methods are illustrated in the configurations tested: inlet swirl — Schemes 26-21A, 26-22A, 26-24A, 26-26A, 26-27A (Figures 53, 54, 55, 56, and 57); vortex spreaders — Schemes 26-25A, 26-28A, and 26-29A (Figures 58, 59, and 60). In an alternative approach to the use of aerodynamic devices for fuel spreading, a design employing multiple pressure atomizing nozzles (six nozzles in a hexagonal arrangement) was also proposed and evaluated (Scheme 26-19B, Figure 61).

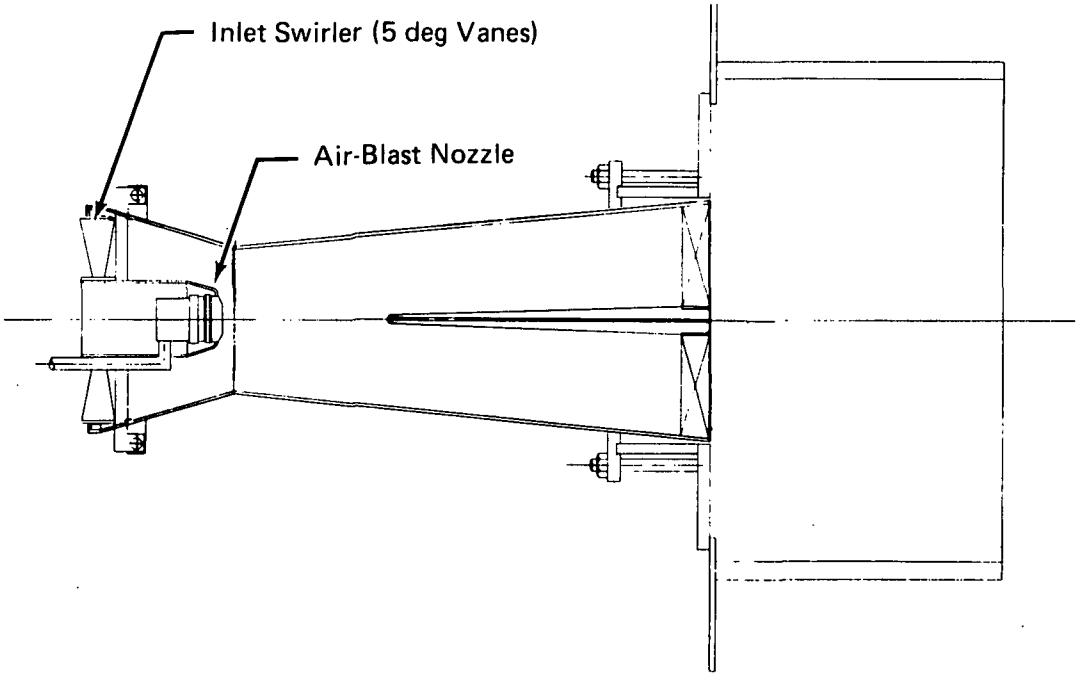

Figure 53. Scheme 26-21A — Original Premix Tube With Air-Blast Nozzle and Inlet Swirl Vanes

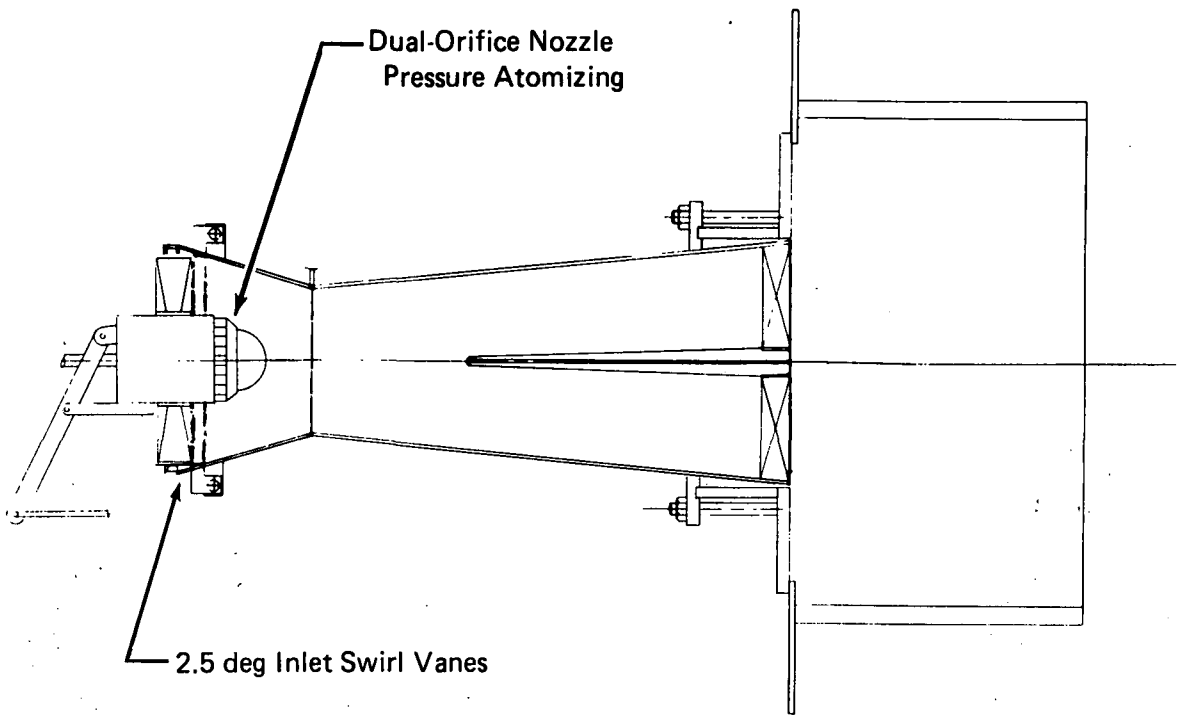

Figure 54. Scheme 26-22A — Original Premix Tube With Dual-Orifice Nozzle

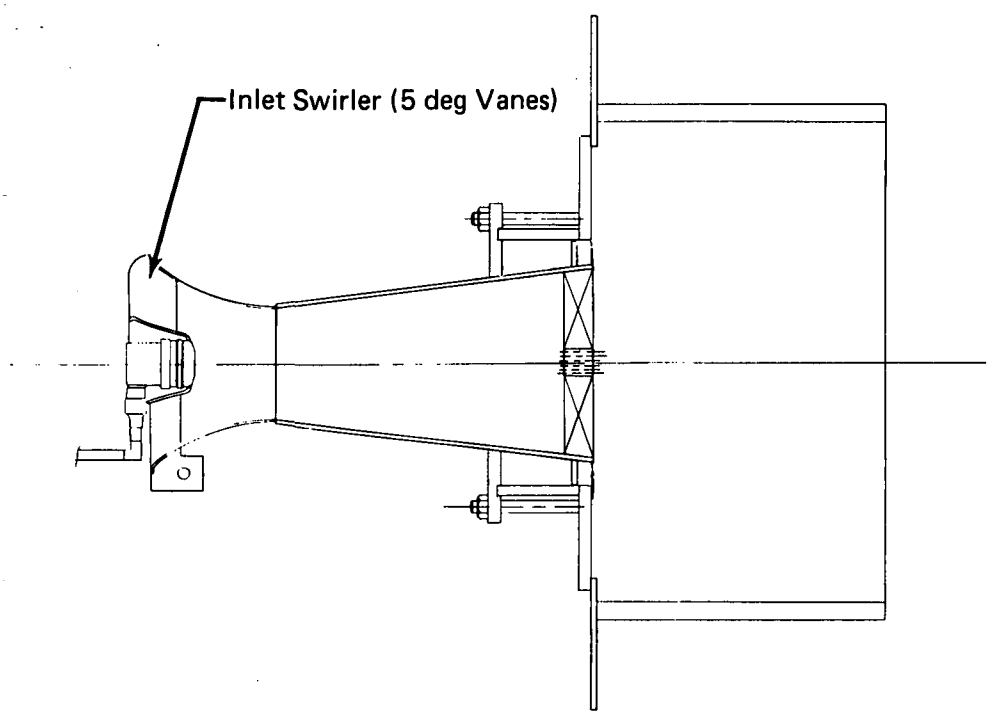

Figure 55. Scheme 22-24A — Short Premix Tube With Air-Blast Nozzle

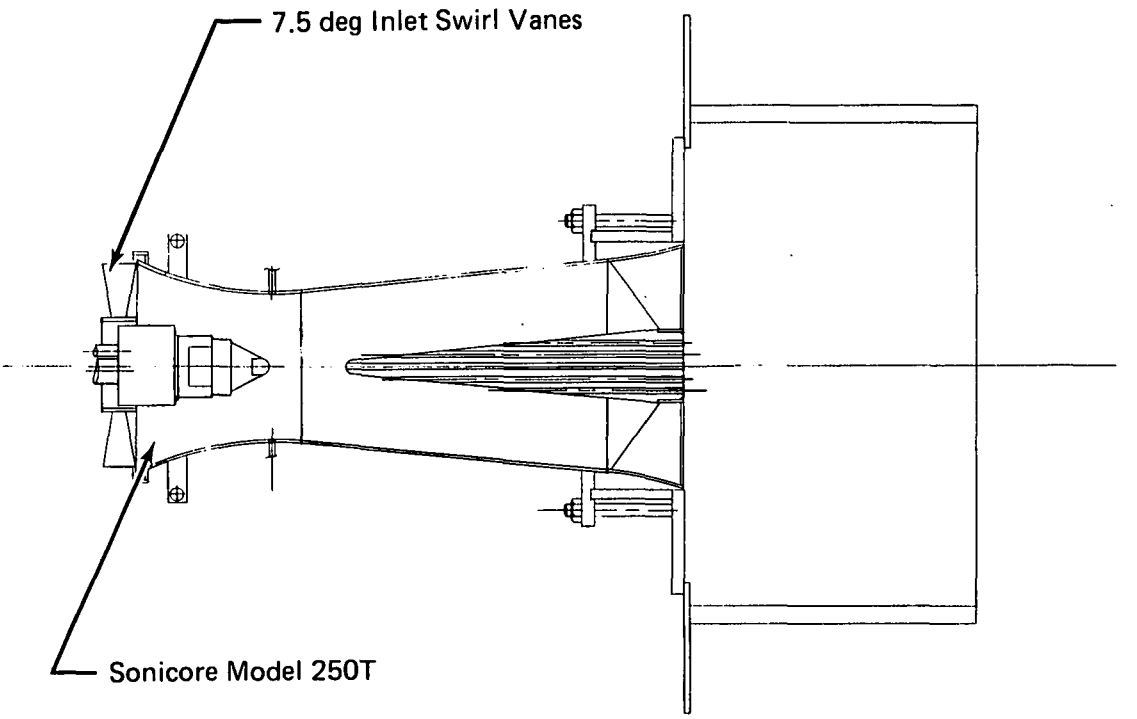

Figure 56. Scheme 22-26A — New Premix Tube With Air-Boost Nozzle and Inlet Swirl

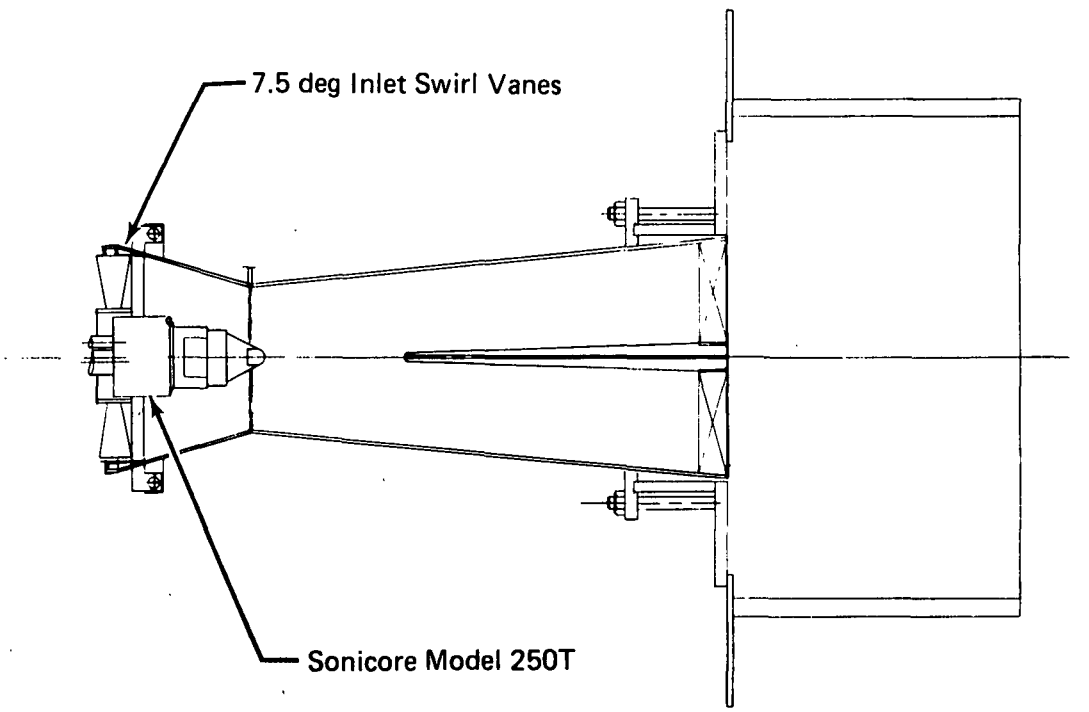

Figure 57. Scheme 22-27A — Original Premix Tube With Air-Boost Nozzle

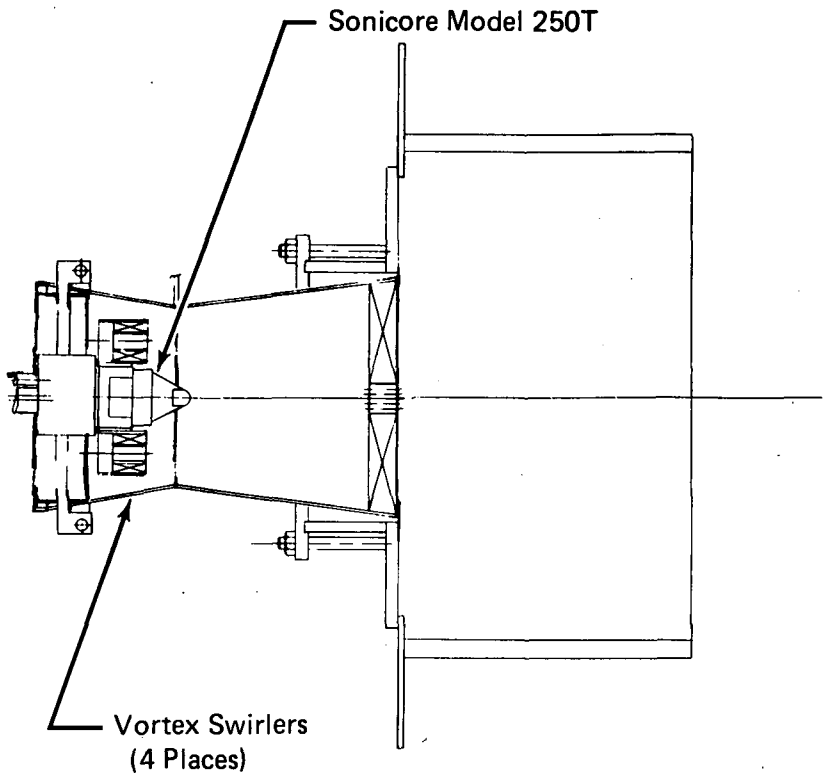

Figure 58. Scheme 22-25A — Short Premix Tube With Air-Boost Nozzle and Vortex Spreaders

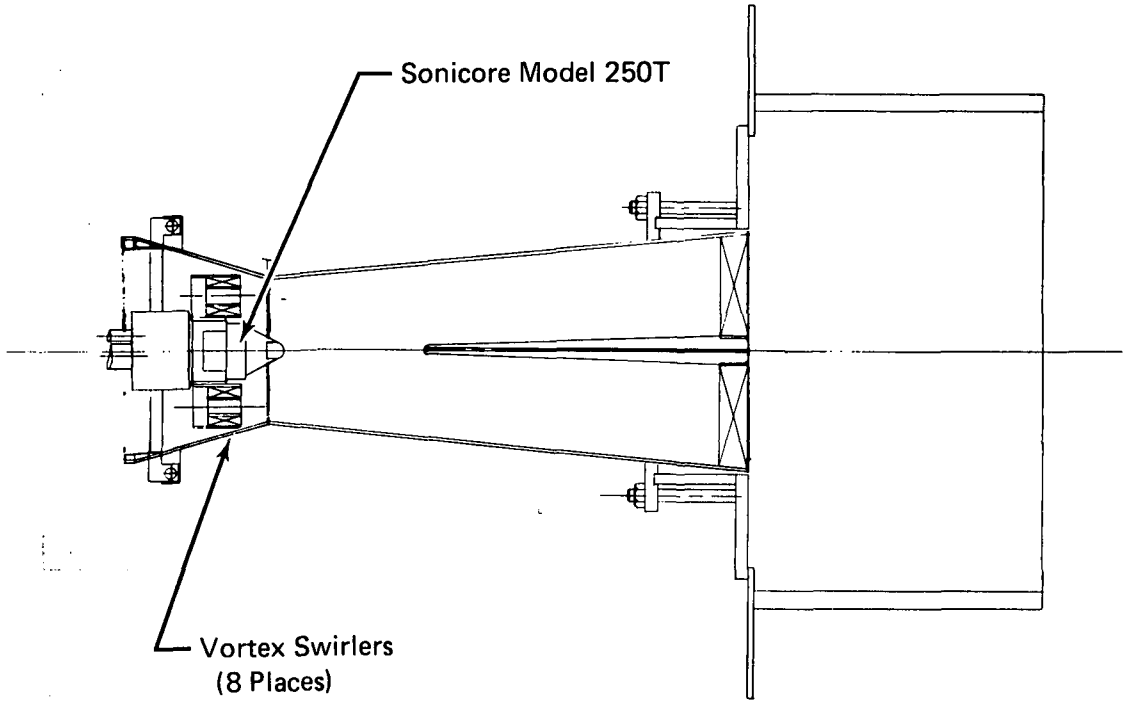

Figure 59. Scheme 22-28A — Original Premix Tube With Air-Boost Nozzle and Vortex Spreaders

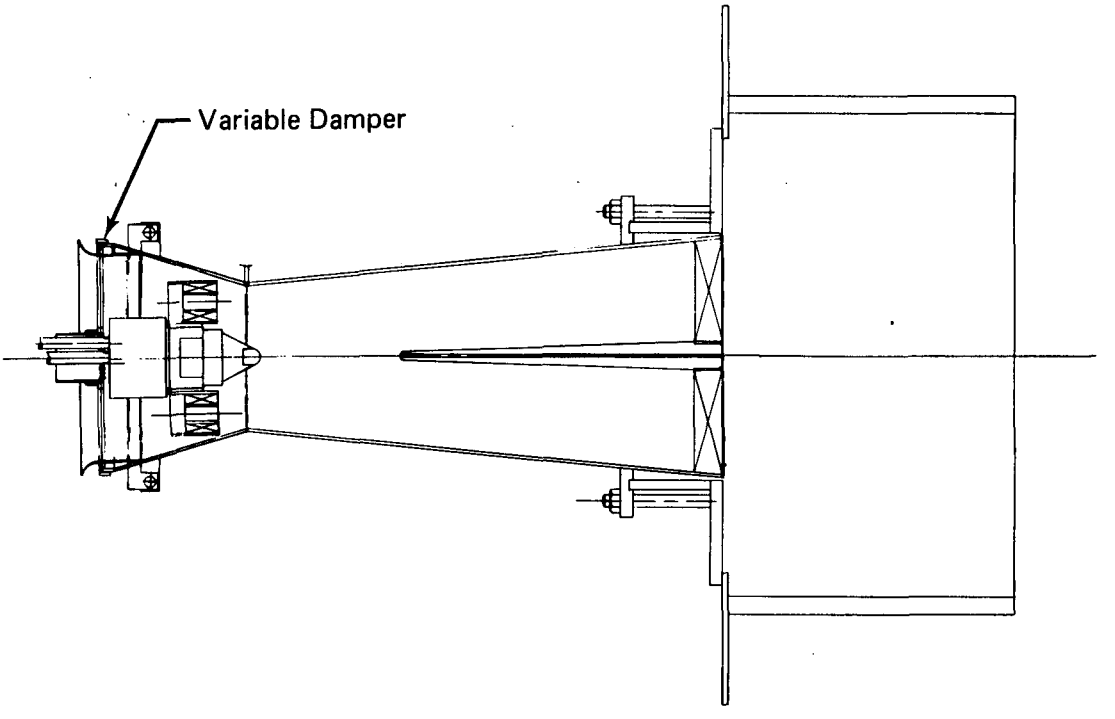

Figure 60. Scheme 22-29A — Original Premix Tube With Air-Boost Nozzle, Vortex Spreaders and Variable Damper

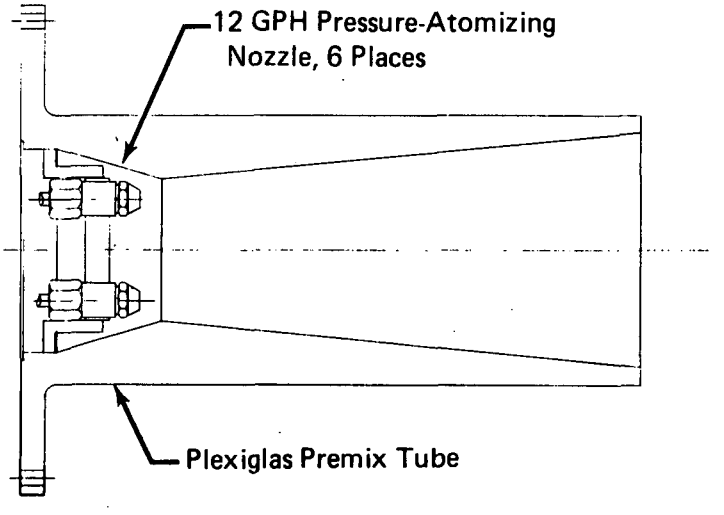

Figure 61. Scheme 22-19B — Configuration for Flow Visualization Test of Six-Nozzle Cluster Fuel Injector

(b) Air-Boost Nozzles

To provide greater atomization capability, energy from an external source can be utilized. "Air-boost" atomization calls for the use of compressed gas as a convenient means of providing a localized source of high energy at the point of fuel injection. A Sonicore nozzle, model 250T, was selected for evaluation in bench testing. Configurations utilizing both inlet swirl vanes and vortex spreaders to promote an even fuel distribution were constructed, as shown in Figures 56 through 60 (Schemes 26-25A through 26-29A). A larger capacity Sonicore nozzle, Model 281T, was also selected for evaluation, and subsequently tested with no provision for aerodynamic spreading of the fuel (Scheme 26-23A, Figure 62).

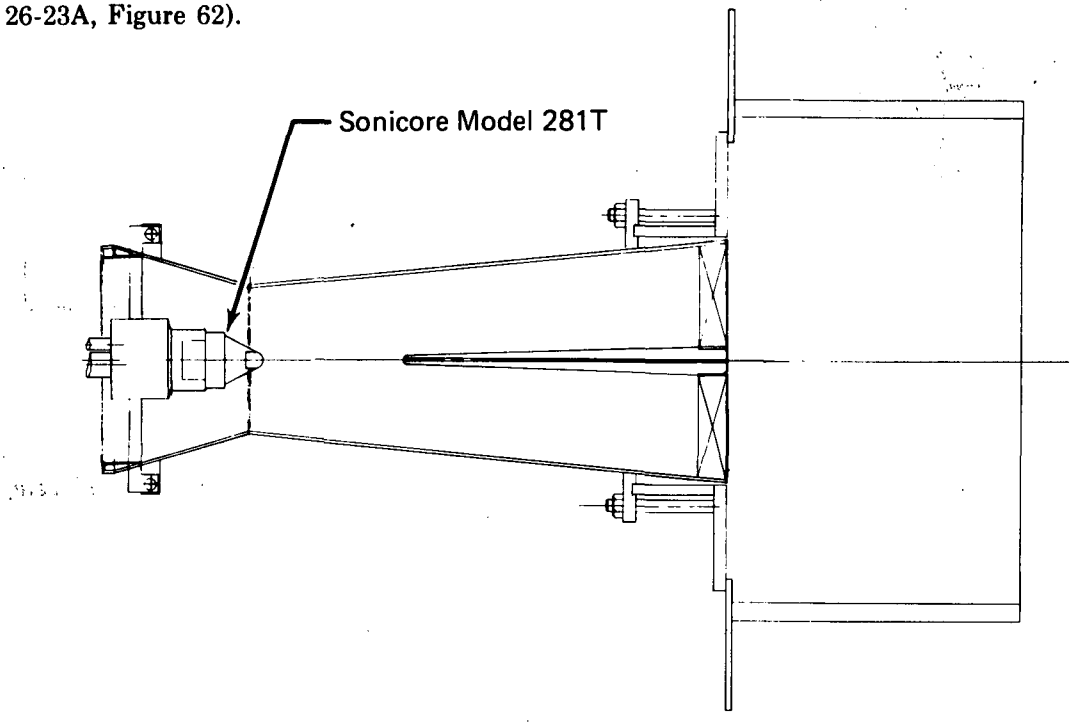

Figure 62. Scheme 22-23A — Original Premix Tube With Air-Boost Nozzle (No Inlet Swirl)

(c) Modified Sprayring Injectors

The sprayring-type injector employed in the original full-scale premix tube design had inherently good fuel distribution characteristics (because of the basic ring arrangement which allows fuel to be introduced through 16 jets into equal-area sectors of the premix passage) but did not provide acceptable atomization of the fuel in initial tests. Two modified designs were proposed: (1) a sprayring having "segmented" or multiple individual splashplates designed to eliminate the pooling of liquid from adjacent fuel jets which had occurred on the surface of the original full-ring splashplate (pooling had been observed in some flow visualization tests); (2) a sprayring with no splashplates, designed to operate a low pressure drop (thereby producing low-velocity fuel jets that do not penetrate to the premix tube wall) — the number of fuel jets was increased from 16 to 64. The two sprayring injector configurations, Schemes 26-18A and 26-20A are shown in Figures 63 and 64.

Component tests were conducted to evaluate the various fuel-injector designs described in the previous section.

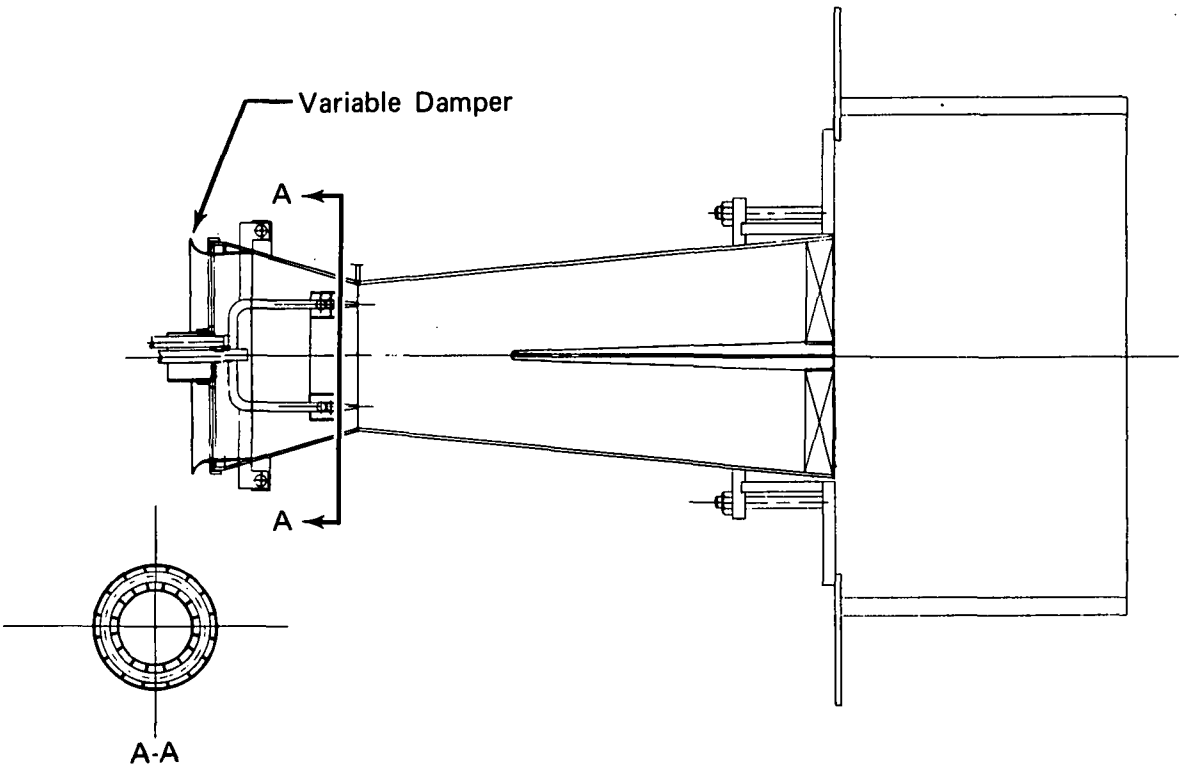

Figure 63. Scheme 22-18A — Original Premix Tube With Spray-Ring Injector and Segmented Splashplates

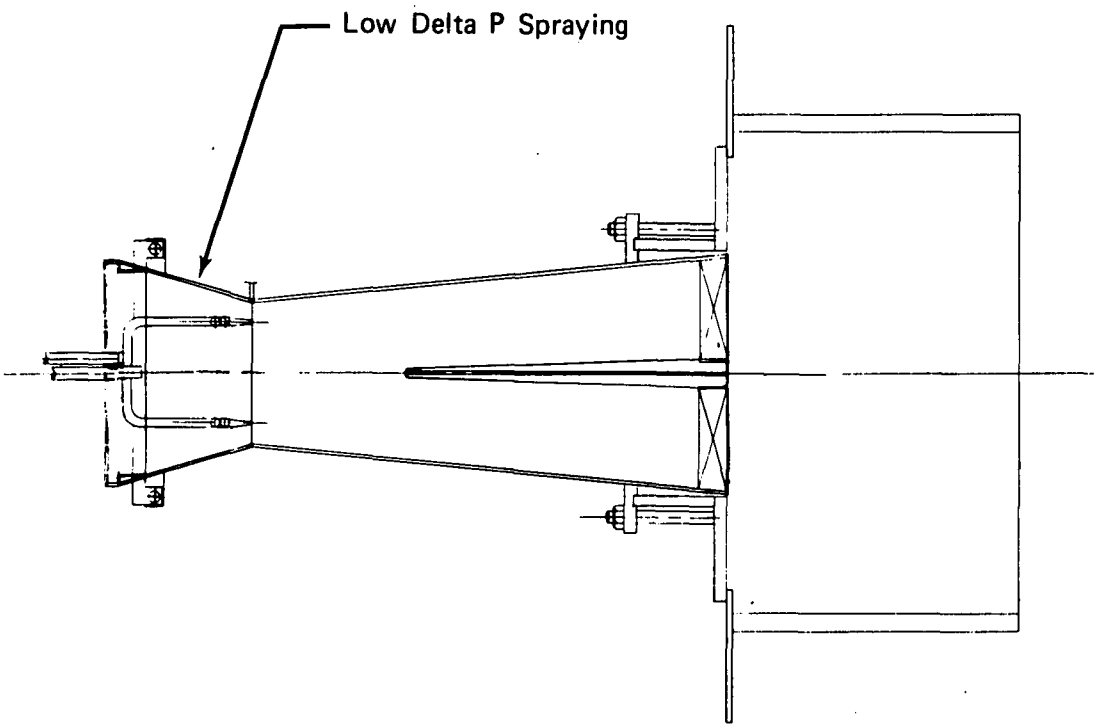

Figure 64. Scheme 22-20A — Original Premix Tube With Low Delta P Spray Ring

The tests performed and the highlights of the results obtained are summarized in Table X. All tests (both flow visualization and combustion tests) were conducted at ambient pressure, and at nominal design-point premixing passage velocities. The rig inlet air was preheated to 600°F in the combustion tests.

As indicated in Table X, the results obtained with segmented splashplates (Scheme 26-18A) indicated no significant improvement in flame quality with respect to the previous full-ring splashplate used on the original sprayring injector. Similarly, the six nozzle cluster design (Scheme 26-19B, utilizing 12 GPH pressure atomizing nozzles) was found to produce a poor distribution of fuel in the flow visualization tests conducted.

The low-delta-P sprayring (Scheme 26-20A) was a generally successful design, producing a good quality flame with only traces of luminous burning.

Among the three types of centrally-mounted fuel nozzles that were evaluated (pressure atomizing, air-blast, and air-boost), flame quality ranged from acceptable (Scheme 26-23A, employing an oversize Sonicore nozzle with no flow-spreading device) to excellent (Schemes 26-28A and 26-29A, Sonicore nozzle with 8 vortex spreaders). In all the central-nozzle schemes except 26-28A and 26-29A, there were local concentrations of fuel (and traces of luminous flame) in the center of the primary combustion flow field.

The most promising configuration (Scheme 26-29A), which was ultimately selected for evaluation in the full-scale combustor, produced an excellent quality flame (no luminous burning) and a uniform fuel distribution. A photograph of the flame obtained with this scheme is presented in Figure 65. The use of an air-boost (Sonicore) nozzle was viewed as a potential drawback, because of the implied requirement for an external boost compressor. However, the very fine atomization produced by the Sonicore nozzle was believed to be a factor in the outstanding premixing performance obtained with this scheme. The selection of Scheme 26-29A for use in the full-scale combustor was made with a view toward establishing a limiting case in which the emission characteristics achievable with very good premixing could be demonstrated.

3.1.4 Revised Premix Tube Designs

In the second verification test series performed using the complete full-scale combustor the air-boost premix tube (Scheme 26-29A, shown in Figure 60) was employed. As described in section 3.2.2, low NO_x concentration levels were demonstrated, a result attributed primarily to the superior atomization characteristics of the air-boost nozzle. At the same time however, preignition of the fuel took place inside the premixing passage and damage to the premix tube swirl vanes was incurred. The damage was similar that encountered in the initial tests of the full-scale combustor.

Subsequent technical activity was directed toward the elimination of preignition in the full-scale premix tube. An in-house design review was held, and it was concluded that modifications to the basic premix-tube configuration specifically aimed at reducing the likelihood of preignition should be made. Two alternative premix tube designs were proposed. Both incorporated modifications specifically aimed at reducing the likelihood of preignition.

TABLE X.
PREMIX TUBE COMPONENT TESTS OF ALTERNATIVE FUEL INJECTORS

Scheme	*Type Test*	*Purpose*	*Results*
26-18A	Combustion	Evaluate sprayring with segmented splashplates	Generally poor quality flame (luminous, opaque) but slightly better than baseline Scheme 26-13A.
26-18B	Flow Visualization	Check fuel atomization and distribution	Segmented splashplates eliminate some local concentrations of liquid.
26-19B	Flow Visualization	Evaluate 6-Nozzle Cluster	Excessive wetting of wall.
26-20A	Combustion	Evaluate low delta P sprayring (no splashplates)	Generally good flame quality (trace of luminous flame).
26-20B	Flow Visualization	Check fuel atomization and distribution	Good atomization; acceptable distribution (fuel spreads almost to wall and to center of passage).
26-21A	Combustion	Evaluate air-blast nozzle with 5 deg inlet swirl vanes	Good flame quality (trace of luminous flame) slight concentration in center.
26-21B	Flow Visualization	Check fuel atomization and distribution	Coarse spray produced by nozzle but atomized by droplet shattering; liquid does not quite spread to wall.
26-22A	Combustion	Evaluate dual orifice nozzle with 2.5 deg inlet swirl vanes	Good flame quality using primary orifice only (secondary too large for ambient testing).
26-22B	Flow Visualization	Check fuel atomization and distribution	Secondary orifice flowed and found to have wider spraycone, may cause wetting of wall at high pressure.
26-23A	Combustion	Evaluate Sonicore nozzle	Acceptable flame quality but concentration of luminous flame in center.
26-24A	Combustion	Evaluate air-blast nozzle with 5 deg inlet swirl vanes in short premix tube	Good flame quality (trace of luminous flame) slight concentration in center.
26-25A	Combustion	Evaluate Sonicore nozzle with 4 vortex spreaders	Good quality flame except slight concentration (trace of luminous flame) in center.
26-26A	Combustion	Evaluate Sonicore nozzle with 7.5 deg inlet swirl vanes in new premix tube	Excellent quality flame except slight concentration in center. Swirl strength improved.
26-27A	Combustion	Evaluate Sonicore nozzle with 7.5 deg inlet swirl vanes	Good quality flame except slight concentration in center.
26-28A	Combustion	Evaluate Sonicore nozzle with 8 vortex spreaders	Excellent quality flame with good distribution.
26-29A	Combustion	Same as 26-28A but with inlet damper installed	Same as 26-28A.

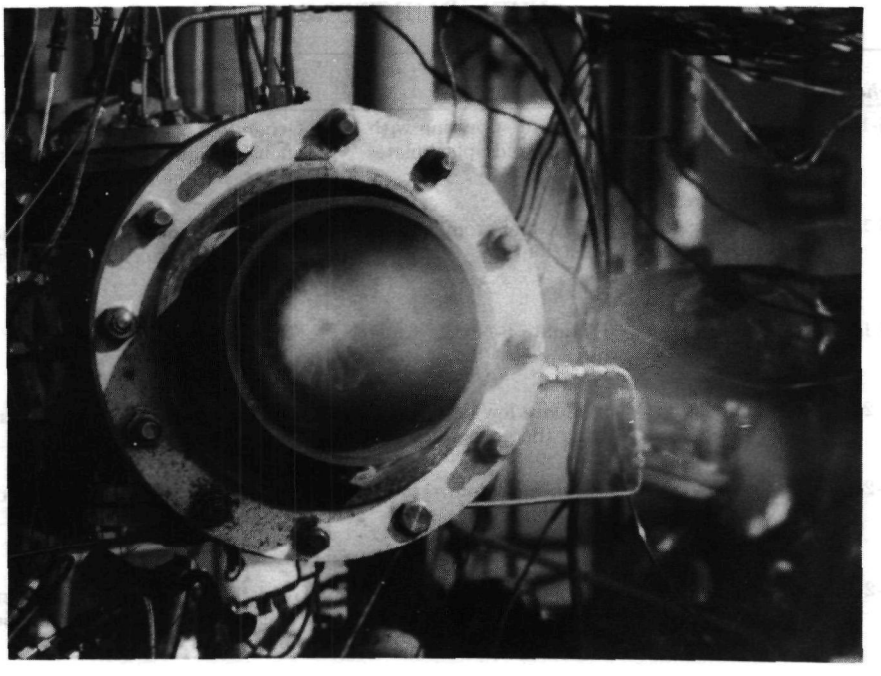

Figure 65. Flame Observed Using Premix Tube (Scheme 26-29A)

The damage to the premix tube swirler incurred during the second series of full-scale combustor tests provided a strong indication that the basic design of the diffusing section of the full-scale premix tube had been a contributing factor in the occurrence of preignition. As part of the design review, a summary comparison was made of the premix tube diffusing passage design and established criteria in the areas of autoignition, passage velocity, and flow separation. In Table XI the key elements of the comparison are identified. It may be seen from Table X that the original premix tube designs met both the autoignition and flow-separation criteria, but failed to satisfy the third criterion of maintaining a mass-average minimum velocity greater than 200 fps. This value was based on experience gained from tests of a variety of different premixing devices, and was considered generally consistent with an alternative criterion that minimum local velocities in the premixing passage be maintained at values greater than 130 fps (a conservative calculation of expected turbulent flamespeed under the design-point conditions specified for the premixing passage of the full-scale combustor was used to determine the value of 130 fps). Because the minimum mass-average velocity in the original basic premix tube design (which occurs at the leading edge of the swirler) is only 130 fps, it was reasoned that lower local velocities were probably present in the flowstream (along the wall or due to profiles in the free stream) during tests of the full-scale combustor, and that conditions favorable for flame stabilization were set up in these regions.

TABLE XI
PREMIX TUBE DESIGN REVIEW SUMMARY*

Parameter	*Criteria*	*Original Premix Tubes (1 & 2)*	*Redesign*
Autoignition	τ res <1 29 ms at 800°F	τ res = 3.6 ms	τ res = 0.8 ms τ res = 1.0 ms
Passage Velocity	$V_{min} >> S_T$ max ~ 130 fps local min ~200 fps avg min	130 fps average minimum	350 fps average minimum
Flow Separation	Conical half-angle of 6 deg or less	5.6 deg	5.6 deg

To provide an additional margin against preignition, it was proposed that passage velocities be increased substantially. To accomplish this objective the length of the diffusing passage and the diameter of the passage at the discharge plane were both reduced. In Figure 66, the revised premix tube diffusing passage design is shown in conjunction with a centrally-mounted air-boost fuel nozzle. A second proposed version of the modified premix tube is shown in Figure 67. This design featured a radial "spoke" spraybar and a smaller throat diameter (to achieve a higher air velocity for improved fuel atomization). In order to meet the design criterion for flow separation (half-angle less than 6 deg) it was necessary to increase the length of the diffusing section in this design. In order to maintain the required premix tube air pressure drop (avoiding an increase due to the adoption of a swirler having a smaller diameter) it was necessary to reduce the swirler vane angle from 45 to 26 deg in both designs, thereby providing the same effective flow area.

The proposed air-boost premix tube configuration was assembled utilizing a Sonicore nozzle and 5 deg inlet swirl for aerodynamic fuel spreading. This configuration, shown in Figure 68, was combustion tested in the component rig facility to determine its general performance. During these tests a bistable mode of flameholding was observed. Near lean blowout the premix tube flame was entirely blue and was anchored at the centerbody of the swirler. At slightly higher equivalence ratios (still fuel lean) the flame had the appearance of being locally fuel-rich in the center. As higher operating equivalence ratios were approached, the mixture apparently exceeded the local (rich) flammability limit in the center of the combustion duct, and the flame lifted from the swirler and became stabilized just downstream at the rig discharge plane where the entrainment of ambient air could take place. Because of the observed fuel-rich region of flame in the center of the combustion duct, and the related lifted-flame phenomenon, it was concluded that the method of fuel spreading employed (inlet swirl) was ineffective at the low fuel flowrates required under bench-test (atmospheric pressure) operating conditions. At low fuel flows the Sonicore nozzle is a very effective atomizer. The small fuel droplets produced tend to follow local air patterns and remain in the stream tubes in which they were deposited by the fuel injector. The influence of the centrifugal force field set up by the inlet swirler is less pronounced for small droplets than for larger droplets, with the result that less spreading of the fuel occurs. At higher fuel flows, the Sonicore nozzle performance declines (larger values of SMD are encountered) with the result that droplet spreading may improve. This result is indicative of a generally undesirable trade-off between atomization and distribution associated with the use of air-boost nozzles.

The second configuration (Scheme 26-33A, Figure 67) was also combustion tested. Results showed that both the atomization and distribution of fuel provided by the radial spraybars were excellent. Because of these results, and because of the greatly increased margin against flashback provided by this design, Scheme 26-33A was selected for testing in the full-scale combustor.

*Refer to Appendix B for SI unit conversion

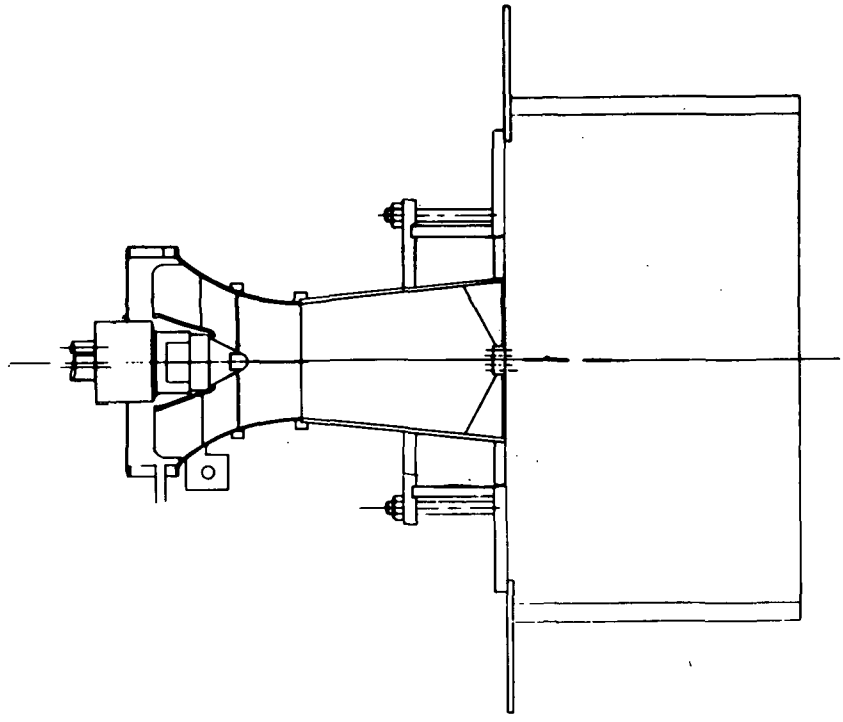

Figure 66. Revised Premix Tube Design Incorporating Air-Boost Nozzle

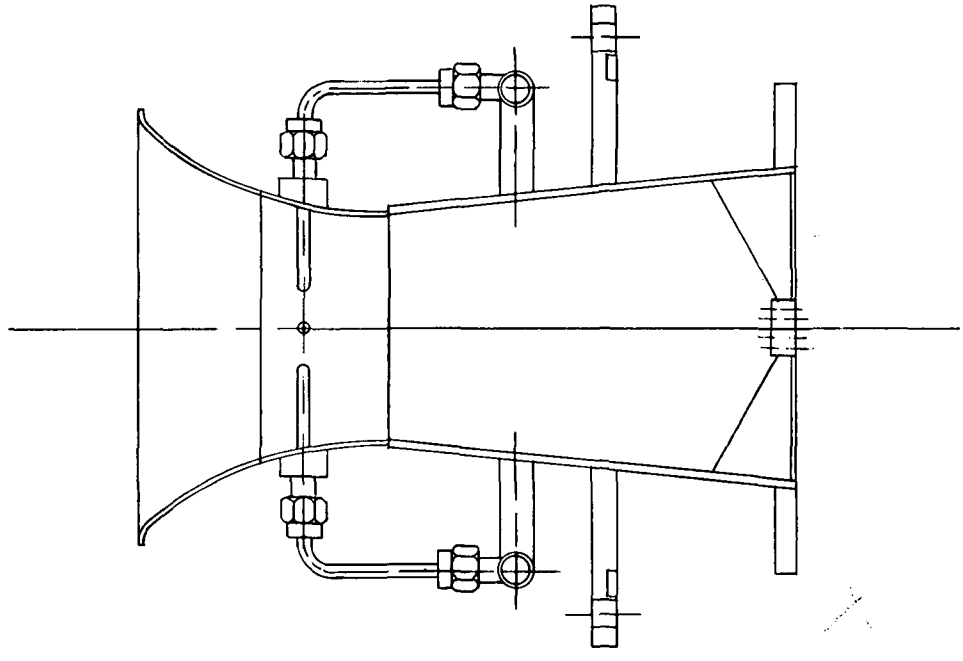

Figure 67. Revised Premix Tube Design Incorporating "Spoke" Fuel Injector

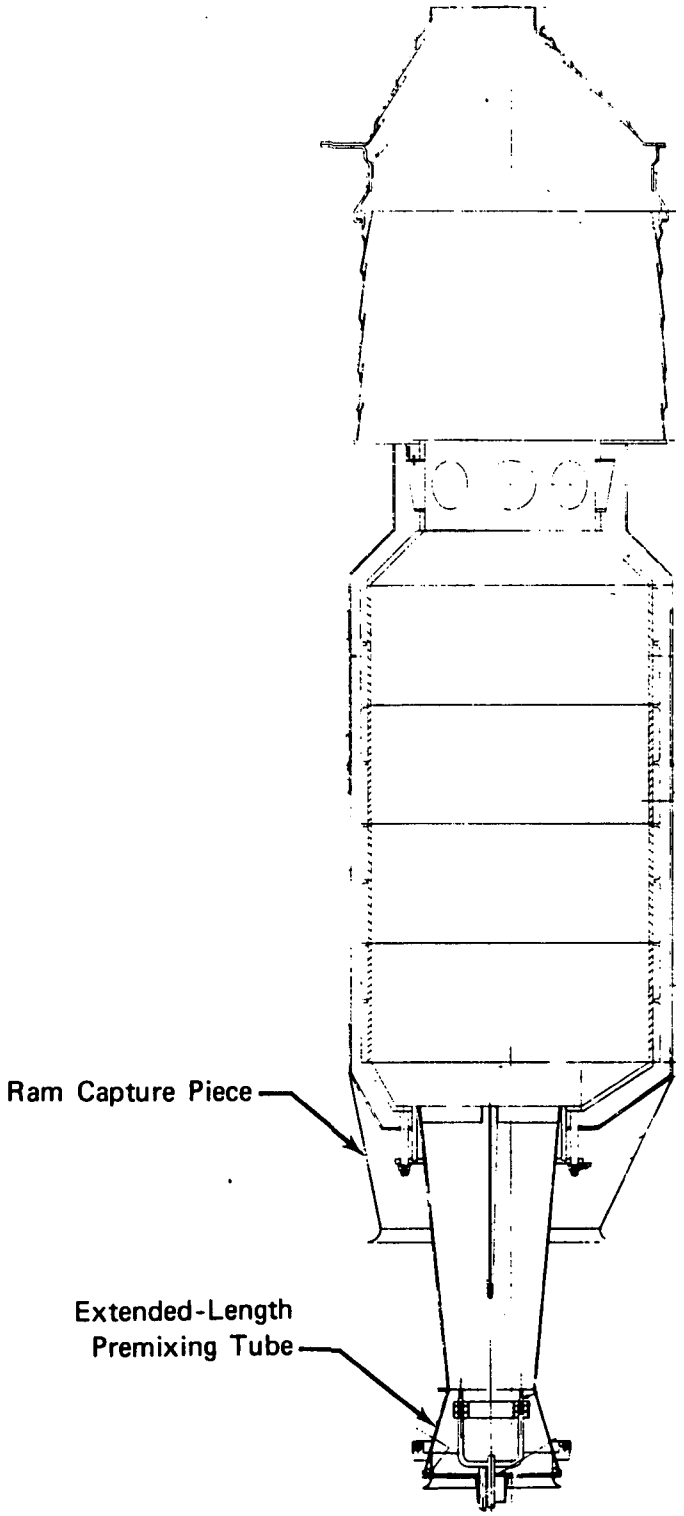

Figure 68. Full-Scale Combustor Scheme FS-01A

3.2 FULL-SCALE COMBUSTOR VERIFICATION TESTS

Verification Testing of the complete full-scale combustor was accomplished in four parts, each consisting of the evaluation of a separate configuration. The first three configurations were variations of the Full-Residence-Time (FRT) version of the combustor utilizing different premix tubes. A major portion of the Phase IV development effort was devoted to evaluation and development of the premix tube. Testing of each of the three FRT combustor configurations was preceded by extensive premix tube component testing (see the discussion of that effort in Section 3.1). The fourth and final configuration consisted of the short-length, engine-compatible version (ECV) of the full-scale combustor tested in conjunction with the premix tube from the third configuration of the FRT combustor.

A general description of the full-scale combustor rig hardware and related equipment was given in Section 2.10.

In this subsection, the full-scale combustor verification tests are described in chronological order and grouped according to the four configurations evaluated.

3.2.1 Initial FRT Configuration (Scheme FS-01A)

Verification testing of the full-scale combustor was initiated as part of a general checkout of rig systems. A brief test of the basic FRT combustor including the extended-length premix tube (Scheme 26-12A, Figure 50), was conducted. The configuration, designated Scheme FS-01A, is shown in Figure 68.

There were several objectives in the initial tests, including the checkout of rig systems, calibration of the combustor with regard to internal airflow distribution (for comparison to the aerodynamic model predictions described in Section 2.8), determination of the general operating characteristics of the combustor, and determination of a basic emission signature.

The results of the tests showed generally satisfactory functioning of rig systems. The combustor internal airflow distribution, as determined by total and static pressure measurements in the primary liner cooling shroud, and by static pressure measurements at the throat of the premix tube, closely matched the analytical model predictions. Problems were identified in the operation of the premix tube, and in the basic combustor emission signature. The test results indicated that the degree of fuel preparation provided by the full-scale premix tube had been substandard, and that local ignition of the fuel-air mixture upstream of the swirl vanes had occurred. Visually the flame (as seen on the video monitor) appeared very luminous with characteristics indicative of diffusion burning. Post-run observations showed locally heavy carbon deposits on the swirler and primary liner as if fuel had run out of the premixing tube along portions of its wall. Also, the center sections of seven swirler vanes were burned through, as a result of the fuel preignition.

The exhaust emission data, shown in Figure 69, indicated that the emission signature associated with the Rich Burn/Quick Quench concept in bench-scale tests had been duplicated in some respects in the full-scale combustor (the NO_x curve, in particular, exhibited a peak and a minimum region or "bucket" similar to the curve shown in Figure 5 for the bench-scale combustor). However, there were significant differences, including the absence of a peak in the CO curve (CO concentrations increased asymptotically as overall equivalence ratio setting was reduced, apparently toward lean blowout of the combustor), and the relatively high NO_x concentration (56 ppmv at 15% O_2, compared to levels of 36 ppmv and lower obtained for the bench-scale combustor) measured in the minimum region of the NO_x curve. These differences in the basic emission signature were consistent with the observed deficiencies in premix tube performance. For example, the apparent asymptotic increase in CO toward lean blowout at low

overall equivalence ratios was consistent with the observed condition of very poor fuel preparation in the primary zone (efficient burning would have been possible only after a sufficient quantity of fuel had been introduced to support combustion in the secondary zone; hence, lean blowout would have been overcome only at the higher overall equivalence ratio settings). The increased NO_x concentration measured at bottom of the NO_x curve bucket (in comparison to bench-scale results) was also consistent with the occurrence of fuel preignition in the premix tube, and, in general, with burning under nonpremixed conditions in the primary zone.

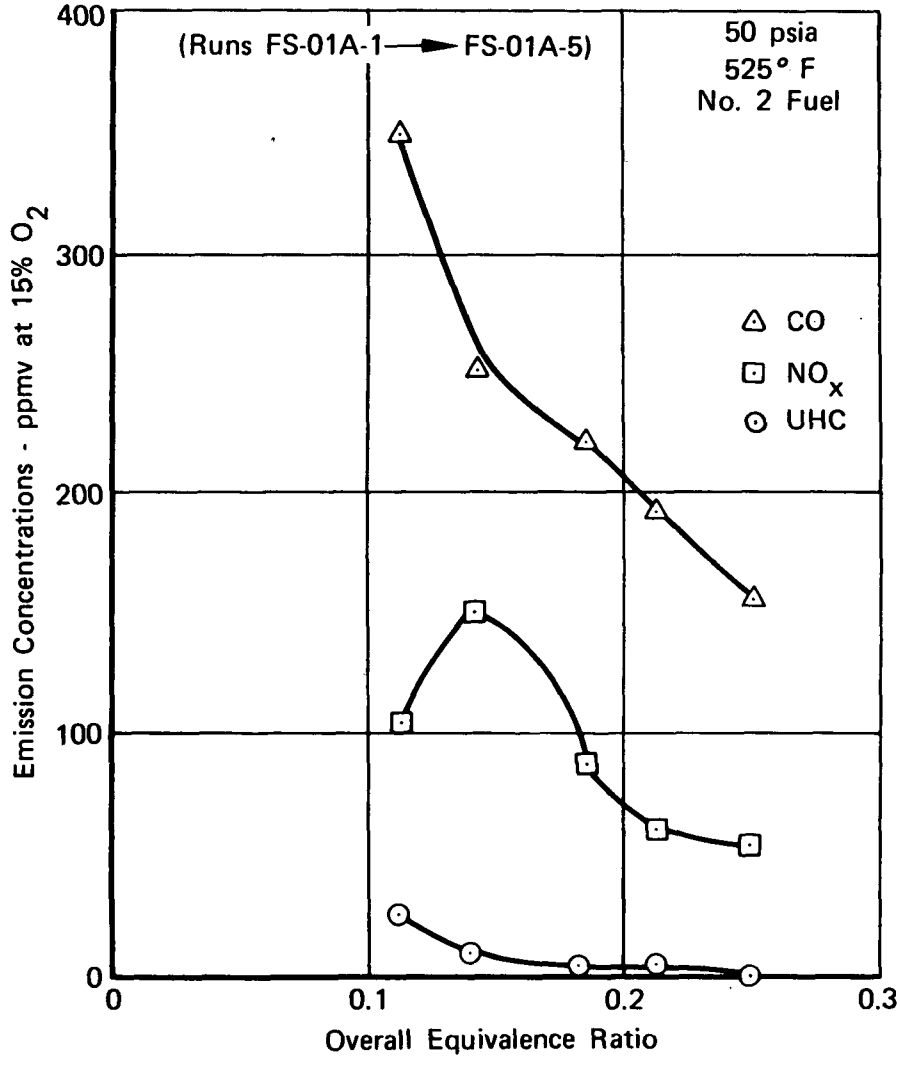

Figure 69. Variation in Emission Concentrations With Overall Equivalence Ratio for Tests Conducted With Scheme FS-01A

The data obtained for Scheme FS-01A during the initial test series are presented in Appendix A, as part of the complete test results for the full-scale combustor. The tables contain the major parameters necessary to specify combustor operating conditions, and contain liner temperature and exhaust emission data.

Several potential causes of the occurrence of flameholding within the premixing passage were proposed and investigated: the possible separation of flow along the wall of the diffusing passage; severe swirler vane separation; fuel collection and flameholding in recirculation zones caused by wakes from the damper; nonuniform approaching airflow; and a possible TEB leak ("TEB" or triethyl borane, a pyroforic liquid, was injected through the premix tube to effect ignition of the combustor). Two of the proposed causes (nonuniform approach airflow and TEB leak) would have accounted for both the observed internal flameholding and the apparent deterioration in the quality of premixing.

After examination of the data and the test rig, no immediate conclusion was reached. Because of the relatively low velocity of airflow entering the plenum section of the rig (in which the combustor was mounted), serious distortions in the airflow approaching the combustor appeared unlikely. Flow separation in the diffusion passage of the premix tube or at any appreciable distance downstream of the damper were considered unlikely because these conditions had not been observed in the initial premix tube component verification tests. Swirler vane separation was viewed as an insufficient cause of the observed fuel preignition without other contributing factors, such as the presence of regions of stagnation of reverse flow inside the premixing passage (separation of the flow passing over the swirler vanes is an accepted occurrence in other proven premix tube designs). The possibility of a steady TEB leak, which would have served as a source of continuous ignition for fuel in the premixing passage, could not be dismissed on the basis of available evidence.

In preparing for further tests of the full-scale combustor, several steps were taken to ensure that the various potential problem areas identified (even though subsequently discounted) would no longer be a factor in the operation of the combustor. Included were the following rig modifications:

a. The front of the burner was elevated so that the burner axis made about a five-degree angle with the plenum case axis. This change was meant to promote a more direct flowpath between the rig entrance duct and the premix tube, and reduce airflow distortions at the premix tube inlet. A comparison of rig configurations before and after this change may be seen in Figures 70 and 71.

b. The rig direct-fired air preheater was relocated to a position two feet upstream of the original location in the duct leading to the rig plenum. This change was made to allow more time for any preheater-induced flow distortions to "wash out," and also give a more uniform temperature profile when the preheater is used.

c. The method of TEB injection was changed to provide for introduction directly into the primary zone of the combustor rather than through the premixing passage. In the initial tests of the full-scale combustor, the possible leakage of TEB into the premixing passage during steady-state operation was postulated as a likely cause of damage to the premix tube swirler. Relocation of the TEB line eliminated this type leakage as a factor in future testing.

d. Additional instrumentation was provided to ascertain airflow profiles into the premix tube. Twelve total pressure probes were added at four circumferential and three radial locations.

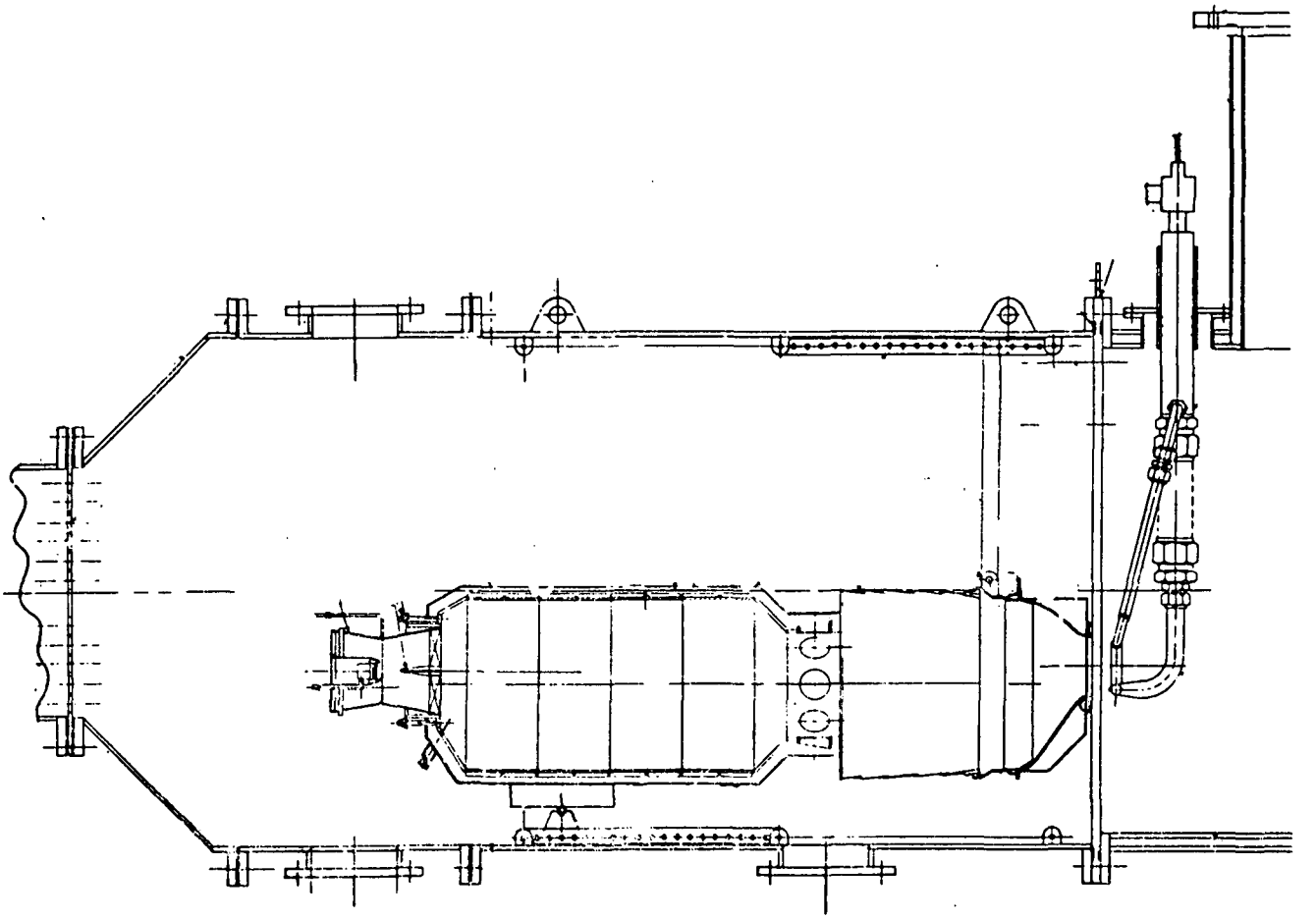

Figure 70. Original Arrangement of the Full-Scale Test Rig

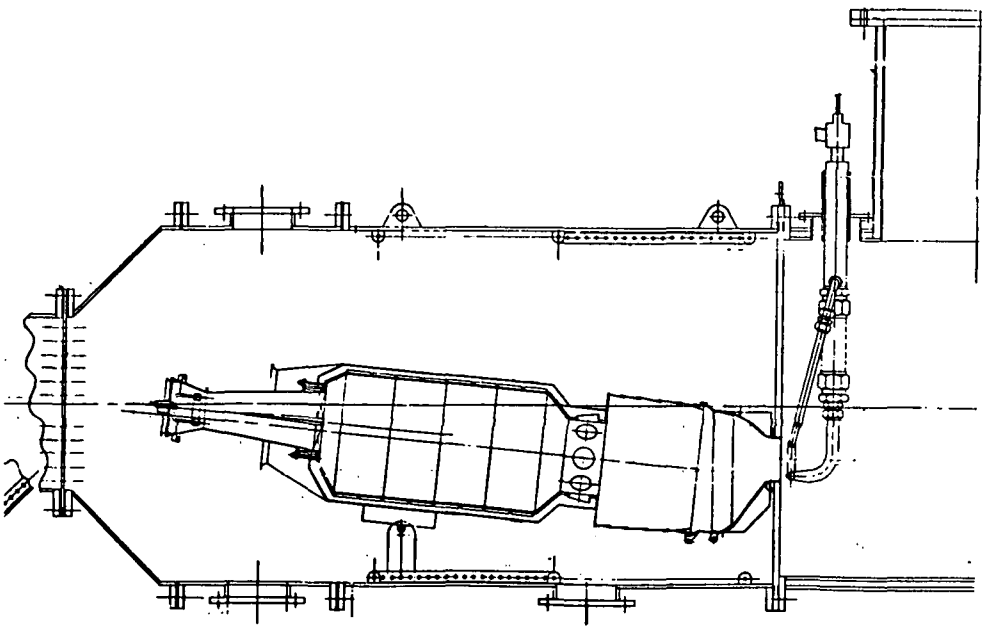

Figure 71. Arrangement of the Full-Scale Test Rig Following Elevation of the Combustor

Two further steps were taken: (1) diagnostic tests of the premix tube were conducted (as described in Section 3.1.2) in the component rig to determine further potential causes of the observed preignition and apparent deterioration in the quality of premixing; (2) at the same time, alternative fuel injector designs were formulated for subsequent evaluation in the component rig (described in Section 3.1.3).

3.2.2 Second FRT Configuration (Scheme FS-02A)

Testing of the full-scale combustor was resumed using an air-boost premixing tube. Diagnostic tests of the initial premix tube design (Figure 50) had indicated that an alternative fuel injector might be required to achieve adequate premixing. A number of modified premix tube configurations incorporating various fuel injectors and fuel-spreading devices were evaluated in subsequent component tests, as described in Section 3.1.3. The air-boost design (Scheme 26-29A, shown in Figure 60) was selected as having outstanding premixing performance (based on observations of flame quality). Because of the inherent penalty associated with the use of air-boost nozzles in a gas turbine combustor (the auxiliary equipment required is bulky and expensive), Scheme 26-29A was chosen with a view toward establishing a limiting case in which the emission characteristics achievable with very good premixing (made possible by the very fine atomization of the air-boost nozzle) could be demonstrated.

The complete combustor configuration, designated Scheme FS-02A, is shown in Figure 72. Scheme FS-02A was identical to Scheme FS-01A, except for substitution of the air-boost premix tube. There were also minor changes in the mounting arrangements for the combustor and the configuration of the rig, as described in Section 3.2.1. A single series of tests was conducted in the full-scale combustor plenum-rig facility at an operating pressure of 50 psia (nominal) and a combustor inlet air temperature of 525°F, using neat No. 2 fuel. The exhaust emission data measured are presented in Figure 73. In Figure 74, a comparison of these results to those obtained in the initial test series is shown. A very low NO_x concentration of 29 ppmv was measured at the bottom of the "bucket" in the NO_x curve. This level was 60% of the program goal of 50 ppmv. No staging of the primary-zone airflow had been attempted in the tests performed. However, it was anticipated that staging could be employed to shift the "bucket" in the NO_x curve to the left and to the right in the manner demonstrated for the bench-scale Rich Burn/Quick Quench combustor, thereby establishing a low NO_x "corridor" over the operating range from idle to full power. Bench-scale rig results had also indicated that the effect of increased operating pressure on NO_x concentration levels would not be significant. A moderate increase in NO_x would be expected, however, due to combustor inlet air temperature levels.

The CO curve in Figure 73 exhibited the same characteristic shape observed in tests of the bench-scale Rich Burn/Quick Quench combustor. The peak in the curve, however, was not as high as the levels measured for the bench-scale combustor (about 300 ppmv, compared to levels as high as 900 ppmv for the bench-scale combustor). The location of the peak also represented a variation in the full-scale combustor results with respect to those obtained for the bench-scale combustor (in representative bench-scale tests, the peak occurred in the vicinity of 0.1 overall equivalence ratio compared to 0.2 in Figure 73). It was expected that the location of the peak in the CO curve could be varied by adjusting the stoichiometry of the secondary zone of the combustor (independent control of the CO characteristics of the combustor, without any appreciable influence on NO_x characteristics, had been demonstrated in this manner in the bench-scale program). By reducing the total quantity of air admitted to the secondary zone (i.e., by reducing the sum of quick-quench airflow plus premix-tube airflow), it was anticipated that a leftward shift of the CO curve would be possible. If this adjustment were made, lower CO concentration levels would be expected in the range of equivalence ratios above 0.2. A reduction in CO concentration levels would also be expected as a result of increasing the inlet-air temperature level.

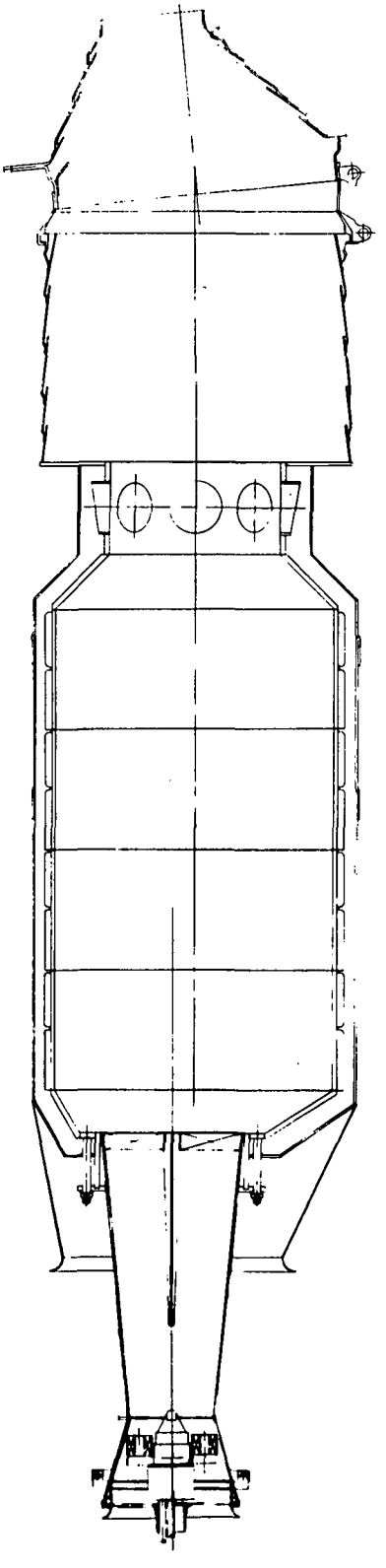

Figure 72. Full-Scale Combustor Scheme FS-02A

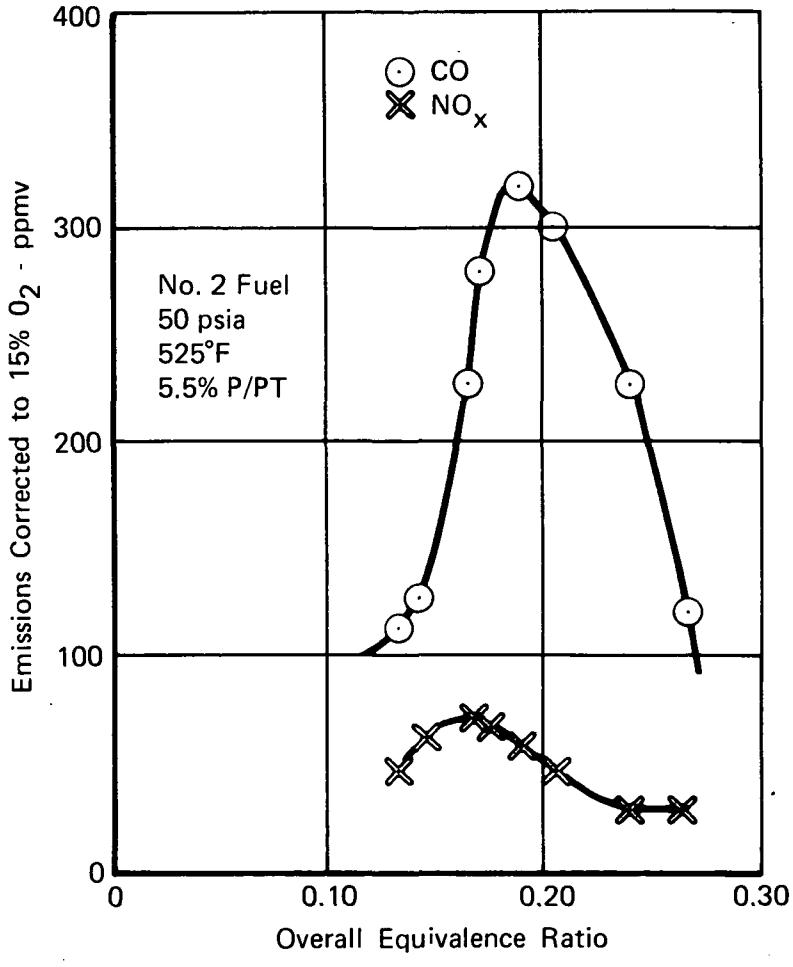

Figure 73. Variation in Emission Concentration With Overall Equivalence Ratio for Tests Conducted With Scheme FS-02A

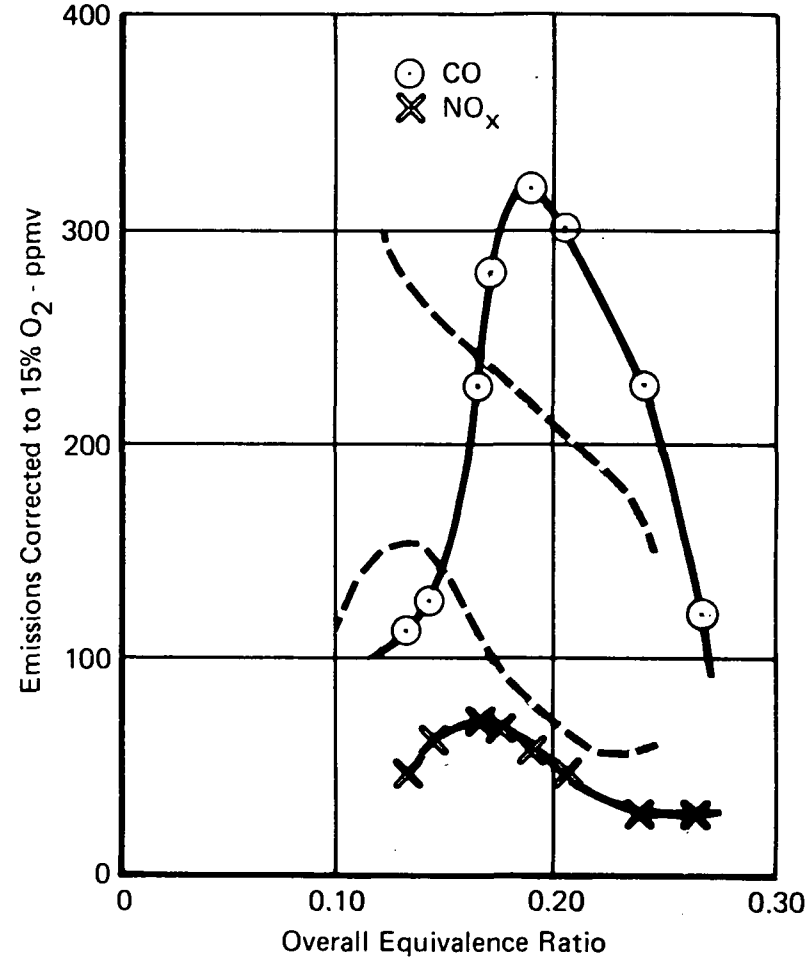

Figure 74. Comparison of Emission Data Obtained for Schemes PS-01A and FS-02A

The evaluation of Scheme FS-02A of the full-scale combustor was limited to a single series of tests because of a repeat occurrence of damage to the premix tube swirler. Inspection of the combustor following the tests, for which data are presented in Figure 73, revealed that half the swirl vanes were missing or severely damaged, apparently due to preignition of the fuel inside the premixing passage. The damage was similar to that incurred in the initial tests of the full-scale combustor.

The very low NO_x concentration levels obtained in the tests of Scheme FS-02A were attributed to the superior fuel atomization characteristics of the air-boost nozzle, and to the effectiveness of the fuel-spreading devices employed (vortex swirlers surrounding the fuel nozzle). At the same time, however, the very promising emission results achieved were seriously compromised by the recurrence of the preignition phenomenon observed in Scheme FS-01A. Subsequent to the second test series, it was decided that modifications to the aerodynamic design of the basic premix tube (which had been the same in the two initial schemes) should be made. Following an in-house review, two revised designs were formulated, as described in Section 3.1.4. In both designs, internal premixing passage velocities were increased substantially; one configuration employed an air-boost nozzle, the other a number of radial "spoke" spraybars. The second, nonair-boost design was ultimately selected for evaluation in Scheme FS-03A of the full-scale combustor.

3.2.3 Third FRT Configuration (Scheme FS-03A)

Testing of the FRT combustor was resumed following a review of the aerodynamic design of the basic premix tube, and the subsequent formulation and preliminary testing of a revised premix tube design. The revised design, which featured higher premixing passage velocities (350 FPS minimum at the full-power setting), and incorporated a radial "spoke" fuel injector, is shown in Figure 67. The combustor configuration (Scheme FS-03A, shown in Figure 75) was identical to that tested previously except for substitution of the redesigned premix tube. In the tests conducted, a constant premix tube airflow setting was maintained. The premix tube variable damper was not used.

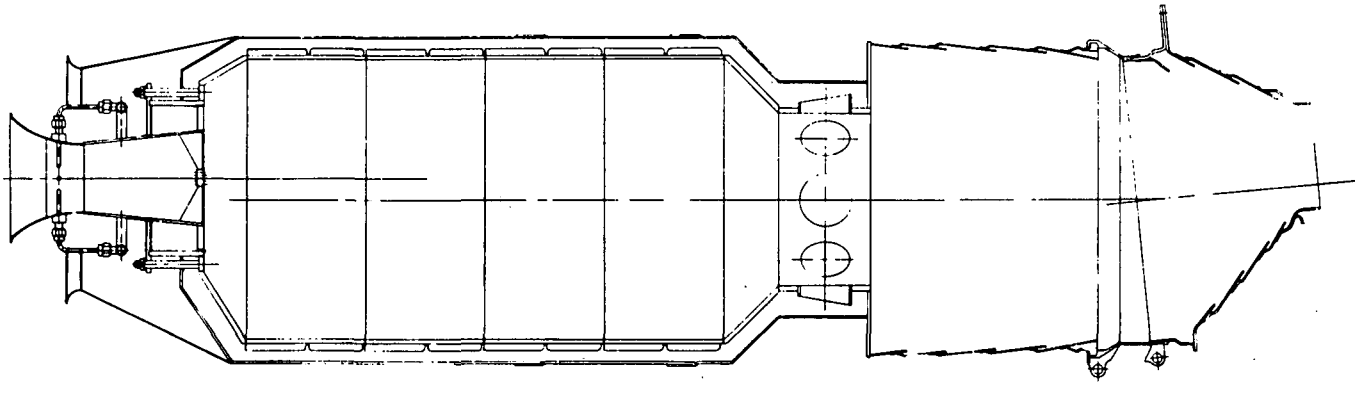

Figure 75. Full-Scale Combustor Scheme FS-03A

3.2.3.1 First Test Series

The experimental evaluation of Scheme FS-03A was accomplished in three parts. In the initial test series, the combustor was tested at 50 psia rig pressure and 450°F inlet air temperature using No. 2 fuel and No. 2 fuel with 0.5% nitrogen (as pyridine). Examination of the combustor following the tests revealed damage to the premix tube swirler, and the presence of a metal instrumentation tag in the premixing passage. The position of the tag, and the pattern of the metal discoloration in the premix tube wall (due to the uneven heating associated with internal flameholding), indicated that the tag had been ingested into the premix tube (having broken free at an upstream site inside the rig) and had lodged against the fuel injector spraybars. The resulting wake inside the premixing passage caused flameholding and damage to seven of the fifteen swirler vanes.

3.2.3.2 Second Test Series

Repairs were made to the premix tube, and the initial test series was partially repeated: data was obtained at 50 psia rig pressure and 400°F inlet air temperature using No. 2 fuel with 0.5% nitrogen (as pyridine). The emission data may be found in Table II of Appendix A for comparison purposes. Because there was no significant change in the emission characteristics of the combustor in these repeat tests, it was decided that the tests using non-nitrogenous No. 2 fuel need not be repeated. A single data point at 100 psia rig pressure was obtained during the second test series prior to a test stand malfunction (U-tube failure resulting in mercury contamination of the control room) which forced the shutdown of the rig.

3.2.3.3 Third Test Series

Data was obtained at 100 psia rig pressure and 575°F inlet air temperature using No. 2 fuel and No. 2 fuel with 0.5% nitrogen (as pyridine) in a third test series. Examination of the combustor before and after the tests showed no further distress to the premix tube swirl vanes. The combustor liner was found to be in good condition except for minor deterioration of the flamespray coating at the entrance to the quick-quench zone. It was noted that a metal band or collar on the combustor had come loose during the third test series. When in place, this band prevents the direct entry of air from the rig plenum into the quick-quench zone of the combustor, forcing it to follow an alternative path through the primary liner cooling passage. In the displaced position, some airflow was allowed to enter the quick-quench section without passing through the cooling shroud. In a separate incident, damage to the rig exit traverse probe was sustained midway through the third test series because of interrupted cooling water flow (due to the failure of a bellows section inside the rig). Five of the nine gas-stream thermocouples were destroyed, and pattern factor data were unavailable for the last five test points.

3.2.3.4 Fourth Test Series

The fourth test series consisted of an evaluation of the operation of the combustor on shale-derived DFM and verification of the previous test results obtained using No. 2 fuel (to determine whether the loosened collar on the quick-quench section of the combustor may have affected performance or emission characteristics).

The data obtained in the four test series conducted are presented in Appendix A of this report. The tables in Appendix A contain the major parameters necessary to specify combustor operating conditions, and contain liner temperature and exhaust emission data for Scheme FS-03A.

A scheme definition sheet for the configuration evaluated (Scheme FS-03A) is presented in Figure 76, showing the design point airflow distribution of the combustor, and the location of liner skin thermocouples. Calculated values of the primary and secondary airflow rates are also presented in Table IV of Appendix A for each test point.

3.2.3.5 Exhaust Emission Data

The exhaust emission data generated during the first of the three test series are presented in Figure 77. The curves obtained for both NO_x and CO exhibit the characteristic shapes documented in numerous tests of bench-scale combustor during Phase II. A minimum NO_x concentration of 26 ppmv (corrected to 15% O_2) was achieved using neat No. 2 fuel. This level compares favorably to the minimum levels achieved in tests of the bench-scale combustor (20 to 36 ppmv at 15% O_2 depending on primary zone residence time) using neat No. 2 fuel. It should be noted, however, that a direct comparison of these results is not possible because of differences in the inlet air temperature (450°F in the current results vs 600°F in the bench-scale data).

The NO_x curve obtained for No. 2 fuel with 0.5% nitrogen is less complete. However, a minimum concentration of 75 ppmv (corrected to 15% O_2) was documented. This level is higher than the minimum levels achieved in tests of the bench-scale combustor (33 to 55 ppmv at 15% O_2 depending on primary zone residence time) using No. 2 fuel with 0.5% nitrogen. Differences in primary zone residence time (60 ms, on a cold-flow basis, for Scheme FS-03A vs values of 80 to 170 ms for various schemes of the bench-scale combustor) may account for the observed increase in the NO_x concentration level. Similarly, differences in the quality of premixing and in the effectiveness of the quick-quench section may exist in the full-scale combustor relative to the bench-scale combustor, and may be a factor in the higher NO_x concentration level.

The CO concentration levels obtained in the first test series are lower than those documented in the bench-scale combustor test program (300 ppmv in Figure 77, at the peak of the CO curve, compared to values as high as 900 ppmv for the bench-scale combustor). Generally, the magnitude of the peak in the CO curve is believed to be related to the effectiveness of mixing in the quick-quench section. A lower peak concentration implies reduced mixing effectiveness. In Figure 77, the relatively low peak concentrations in the CO curves, and the slightly higher minimum NO_x concentrations already noted, were both consistent with the view that the rate of mixing achieved in the quick-quench section of the full-scale combustor (Scheme FS-03A) may have been somewhat less than that achieved in the bench-scale combustor.

The data generated during the first test series (Figure 77) also reflected the influence (if any) of damage to the premix tube swirl vanes. It was believed that ingestion of the metal instrumentation tag (which caused flameholding in the premixing passage and resultant damage to the vanes) occurred near the end of the first test series during the runs conducted using No. 2 fuel with pyridine additive (after completion of tests with neat No. 2 fuel, and after a brief interruption to replenish the stand fuel supply). The effect of the damage (and of burning in the premixing passage) on the exhaust emission data in Figure 77 was unknown. However, a comparison of the results in question with those generated in subsequent testing (in the second test series described below) had shown only minor differences in the basic emission characteristics and concentration levels.

Exhaust emission data generated during the second test series are presented in Figure 78. The second test series was conducted to determine whether the data from the first series may have been biased by damage to the premix tube. A comparison of the curves for NO_x and CO in Figure 78 to those in Figure 77, showed general agreement with regard to the characteristic shapes and the emission concentration levels, with the following exceptions.

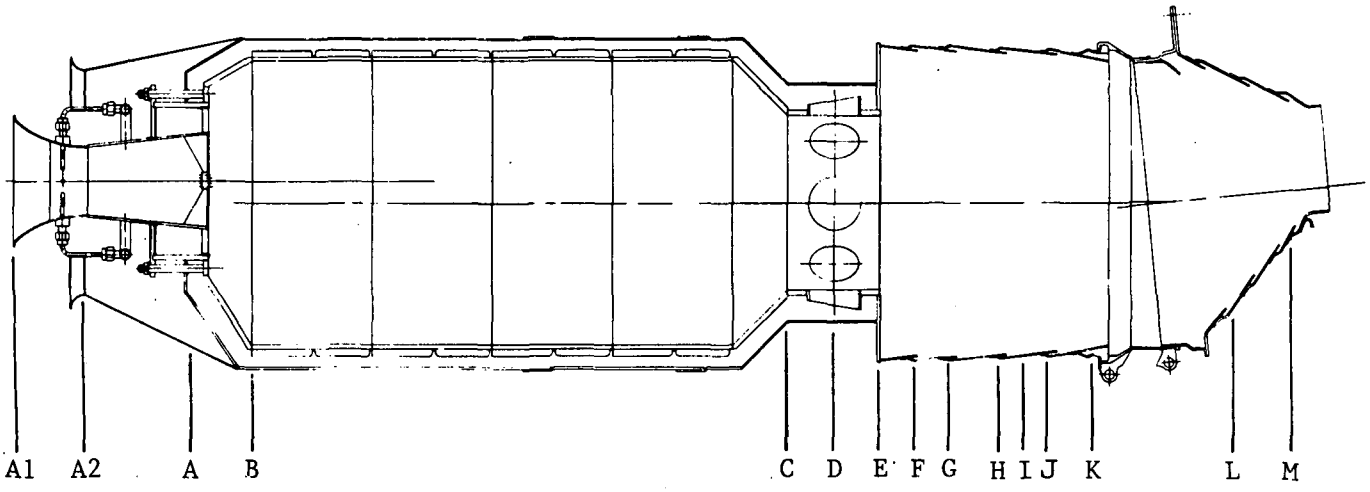

LB	AREF	L/D	VOLREF	ACDSUM
46.14	88.20	4.35	2590.0	24.12

STATION	AX	ACD	WACUM	PHI
A1	13.847	0.0	0.0	0.0
A2	4.335	0.0	0.0	0.0
A	8.038	4.978	20.641	1.285
B	75.391	0.0	20.641	1.285
C	28.260	0.0	20.641	1.285
D	28.260	10.854	65.649	0.404
E	72.346	0.0	65.649	0.404
F	72.346	0.420	67.391	0.394
G	72.346	0.523	69.559	0.381
H	72.346	0.447	71.413	0.371
I	72.346	5.049	92.349	0.287
J	72.346	0.224	93.278	0.284
K	72.346	0.829	96.716	0.274
L	72.346	0.792	100.000	0.265
M	39.337	0.0	100.000	0.265

HEADER	AXIAL LOC	RAD LOC	CIRCUM LOC
TLIN 1	7.72	4.80	0.0
TLIN 2	12.74	5.00	0.0
TLIN 3	17.59	5.00	0.0
TLIN 4	22.44	5.00	0.0
TLIN 5	31.97	4.80	0.0
TLIN 6	36.67	4.80	0.0

Figure 76. Burner Scheme Definition (Scheme FS-03A)

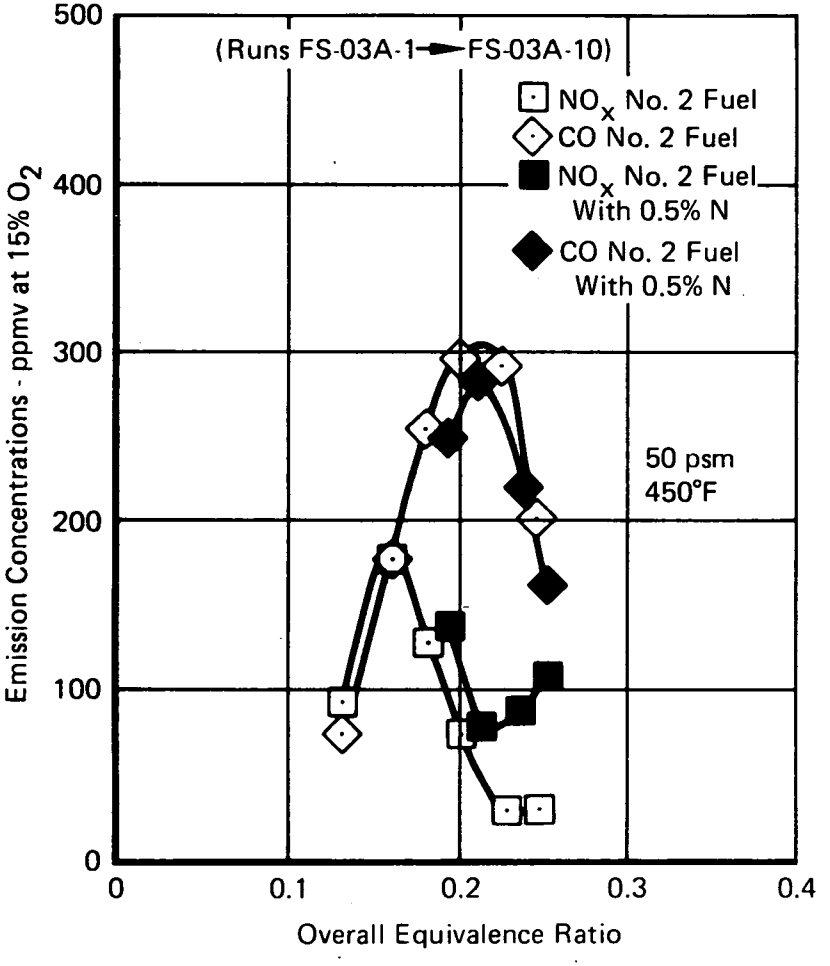

Figure 77. Variation in Emission Concentrations With Overall Equivalence Ratio for Scheme PS-03A, First Test Series

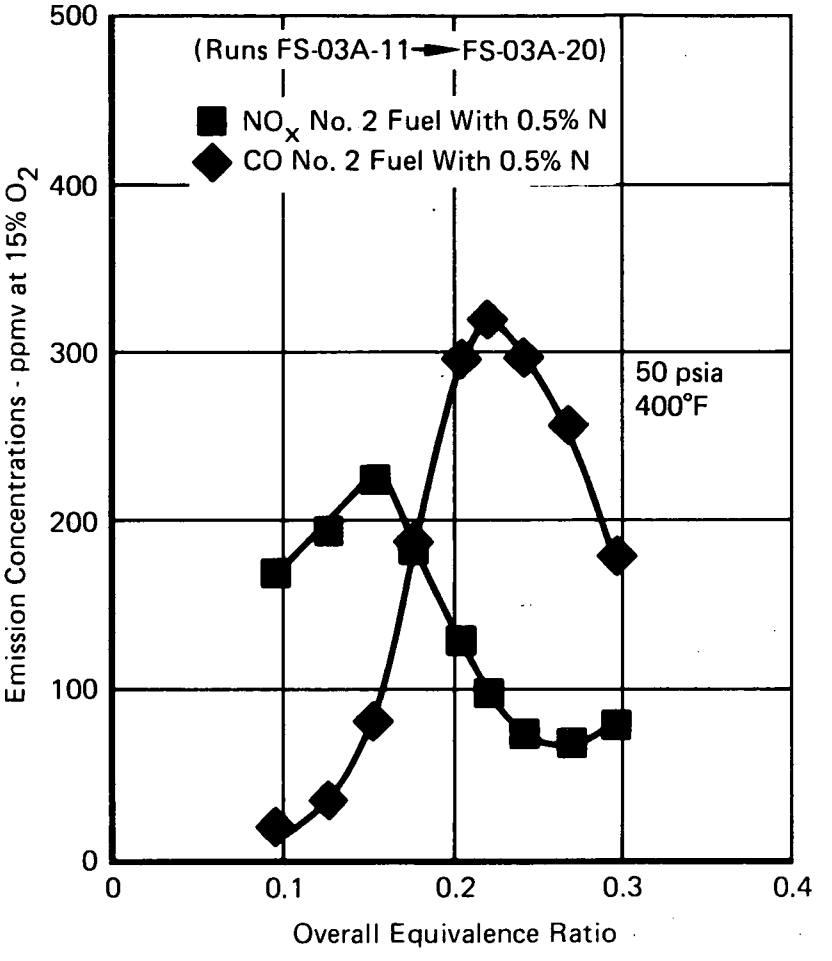

Figure 78. Variation in Emission Concentrations With Overall Equivalence Ratio for Scheme PS-03A, Second Test Series

First, the peaks in the CO and NO_x curves in Figure 78 were broader (covering a somewhat wider range of equivalence ratios on the abscissa) than those in Figure 77. Similarly, the bucket in the NO_x curve in Figure 78 was broader than the one in Figure 77. It was believed that these differences were the result of slightly lower inlet air temperatures in the second test series (400°F compared to 450°F in the first test series, as shown in Table I of Appendix A). Inlet air temperature was not independently controllable at the full-scale combustor test facility without the use of a direct-fired heater burner. To avoid the introduction of heater burner emissions as an unknown element in the initial test results, the temperature of the rig inlet air was allowed to vary in accordance with the levels available from the stand (slave engine) supply. A lower inlet temperature can be expected to promote the formation of CO (due to uniformly lower gas temperatures and increased quenching in the mixing regions of the combustor), and to reduce the rate of formation of thermal NO_x, resulting in generally higher CO concentration levels, and generally lower NO_x levels over the entire range of equivalence ratios tested. These changes would give the appearance of an increase in breadth to both the CO and NO_x curves.

A lower inlet air temperature might also be expected to cause a reduction in the degree of fuel prevaporization achieved in the premix tube of the combustor, and, as a result, serve to further reduce the slope of the NO_x vs equivalence ratio curve (the rate of formation of NO_x is more sharply responsive to changes in the burner equivalence ratio when premixed than under nonpremixed conditions). This effect may also have contributed to the increased breadth of the NO_x curve peak in Figure 78.

The second difference that can be noted in comparing the data of Figure 78 to those of Figure 77 is the shift in location of the NO_x curve bucket (from 0.22 equivalence ratio in Figure 77 to 0.27 equivalence ratio in Figure 78). The shift implies an increase in premix tube airflow in the second test series of about 20%. This result is consistent with the view that premix tube airflow in the first test series was too low as a result of the blockage created by ingestion of the metal instrumentation tag, and the resultant increase in pressure drop created by burning in the premixing passage.

Exhaust emission data generated during the third test series are shown in Figure 79. Tests were conducted at 100 psia rig pressure and 575°F inlet air temperature. The combustor configuration (Scheme FS-03A) was the same as that tested in the first two test series; however, it is likely that some change in operating characteristics may have resulted from the loosening of the metal band on the combustor liner. This incident occurred at some point during the third test series. Comparison of the NO_x and CO data for No. 2 fuel with 0.5% N in Figure 79 to those generated at 50 psia rig pressure and 400°F inlet air temperature during the second test series (Figure 78), shows the following similarities and differences.

1. The peaks and buckets in the NO_x curves occur at the same values of overall equivalence ratio. The peak NO_x concentration in Figure 79 is substantially higher (442 ppmv) than that in Figure 78 (226 ppmv) in keeping with the higher rig pressure and higher inlet air temperature. The minimum NO_x concentration in Figure 79 (79 ppmv) is only slightly higher than that in Figure 78 (70 ppmv) indicating the absence of any appreciable effect of increased pressure and increased inlet air temperature at the bottom of the NO_x curve bucket. This result is consistent with the bench-scale data, which also indicated only a slight increase in the minimum attainable NO_x concentration with increased rig pressure and inlet air temperature (see Table VI of Appendix A).

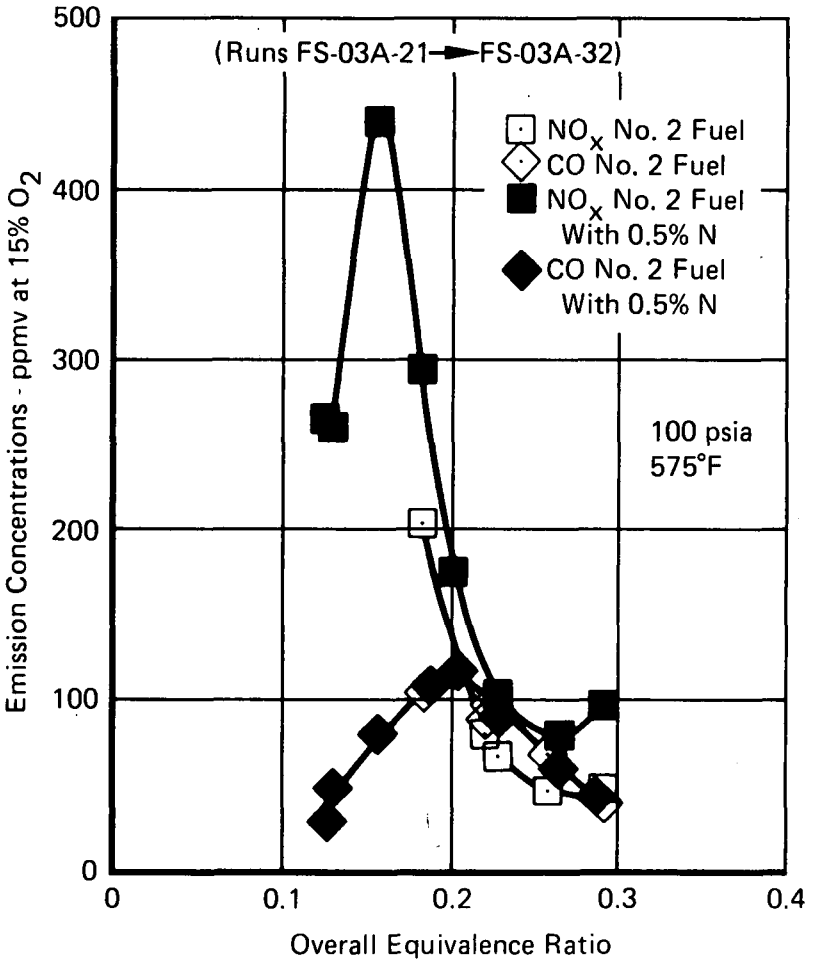

Figure 79. Variation in Emission Concentrations With Overall Equivalence Ratio for Scheme PS-03A, Third Test Series

2. The peak CO concentration in Figure 79 is 116 ppmv, substantially lower than the peak value of 322 ppmv in Figure 78. This difference was expected because of the increased rig pressure and increased inlet air temperature in the third test series. As discussed earlier in this section, the peak CO concentrations measured at 50 psia rig pressure (in the first and second test series, Figures 77 and 78) were substantially lower than those documented at the same rig pressure in the bench-scale test program. In the third test series, these characteristically lower values were further reduced (due to increased rig pressure and inlet air temperature) to the extent that six of eight measured CO concentrations were less than the program goal of 100 ppmv.

In Figure 80, the variation in emission concentrations with overall equivalence ratio for tests of the fourth test series conducted with Scheme FS-03A firing shale DFM is shown; these data, obtained at 50 psia rig pressure and 475°F inlet air temperature, can be compared to the results for Scheme FS-03A firing No. 2 fuel and No. 2 fuel with 0.5% nitrogen shown in Figures 77 and 78. The following observations concerning the two sets of data can be made: (1) NO_x concentrations measured at the bottoms of the NO_x curve "buckets" may be seen to vary with fuel nitrogen content in the expected manner (26 ppmv for No. 2 fuel with 0% nitrogen, 64 ppmv for shale DFM with 0.24% nitrogen, and 75 ppmv for No. 2 fuel with 0.5% nitrogen); (2) the peaks in the NO_x and CO curves for the two sets of data coincide (occur at the same values of overall equivalence ratio on the abscissa); and (3) the peak concentration in the CO curve in Figure 86 (data for shale DFM) is somewhat higher than the peak concentration measured for No. 2 fuel (360 ppmv compared to 300 ppmv, both corrected to 15% O_2). Taken as a whole, these results indicate that the emission characteristics of the combustor obtained during the firing of shale DFM conformed generally to expectations. The slight increase in CO concentration levels in the shale DFM tests, which is not a significant difference, may be attributable to minor variations in the configuration of the combustor hardware or other rig-related factors or may be due to fuel-related effects.

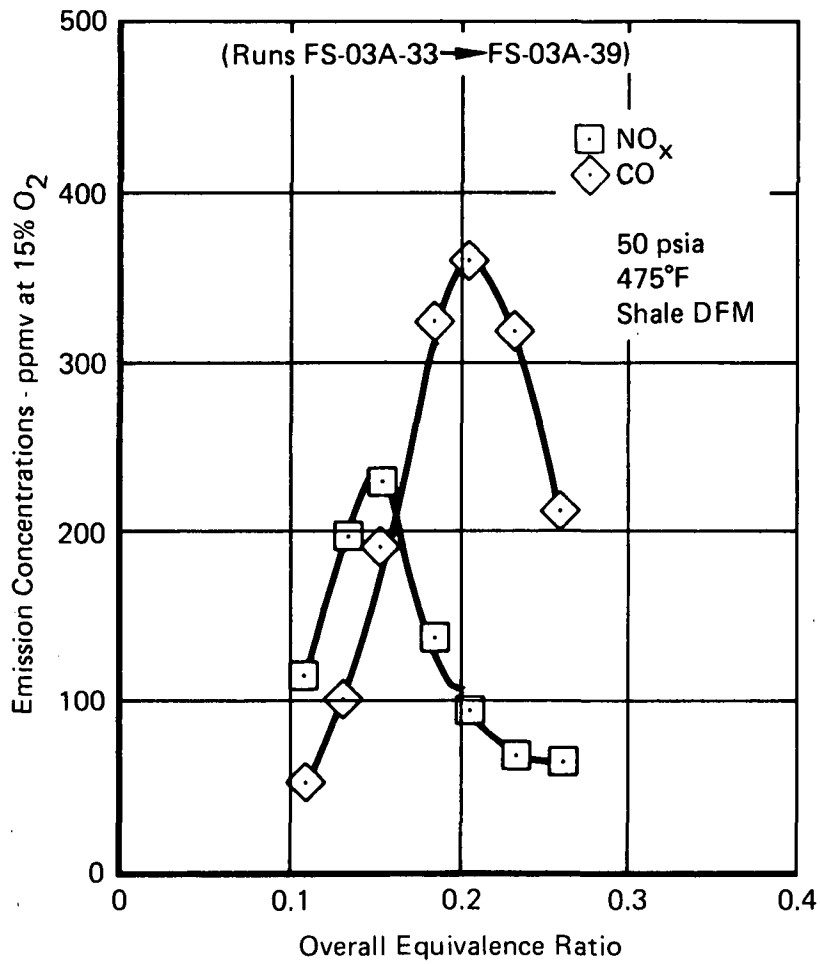

Figure 80. Variation in Emission Concentrations With Overall Equivalence Ratio for Scheme PS-03A, Fourth Test Series

In Figure 81, the data generated at 100 psia rig pressure and 570°F inlet air temperature for Scheme FS-03A firing shale DFM are presented; these results can be compared to the data for Scheme FS-03A firing No. 2 fuel and No. 2 fuel with 0.5% nitrogen presented in Figure 79. It may be seen that comments made previously concerning results obtained at 50 psia rig pressure apply to the 100 psia data as well: (1) the NO_x curve "buckets" vary with fuel nitrogen content in the expected manner (44 ppmv for No. 2 fuel, 64 ppmv for shale DFM, and 79 ppmv for No. 2 fuel with 0.5% pyridine); (2) peaks in the NO_x and CO curves coincide; and (3) CO concentration levels in the shale DFM tests are somewhat higher than the levels obtained for No. 2 fuel.

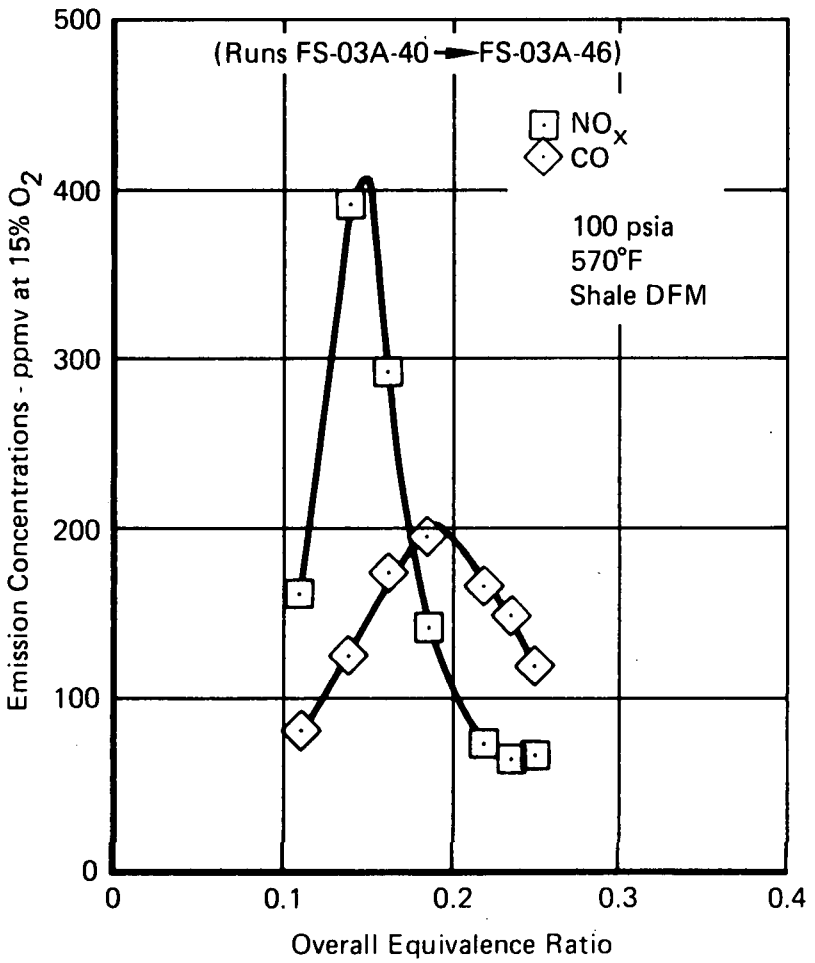

Figure 81. Variation in Emission Concentrations With Overall Equivalence Ratio for Scheme PS-03A, Fifth Test Series

The last two comments also apply to the data generated at 100 psia rig pressure and 570°F inlet air temperature for Scheme FS-03A firing neat No. 2 fuel (shown in Figure 82). These data can be compared to the results shown in Figure 79, obtained for the same (nominal) burner configuration and the same fuel. NO_x concentration levels at the bottoms of the NO_x curve "buckets" were essentially the same (44 ppmv vs 45 ppmv) in the two test series. The only notable difference in the data is the generally higher CO concentration level

obtained during the repeat tests. Because the combustor configurations tested were identical except for the loosened quick-quench collar, which had been a factor in the initial test series, it was concluded that the mixing effectiveness of the quick-quench section may have been compromised in the initial tests resulting in a less distinct peak in the CO curve (a uniformly lower CO concentration level). This result, which did not constitute a major difference, was the only apparent effect of the loosened quick-quench collar.

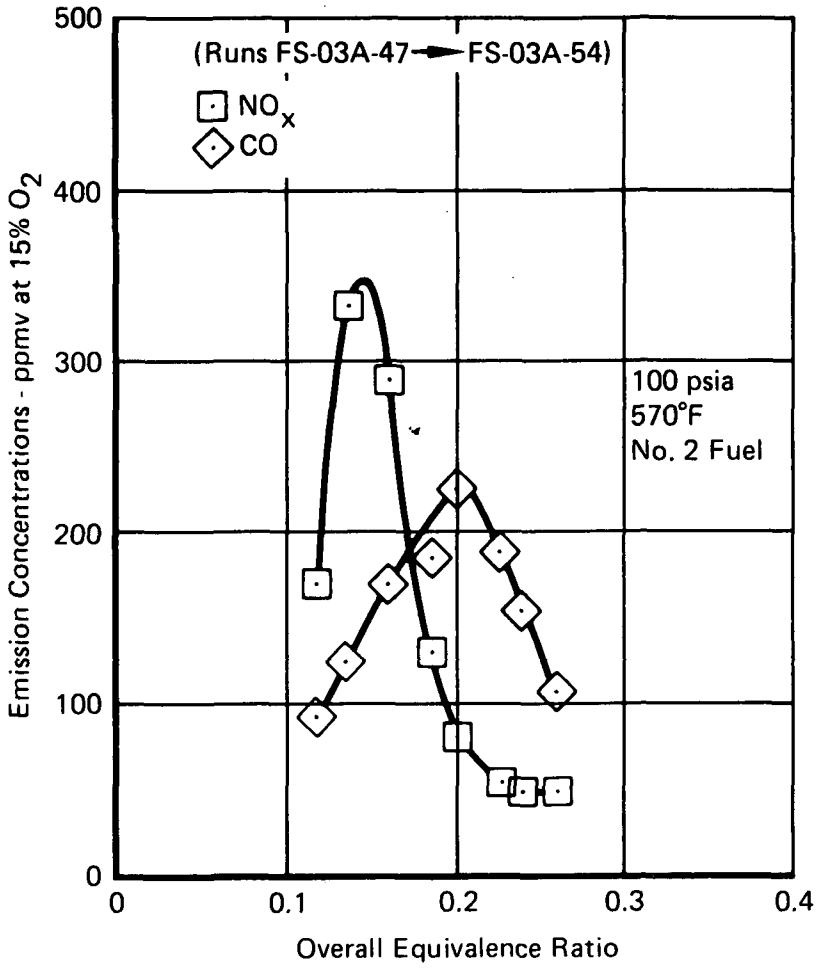

Figure 82. Variation in Emission Concentrations With Overall Equivalence Ratio for Scheme PS-03A, Sixth Test Series

3.2.3.6 Exit Temperature Profiles and Combustor Liner Temperatures

Combustor exit gas stream temperatures were measured using a rig radial traverse probe. Thermocouples are provided at nine locations equally spaced over the circumference of the annular exit transition piece. In the tests concluded, readings were taken at a single radial position near mid-span. The radial traverse capability of the probe was not used in order to maximize the run time available for generating a basic emission signature of the combustor.

Representative exit thermocouple data are presented in Figure 83. A strong central peak is evident in the circumferential profile, with peak-to-peak minimum differentials as great as 1400°F. Values of temperature pattern factor (peak-to-average temperature differentials normalized to overall temperature rise) are presented in Table V of Appendix A and Figure 84. The range of values obtained (0.3 to 0.7) is substantially higher than the generally accepted

target range of 0.2 to 0.3. Examination of the curves in Figure 83 indicates that the peak temperatures occur in a region occupying about one-third of the circumference (three of nine thermocouples) at the exit of the annular transition duct. These peak temperatures appear to represent the same "top-hat" profile that exists at the discharge plane of the quick-quench section (where a jet occupying about one-third the local cross-sectional area enters the aft dilution section). It can be expected that this top-hat temperature profile will persist in the flow as it passes through the aft dilution section and through the transition duct (a distance of about 2.5 jet diameters), and will appear at the exit plane of the combustor. In Figure 83, lines indicating the magnitude of the top-hat profile at the end of the quick-quench section (assuming complete mixing within the jet) are superimposed on the exit-plane circumferential profiles. It can be seen that there is close agreement between the measured peak exit temperatures and the ideal quick-quench section temperatures. This result has two important implications. First, the high values of temperature pattern factor in Figure 84 and Table V of Appendix A appear to be the result of ineffective mixing in the aft dilution section of the combustor. Because of high-velocity flow in the center of the passage, it is not unexpected that penetration and mixing in this section may be ineffective. Second, it is noteworthy that no temperature reading at the exit plane of the combustor exceeds the ideal (mixed out) temperature of the quick-quench section by a significant amount. To illustrate this feature of the data, computations of temperature pattern factor were performed for gases at the quick-quench section on the assumption that the peak temperatures measured at the combustor exit plane are equal to those that exist at the end of the quick-quench section. Values of this parameter, TPFQQ, are plotted in Figure 85 as a function of overall equivalence ratio. The maximum value obtained, 0.096, is well below the generally accepted target range of 0.2 to 0.3. Although this parameter has been computed indirectly, and may, therefore, be subject to error (for example, some of the values of TPFQQ are slightly negative, indicating that the peak exit temperature was actually lower than the quick-quench section temperature due to mixing in the aft dilution section), the very low values obtained indicate that excellent mixing was achieved in the quick-quench section of the combustor.

The effect of fuel type on combustor liner temperature levels in the fourth test series is illustrated in Figure 86. Data from skin thermocouples attached to the outer surface of the primary combustor liner (parameters T_{LIN1} through $T_{LIN\ 6}$ in Table IV; T/C locations shown in Figure 7) have been used to compute values of the liner temperature rise factor (LTRF). This parameter, defined in Figure 86, provides a basis of comparison for No. 2 fuel and shale-derived DFM in terms of the overall average liner temperature rise (normalized to burner ideal temperature rise). Results indicated that the shale DFM produced a slightly higher liner temperature rise (a difference as great as 4% of the burner ideal temperature rise at some equivalence ratio settings).

A further effect of the use of shale DFM is illustrated in Figures 87 and 88. Photographs of the premix tube swirler and premixing passage show a minor buildup of carbon on the surfaces of these parts. For comparison, the condition of the swirler following tests with No. 2 fuel is shown in Figure 89. It is believed that the deposits shown were the result of DFM fuel contamination (the distillate fuel used in this test program contains heavy earth waxes that were acquired at the refinery when processed fuel was placed in tanks originally used for crude shale) and are not a characteristic of shale-derived fuels in general.

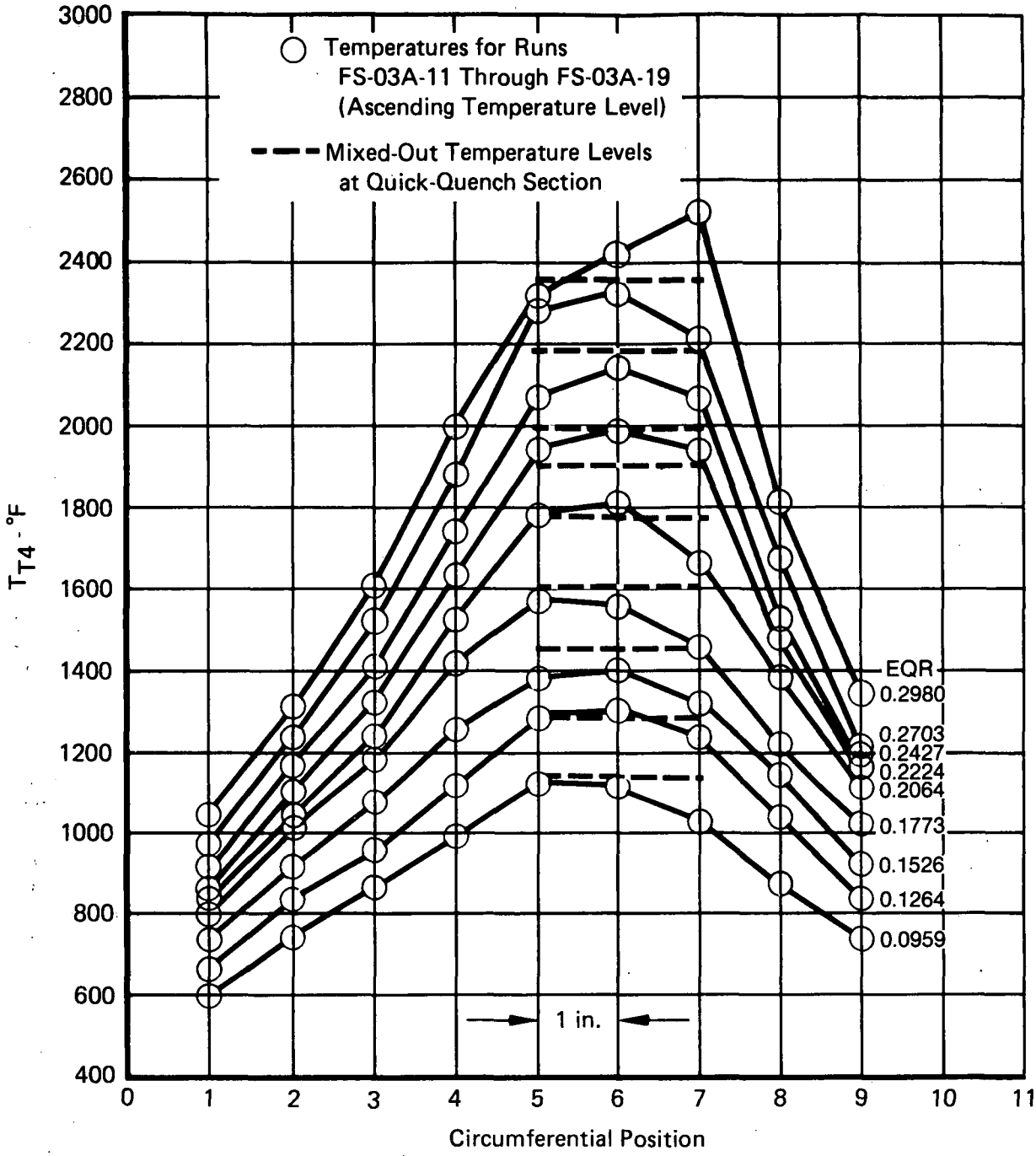

Figure 83. Exit Temperature Profiles (Second Test Series, Probe at Mid-Span)

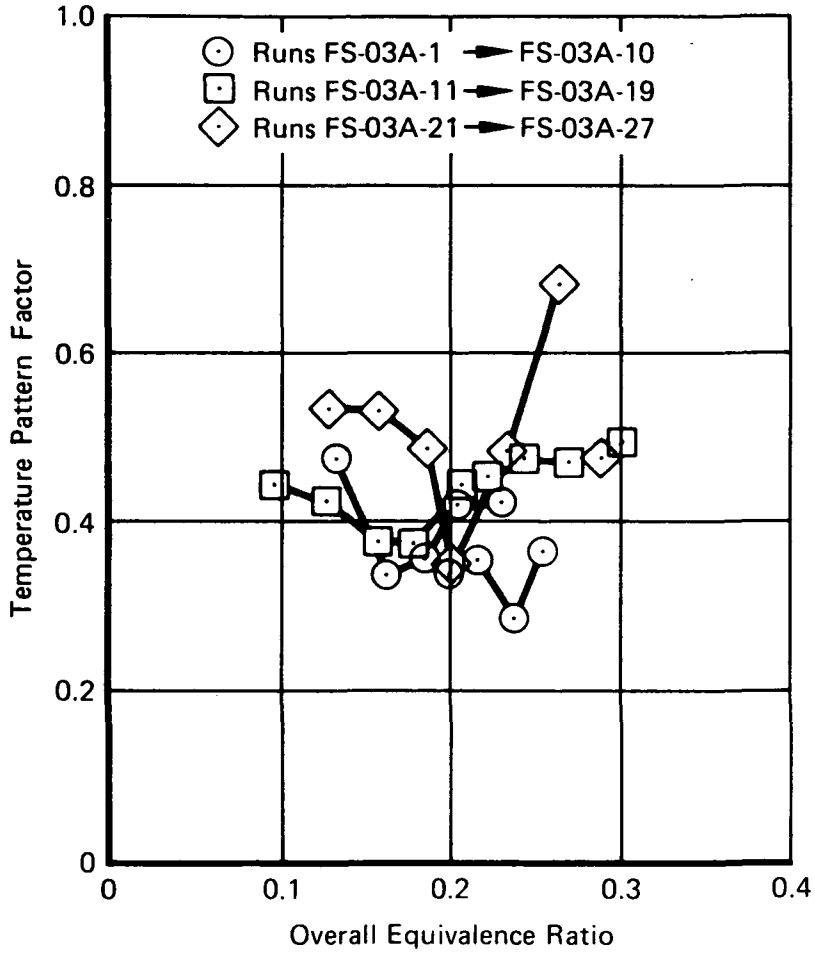

Figure 84. Variation in Temperature Pattern Factor With Overall Equivalence Ratio

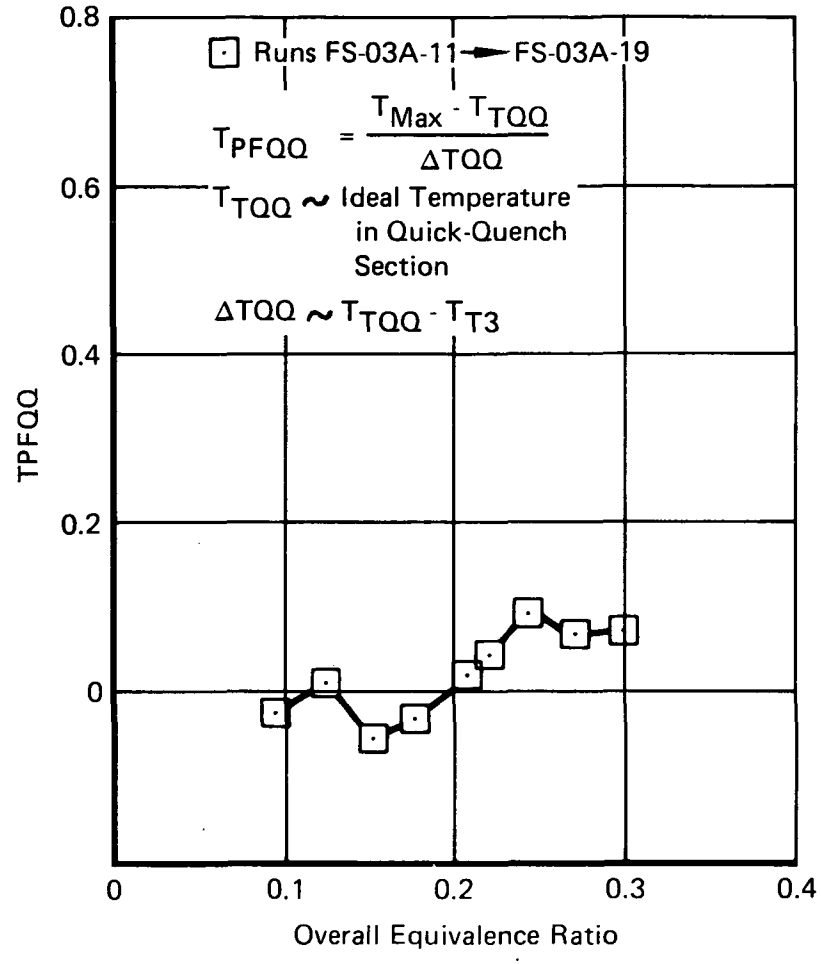

Figure 85. Variation in Quick-Quench Section Pattern Factor (TPFQQ) With Overall Engine Ratio (Second Test Series)

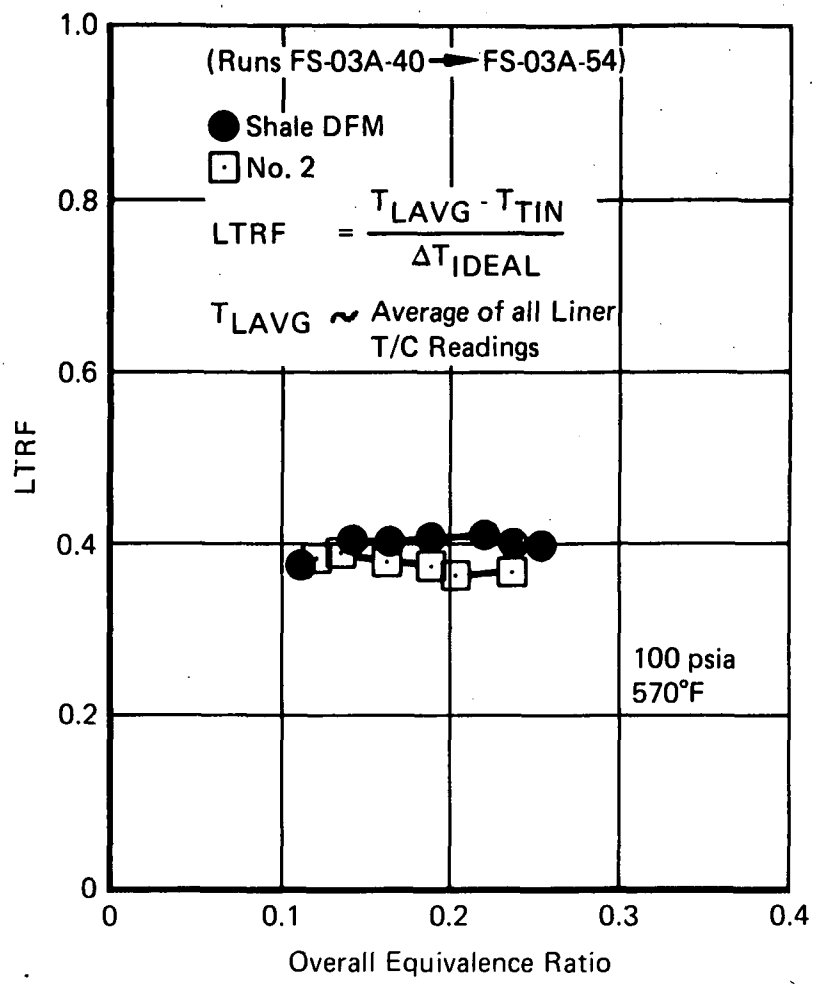

Figure 86. Variation in Liner Temperature Rise Factor (LTRF) With Overall Equivalence Ratio and Fuel Type

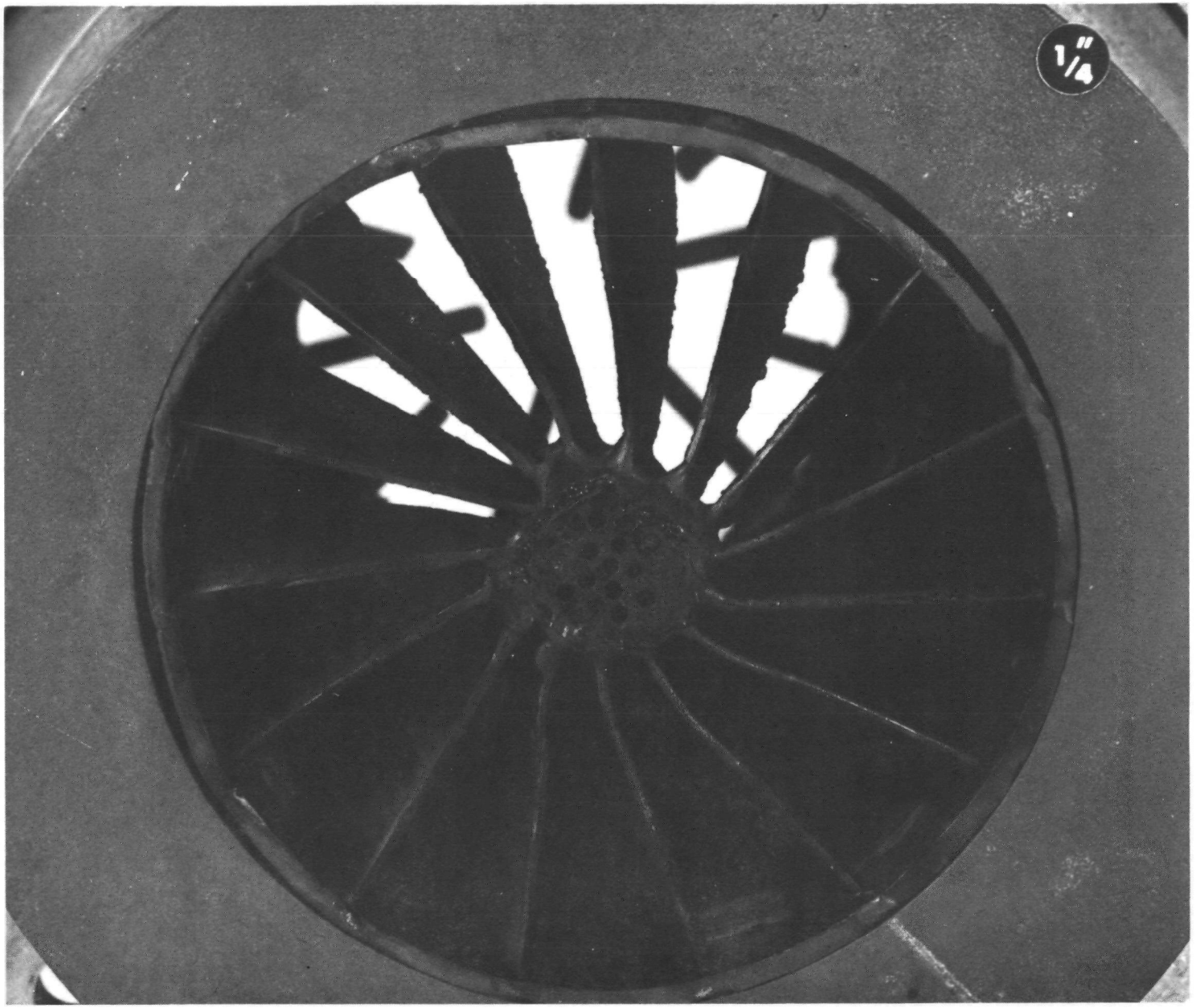

Figure 87. Condition of Premix Tube Swirler Following Tests With Shale Derived DFM

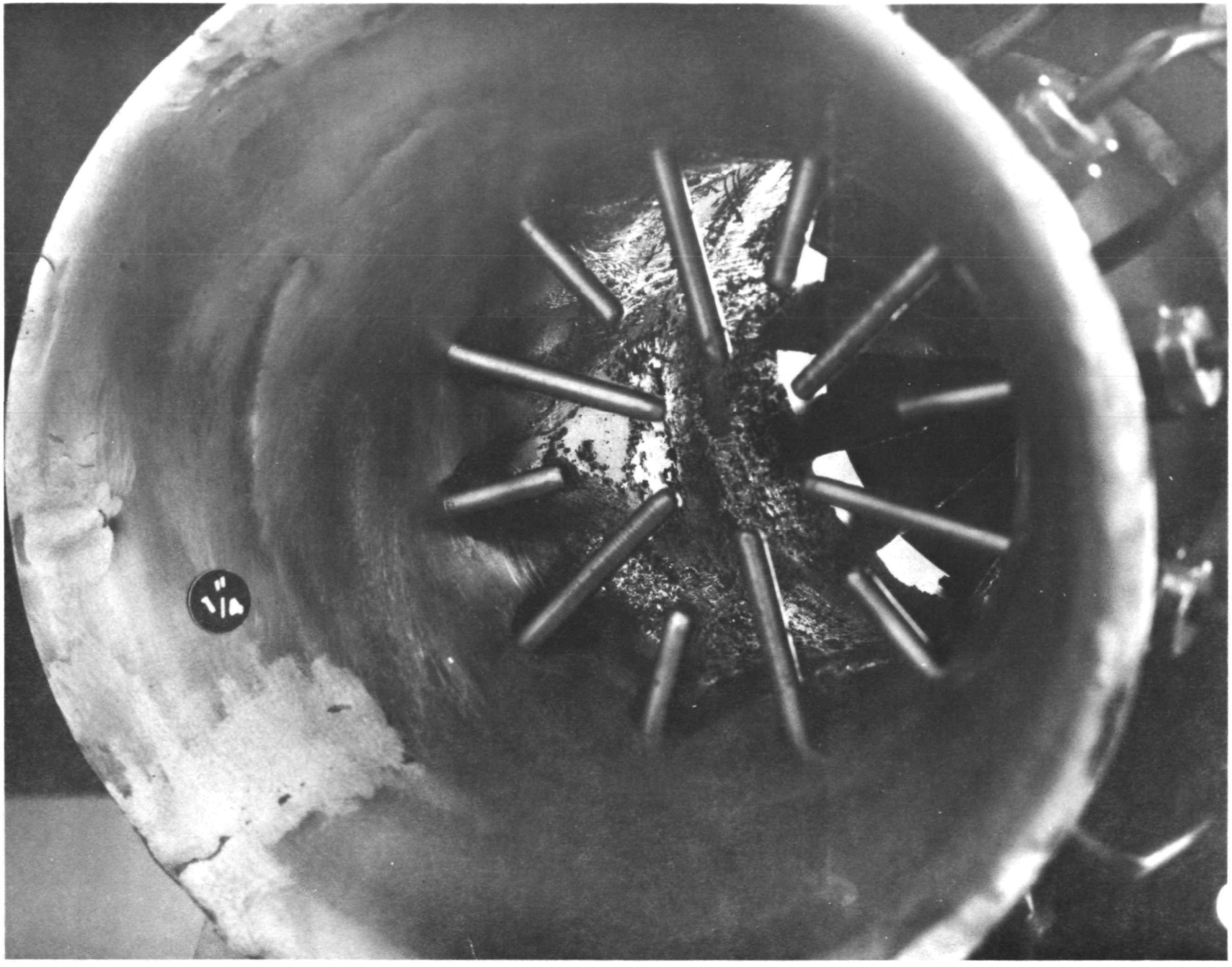

Figure 88. Condition of Premixing Passage Following Tests With Shale Derived DFM

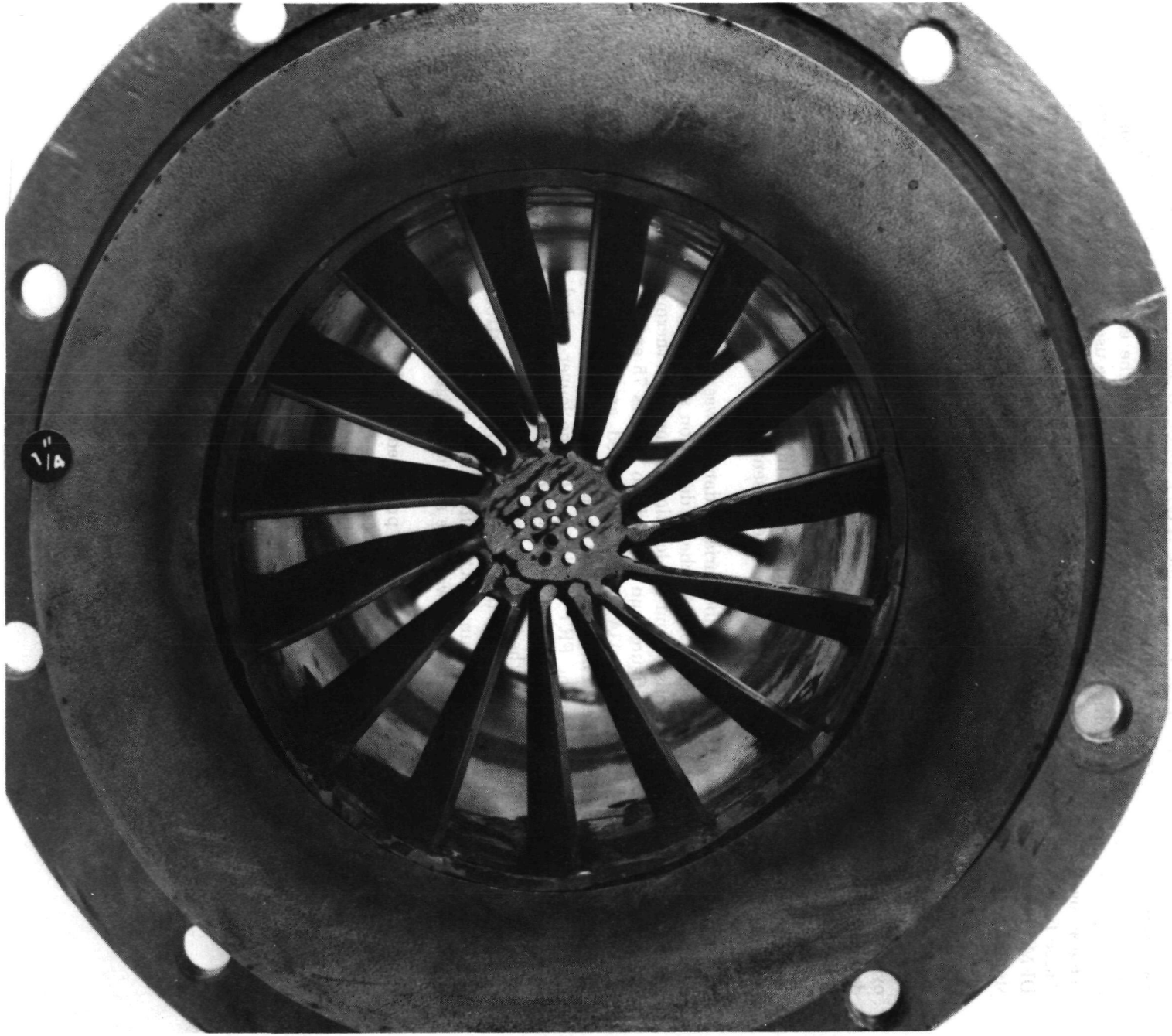

Figure 89. Condition of Premix Tube Swirler Following Tests With No. 2 Fuel

3.2.4 Evaluation of the ECV Configuration (Scheme FS-04A)

Following tests of the full-residence-time (FRT) configuration, the combustor hardware was reworked to the short-length engine-compatible version (ECV). Testing of this configuration was accomplished in two test series, one directed toward the establishment of a basic emission signature, and the other providing a demonstration of the use of variable geometry to achieve low NO_x concentration levels over a wide range of combustor operating conditions. Three fuels were fired: No. 2 fuel; No. 2 with 0.5% nitrogen (as pyridine); and shale-derived DFM. The results obtained indicate that the emission signature of the ECV combustor is similar to that obtained previously for the FRT version. However, the NO_x concentration levels measured were the same to slightly lower than those measured for the FRT combustor. This result was unexpected, and apparently occurred due to better placement of the penetration air jets in the aft dilution section of the combustor. Operation of the premix tube variable damper was successfully accomplished, and NO_x levels less than the program goals were demonstrated over the entire power range. Toward the end of the final test series, pieces of the premix tube damper broke loose (due to fatigue failure of tack welds). There was some damage to the premix tube swirler as a result. Because the problem experienced was mechanical in origin, this occurrence did not indicate any deficiency in the aerodynamic design of the premix tube or the variable damper. Aside from the damage to the premix tube, the combustor was found to be in good condition. Complete details of the tests are presented in this section.

In the initial tests, the premix tube variable damper was not used. The configuration, Scheme FS-04A, is shown in Figure 90. A scheme definition sheet, showing the design point airflow distribution of the combustor and the location of liner skin thermocouples, is shown in Figure 91. Comparison of these figures can be made to Figures 75 and 76, in which details of the FRT combustor (Scheme FS-03A) previously tested are given. The FRT and ECV combustor configurations differed in three main areas: (1) primary zone length in the ECV was 12.5 in. compared to 18 in. in the FRT combustor; (2) the louver-cooled dilution piece just downstream of the quick-quench section in the FRT combustor was removed, yielding a reduction of 8 in. in the length of the secondary zone; (3) the final dilution airflow, which was introduced at Station I in Scheme FS-03A (see Figure 76), was introduced through axially-directed holes in the wall of the dump section in Scheme FS-04A (Station E in Figure 91). Photographs of the ECV combustor hardware are shown in Figures 92 and 93.

The data obtained in the two test series are presented in Tables I through V of Appendix A. The tables contain the major parameters necessary to specify combustor operating conditions, and contain liner temperature and exhaust emission data.

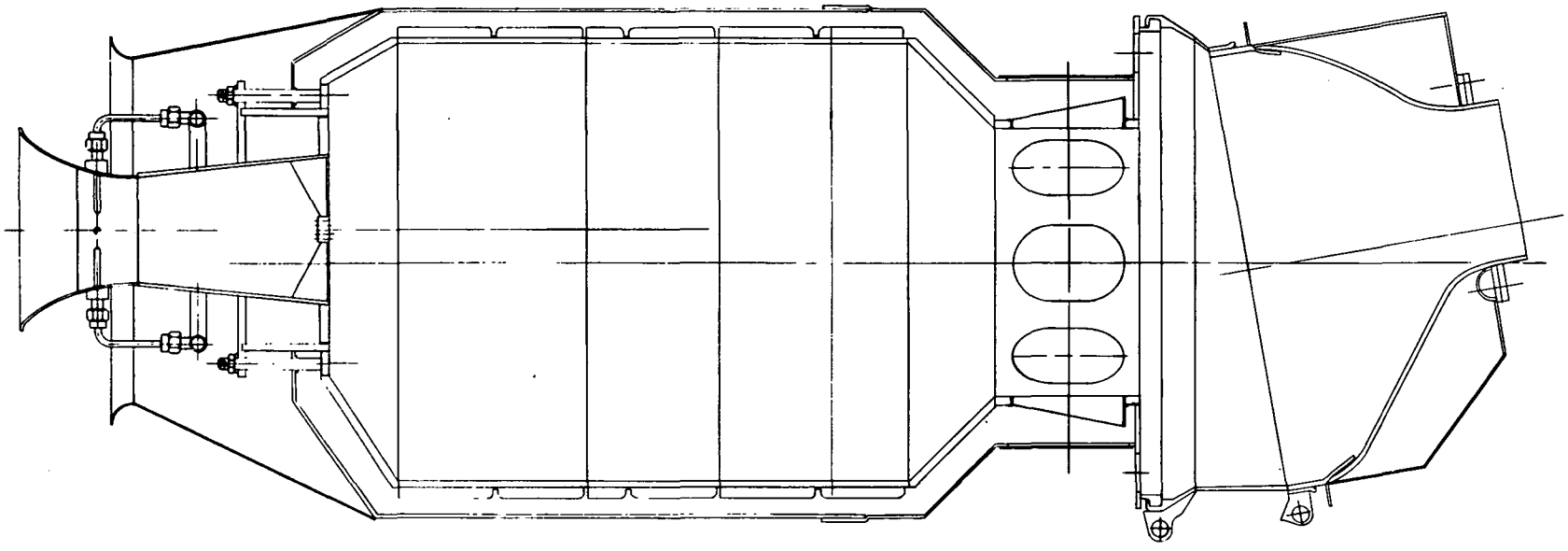

Figure 90. Full Scale Combustor Scheme FS-04A

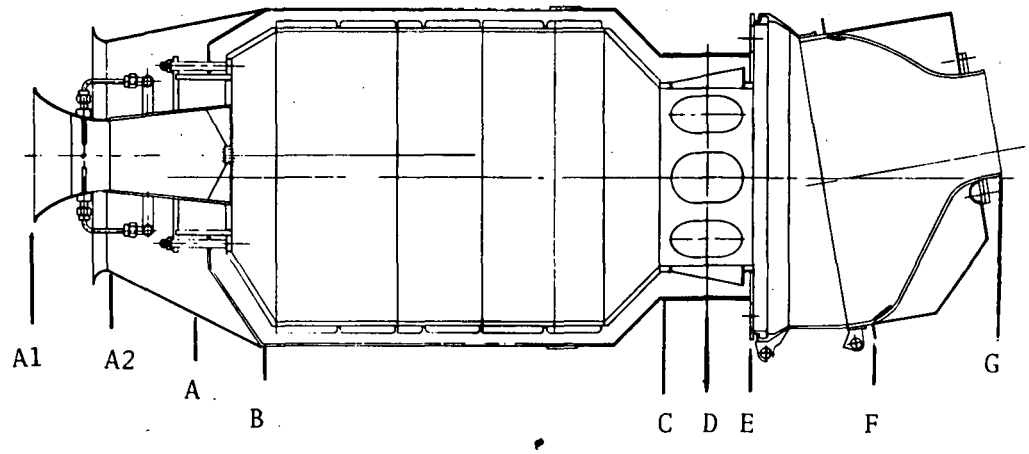

LB	AREF	L/D	VOLREF	ACDSUM
33.50	88.20	3.16	1505.0	27.26

STATION	AX	ACD	WACUM	PHI
A1	13.847	0.0	0.0	0.0
A2	4.335	0.0	0.0	0.0
A	8.038	5.468	20.058	1.285
B	75.391	0.0	20.058	1.285
C	28.260	0.0	20.058	1.285
D	28.260	10.953	60.234	0.428
E	72.346	10.049	97.095	0.266
F	72.346	0.792	100.000	0.258
G	39.337	0.0	100.000	0.258

HEADER	AXIAL LOC	RAD LOC	CIRCUM LOC
TL1N1	7.50	4.8	Avg
TL1N2	10.50	5.0	180
TL1N3	14.80	5.0	90
TL1N4	14.80	5.0	180
TL1N5	14.80	5.0	270
TL1N6	21.50	3.4	0
TL1N7	21.50	3.4	90
TL1N8	21.50	3.4	270

Figure 91. Burner Scheme Definition (Scheme FS-04A)

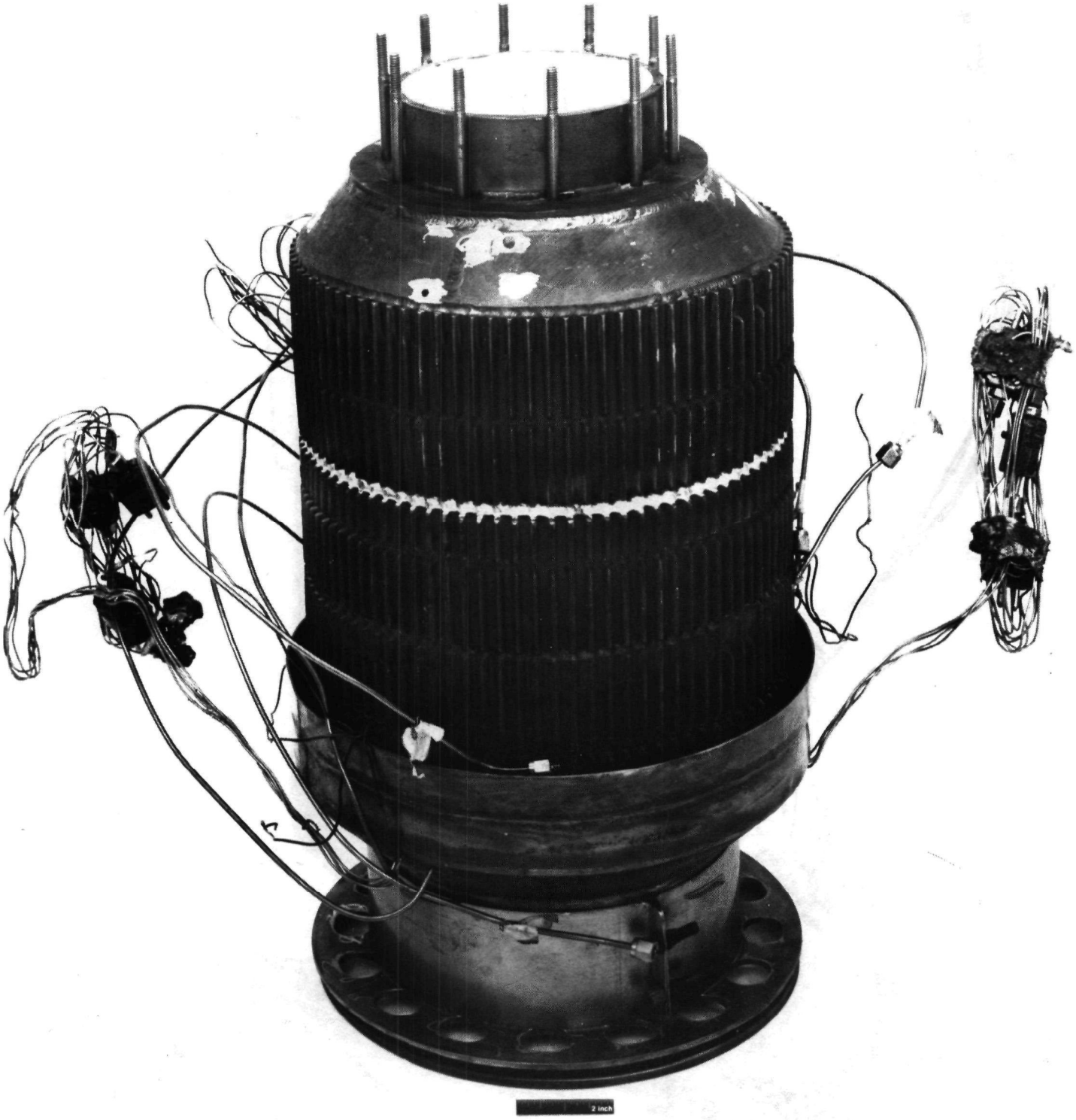

Figure 92. ECV Combustor During Assembly

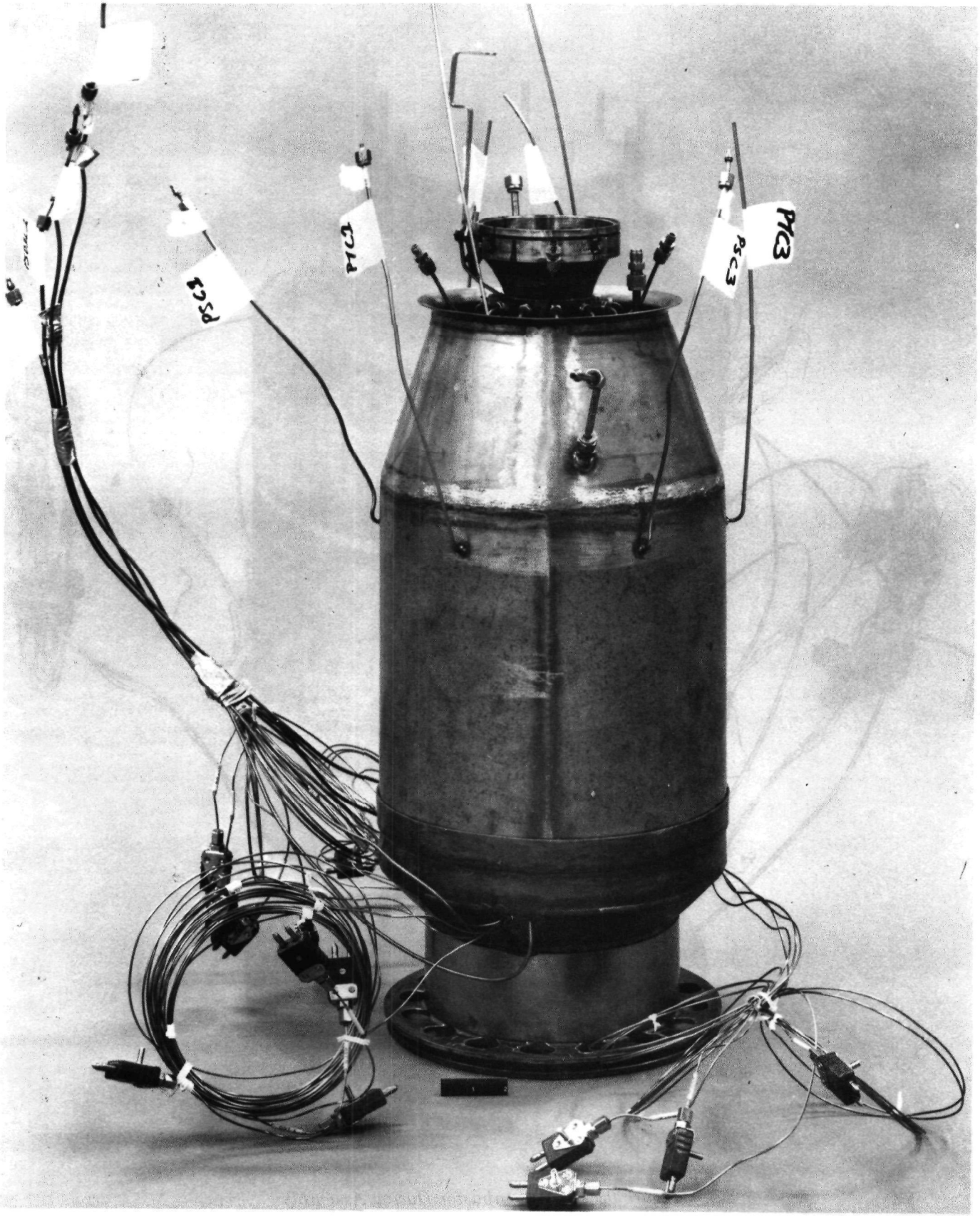

Figure 93. ECV Combustor Fully Assembled Except for Variable Damper

3.2.4.1 *First Test Series*

Emission-signature data were generated at 100 psia rig pressure and 560°F inlet air temperature for Scheme FS-04A in the initial test series. The results for No. 2 fuel, No. 2 fuel with 0.5% nitrogen (as pyridine), and shale-derived DFM are shown in Figures 94 through 96. Comparison of the data in Figure 94 (for No. 2 fuel) can be made to those shown in Figure 82 for the FRT combustor. The two sets of data are similar in that the peaks in the CO curves occur at approximately the same value (about 0.20) of overall equivalence ratio. Minimum NO_x concentrations for the two combustors also occur within the same basic range of overall equivalence ratios (0.20 to 0.27). The principal differences exist in the CO concentration levels measured (594 ppmv at the peak of the curve for the ECV combustor vs 224 ppmv for the FRT combustor, both corrected to 15% O_2), and in the minimum NO_x concentrations recorded (38 ppmv for the ECV combustor vs 45 ppmv for the FRT combustor). Taken as a whole, the results obtained indicate that the two combustors have comparable emission characteristics (as expected), and that the anticipated increase in NO_x in the ECV configuration (because of a reduced primary zone residence time) did not take place. As shown, there was instead a general increase in the CO concentration level, along with the unexpected decline in the minimum achievable NO_x concentration level. The initial interpretation of these results was that a tradeoff had been effected between NO_x and CO in the aft dilution section of the combustor. It was reasoned that in the previous FRT configuration (Scheme FS-03A), partially mixed gases in the region of jet-induced recirculation at the dump plane of the quick-quench section may have supported combustion reactions that contributed to the formation of NO_x. The direct introduction of penetration air into this region in the ECV combustor (Scheme FS-04A) would have terminated these reactions, resulting in a net decline in NO_x and an increase in CO. This hypothesis implies that the mixing process initiated within the quick-quench section is incomplete at the dump plane of the combustor (not an unreasonable assumption because the dump plane is only one-half inch downstream of the trailing edge of the penetration jets). Subsequent findings, however, have made it necesary to modify the hypothesis. Examination of the combustor following the first test series revealed a crack in the premix tube fuel manifold. During the tests in question, fuel had leaked onto the outer surface of the combustor dome (see Figure 97) and had been ingested into the primary liner cooling passage. Fuel entering the passage would ultimately be discharged through the quick-quench slots. The introduction of raw fuel into the combustor at this location under highly turbulent, overall fuel-lean conditions would account for the increased CO concentration levels observed in the first test series. An increase in unburned hydrocarbon concentration levels would also be expected, and as may be seen in Figures 94 through 96, did also occur (concentration levels as high as 33 ppmv were measured compared to the usual levels of 5 ppmv or less). In the second test series (after the manifold had been repaired), CO concentration levels were found to be lower and generally comparable to those obtained for the FRT combustor. The conclusion drawn from these results was that the net decline in NO_x concentration levels in the shorter (ECV) combustor has been the result of a more effective quenching process brought about by the introduction of a substantial portion of the combustor airflow (36%) through axially-directed holes in the wall of the dump section of the combustor. It appears that this airflow may have purged the dump region of the partially mixed reacting gases which have contributed to the production of NO_x in the FRT combustor. The fact that a net reduction in overall NO_x concentration levels could result from this change indicates that the local reduction achieved was substantial enough to offset any increase in NO_x production due to a shorter primary zone residence time.

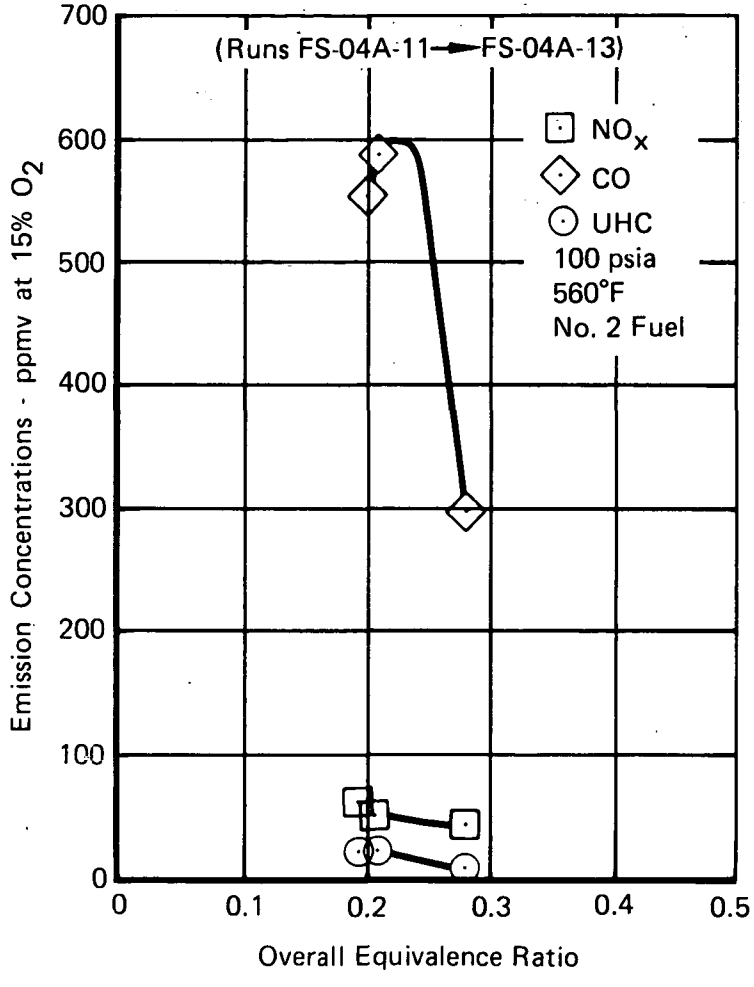

Figure 94. Variation in Emission Concentrations With Overall Equivalence Ratio for Scheme FS-04A Firing No. 2 Fuel

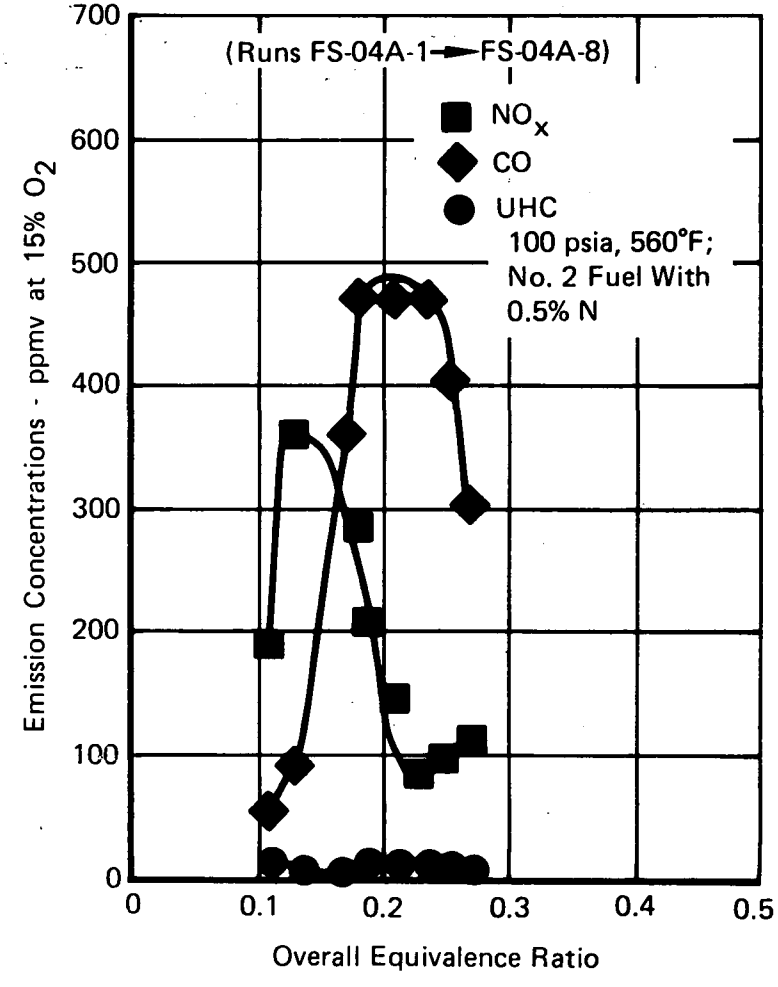

Figure 95. Variation in Emission Concentrations With Overall Equivalence Ratio for Scheme FS-04A Firing No. 2 Fuel With 0.5% N

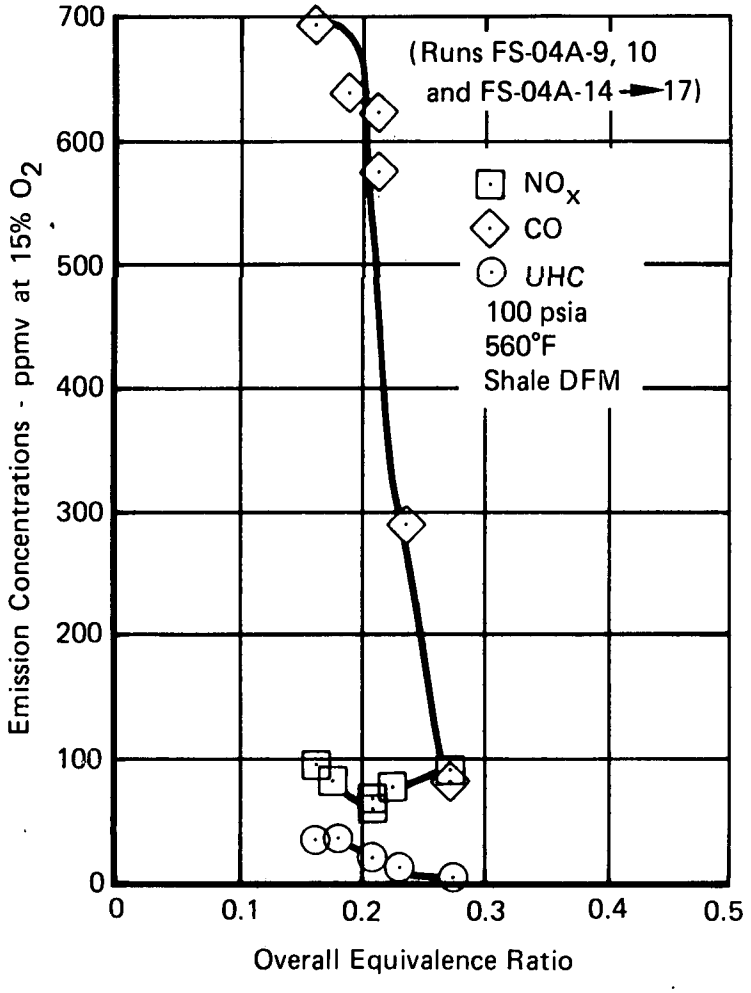

Figure 96. Variation in Emission Concentrations With Overall Equivalence Ratio for Scheme FS-04A Firing Shale DFM

Figure 97. Evidence of Fuel Leak Caused by Cracked Manifold

3.2.4.2 *Second Test Series*

In the second test series, the premix tube damper was installed and tests were performed at inlet conditions representing three engine power settings (see Table XII). The configuration evaluated, Scheme FS-04B, is shown in Figure 98. In Figure 99, a photograph of the premix tube assembly with the variable damper mechanism attached is shown.

TABLE XII
RIG TEST CONDITIONS SIMULATING
VARIOUS ENGINE POWER SETTINGS

	T_{T3} (°F)	P_{T3} (psia)	Primary Airflow (%)
Idle	320[1]	40	11
50% Power	550	96	16
100% Power	780[2]	100[3]	21

Notes:
[1]Lowest attainable rig setting. Engine value is 280°F.
[2]Direct-fired rig heater burner required, resulting in vitiation of inlet air.
[3]Highest rig pressure. Engine value is 188 psia.

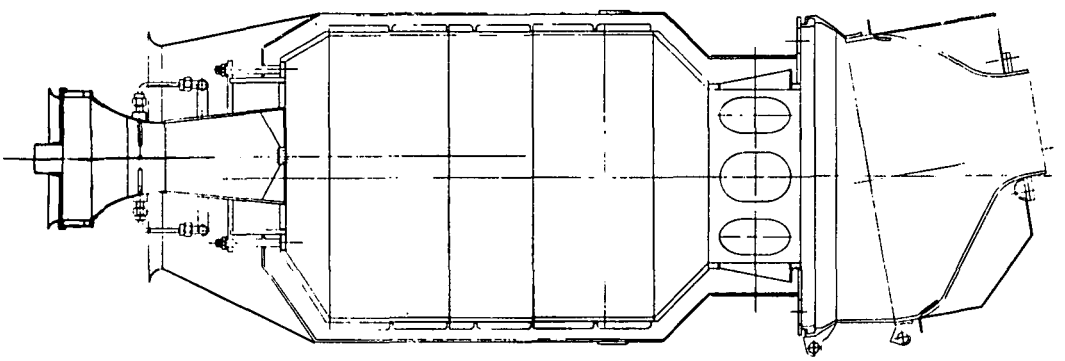

Figure 98. Full-Scale Combustor Scheme FS-04B

Test results obtained firing No. 2 fuel with 0.5% nitrogen (as pyridine) are shown in Figure 100. At the idle setting, a minimum NO_x concentration of 95 ppmv (corrected to 15% O_2) was measured at 0.18 overall equivalence ratio. This concentration is somewhat higher than the levels measured at the 50 and 100% power points (84 and 81 ppmv, respectively), indicating that the low inlet air temperature associated with the idle setting (320°F nominal) has a detrimental effect on fuel vaporization (causing an increase in the occurrence of droplet burning, and resultant higher NO_x). The low inlet air temperature and the low rig pressure (40 psia) also contributed to an increase in CO concentration levels (753 ppmv near the peak of the curve, corrected to 15% O_2) at the idle setting.

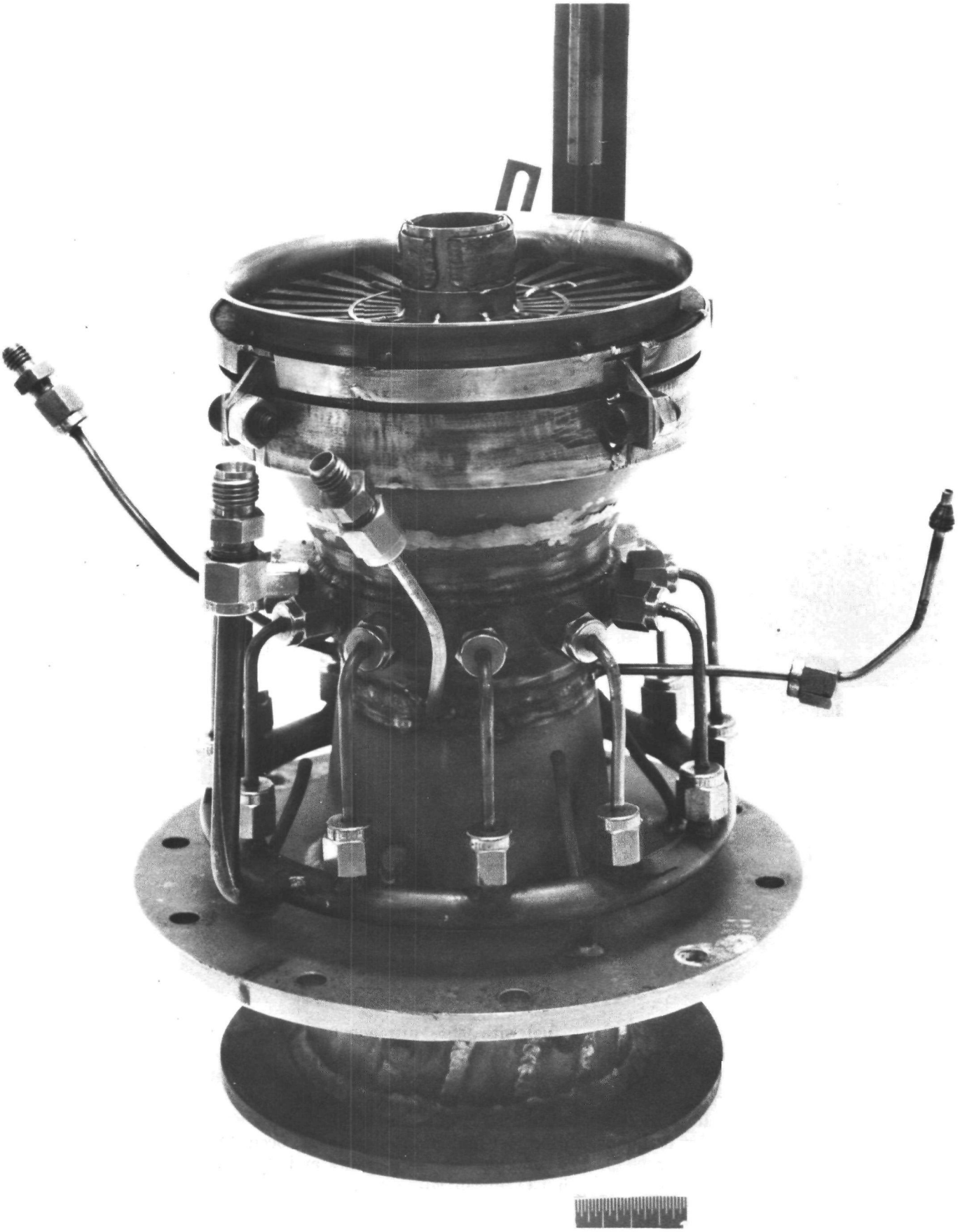

Figure 99. Premix Tube With Variable Damper Attached

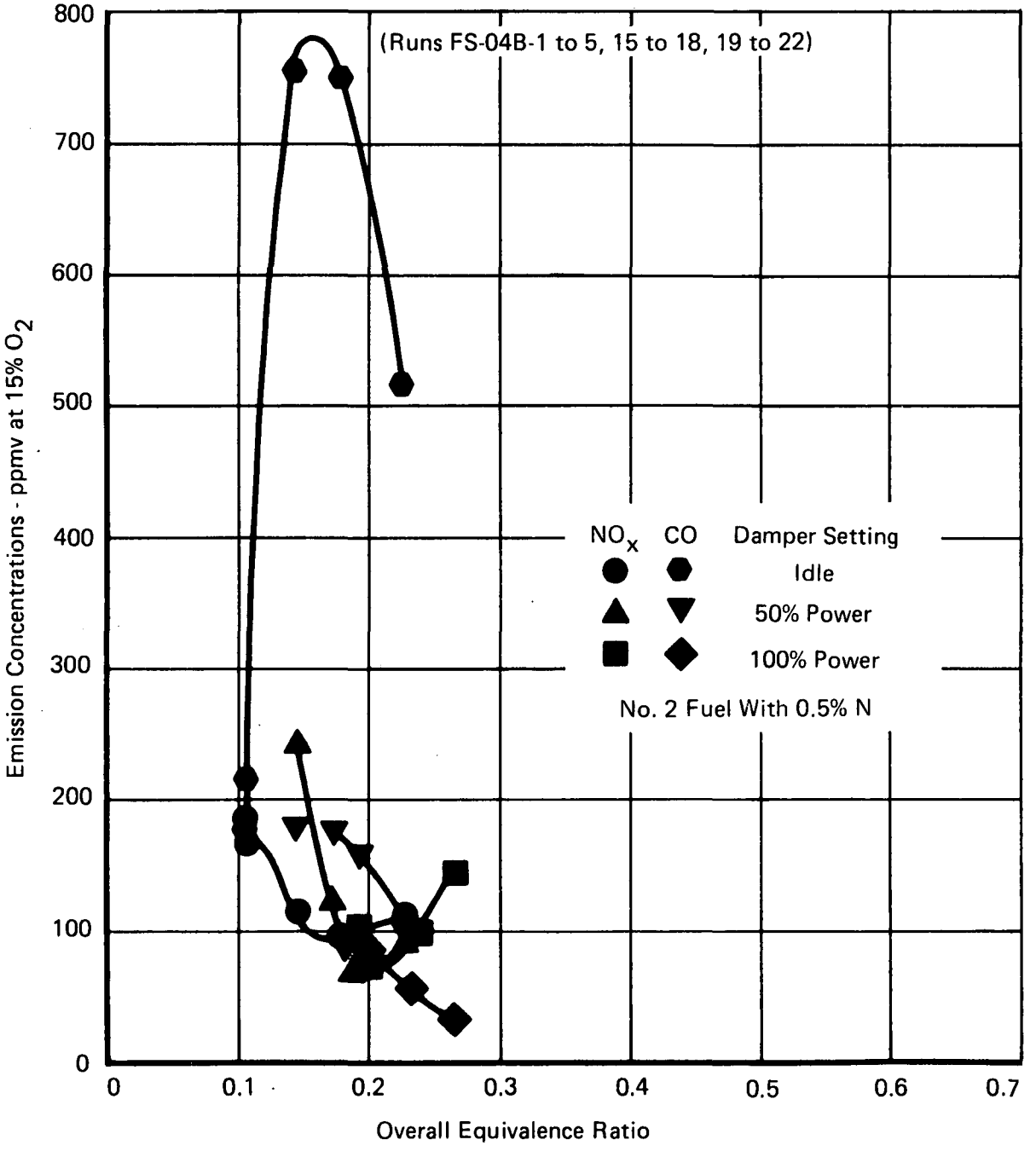

Figure 100. Variation in Emission Concentrations With Overall Equivalence Ratio for Scheme FS-04B Firing No. 2 Fuel With 0.5% N

The intermediate and baseload power settings (50 and 100% power) are meant to differ in primary zone airflow (Table XII) as well as rig inlet conditions. Although the damper setting was varied in going from the 50 to the 100% power points, it appears that no appreciable increase in primary airflow was effected (the minimum point in the NO_x curve for 50% power occurs at 0.19 overall equivalence ratio compared to 0.20 for 100% power). Apparently the residual blockage of the damper device in its full-open position caused a reduction in premix tube airflow with respect to the quantity that can be passed when the device is completely removed (in Figure 95, data obtained with the damper removed show a minimum point in the NO_x curve at 0.24 overall equivalence ratio, indicating an increase in primary airflow from about 15% to about 18% of the total combustor airflow). Aside from the intended difference in primary airflow setting, the 50 and 100% power points differ primarily in inlet air temperature (550°F vs 780°F, per Table XIII). At the higher temperature, the rig direct-fired heater burner is operated. The rig supply limit of 100 psia precludes testing at 188 psia, the full baseload pressure; therefore, the difference between the 50 and 100% point rig pressure conditions is only 4 psi.

In Figure 100, it may be seen that the NO_x curves for the 50 and 100% power points are nearly identical, reflecting the similarity in primary zone airflow rates and rig pressure, and indicating that the increase in inlet air temperature had no appreciable effect (the NO_x concentrations at the 100% power point were corrected by subtracting the 12 ppmv contribution of the heater burner, separately measured, from the raw data). Figure 100 also shows that the maximum CO concentration measured at the 100% power point was 86 ppmv, compared to 182 ppmv at the 50% power point, a decrease due almost entirely to the higher inlet air temperature (CO concentrations at the 100% power point were also corrected by subtracting the 37 ppmv contribution of the heater burner from the raw data).

Test results obtained firing shale-derived DFM are shown in Figure 101. Data points were recorded at the bottom of the NO_x curve bucket for the idle setting and for the 50% power setting (minimum NO_x concentrations were ascertained by monitoring the gas analyzer reading while adjusting rig fuel flow). A minimum concentration of 80 ppmv (corrected to 15% O_2) was documented at idle; at the 50% power setting, 75 ppmv (corrected to 15% O_2) was achieved. Data were not recorded at the 100% power setting because of the close similarity of that point to the 50% power point (there had been no appreciable difference in NO_x concentrations measured at the two points in the previous tests conducted with pyridine-spiked No. 2 fuel). The CO data shown in Figure 101 are comparable to those shown in Figure 100 for pyridine-spiked No. 2 fuel.

In Figure 102, test results obtained firing non-nitrogenous No. 2 fuel are presented. As in the case of shale-derived DFM, data were recorded only at the idle and 50% power points. Minimum NO_x concentrations of 49 and 43 ppmv (corrected to 15% O_2) were demonstrated at the idle and 50% power settings. The CO characteristics were comparable to those obtained for the other two fuels.

For purposes of comparison, the NO_x characteristics obtained for the three fuels at the idle and 50% power points are summarized in Figure 103. Minimum concentrations of 49, 80, and 95 ppmv (corrected to 15% O_2) were measured at idle for No. 2 fuel (0% nitrogen), shale DFM (0.24% nitrogen), and pyridine-spiked No. 2 fuel (0.5% nitrogen), respectively. At 50% power, the minimum concentrations were 43, 75, and 84 ppmv (corrected to 15% O_2) respectively, for the same three fuels.

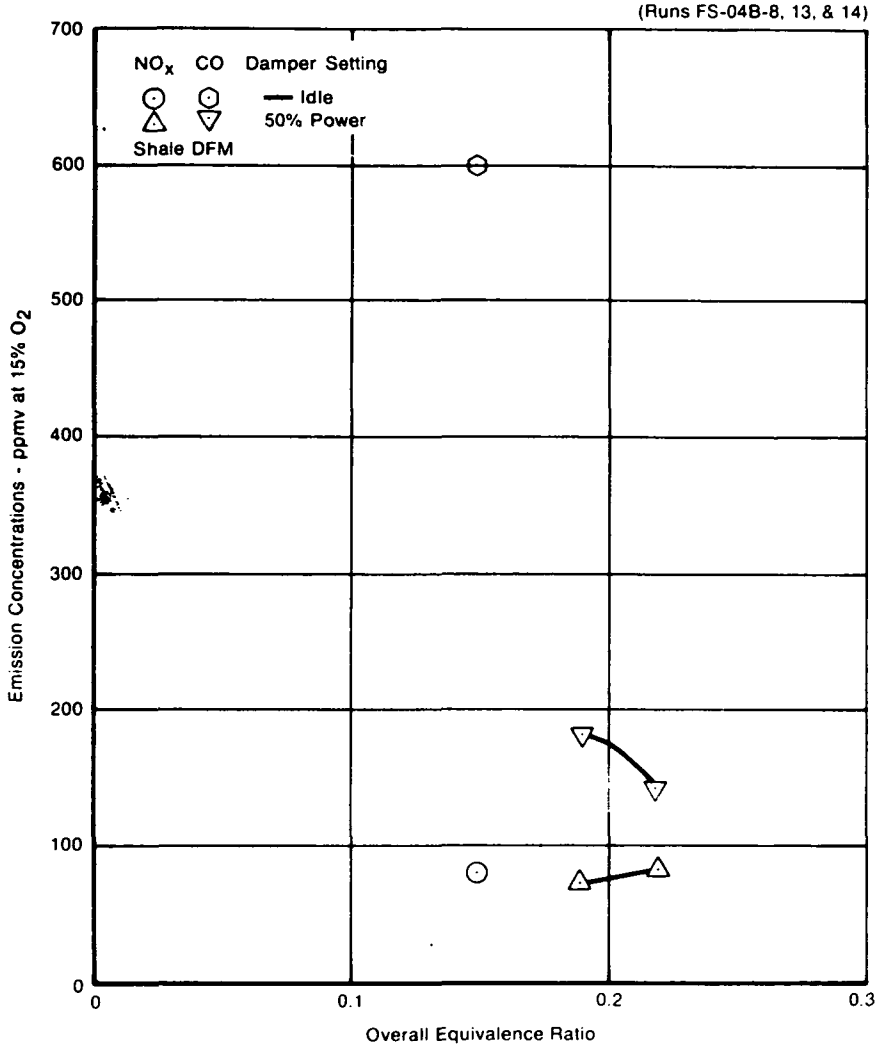

Figure 101. Variation in Emission Concentrations With Overall Equivalence Ratio for Scheme FS-04B Firing Shale DFM

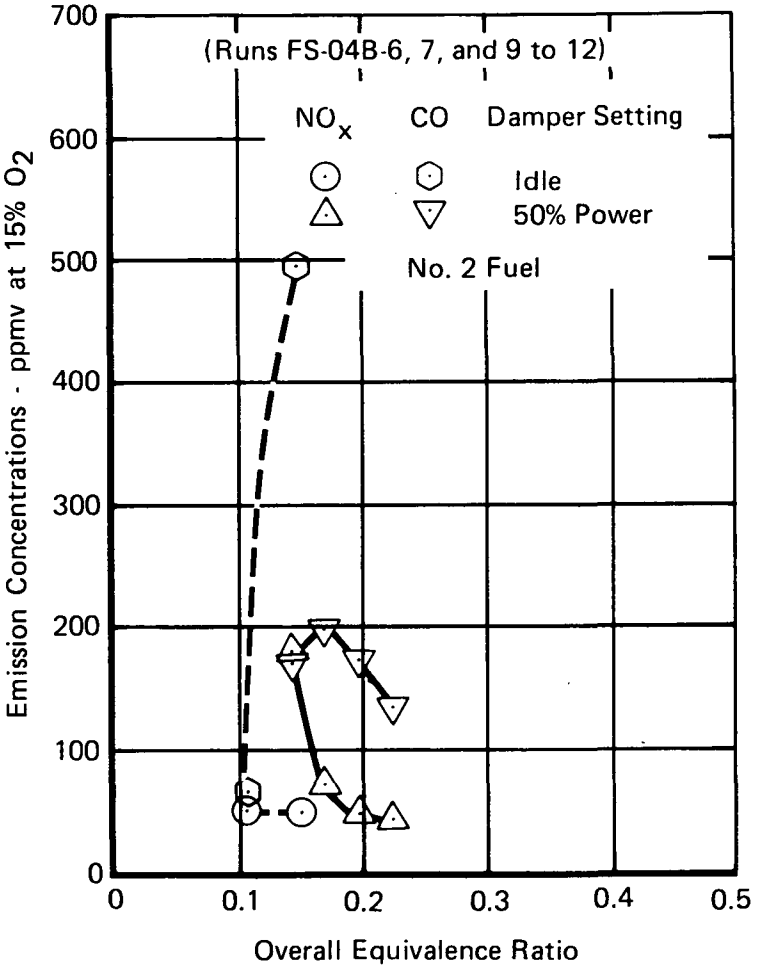

Figure 102. Variation in Emission Concentrations With Overall Equivalence Ratio for Scheme FS-04B Firing No. 2 Fuel

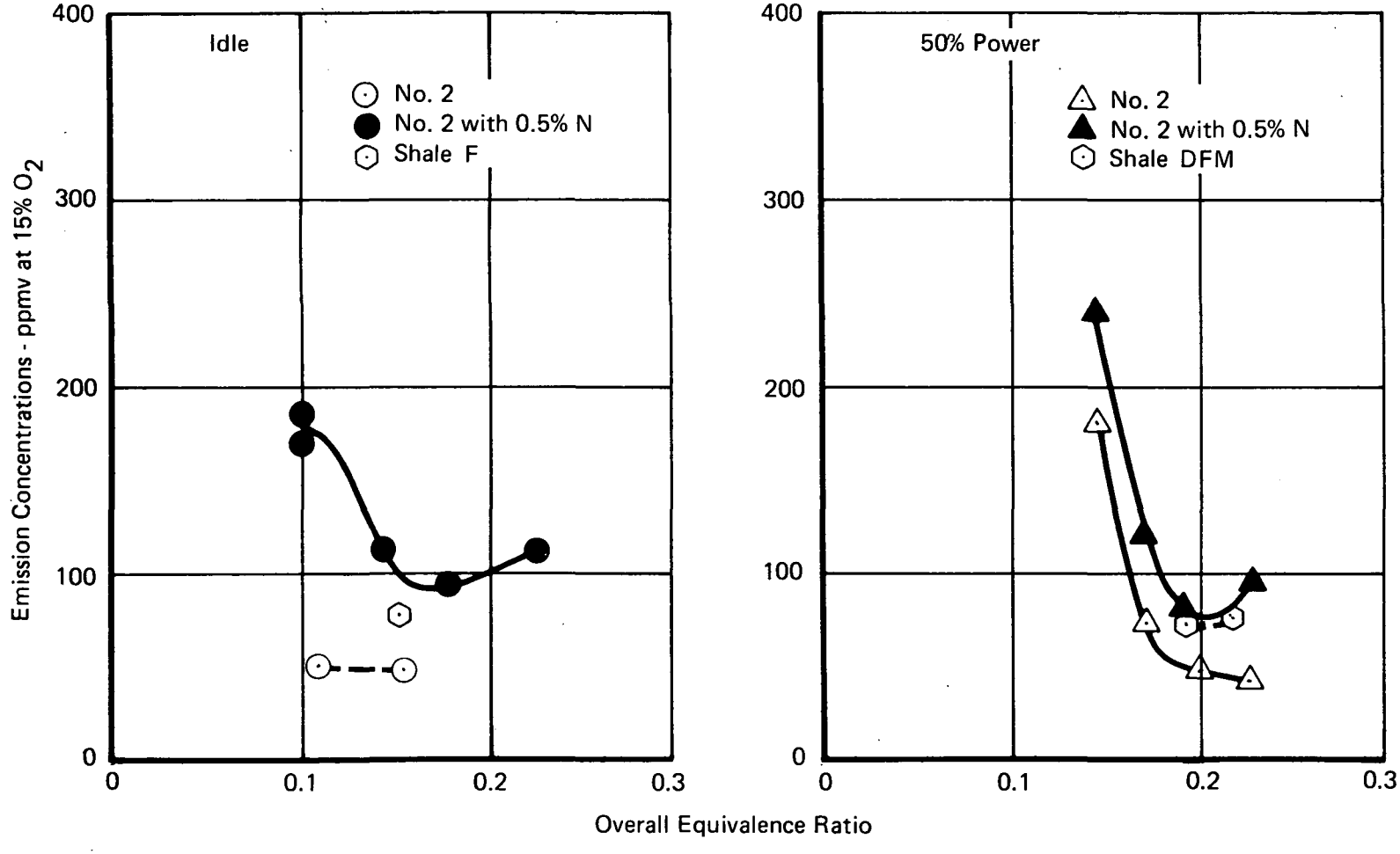

Figure 103. Comparison of NO_x Characteristics at the Idle and 50% Power Settings; Showing Variation With Fuel Type

Composite results showing the use of the premix tube damper to vary the NO_x characteristics of the combustor are presented in Figure 104. The data shown are from tests conducted using No. 2 fuel with 0.5% nitrogen. Because of the close proximity of the 50 and 100% power settings (due to the lack of full modulation capability of the premix tube damper at these two points, and the nearly identical rig pressure levels), composite results are shown for data generated using both Scheme FS-04A and FS-04B (in Scheme FS-04A, the absence of the damper resulted in greater premix tube airflow, providing data representative of a higher power setting), as well as Scheme FS-04B (which had the damper attached) alone. Using data from both schemes, the movement of the NO_x curve bucket from 0.17 to 0.235 overall equivalence ratio can be demonstrated.

Examination of the combustor following the second test series indicated that pieces of the premix tube damper had broken loose during the test (due to fatigue failure of tack welds). One piece was ingested into the premix tube where it lodged against several spraybars. There was some damage to the premix tube swirler, as a result of flameholding inside the premix passage, in the wake of the ingested part. This occurrence was due to mechanical failure and does not, we believe, reflect any deficiency in the aerodynamic design of the premix tube. Otherwise, the burner was found to be in good condition, with the exception of some deterioration in the flamespray coating and the failure of several tack welds on the guide chutes in the quick-quench section.

3.2.5 Liner Temperatures

The effect of fuel type on liner temperature levels in the FRT combustor was reported in Section 3.4.3. Data from skin thermocouples attached to the outer surface of the combustor liner were used to compute values of the liner temperature rise factor (LTRF). This parameter provides a basis of comparison for two fuels (in this case No. 2 fuel and shale-derived DFM) in terms of the overall average liner temperature rise (normalized to burner ideal temperature rise).

Although only five liner thermocouples were available, and although the "liner temperature rise" computed can be expected to vary in absolute value with the number and placement of thermocouples, with the movement of the flamefront inside the combustor, and with other factors, LTRF is a useful indicator of the relative change in liner temperatures when identical tests (same combustor configuration and operating conditions) are conducted using two separate fuels. Results for the FRT combustor indicated that the shale DFM produced an increase in liner temperature rise, as great as 4% of the burner ideal temperature rise greater at some settings, when compared to No. 2 fuel.

During the rework of the combustor hardware (from the FRT to the ECV configuration), the five original skin thermocouples were destroyed. They were replaced by ten thermocouples on the ECV combustor, at the locations shown in Figure 91. It was planned that these thermocouples would provide more complete liner temperature data, including absolute readings at additional locations and a greater base for the LTRF.

Data for the ECV combustor are presented in Table IV, Appendix A. The maximum individual temperature recorded was 1908°F; however, this reading was taken just prior to failure of the cable leading to the thermocouple in question and may not be accurate (the output from several thermocouples was lost due to the battering of cables on the outside of the rig in hot gas flowing from a leaking gasket). Several other readings of 1800 to 1860°F were also recorded.

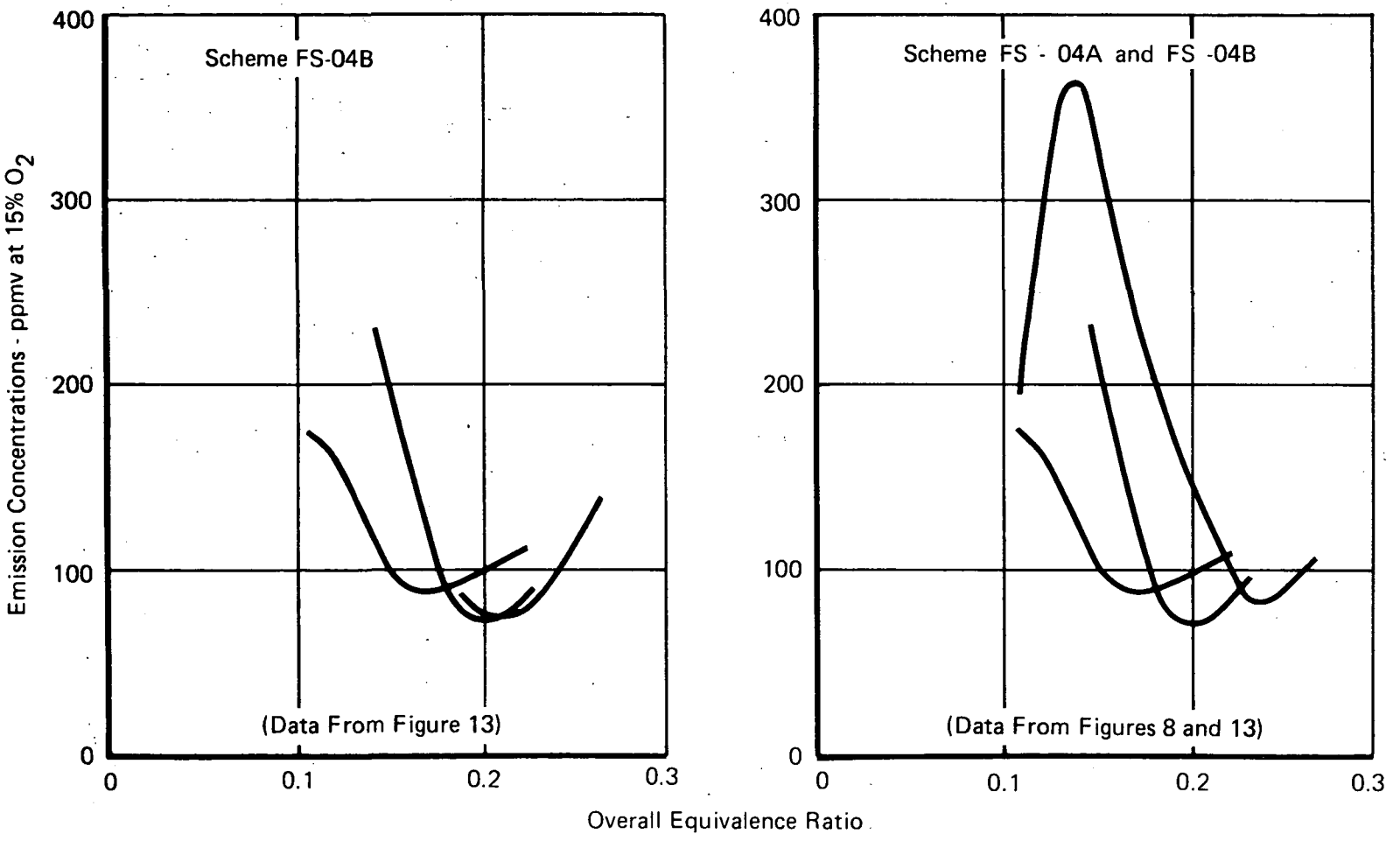

Figure 104. Composite Results Showing Use of the Premix Tube Damper to Vary NO_x Characteristics of the Combustion

Computations of the LTRF were performed as planned; however, the values obtained are significantly different from those presented in Figure 86 (for the FRT combustor). Two of the five readings used in the prior FRT computation were taken from thermocouples located in the aft dilution section of the combustor where the liner temperatures are relatively low. The other three were located in sections of the primary zone that appear relatively insensitive to flamefront movement (in some other sections of the combustor, readings can actually decline as the firing rate is increased, due to the shifting of zones of high heat release). As a result of this particular placement of thermocouples in the FRT combustor, values computed for the average liner temperature rise tend to be low, and then increase in direct proportion to the burner ideal temperature rise. LTRF for the FRT combustor was essentially constant at a value of about 0.4 (see Figure 86).

By contrast, values of LTRF computed for the ECV combustor, which are shown in Figure 105, are considerably higher (0.4 to 1.4) and vary inversely with the combustor overall equivalence ratio. Examination of the temperature data in Table IV shows that all thermocouples exhibit high readings at some or all of the overall equivalence ratio settings (low temperatures measured on the liner of the aft dilution section, which was removed in the ECV combustor, are no longer present). Parameters T_{LIN1} through T_{LIN5} also show trends opposite to the burner ideal temperature rise, presumably the result of flamefront movement. As a consequence, the values of average liner temperature rise computed from these data are higher than those obtained for the FRT combustor, and more nearly invariant with burner ideal temperature rise. When normalized to the ideal burner temperature rise in the computation of LTRF, the average liner temperature rise declines sharply with increasing overall equivalence ratio. The data in Figure 105 thus indicate that relatively high temperatures exist in some portions of the combustor liner even at low overall equivalence ratios, and that shifting of the temperature pattern occurs as the setting is increased. The spread between the maximum liner temperatures measured at the low-power and full-power settings does not appear to be great.

Interpretation of the LTRF data in Figure 105 to determine the effect of fuel type (No. 2 fuel vs shale DFM) on liner temperature rise was not possible because of scatter in the ECV combustor data. The emergence of scatter in comparison to the previous data obtained for the FRT combustor may have been a result of the strong dependence of LTRF on overall equivalence ratio in the case of the ECV combustor.

3.2.6 Residence Time Effects

Bench-scale data indicating the dependence of the minimum attainable NO_x concentration on primary zone residence time were presented in Figure 7. In Figure 106, full-scale combustor data for the FRT and ECV configurations are compared to the previous bench-scale results. For the purposes of these comparisons, effective primary zone volumes of 0.818 ft^3 and 0.568 ft^3 were assumed for the FRT and ECV configurations, respectively. Values of the primary airflow rate, inlet air temperature, and pressure were taken from the data tables in Appendix A. For the FRT combustor, test points FS-03A-26 and FS-03A-54 were selected as representative; FS-04A-6 and FS-04A-13 were selected for the ECV combustor. The residence time values shown are based on the cold flow characteristics of the combustor, and were computed as follows for test FS-04A-6:

- air density at 564°F and 100.4 psia = 0.265 lb/ft^3
- primary zone volume = 0.568 ft^3
- primary zone airflow = 3.618 lb/sec

τ_{res} = (0.265) (0.568)/3.618 = 0.042 sec

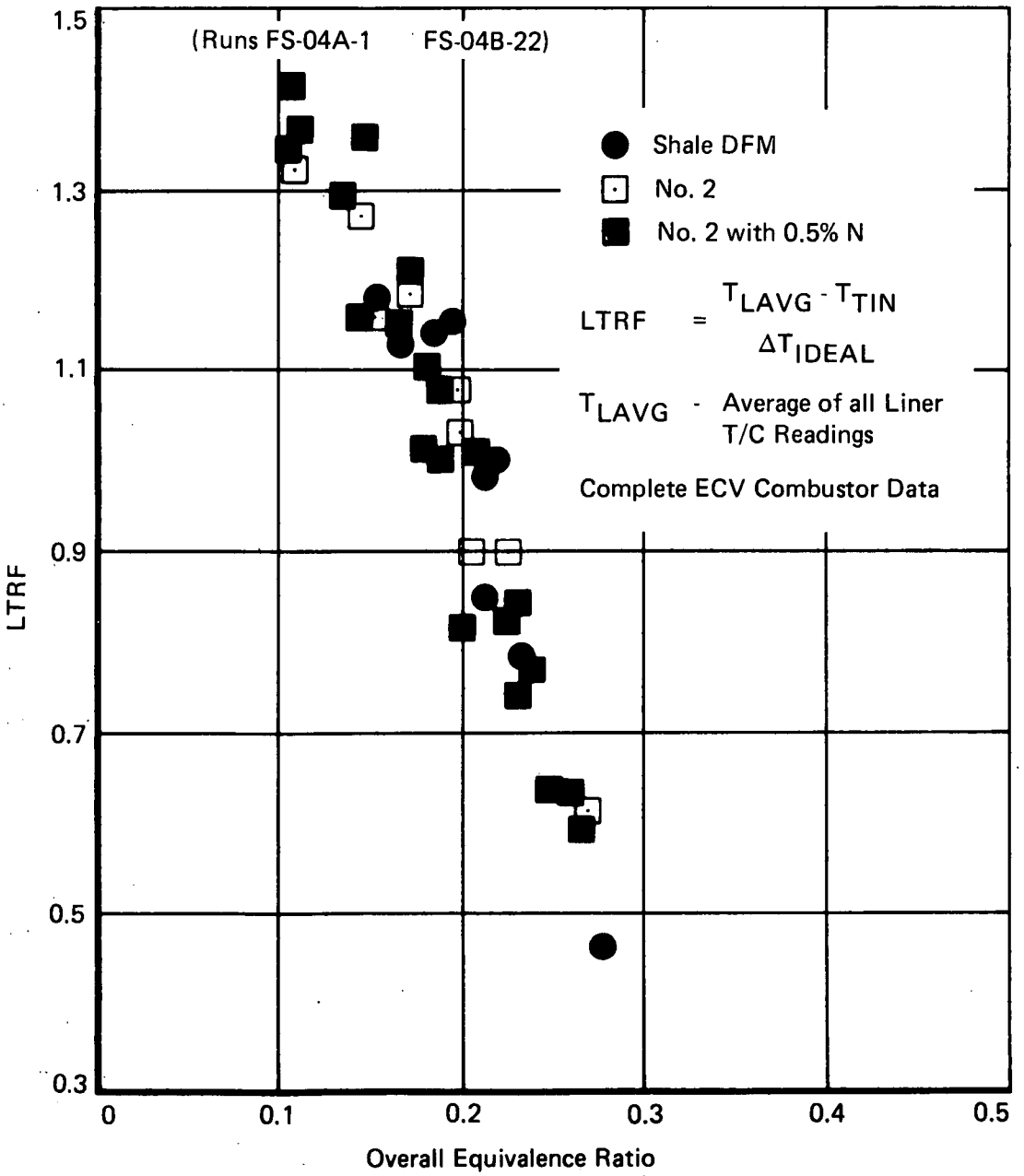

Figure 105. Variation in Liner Temperature Rise Factor (LTRF) With Overall Equivalence Ratio for Tests Conducted with the ECV Combustor

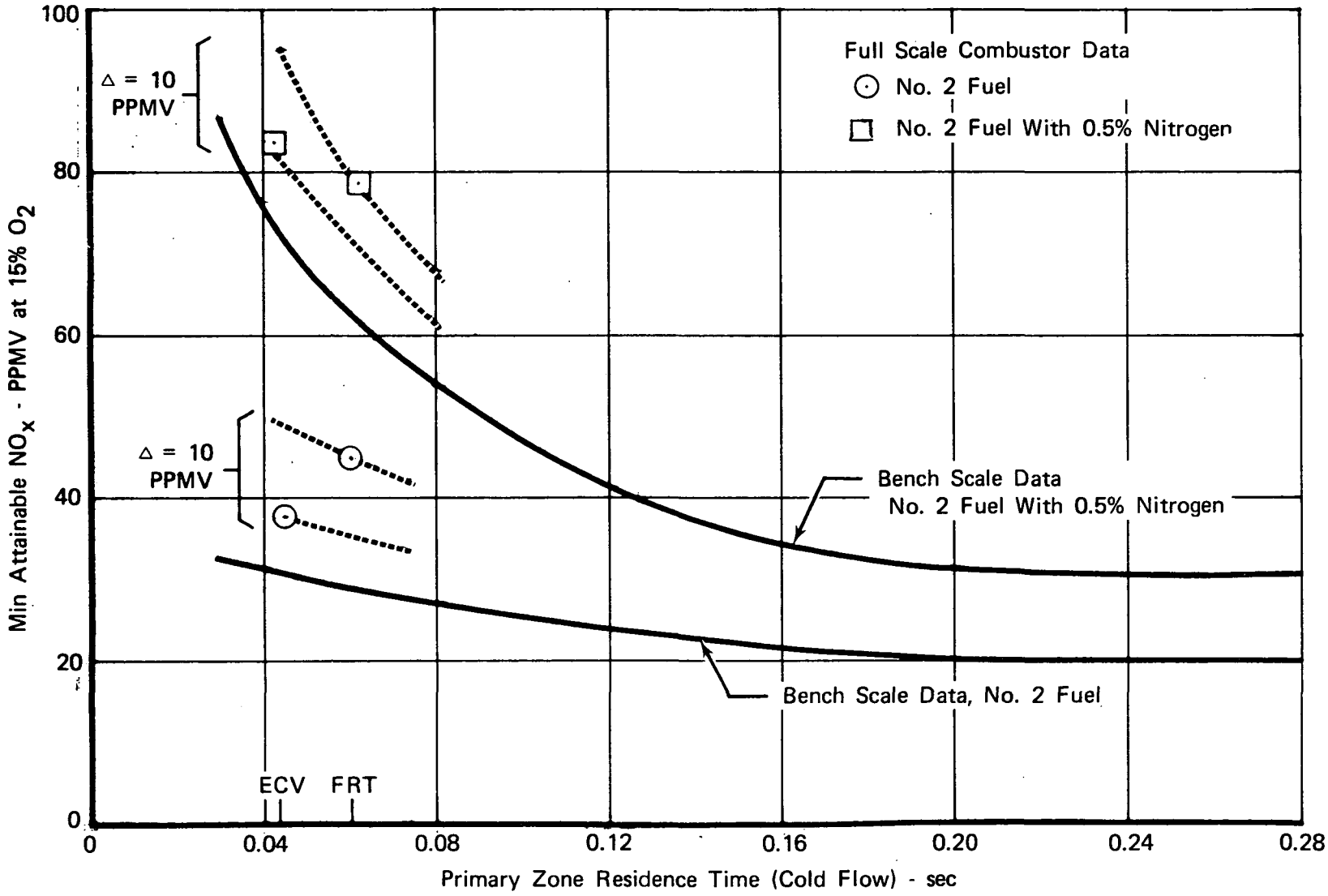

Figure 106. Variation in Minimum NO_x Concentration With Primary Residence Time

The results in Figure 106 indicate that the full-scale combustor data points lie above the curves for the bench-scale combustor. It is noteworthy that there is a decline in the minimum attainable NO_x concentration for the ECV combustor (42 msec) compared to the FRT combustor (61 msec) when firing No. 2 fuel. This result, which was discussed earlier in this section, has been attributed to the purging effect of the axially-directed penetration airflow that was introduced through the wall of the dump section of the ECV combustor (at Station E in Figure 91). By eliminating a region of recirculating gases that may have contributed to thermal NO_x formulation in the FRT combustor (fuel-nitrogen NO_x formation is less likely to depend upon a region of increased residence time), this change appears to have produced a decline of about 10 ppmv (in 15% O_2 units) in the minimum attainable NO_x concentration. As indicated in Figure 106, the same 10 ppmv increment matches the separation in curves that can be projected through the two data points for No. 2 fuel with 0.5% nitrogen. It is reasonable to expect that a decline in thermal NO_x due to the altered airflow distribution would appear in these results as well, and that the fuel-nitrogen NO_x characteristics would be largely unaffected.

SECTION 4

CONCLUSIONS FROM PHASES III AND IV

With the completion of Phases III and IV of the program, several conclusions were drawn:

1. The Rich Burn/Quick Quench combustor concept was successfully transferred from subscale to a size representative of a 25 megawatt (Mw) gas turbine engine (GTE) combustor. Indicative of this transformation was the demonstration of the same emission trends in the larger size combustor as seen in the subscale combustors of Phase II.

2. *Substantial emission reductions, representing improvements better than* the emission goals of the program, were demonstrated — while operating on both non-nitrogenous and nitrogen bearing fuels at pressures up to nearly seven atm. Because Phase II results showed that the NO_x emissions of this combustion concept are independent of pressure level, it is reasonable to expect that similar emission levels wold be achieved at pressure levels typical of full-power conditions of a 25-Mw GTE.

3. Two lengths of the Rich Burn/Quick Quench combustor were tested in Phase IV: one with about twice the length of a typical 25-Mw GTE combustor; the other, sized to fit a typical in-line engine case envelope. Both lengths of the combustor met the emission goals of the program.

4. Variable geometry was successfully employed to vary the airflow admitted into the primary combustion volume. This demonstrated the ability to meet the program emission goals over the range of operating conditions experienced in a typical 25-Mw GTE.

5. The method of final dilution air addition was shown to be important in NO_x formation within the secondary zone.

6. The Rich Burn/Quick Quench combustor also met the program emission goal while operating on a shale-derived diesel fuel marine. This indicates the potential for handling other alternative fuels (both shale oil and coal derived) by this combustion concept.

7. From the data gathered in Phase IV, the following areas of further development were indicated:

   - Improvements in the exit temperature pattern factor.
   - Primary zone liner cooling techniques and advanced materials for the primary zone liner.
   - Alternative fuel preparation devices to handle heavy fuels and allow easier control of airflow.
   - Operation of the combustor on other alternative fuels and at full engine conditions.

LIST OF SYMBOLS

The following symbols are used in the test data summaries contained in Tables I through V.

Symbol	*Definition*	*Units*
EQR	Combustor overall fuel-air equivalence ratio determined from metered fuel and air flowrates	—
PTIN	Combustor inlet total pressure	psia
TTIN	Combustor inlet total temperature	°F
WA	Total combustor airflow rate	pps
LPL	Combustor total pressure loss	%
FUEL	Fuel type. "2" designates No. 2 fuel oil. "2P" designates No. 2 fuel with pyridine (0.5%N)	—
PHIP	Primary zone equivalence ratio	—
NOX15	NO_x concentration corrected to 15% O_2	ppmv
NO15	NO concentration corrected to 15% O_2	ppmv
CO15	CO concentration corrected to 15% O_2	ppmv
UHC15	Unburned hydrocarbon concentration corrected to 15% O_2	ppmv
CO2	CO_2 concentration, uncorrected, as measured	pctv
O2	O_2 concentration, uncorrected, as measured	pctv
CFRAC	Carbon balance parameter; total carbon out divided by total carbon in	—
EFFGA	Combustion efficiency from gas analysis measurements	%
TLIN1 Through TLIN6	Combustor liner temperatures, measured at locations defined in Figure 5	°F
WAPRI	Primary zone airflow rate	pps
WASEC	Secondary zone (quick-quench) airflow rate	pps
FA	Overall fuel-air ratio determined from metered fuel and air flowrates	—
TPF	Temperature pattern factor	—

REFERENCES

1. Mosier, S. A., "Advanced Combustion Systems for Stationary Gas Turbines," EPA-600/7-77-073e, July 1977, Presented at Second Stationary Source Combustion Symposium, August 1977.

2. Lefebvre, A. H. and Herbert, M. V.; "Heat Transfer Processes in Gas Turbine Combustion Chambers," Proceedings of the Institute of Mechanical Engineers (London), Vol. 174, No. 12, 1960, pp. 463-478.

3. Rizkalla, A. A., and A. H. Lefebrve, "The Influence of Air and Liquid Properties on Airblast Atomization," Joint Fluids Engineering and ASME Conference, Montreal, Quebec, 13-15 May 1974.

4. Adelberg, M., "Mean Drop Size Resulting from the Injection of a Liquid Jet Into a High-Speed Gas Stream (Including Corrections to August 1967 Paper)," *AIAA Journal*, Vol. 6, No. 6, June 1968.

5. Ingebo, Robert D., and Hampton H. Foster, "Drop-Size Distribution for Crosscurrent Breakup of Liquid Jets III Airstreams," NACA Technical Note 4087, October 1957.

6. Weiss, Maldem A., and Charles H. Worsham, "Atomization in High Velocity Airstreams," *ARS Journal,* Vol. 29, No. 4, April 1959.

7. Nukiyama, S. and Y. Tanasawa, "Experiments on the Atomization of Liquids in an Air Stream," Droplet-Size Distribution in an Atomized Jet, transl. by E. Hope, Rept. 3, 18 March 1960, Defense Research Board, Department of National Defense, Ottawa, Canada; transl. from *Transactions of the Society of Mechanical Engineers (Japan)*, Vol. 5, No. 18, February 1939.

8. Kurzius, S. C., and F. H. Raab, "Measurement of Droplet Sizes in Liquid Jets Atomized in Low-Density Supersonic Streams," Rept. TP 152, March 1967, Aerochem Research Labs., Princeton, N. J.

9. Lorenzetto, G. E. and A. H. Lefebrve, "Measurements of Drop Size on a Plain-Jet Airblast Atomizer," *AIAA* 1976.

10. Ingebo, Robert D., "Effect of Airstream Velocity on Mean Drop Diameters of Water Sprays Produced by Pressure and Air Atomizing Nozzles," *Gas Turbine Combustion and Fuels Technology*, ASME, 27 November through 2 December 1977. Edited by E. Karl Bastress.

11. Dombrowski, N., and W. R. Johns, "The Aerodynamic Instability and Disintegration of Viscous Liquid Sheets," *Chem. Eng. Sci.*, Vol. 18, 1963.

12. Wolfe, H. E., and W. H. Andersen, "Kinetics, Mechanism, and Resultant Droplet Sizes of the Aerodynamic Breakup of Liquid Drops," Aerojet - General Corporation, Downey, California, Report No. 0395-04 (18) SP/April 1964/Copy 23.

13. Donaldson, Coleman, Snedeker, and Richard, "Experimental Investigation of the Structure of Vortices in Simple Cylindrical Vortec Chamber," ARAP Report No. 47, December 1962.

14. Chelko, Louis, "Penetration of Liquid Jets into a High Velocity Airstream," NACA E50F21, 14 August 1950.

15. Koplin, M. A., K. P. Horn, and R. E. Reichenbach, "Study of a Liquid Injectant Into a Supersonic Flow," *AIAA Journal*, Vol. 6, No. 5, May 1968, pp. 853-858.

16. Tacina, Robert, "Experimental Evaluation of Premixing/Prevaporizing Fuel Injection Concepts for a Gas Turbine Catalytic Combustor," *Gas Turbine Combustion and Fuels Technology*, ASME, 27 November through 2 December 1977, Edited by E. Karl Bastress.

APPENDIX A

DATA LISTINGS

TABLE I
COMBUSTOR OPERATING PARAMETER DATA

Test No.	EQR	PTIN	TTIN	WA	LPL	Fuel
FS-01A-1	0.1381	55.1	501.0	7.298	3.57	2
FS-01A-2	0.2108	54.9	509.7	6.913	3.22	2
FS-01A-3	0.1817	54.9	512.3	6.886	3.31	2
FS-01A-4	0.2456	54.6	516.3	6.764	3.06	2
FS-01A-5	0.1148	54.4	514.7	7.294	3.43	2
FS-02A-1	0.1715	16.1	488.0	2.501	4.78	2
FS-02A-2*	0.2006	16.1	488.0	2.501	4.78	2
FS-02A-3*	0.2253	16.1	488.0	2.501	4.78	2
FS-02A-4*	0.2529	16.1	488.0	2.501	4.78	2
FS-02A-5*	0.2776	16.1	488.0	2.501	4.78	2
FS-02A-6*	0.3023	16.1	488.0	2.501	4.78	2
FS-02A-7*	0.3285	16.1	488.0	2.501	4.78	2
FS-02A-8*	0.1279	50.5	539.7	9.354	5.90	2
FS-02A-9*	0.1439	50.5	539.7	9.354	5.90	2
FS-02A-10*	0.1570	50.5	539.7	9.354	5.90	2
FS-02A-11*	0.1701	50.5	539.7	9.354	5.90	2
FS-02A-12*	0.1831	50.5	539.7	9.354	5.90	2
FS-02A-13*	0.1962	50.5	539.7	9.354	5.90	2
FS-02A-14*	0.2296	50.5	539.7	9.354	5.90	2
FS-02A-15*	0.2616	50.5	539.7	9.354	5.90	2
FS-03A-1	0.1323	49.9	453.0	8.315	5.51	2
FS-03A-2	0.1613	50.8	456.0	8.158	5.41	2
FS-03A-3	0.1831	50.9	460.0	8.184	5.50	2
FS-03A-4	0.2035	50.2	461.0	8.477	5.87	2
FS-03A-5	0.2296	50.2	453.0	8.296	5.77	2
FS-03A-6	0.2485	50.8	468.3	8.108	5.61	2
FS-03A-7	0.2544	50.6	470.0	7.984	5.53	2P
FS-03A-8	0.2369	50.0	470.0	8.070	5.70	2P
FS-03A-9	0.2151	51.2	470.0	7.804	5.37	2P
FS-03A-10	0.1977	50.1	470.0	7.599	5.78	2P
FS-03A-11	0.0959	50.4	395.0	8.867	5.75	2P
FS-03A-12	0.1264	49.9	398.0	8.565	5.61	2P
FS-03A-13	0.1526	49.9	399.0	8.395	5.61	2P
FS-03A-14	0.1773	50.2	402.0	8.227	5.48	2P
FS-03A-15	0.2064	49.9	403.0	8.015	5.22	2P
FS-03A-16	0.2224	50.0	405.0	8.255	5.40	2P
FS-03A-17	0.2427	50.4	402.0	8.108	5.26	2P
FS-03A-18	0.2703	50.1	402.0	8.230	5.39	2P
FS-03A-19	0.2980	50.3	404.0	8.081	5.18	2P
FS-03A-20	0.1294	98.4	549.0	17.310	5.79	2P
FS-03A-21	0.1264	99.9	568.0	16.272	5.61	2P
FS-03A-22	0.1570	100.0	574.0	15.705	5.40	2P
FS-03A-23	0.1846	100.1	576.0	15.683	5.50	2P
FS-03A-24	0.2006	100.1	577.0	16.348	5.55	2P
FS-03A-25	0.2311	100.4	580.0	15.991	5.53	2P
FS-03A-26	0.2645	98.9	581.0	15.538	5.36	2P
FS-03A-27	0.2878	98.1	580.0	15.742	5.71	2P
FS-03A-28	0.1831	100.5	578.0	15.688	4.99	2
FS-03A-29	0.2209	100.1	579.0	14.905	4.81	2
FS-03A-30	0.2282	99.7	580.0	16.194	5.76	2
FS-03A-31	0.2587	100.5	579.0	15.851	5.62	2
FS-03A-32	0.2907	99.6	582.0	15.447	5.52	2
FS-03A-33	0.1098	50.2	460.0	9.221	5.38	S
FS-03A-34	0.1344	50.2	473.0	9.158	5.28	S
FS-03A-35	0.1546	50.4	479.0	9.184	5.36	S
FS-03A-36	0.1864	50.0	483.0	8.824	5.30	S
FS-03A-37	0.2066	50.0	485.0	8.907	5.50	S
FS-03A-38	0.2326	50.2	487.0	8.718	5.48	S
FS-03A-39	0.2616	50.1	488.0	8.563	5.39	S
FS-03A-40	0.1113	100.3	561.0	18.188	5.63	S
FS-03A-41	0.1402	99.6	566.0	17.326	5.47	S
FS-03A-42	0.1633	99.7	568.0	17.415	5.57	S
FS-03A-43	0.1879	100.8	569.0	17.301	5.46	S
FS-03A-44	0.2211	100.3	570.0	16.558	5.24	S
FS-03A-45	0.2370	100.3	570.0	17.086	5.63	S
FS-03A-46	0.2514	100.5	570.0	16.939	5.52	S
FS-03A-47	0.1192	100.4	568.0	17.085	5.09	2
FS-03A-48	0.1337	100.0	567.0	18.373	5.99	2
FS-03A-49	0.1613	100.5	567.0	17.797	5.62	2
FS-03A-50	0.1875	101.1	568.0	17.309	5.25	2
FS-03A-51	0.2020	97.2	569.0	18.187	6.32	2
FS-03A-52	0.2282	98.1	568.0	17.856	6.26	2
FS-03A-53	0.2413	98.3	569.0	17.740	6.15	2
FS-03A-54	0.2602	99.1	570.0	17.558	6.05	2
FS-04A-1	0.1090	99.4	563.0	18.674	5.93	2P
FS-04A-2	0.1352	100.9	564.0	18.356	5.55	2P
FS-04A-3	0.1642	99.4	563.0	17.540	5.39	2P
FS-04A-4	0.1817	98.5	564.0	17.963	5.73	2P
FS-04A-5	0.2078	99.3	563.0	17.657	5.49	2P
FS-04A-6	0.2355	100.4	564.0	17.332	5.43	2P
FS-04A-7	0.2660	100.3	562.0	16.844	5.14	2P
FS-04A-8	0.2514	99.9	561.0	17.114	5.31	2P
FS-04A-9	0.1850	99.3	565.0	17.724	5.79	S
FS-04A-10	0.2124	99.9	565.0	17.310	5.56	S
FS-04A-11	0.1977	99.8	564.0	16.575	5.07	2
FS-04A-12	0.2035	96.2	563.0	17.700	6.38	2
FS-04A-13	0.2689	97.5	564.0	16.823	5.79	2
FS-04A-14	0.2326	100.9	573.0	16.939	5.60	S
FS-04A-15	0.2760	100.9	575.0	16.277	5.36	S
FS-04A-16	0.2110	99.2	574.0	17.126	6.09	S
FS-04A-17	0.1647	99.2	574.0	17.136	6.14	S
FS-04B-1	0.1773	40.0	309.0	7.479	4.91	2P
FS-04B-2	0.1032	39.8	317.0	8.091	6.05	2P
FS-04B-3	0.2253	41.4	318.0	7.451	4.51	2P
FS-04B-4	0.1453	39.1	318.0	7.496	6.53	2P
FS-04B-5	0.1032	41.1	318.0	6.759	3.35	2P
FS-04B-6	0.1061	39.4	314.0	7.705	6.11	2
FS-04B-7	0.1497	39.2	315.0	7.519	5.64	2
FS-04B-8	0.1532	41.2	327.0	8.040	5.25	S
FS-04B-9	0.1439	92.6	549.0	17.555	5.73	2
FS-04B-10	0.1701	93.8	556.0	17.273	5.39	2
FS-04B-11	0.1962	94.0	559.0	16.859	5.23	2
FS-04B-12	0.2238	95.2	562.0	16.658	5.16	2
FS-04B-13	0.2168	95.6	561.0	16.802	5.04	S
FS-04B-14	0.1922	95.4	562.0	17.070	5.15	S
FS-04B-15	0.2267	95.6	562.0	16.833	4.98	2P
FS-04B-16	0.1904	93.4	563.0	17.149	5.42	2P
FS-04B-17	0.1701	92.2	563.0	17.421	5.59	2P
FS-04B-18	0.1453	93.0	562.0	17.464	5.33	2P
FS-04B-19	0.2006	97.6	782.0	16.702	5.39	2P
FS-04B-20	0.2296	99.2	778.0	16.255	6.14	2P
FS-04B-21	0.2631	99.4	777.0	16.255	5.73	2P
FS-04B-22	0.1846	99.4	783.0	15.952	5.19	2P

*Values listed are approximate — only emissions and fuel flow were read, airflow was maintained nearly constant.

TABLE II
EMISSION CONCENTRATION DATA

Test No.	EQR	PHIP	NO_{x15}	NO_{15}	CO_{15}	UHC_{15}	Test No.	EQR	PHIP	NO_{x15}	NO_{15}	CO_{15}	UHC_{15}
FS-01A-1	0.1381	0.7485	150.3	137.1	251.0	7.8	FS-03A-38	0.2326	1.1501	67.4	45.0	320.2	2.1
FS-01A-2	0.2108	1.2629	60.7	56.1	192.5	1.4	FS-03A-39	0.2616	1.3075	64.0	47.5	213.4	1.5
FS-01A-3	0.1817	1.0080	84.9	77.8	220.5	1.5	FS-03A-40	0.1113	0.5758	161.4	128.6	81.3	9.7
FS-01A-4	0.2456	1.6139	55.6	53.2	154.8	1.0	FS-03A-41	0.1402	0.7352	392.5	342.3	124.4	5.0
FS-01A-5	0.1148	0.5954	104.7	86.6	348.8	20.7	FS-03A-42	0.1633	0.8431	292.7	244.4	174.2	3.1
							FS-03A-43	0.1879	0.9761	141.8	101.2	195.5	2.2
FS-02A-1	0.1715	0.7114	37.4	37.0	451.2	—	FS-03A-44	0.2211	1.1320	72.4	47.3	165.6	1.6
FS-02A-2*	0.2006	0.8333	40.2	40.2	608.9	—	FS-03A-45	0.2370	1.2275	63.5	42.1	149.9	1.4
FS-02A-3*	0.2253	0.9350	36.7	36.4	671.8	—	FS-03A-46	0.2514	1.2944	65.7	47.0	118.3	1.3
FS-02A-4*	0.2529	1.0501	27.7	27.4	516.3	—	FS-03A-47	0.1192	0.6145	169.2	141.2	89.4	5.0
FS-02A-5*	0.2776	1.1518	22.6	22.6	328.4	—	FS-03A-48	0.1337	0.6865	330.6	289.7	122.1	4.0
FS-02A-6*	0.3023	1.2534	19.9	19.9	189.4	—	FS-03A-49	0.1613	0.8170	290.1	240.9	166.8	2.2
FS-02A-7*	0.3285	1.3618	19.4	19.4	143.4	—	FS-03A-50	0.1875	0.9468	128.9	94.1	183.1	1.3
FS-02A-8*	0.1279	0.6141	37.1	28.8	92.5	—	FS-03A-51	0.2020	1.0369	81.0	50.0	224.8	1.3
FS-02A-9*	0.1439	0.6893	74.5	65.3	144.5	—	FS-03A-52	0.2282	1.1557	51.0	31.3	185.2	1.1
FS-02A-10*	0.1570	0.7520	75.9	61.1	248.2	—	FS-03A-53	0.2413	1.2243	46.2	29.7	151.9	1.0
FS-02A-11*	0.1701	0.8147	71.3	54.8	309.5	—	FS-03A-54	0.2602	1.3115	44.9	32.9	105.3	0.9
FS-02A-12*	0.1831	0.8773	62.2	55.3	343.7	—							
FS-02A-13*	0.1962	0.9400	51.9	46.5	332.4	—	FS-04A-1	0.1090	0.5242	194.2	192.4	55.3	10.0
FS-02A-14*	0.2296	1.0967	32.9	30.9	244.0	—	FS-04A-2	0.1352	0.6620	364.4	359.5	86.1	5.1
FS-02A-15*	0.2616	1.2533	31.1	30.3	121.5	—	FS-04A-3	0.1642	0.7949	289.2	184.7	363.4	8.9
							FS-04A-4	0.1817	0.8879	201.0	93.0	481.7	11.4
FS-03A-1	0.1323	0.6158	91.8	83.0	72.9	7.3	FS-04A-5	0.2078	1.0062	143.4	56.8	481.1	10.7
FS-03A-2	0.1613	0.7279	177.5	150.3	175.9	7.1	FS-04A-6	0.2355	1.1301	83.5	31.2	481.0	10.8
FS-03A-3	0.1831	0.8398	128.4	92.5	255.9	4.1	FS-04A-7	0.2660	1.2649	110.6	61.7	306.9	3.1
FS-03A-4	0.2035	0.9301	73.0	49.1	296.2	3.0	FS-04A-8	0.2514	1.1870	101.6	45.0	402.0	5.5
FS-03A-5	0.2296	1.1185	25.9	15.4	291.4	3.5	FS-04A-9	0.1850	0.9369	87.0	28.1	641.5	33.8
FS-03A-6	0.2485	1.1305	29.8	20.9	202.3	2.8	FS-04A-10	0.2124	0.9405	65.3	22.0	585.3	21.6
FS-03A-7	0.2544	1.0775	107.8	85.7	160.9	2.8	FS-04A-11	0.1977	—	59.0	18.2	561.6	23.7
FS-03A-8	0.2369	1.0138	89.9	68.7	218.3	2.8	FS-04A-12	0.2035	1.0417	46.4	15.0	594.1	24.4
FS-03A-9	0.2151	0.9528	75.2	53.1	284.7	2.9	FS-04A-13	0.2689	1.3399	37.9	18.4	294.5	5.4
FS-03A-10	0.1977	0.8095	136.0	105.6	249.5	3.0	FS-04A-14	0.2326	1.1988	70.3	33.7	291.6	7.8
FS-03A-11	0.0959	0.4681	171.8	170.4	18.1	6.4	FS-04A-15	0.2760	1.3543	93.7	74.8	81.4	2.2
FS-03A-12	0.1264	0.6155	193.8	186.1	33.8	4.9	FS-04A-16	0.2110	1.0679	57.8	17.3	622.6	20.3
FS-03A-13	0.1526	0.7421	226.0	211.5	79.3	3.7	FS-04A-17	0.1647	0.9126	100.7	28.8	698.5	32.5
FS-03A-14	0.1773	0.8918	185.2	183.7	189.0	3.1							
FS-03A-15	0.2064	0.9989	129.4	102.6	296.5	2.7	FS-04B-1	0.1773	—	95.1	79.2	748.8	7.1
FS-03A-16	0.2224	1.0806	96.3	67.5	322.4	1.9	FS-04B-2	0.1032	—	185.4	174.5	218.0	10.6
FS-03A-17	0.2427	1.1646	73.1	45.2	298.4	1.4	FS-04B-3	0.2253	—	113.2	100.1	517.5	5.1
FS-03A-18	0.2703	1.3063	69.8	44.0	256.6	1.2	FS-04B-4	0.1453	—	115.6	103.8	752.8	8.3
FS-03A-19	0.2980	1.4452	80.8	62.8	181.4	1.1	FS-04B-5	0.1032	—	173.5	166.4	183.4	—
FS-03A-20	0.1294	0.6482	258.3	232.5	47.5	4.4	FS-04B-6	0.1061	—	51.0	44.2	65.9	—
FS-03A-21	0.1264	0.5650	265.8	246.7	53.1	21.8	FS-04B-7	0.1497	—	49.2	39.1	494.0	—
FS-03A-22	0.1570	0.7001	442.0	401.4	79.8	14.1	FS-04B-8	0.1532	—	80.0	41.8	601.6	—
FS-03A-23	0.1846	0.8121	294.2	254.2	105.6	9.3	FS-04B-9	0.1439	—	181.1	155.1	171.2	—
FS-03A-24	0.2006	0.9125	180.0	150.5	115.6	11.4	FS-04B-10	0.1701	—	73.4	48.2	200.0	—
FS-03A-25	0.2311	1.0351	104.9	82.2	97.6	6.1	FS-04B-11	0.1962	—	48.2	28.5	174.5	—
FS-03A-26	0.2645	1.1917	79.2	67.6	60.7	4.0	FS-04B-12	0.2238	—	43.0	28.9	134.3	—
FS-03A-27	0.2878	1.2880	95.9	87.8	42.0	3.5	FS-04B-13	0.2168	—	81.2	57.0	143.8	—
FS-03A-28	0.1831	0.8462	203.6	162.6	103.4	3.8	FS-04B-14	0.1922	—	75.4	52.5	174.6	—
FS-03A-29	0.2209	1.0007	81.9	59.8	88.0	3.0	FS-04B-15	0.2267	—	94.1	80.7	105.8	—
FS-03A-30	0.2282	1.0385	67.3	48.2	96.4	2.7	FS-04B-16	0.1904	—	83.6	58.2	161.0	—
FS-03A-31	0.2587	1.1595	48.2	37.3	69.8	2.3	FS-04B-17	0.1701	—	120.0	86.6	178.6	—
FS-03A-32	0.2907	1.2977	43.7	39.9	37.5	1.8	FS-04B-18	0.1453	—	239.3	196.3	181.6	—
FS-03A-33	0.1098	0.5434	114.5	111.6	50.1	15.3	FS-04B-19	0.2006	—	81.1*	67.7*	85.9	—
FS-03A-34	0.1344	0.6642	196.9	182.7	100.6	8.9	FS-04B-20	0.2296	—	97.8*	93.0*	56.0	—
FS-03A-35	0.1546	0.7623	230.9	210.9	191.0	6.3	FS-04B-21	0.2631	—	143.3*	140.6*	34.8	—
FS-03A-36	0.1864	0.9154	138.4	109.2	325.4	3.5	FS-04B-22	0.1846	—	95.5*	82.7*	93.0	—
FS-03A-37	0.2066	1.0317	93.3	65.2	362.9	2.6							

*Corrected for oxides of nitrogen from vitiation of inlet air.

TABLE III
GAS ANALYSIS PARAMETER DATA

Test No.	*EQR*	*CO_2*	*O_2*	*CFRAC*	*EFFGA*	*Test No.*	*EQR*	*CO_2*	*O_2*	*CFRAC*	*EFFGA*
FS-01A-1	0.1381	2.04	18.22	1.0583	99.67	FS-03A-38	0.2326	3.24	17.23	0.9943	99.61
FS-01A-2	0.2108	3.13	16.60	1.0691	99.76	FS-03A-39	0.2616	3.71	16.36	1.0096	99.74
FS-01A-3	0.1817	2.65	17.25	1.0499	99.73	FS-03A-40	0.1113	1.55	18.96	0.9805	99.87
FS-01A-4	0.2456	3.65	15.83	1.0699	99.81	FS-03A-41	0.1402	2.00	18.32	1.0029	99.83
FS-01A-5	0.1148	1.67	18.45	1.0407	99.51	FS-03A-42	0.1633	2.30	17.94	1.0014	99.78
						FS-03A-43	0.1879	2.65	17.47	1.0049	99.76
FS-02A-1	0.1715	2.36	16.75	0.9918	99.46	FS-03A-44	0.2211	3.12	16.73	1.0035	99.80
FS-02A-2*	0.2006	2.70	16.45	0.9745	99.27	FS-03A-45	0.2370	3.37	16.31	1.0085	99.82
FS-02A-3*	0.2253	3.09	15.86	0.9948	99.19	FS-03A-46	0.2514	3.59	15.98	1.0135	99.85
FS-02A-4*	0.2529	3.54	15.26	1.0122	99.38	FS-03A-47	0.1192	1.71	18.64	1.0154	99.88
FS-02A-5*	0.2776	3.90	14.81	1.0142	99.60	FS-03A-48	0.1337	1.95	18.37	1.0317	99.84
FS-02A-6*	0.3023	4.27	14.27	1.0194	99.77	FS-03A-49	0.1613	2.34	17.83	1.0316	99.79
FS-02A-7*	0.3285	4.67	13.76	1.0271	99.83	FS-03A-50	0.1875	2.72	17.30	1.0298	99.78
FS-02A-8*	0.1279	2.16	17.55	1.1931	99.89	FS-03A-51	0.2020	2.97	16.95	1.0475	99.73
FS-02A-9*	0.1439	2.44	17.32	1.2059	99.83	FS-03A-52	0.2282	3.35	16.48	1.0473	99.77
FS-02A-10*	0.1570	2.61	16.84	1.1879	99.70	FS-03A-53	0.2413	3.54	16.14	1.0515	99.81
FS-02A-11*	0.1701	2.81	16.52	1.1821	99.63	FS-03A-54	0.2602	3.84	15.67	1.0572	99.87
FS-02A-12*	0.1831	3.07	16.15	1.2014	99.59						
FS-02A-13*	0.1962	3.27	15.86	1.1941	99.60	FS-04A-1	0.1090	1.63	19.86	1.0572	99.90
FS-02A-14*	0.2296	3.84	15.05	1.2028	99.71	FS-04A-2	0.1352	2.02	19.80	1.0617	99.88
FS-02A-15*	0.2616	4.44	14.27	1.2156	99.85	FS-04A-3	0.1642	2.39	19.74	1.0454	99.53
						FS-04A-4	0.1817	2.65	17.39	1.0532	99.38
FS-03A-1	0.1323	2.01	18.63	1.0752	99.89	FS-04A-5	0.2078	3.04	17.95	1.0585	99.39
FS-03A-2	0.1613	2.44	17.89	1.0773	99.77	FS-04A-6	0.2355	3.43	17.17	1.0502	99.38
FS-03A-3	0.1831	2.78	18.39	1.0802	99.68	FS-04A-7	0.2660	3.86	16.08	1.0491	99.62
FS-03A-4	0.2035	3.04	17.09	1.0640	99.64	FS-04A-8	0.2514	3.64	16.33	1.0462	99.50
FS-03A-5	0.2296	3.50	17.09	1.0927	99.64	FS-04A-9	0.1850	2.64	17.83	1.0253	99.11
FS-03A-6	0.2485	3.79	16.08	1.0931	99.75	FS-04A-10	0.2124	3.00	17.53	1.0180	99.22
FS-03A-7	0.2544	3.75	15.84	1.0531	99.80	FS-04A-11	0.1977	2.86	17.67	1.0493	99.25
FS-03A-8	0.2369	3.44	16.13	1.0372	99.73	FS-04A-12	0.2035	3.01	17.53	1.0686	99.20
FS-03A-9	0.2151	3.08	16.51	1.0196	99.65	FS-04A-13	0.2689	3.96	16.75	1.0620	99.63
FS-03A-10	0.1977	2.85	16.73	1.0247	99.69	FS-04A-14	0.2326	3.44	16.91	1.0606	99.62
FS-03A-11	0.0959	1.32	19.37	0.9677	99.96	FS-04A-15	0.2760	4.00	16.13	1.0334	99.89
FS-03A-12	0.1264	1.69	18.87	0.9480	99.94	FS-04A-16	0.2110	3.09	17.37	1.0515	99.18
FS-03A-13	0.1526	2.00	18.30	0.9339	99.89	FS-04A-17	0.1647	2.33	18.34	1.0220	99.05
FS-03A-14	0.1773	2.33	17.80	0.9466	99.76						
FS-03A-15	0.2064	2.74	17.27	0.9555	99.63	FS-04B-1	0.1773	2.40	17.81	0.9828	99.08
FS-03A-16	0.2224	2.97	16.86	0.9645	99.61	FS-04B-2	0.1032	1.38	18.97	0.9586	99.70
FS-03A-17	0.2427	3.28	16.29	0.9782	99.64	FS-04B-3	0.2253	3.13	16.60	1.0046	99.36
FS-03A-18	0.2703	3.58	15.87	0.9577	99.69	FS-04B-4	0.1453	1.92	18.11	0.9584	99.07
FS-03A-19	0.2980	3.95	15.31	0.9576	99.78	FS-04B-5	0.1032	1.38	18.86	0.9585	99.49
FS-03A-20	0.1294	1.79	18.40	0.9857	99.93	FS-04B-6	0.1061	1.47	18.78	0.9818	99.92
FS-03A-21	0.1264	1.88	18.79	1.0599	99.86	FS-04B-7	0.1497	2.20	17.60	1.0610	99.41
FS-03A-22	0.1570	2.34	17.86	1.0608	99.86	FS-04B-8	0.1532	2.22	17.77	1.0425	99.28
FS-03A-23	0.1846	2.72	17.32	1.0579	99.84	FS-04B-9	0.1439	2.06	17.77	1.0202	99.80
FS-03A-24	0.2006	2.98	16.98	1.0614	99.82	FS-04B-10	0.1701	2.49	17.32	1.0482	99.76
FS-03A-25	0.2311	3.40	16.28	1.0575	99.86	FS-04B-11	0.1962	2.86	16.74	1.0451	99.79
FS-03A-26	0.2645	4.02	15.58	1.0892	99.91	FS-04B-12	0.2238	3.29	16.09	1.0555	99.84
FS-03A-27	0.2878	4.36	14.98	1.0888	99.94	FS-04B-13	0.2168	3.17	16.32	1.0407	99.83
FS-03A-28	0.1831	2.79	16.88	1.0903	99.86	FS-04B-14	0.1922	2.87	16.79	1.0660	99.79
FS-03A-29	0.2209	3.34	16.15	1.0843	99.88	FS-04B-15	0.2267	3.29	16.15	1.0418	99.87
FS-03A-30	0.2282	3.47	15.92	1.0887	99.87	FS-04B-16	0.1904	2.89	16.85	1.0813	99.81
FS-03A-31	0.2587	3.89	15.37	1.0821	99.91	FS-04B-17	0.1701	2.45	17.23	1.0254	99.79
FS-03A-32	0.2907	4.39	14.57	1.0854	99.95	FS-04B-18	0.1453	2.11	17.77	1.0399	99.78
FS-03A-33	0.1098	1.55	19.18	0.9854	99.89	FS-04B-19	0.2006	3.64*	15.71*	1.0303	99.92
FS-03A-34	0.1344	1.88	18.75	0.9889	99.85	FS-04B-20	0.2296	4.03*	15.08*	1.0393	99.94
FS-03A-35	0.1546	2.17	18.44	0.9946	99.75	FS-04B-21	0.2631	4.61*	14.16*	1.0689	99.96
FS-03A-36	0.1864	2.59	17.88	0.9923	99.60	FS-04B-22	0.1846	3.34*	15.86*	1.0301	99.91
FS-03A-37	0.2066	2.90	17.44	0.9973	99.56						

*Includes effect of vitiated inlet air.

TABLE IV
COMBUSTOR LINER TEMPERATURE DATA

Test No.	EQR	(Dome Avg) $TLIN_1$	BST3 $TLIN_2$	BST6 $TLIN_3$	BST7 $TLIN_4$	BST8 $TLIN_5$	BST9 $TLIN_6$	BST10 $TLIN_7$	BST12 $TLIN_8$
FS-01A-1	0.1381	1066	960	1030	1021	556	659		
FS-01A-2	0.2108	1410	1226	1403	1392	637	787		
FS-01A-3	0.1817	1366	1175	1305	1289	600	728		
FS-01A-4	0.2456	1279	1301	1496	1513	688	828		
FS-01A-5	0.1148	1130	916	915	900	556	640		
FS-02A-1	0.1715	1025	1193	1244	1192	570	691		
FS-02A-2*	0.2006	—	—	—	—	—	—		
FS-02A-3*	0.2253	—	—	—	—	—	—		
FS-02A-4*	0.2529	—	—	—	—	—	—		
FS-02A-5*	0.2776	—	—	—	—	—	—		
FS-02A-6*	0.3023	—	—	—	—	—	—		
FS-02A-7*	0.3285	—	—	—	—	—	—		
FS-02A-8*	0.1279	1115	1136	1166	1106	602	701		
FS-02A-9*	0.1439	—	—	—	—	—	—		
FS-02A-10*	0.1570	—	—	—	—	—	—		
FS-02A-11*	0.1701	—	—	—	—	—	—		
FS-02A-12*	0.1831	—	—	—	—	—	—		
FS-02A-13*	0.1962	—	—	—	—	—	—		
FS-02A-14*	0.2296	—	—	—	—	—	—		
FS-02A-15*	0.2611	—	—	—	—	—	—		
FS-03A-1	0.1323	1033	1208	1304	1314	505	592		
FS-03A-2	0.1613	1075	1280	1431	1427	522	644		
FS-03A-3	0.1831	1123	1358	1501	1502	533	677		
FS-03A-4	0.2035	1136	1399	1537	1533	537	695		
FS-03A-5	0.2296	1120	1430	1552	1547	538	709		
FS-03A-6	0.2485	1065	972	1171	1298	578	783		
FS-03A-7	0.2544	1097	942	1160	1308	573	770		
FS-03A-8	0.2369	1078	902	1126	1280	565	755		
FS-03A-9	0.2151	1210	989	1244	1445	572	757		
FS-03A-10	0.1977	1103	1228	1452	1486	599	727		
FS-03A-11	0.0959	871	810	1054	—	428	481		
FS-03A-12	0.1264	895	—	1142	1108	440	520		
FS-03A-13	0.1526	964	—	1240	1221	451	555		
FS-03A-14	0.1773	1023	—	1338	1331	463	582		
FS-03A-15	0.2064	1080	—	1429	1403	472	616		
FS-03A-16	0.2224	1090	—	1461	1434	473	624		
FS-03A-17	0.2427	1102	—	1498	1490	480	651		
FS-03A-18	0.2703	1134	—	1532	1540	490	661		
FS-03A-19	0.2980	1122	—	1605	1304	519	689		
FS-03A-20	0.1294	1025	—	1385	1263	590	660		
FS-03A-21	0.1264	1045	—	1398	1259	609	679		
FS-03A-22	0.1570	1107	—	1501	1391	626	711		
FS-03A-23	0.1846	1173	—	1570	1465	640	742		
FS-03A-24	0.2006	1214	—	1666	1503	635	757		
FS-03A-25	0.2311	1255	—	1724	1575	647	804		
FS-03A-26	0.2645	1291	—	1761	1645	671	854		
FS-03A-27	0.2878	1287	—	1717	1661	695	868		
FS-03A-28	0.1831	1193	—	1633	1480	637	781		
FS-03A-29	0.2209	1295	—	1745	1605	650	790		
FS-03A-30	0.2282	1247	—	1711	1566	648	801		
FS-03A-31	0.2587	1275	—	1751	1622	663	847		
FS-03A-32	0.2907	1296	—	1666	1628	694	882		
FS-03A-33	0.1098	943	—	1237	1137	499	543		
FS-03A-34	0.1344	948	—	1351	1269	520	570		
FS-03A-35	0.1546	960	—	1425	1354	533	590		
FS-03A-36	0.1864	1004	—	1523	1453	544	612		
FS-03A-37	0.2066	1047	—	1566	1502	553	627		
FS-03A-38	0.2326	1104	—	1637	1595	564	648		
FS-03A-39	0.2616	1177	—	1666	1699	586	679		
FS-03A-40	0.1113	989	—	1366	1233	597	632		
FS-03A-41	0.1402	1076	—	1542	1390	611	655		
FS-03A-42	0.1633	1113	—	1601	1459	618	669		
FS-03A-43	0.1879	1168	—	1684	1532	628	688		
FS-03A-44	0.2211	1228	—	1777	1657	645	717		

TABLE IV
COMBUSTOR LINER TEMPERATURE DATA (Continued)

Test No.	EQR	(Dome Avg) $TLIN_1$	BST3 $TLIN_2$	BST6 $TLIN_3$	BST7 $TLIN_4$	BST8 $TLIN_5$	BST9 $TLIN_6$	BST10 $TLIN_7$	BST12 $TLIN_8$
FS-03A-45	0.2370	1224	—	1788	1690	655	728		
FS-03A-46	0.2514	1234	—	1806	1713	663	744		
FS-03A-47	0.1192	1027	—	1421	1290	607	649		
FS-03A-48	0.1337	1041	—	1474	1347	610	656		
FS-03A-49	0.1613	1085	—	1550	1428	618	673		
FS-03A-50	0.1875	1120	—	1587	1473	628	691		
FS-03A-51	0.2020	1124	—	1599	1480	629	696		
FS-03A-52	0.2282	—	—	1651	1555	638	715		
FS-03A-53	0.2413	1191	—	1683	1602	645	728		
FS-03A-54	0.2602	—	—	1727	1656	660	747		
FS-04A-1	0.1090	1128	1049	1195	1223	1254	1438	1403	1423
FS-04A-2	0.1352	1171	1157	1318	1387	1358	1581	1581	1576
FS-04A-3	0.1642	1211	1211	1371	1464	1405	1706	1578	1684
FS-04A-4	0.1817	1265	1251	1419	1492	1388	1786	1643	1707
FS-04A-5	0.2078	1277	1300	1463	1534	1440	1793	1715	1706
FS-04A-6	0.2355	1279	980	1416	1218	944	1783	1715	1693
FS-04A-7	0.2660	1133	725	1179	920	828	1834	1695	1804
FS-04A-8	0.2514	1143	729	1228	920	848	1827	1746	1771
FS-04A-9	0.1850	1411	1239	1475	1533	1335	1783	1679	1665
FS-04A-10	0.2124	1394	1129	1490	1478	1213	1791	1708	1703
FS-04A-11	0.1977	1387	1213	1494	1498	1144	1763	1671	1641
FS-04A-12	0.2035	1299	1090	1422	1414	858	1726	1640	1600
FS-04A-13	0.2689	1251	950	1167	1096	921	1642	1583	1639
FS-04A-14	0.2326	1182	969	1423	1138	1123	1860	1622	1908
FS-04A-15	0.2760	1052	834	1037	885	924	1858	1339	—
FS-04A-16	0.2110	1166	1077	1264	1497	1512	1785	1550	—
FS-04A-17	0.1647	1171	1337	1459	1522	1439	1740	1603	—
FS-04B-1	0.1773	1093	919	1193	1276	1185	1172	—	—
FS-04B-2	0.1032	892	807	1043	1022	880	1258	—	—
FS-04B-3	0.2253	1155	862	1265	1224	1293	1179	—	—
FS-04B-4	0.1453	998	865	1138	1163	1080	1513	—	—
FS-04B-5	0.1032	921	793	1141	1105	893	1246	—	—
FS-04B-6	0.1061	858	791	1057	1168	939	1236	—	—
FS-04B-7	0.1497	978	901	1180	1231	1095	1512	—	—
FS-04B-8	0.1532	1040	903	1278	1290	1087	1543	—	—
FS-04B-9	0.1439	1288	1095	1435	1477	1309	1692	—	—
FS-04B-10	0.1701	1371	1192	1494	1549	1430	1750	—	—
FS-04B-11	0.1962	1424	1258	1526	1535	1479	1775	—	—
FS-04B-12	0.2238	1418	1177	1391	1382	1488	1783	—	—
FS-04B-13	0.2168	1488	1246	1455	1468	1588	1837	—	—
FS-04B-14	0.1922	1456	1281	1580	1619	1524	1823	—	—
FS-04B-15	0.2267	1401	1206	1541	1422	—	1367	—	—
FS-04B-16	0.1904	1478	1334	1523	1526	—	1500	—	—
FS-04B-17	0.1701	1460	1347	1478	1546	—	1605	—	—
FS-04B-18	0.1453	1383	1295	1422	1531	—	1670	—	—
FS-04B-19	0.2006	1504	1309	1490	1510	—	1604	—	—
FS-04B-20	0.2296	1488	1323	1588	1315	—	1750	—	—
FS-04B-21	0.2631	1490	1248	1551	1234	—	1720	—	—
FS-04B-22	0.1846	1492	1366	1650	—	—	1797	—	—

TABLE V
PERFORMANCE PARAMETER DATA

Test No.	*EQR*	*WAPRI*	*WASEC*	*VREF*	*EFFMB*	*TPF*
FS-01A-1	0.1381	1.350	2.861	16.7	121.1	0.53
FS-01A-2	0.2108	1.155	2.613	14.5	125.9	0.52
FS-01A-3	0.1817	1.243	2.667	15.6	124.4	0.51
FS-01A-4	0.2456	1.031	2.537	13.1	127.6	0.56
FS-01A-5	0.1148	1.411	2.818	18.0	121.0	0.53
FS-02A-1	0.1715	0.603	0.994	25.2	84.4	0.91
FS-02A-2*	0.2006	0.603	0.994	25.2	—	—
FS-02A-3*	0.2253	0.603	0.994	25.2	—	—
FS-02A-4*	0.2529	0.603	0.994	25.2	—	—
FS-02A-5*	0.2776	0.603	0.994	25.2	—	—
FS-02A-6*	0.3023	0.603	0.994	25.2	—	—
FS-02A-7*	0.3285	0.603	0.994	25.2	—	—
FS-02A-8*	0.1279	1.956	3.857	27.5	98.6	0.70
FS-02A-9*	0.1439	1.956	3.857	27.5	—	—
FS-02A-10*	0.1570	1.956	3.857	27.5	—	—
FS-02A-11*	0.1701	1.956	3.857	27.5	—	—
FS-02A-12*	0.1831	1.956	3.857	27.5	—	—
FS-02A-13*	0.1962	1.956	3.857	27.5	—	—
FS-02A-14*	0.2296	1.956	3.857	27.5	—	—
FS-02A-15*	0.2616	1.956	3.857	27.5	—	—
FS-03A-1	0.1323	1.790	3.217	23.2	116.0	0.48
FS-03A-2	0.1613	1.805	3.262	23.1	110.6	0.34
FS-03A-3	0.1831	1.787	3.210	22.9	113.6	0.36
FS-03A-4	0.2035	1.858	3.189	24.2	115.3	0.43
FS-03A-5	0.2296	1.702	3.344	21.9	116.4	0.43
FS-03A-6	0.2485	1.781	3.198	23.1	104.4	0.40
FS-03A-7	0.2544	1.885	3.245	24.6	103.4	0.37
FS-03A-8	0.2369	1.888	3.170	24.9	108.9	0.29
FS-03A-9	0.2151	1.767	3.164	22.8	104.1	0.36
FS-03A-10	0.1977	1.861	3.030	24.5	109.1	0.34
FS-03A-11	0.0959	1.828	3.545	22.0	111.2	0.45
FS-03A-12	0.1264	1.766	3.899	21.6	107.6	0.43
FS-03A-13	0.1526	1.732	3.839	21.2	103.5	0.38
FS-03A-14	0.1773	1.630	3.844	19.9	105.6	0.38
FS-03A-15	0.2064	1.660	3.704	20.4	104.8	0.45
FS-03A-16	0.2224	1.696	3.701	20.8	109.4	0.46
FS-03A-17	0.2427	1.688	3.783	20.5	109.5	0.48
FS-03A-18	0.2703	1.700	3.707	20.8	109.1	0.48
FS-03A-19	0.2980	1.666	3.650	20.3	108.9	0.50
FS-03A-20	0.1294	3.446	7.768	25.1	113.4	0.53
FS-03A-21	0.1264	3.642	7.179	26.6	108.1	0.54
FS-03A-22	0.1570	3.527	7.008	25.9	108.8	0.54
FS-03A-23	0.1846	3.552	6.940	26.1	110.5	0.49
FS-03A-24	0.2006	3.603	6.990	26.5	111.3	0.35
FS-03A-25	0.2311	3.564	6.880	26.2	109.7	0.49
FS-03A-26	0.2645	3.455	6.484	25.8	110.3	0.69
FS-03A-27	0.2878	3.521	6.521	26.5	108.7	0.48
FS-03A-28	0.1831	3.397	6.604	24.9	101.6	—
FS-03A-29	0.2209	3.290	6.338	24.3	103.3	—
FS-03A-30	0.2282	3.564	6.633	26.4	104.2	—
FS-03A-31	0.2587	3.528	6.598	25.9	104.3	—
FS-03A-32	0.2907	3.466	6.502	25.7	103.9	—
FS-03A-33	0.1098	1.874	4.005	24.3	140.6	—
FS-03A-34	0.1344	1.846	3.975	24.3	144.3	—
FS-03A-35	0.1546	1.858	4.022	24.5	148.3	—
FS-03A-36	0.1864	1.791	3.899	23.9	151.9	—
FS-03A-37	0.2066	1.789	3.836	24.0	157.3	—
FS-03A-38	0.2326	1.763	3.783	23.6	158.2	—
FS-03A-39	0.2616	1.715	3.778	23.0	166.5	—
FS-03A-40	0.1113	3.515	7.766	25.4	139.1	—
FS-03A-41	0.1402	3.317	7.708	24.2	151.3	—
FS-03A-42	0.1633	3.358	7.680	24.6	152.0	—
FS-03A-43	0.1879	3.318	7.277	24.0	157.3	—
FS-03A-44	0.2211	3.233	7.258	23.5	161.3	—
FS-03A-45	0.2370	3.308	7.424	24.1	166.4	—

TABLE V
PERFORMANCE PARAMETER DATA (Continued)

Test No.	*EQR*	*WAPRI*	*WASEC*	*VREF*	*EFFMB*	*TPF*
FS-03A-46	0.2514	3.296	7.477	24.0	168.9	—
FS-03A-47	0.1192	3.312	7.571	24.0	144.4	—
FS-03A-48	0.1337	3.579	7.974	26.1	152.6	—
FS-03A-49	0.1613	3.508	7.813	25.4	158.0	—
FS-03A-50	0.1875	3.438	7.674	24.8	165.0	—
FS-03A-51	0.2020	3.549	7.745	26.6	166.6	—
FS-03A-52	0.2282	3.528	7.643	26.2	174.4	—
FS-03A-53	0.2413	3.490	7.599	25.9	172.1	—
FS-03A-54	0.2602	3.477	7.574	25.6	172.9	—
FS-04A-1	0.1090	3.895	6.476	28.4	119.1	—
FS-04A-2	0.1352	3.745	6.856	27.0	107.6	—
FS-04A-3	0.1642	3.615	5.962	26.4	103.8	—
FS-04A-4	0.1817	3.671	6.755	27.1	110.4	—
FS-04A-5	0.2078	3.639	6.711	26.6	113.2	—
FS-04A-6	0.2355	3.618	6.622	26.2	130.1	—
FS-04A-7	0.2660	3.540	6.509	25.6	140.3	—
FS-04A-8	0.2514	3.628	6.549	26.3	133.8	—
FS-04A-9	0.1850	3.502	6.928	25.7	125.1	—
FS-04A-10	0.2124	3.901	6.860	28.4	132.8	—
FS-04A-11	0.1977	—	7.088	—	129.9	—
FS-04A-12	0.2035	3.461	6.739	26.1	135.3	—
FS-04A-13	0.2689	3.377	6.764	25.2	146.0	—
FS-04A-14	0.2326	3.283	7.885	23.8	119.1	—
FS-04A-15	0.2760	3.325	8.340	24.2	109.1	—
FS-04A-16	0.2110	3.392	7.706	25.1	114.9	—
FS-04A-17	0.1647	3.088	7.736	22.8	101.4	—
FS-04B-1	0.1773	—	2.924	—	147.1	—
FS-04B-2	0.1032	—	3.434	—	132.9	—
FS-04B-3	0.2253	—	3.092	—	152.7	—
FS-04B-4	0.1453	—	3.078	—	135.3	—
FS-04B-5	0.1032	—	2.719	—	—	—
FS-04B-6	0.1061	—	3.112	—	—	—
FS-04B-7	0.1497	—	2.882	—	—	—
FS-04B-8	0.1532	—	3.008	—	—	—
FS-04B-9	0.1439	—	6.684	—	—	—
FS-04B-10	0.1701	—	6.618	—	—	—
FS-04B-11	0.1962	—	6.402	—	—	—
FS-04B-12	0.2238	—	6.380	—	—	—
FS-04B-13	0.2168	—	6.486	—	—	—
FS-04B-14	0.1922	—	6.598	—	—	—
FS-04B-15	0.2267	—	6.924	—	—	—
FS-04B-16	0.1904	—	6.571	—	—	—
FS-04B-17	0.1701	—	7.256	—	—	—
FS-04B-18	0.1453	—	7.451	—	—	—
FS-04B-19	0.2006	—	6.581	—	—	—
FS-04B-20	0.2296	—	6.442	—	—	—
FS-04B-21	0.2631	—	6.319	—	—	—
FS-04B-22	0.1846	—	6.417	—	—	—

APPENDIX B

SI UNIT CONVERSION TABLE

English	*SI*	*Multiply by*
°F	°C	°C = (5/g)(°F−32)
in.	cm	2.54
$in.^2$	cm^2	0.1550
$in.^3$	liters	0.0164
ft	m	0.3048
ft^2	m^2	0.0929
ft^3	m^3	0.0283
ft/sec	m/sec	0.3048
in. Hg	N/m^2	3.3863
lb_m/sec	kg/sec	0.4535
lb_m/hr	kg/hr	0.4535
gal	m^3	0.003785
Btu/ft^2 hr	w/m^2	315.24808
psi	N/m^2	6894.7572

TECHNICAL REPORT DATA
(Please read Instructions on the reverse before completing)

1. REPORT NO.	2.	3. RECIPIENT'S ACCESSION NO.
EPA-600/7-80-017c		

4. TITLE AND SUBTITLE	5. REPORT DATE
Advanced Combustion Systems for Stationary Gas Turbine Engines: Volume 3. Combustor Verification Testing	January 1980
	6. PERFORMING ORGANIZATION CODE

7. AUTHOR(S)	8. PERFORMING ORGANIZATION REPORT NO.
R.M. Pierce, C.E. Smith, and B.S. Hinton	FR-11405

9. PERFORMING ORGANIZATION NAME AND ADDRESS	10. PROGRAM ELEMENT NO.
Pratt and Whitney Aircraft Group United Technologies Corporation P.O. Box 2691 West Palm Beach, Florida 33402	INE829
	11. CONTRACT/GRANT NO. 68-02-2136

12. SPONSORING AGENCY NAME AND ADDRESS	13. TYPE OF REPORT AND PERIOD COVERED
EPA, Office of Research and Development Industrial Environmental Research Laboratory Research Triangle Park, NC 27711	Final; 1/78 - 4/79
	14. SPONSORING AGENCY CODE EPA/600/13

15. SUPPLEMENTARY NOTES IERL-RTP project officer is W.S. Lanier, Mail Drop 65, 919/541-2432.

16. ABSTRACT The reports describe an exploratory development program to identify, evaluate, and demonstrate dry techniques for significantly reducing NOx from stationary gas turbine engines. (Volume 1 describes Phase I research activities to compile a series of combustor design concepts which could potentially meet the program goals, and Volume 2 describes the Phase II bench-scale evaluation of those techniques: the rich-burn/quick-quench (RB/QQ) concept was found to be effective in limiting pollutant emissions when burning either clean fuels or fuels containing significant amounts of chemically bound nitrogen.) Volume 3 describes the scaleup of the RB/QQ model to a full-scale (25 MW) gas turbine combustor, and documents test results from the full-scale evaluations. Test results were very positive, showing that the RB/QQ concept can reduce NOx to approximately 45 ppm (at zero % O2) for clean distillate oil and to approximately 75 ppm for a distillate oil doped to 0.5% nitrogen, as pyridine. CO emissions below the 100 ppm program goal were also demonstrated. These tests also indicate that the new combustor concept may be capable of low emission performance on petroleum residual oil and synthetic liquid fuels such as SRC II or shale oil. Results from testing on those fuels is included in Volume 4, an addendum.

17. KEY WORDS AND DOCUMENT ANALYSIS

a. DESCRIPTORS	b. IDENTIFIERS/OPEN ENDED TERMS	c. COSATI Field/Group	
Pollution	Pollution Control	13B	13H
Gas Turbine Engines	Stationary Sources	21E	21D
Stationary Engines	Combustor Design	21K	
Nitrogen Oxides	Staged Combustion	07B	
Carbon Monoxide	Dry Controls		
Combustion	Fuel Preparation	21B	
Combustion Chambers	Fuel-bound Nitrogen		
Atomizing			
Shale Oil			

18. DISTRIBUTION STATEMENT	19. SECURITY CLASS *(This Report)*	21. NO. OF PAGES
Release to Public	Unclassified	152
	20. SECURITY CLASS *(This page)*	22. PRICE
	Unclassified	

EPA Form 2220-1 (9-73)